Friction, Wear, Wear Debris and Functional Biocompatibility of Cartilage Substitution Biomaterials

Serena Louisa Russell

Submitted in accordance with the requirements for the degree of Doctor of Philosophy

The University of Leeds
School of Mechanical Engineering
School of Biological Sciences

September 2010

Acknowledgements

Thank you to my supervisors Dr. Joanne Tipper (and for all the stories about your children), Prof. Eileen Ingham, Prof. Zhongmin Jin and Prof. John Fisher – your support, advice and words of encouragement have kept me motivated, which helped me to attended my monthly supervision meetings with optimism and a smile(!), even though there was a long anticipated wait for the materials.

I would also like to thank RW Injection Moulding Company for moulding some of the materials for this thesis, without which I would have had very few results! Thanks to Dr. Wojciech Swieszkowski from Warsaw University who provided the hydrogels. EPSRC and DePuy International sponsored this project for which I would like to thank.

I would like to extend my appreciation for the support and patience of the technical staff, particularly Mr. Phil Wood and Mr. Adrian Eagles. I would like to thank those of you who made my time here enjoyable and for giving me so many memories. A special thank you to Jia, Catherine, Cecilia and Rachel for the many coffee breaks and much needed chats! I will always remember the amusing conversations in office 442c – I appreciate you all welcoming me to the office. I have been fortunate to have worked in both Mechanical Engineering and Microbiology and made so many friends thank you for being helpful and very sociable. It has been a pleasure to work with so many friendly and sociable people.

I would like to thank my beautiful niece and nephew for keeping me amused and definitely keeping me on my toes – I have more time to play with you now! To my sister and brothers, I appreciate your love and support. I am grateful to my cousin (and her family) for the many chats over many, many, many bottles of red wine – your kind words, advice and support were very much valued.

Lastly, but by no means least – a huge thank you to my parents for their love, support, words of encouragement, motivation, the many laughs – the list goes on! I could not have finished this without you both. Thank you so much for always being there for me when I needed you and for believing in me. Love you always!

Abstract

The friction, wear and biological response to hydrogels, thermoset and thermoplastic polyurethanes were investigated in order to determine their suitability as potential cartilage substitution biomaterials. A single station pin-on-plate friction rig was utilised to determine the friction properties of these materials when articulated against articular cartilage plates and stainless steel plates. These materials were also reciprocated against stainless steel plates with smooth and rough surfaces using a six station multidirectional wear rig to generate clinically relevant sized wear particles which were characterised in terms of particle number and area as a function of size. Aseptically generated wear particles from the thermoset and thermoplastic polyurethanes were generated utilising a single station pin-on-plate wear rig and cultured with peripheral blood mononuclear cells to establish their biological activity by assessing the release of four cytokines (tumour necrosis factor-alpha, interleukin-1β, interleukin-6 and interleukin-8) using an enzyme-linked immunosorbent assay.

Friction tests demonstrated that articular cartilage (articulated against itself) exhibited a low coefficient of friction which was concurrent with the literature. The thermoplastic polyurethanes and hydrogels (against articular cartilage) exhibited statistically similar friction characteristics compared to articular cartilage against itself, however, the hydrogels generated considerable wear. In contrast, the friction characteristics of the thermoset polyurethanes were significantly higher than the friction of articular cartilage against itself. When wear particles were generated against stainless steel plates with smooth and rough surfaces, it was clear that the largest percentage number of particles were either < 0.1 or 0.1-1.0 μm in size, however, the percentage area of these particles was more variable and was either in the 0.1-1.0 μm, 1-10 μm or > 10 μm size range. Diprane 50D was the least biologically active material, as cells from two donors out of three were stimulated to release elevated levels of cytokines. Diprane 50D and Corethane 55D were the only two materials to stimulate cells from donors to significantly release three cytokines out of four. All other materials stimulated an elevated level of all four cytokines from cells from all three donors.

Table of Contents

List of Figures

List of Tables

List of Abbreviations

µl	Microlitre
µm	Micrometer
μm^3	Micrometer cubed
AC	Articular cartilage
ACI	Autologous chondrocyte implantation
ACL	Anterior cruciate ligament
ADAMTS	A disintegrin and metalloproteinase with thrombospondin motifs'
Bcl-2	B-cell lymphoma 2 (human proto-oncogene)
BMP	Bone morphogenetic protein
BMP	Bone morphogenetic proteins
BMP-2	Bone morphogenetic protein-2
BMP-7	Bone morphogenetic protein-7
BSA	Bovine serum albumin
BSD	Back scatter detector
BW	Body weight
Chem 90A	Chemtura 90A
cm^2	Centimeter cubed
CO^2	Carbon dioxide
Cor 55D	Corethane 55D
Dip 50D	Diprane 50D
ECM	Extracellular matrix
EGF	Epidermal growth factor
EHL	Elastohydrodynamic lubrication
ELISA	Enzyme-linked immunosorbant assay
FBS	Foetal bovine serum
FEGESEM	Field emission gun environmental scanning electron microscopy
FEGSEM	Field emission gun scanning electron microscopy
FS	FluoSphere
g	Grams
GAG	Glycosaminoglycan
h	Hour
$H_{12}MDI$	Methylene bis (p-cyclohexyl isocyanate)

HA	Hyaluronan
HABR	Hyaluronan-binding region
HBA	Heated blood agar
HDI	Hexamethylene diisocyanate
HEPES	N-(2-hydroxyethyl) piperazine-N'-(2-ethanesulfonic acid)
HRP	Horse radish peroxidise
Hz	Hertz
IGF-1	Insulin growth factor-1
IL-1	Interleukin-1
IL-10	Interleukin-10
IL-11	Interleukin-11
IL-12	interleukin-12
IL-13	Interleukin-13
IL-17	Interleukin-17
IL-18	Interleukin-18
IL-4	Interleukin-4
IL-6	Interleukin-6
IL-8	Interleukin-8
IL-ra	Interleukin receptor antagonist
INF-γ	Interferon gamma
iNOS	inducible Nitric oxide synthase
KDa	kilo Daltons
KN	kilo Newton
KOH	Potassium hydroxide
KV	kilo Volts
LCL	Lateral collateral ligament
LIF	Leukaemia inhibitory factor
LS	Least square
LVDT	Linear variable differential transformer
MCL	Medial collateral ligament
MDI	Methylene diphenyl diisocyanate
mg	Milligram
Min	Minutes
ml	Millilitre

mm	Millimeter
mm^2	Millimeter squared
mm^3	Millimeter cubed
MMP	Matrix metalloproteinase
MMP-13	Matrix metalloproteinase-13
MMP-3	Matrix metalloproteinase-3
MMP-9	Matrix metalloproteinase-9
MPa	Mega pascals
mRNA	Messenger ribonucleic acid
MTT	3-(4,5-dimethylthiazol-2-yl)-2,5-diphenyltetrazolium bromide
MW	Molecular weight
N	Newtons
NA	Nutrient agar
ng	Nanogram
$ng.ml^{-1}$	Nanogram per millilitre
NICE	National Institute for Health and Clinical Excellence
OA	Osteoarthritis
Pa s	Pascal per second
PBMNC	Peripheral blood mononuclear cells
PBS	Phosphate buffered saline
PC	Personal computer
PCL	Polycaprolactone
PE	Polyethylene
pg	picogram
PG	Proteoglycan
$pg.ml^{-1}$	Picogram per millilitre
PMMA	Polymethyl methacrylate
PTR	Proteoglycan tandem repeats
PU	Polyurethane
PVA	Polyvinyl alcohol
PVA/PVP	Polyvinyl alcohol/polyvinyl pyrrolidone
PVP	Polyvinyl pyrrolidone
RA	Rheumatoid arthritis
rpm	Revolutions per minute

RPMI	Rosslyn Park Memorial Institute 1640 culture medium
RTM	Transport medium
SAB	Saboraud dextrose agar
SAL	Surface amorphous layer
SDS	Sodium dodecyl sulphate
SDS-HCl	Sodium dodecyl sulphate-hydrochloric acid
SLRP	Small leucine-rich proteoglycans
SOX-9	SRY (sex determining region Y) – box 9
SS	Stainless steel
TDI	toluene diisocyanate
Tec 51D	Tecoflex 51D
Tec 94A	Tecoflex 94A
TGF-β	Transforming growth factor beta
TIMP	Tissue inhibitor of metalloproteinases
TJR	Total joint replacement
TMB	Tetramethylbenzidine
TNF-α	Tumour necrosis factor alpha
TPU	Thermoplastic polyurethane
UHMWPE	Ultra high molecular weight polyethylene
UK	United Kingdom
USA	United States of America
v/v	Volume/volume
VSI	Vertical scanning interferometry
w/v	Weight/volume
WLI	White light interferometer

Chapter One

Literature Review

1.1 Introduction

Osteoarthritis (OA) is a debilitating disease that mainly affects the large weight bearing joints (i.e. the hip and the knee), nevertheless this disease can also have an effect on smaller joints, such as those present in the fingers (Aigner *et al.*, 2006). The exact cause of OA is not fully understood and the initial mechanisms involved during the onset of OA are still under scrutiny after many years of investigations. OA involves the destruction of articular cartilage (AC), bone and the surrounding tissues of the joints (Aigner *et al.*, 2006). As the cartilage wears, the underlying subchondral bone becomes exposed and comes in contact with the opposing side of the joint. This leads to excruciating pain, joint stiffening and eventually loss of joint movement. There are limited treatments available for the management of OA and, total joint replacement is a last resort.

There are a vast range of medical devices used currently for the replacement of knee and hip joints. It becomes necessary to replace a natural joint due to the development of degenerative diseases such OA. Initially, total joint (both knee and hip) replacements were conducted in patients over the age of 65. However, more recently the age bracket has decreased dramatically to include those in the age group of 45-65 (Katz, 2006). The occurrence of inflammatory joint diseases (i.e. osteoarthritis and rheumatoid arthritis) has increased over the years, and in turn has increased the requirement for surgical intervention. This may be a result of patients not tolerating pain, and hence seeking medical interventions earlier, rather than an increased number of people developing these diseases. Total joint replacements are invasive procedures and revision operations are increasing due to loosening of the implant. Prostheses may only last 10 to 15 years post-implantation as a result of adverse biological reactions to wear products, which leads to osteolysis and aseptic loosening (Ingham and Fisher, 2005).

To further understand why these implants have a limited 'lifespan' we must recognise the biological mechanisms (host response) that occur, post-implantation. The host response refers to the *in vivo* process of cellular invasion once a biomaterial has been implanted. This process involves a number of events following surgery, which include blood-device interactions, deposition of new matrix, acute/chronic inflammation, development of granulation tissue, and foreign body response followed by fibrous capsule formation (Anderson, 2001).

The generation of wear particles is a major issue associated with all joint replacements (Matthews *et al.*, 2000). Wear particles promote the recruitment of various cell types, particularly macrophages. Macrophages release cytokines, which act on other cells in an anabolic or catabolic manner and these actions eventually lead to osteolysis. Macrophages ingest wear particles in order to try to digest and eliminate them from the body, a process referred to as phagocytosis. However, the uptake of wear particles is highly dependent on their size (Wang *et al.*, 1997). It has been reported that particles in the size range of 1.0-10 μm elicit the biological response that leads to osteolysis and implant loosening (Green *et al.*, 1998; Matthews *et al.*, 2000; Tipper *et al.*, 2006). Furthermore, the long term effects of these ingested particles are not fully understood.

The release of wear debris is associated with friction and wear of the devices. Therefore, it is essential to establish the friction and wear characteristics of any potential biomaterial; particularly those that are intended to substitute small osteochondral defects as opposed to replacing the natural joint, as these materials will replace AC. Potential cartilage substitution biomaterials should mimic the mechanical properties of native cartilage and possess similar friction and wear characteristics to this biological tissue. As a result, understanding these very properties with regards to natural AC is imperative, if potential biomaterials are to substitute this complex tissue.

1.2 Classification of joints

Joints are distinguished by their structure and function. Structural differences are defined by the material that attaches to the bone and the presence of a joint cavity - the joint cavity can be composed of a fibrous, cartilaginous or a synovial membrane. The functional part of a joint can be established by the motion of the joint (Marieb, 2004). There are three types of joint motion, i) synarthroses, (*syn* – together, *arthro* – joint) are joints that have no

movement, ii) amphiarthroses, (*amphi* – both sides) are joints with slight movement, and iii) diarthroses, (*dia* – apart) are joints that move freely and where the surfaces are covered with hyaline cartilage (Freeman, 1979; Marieb, 2004; Seely *et al.* 2005). Synarthroses generally have fibrous or cartilaginous structures (e.g. joints in the skull), while amphiarthroses are usually cartilaginous structures, and these types of joints are found mainly in the trunk of the body (e.g. joints between vertebrae). Diarthroses (or diarthrodial joints) are also synovial joints and are present in the limbs [hips and knees] (Marieb, 2004). This can be seen in the knee and hip joints, which are encapsulated by a synovial membrane. This review will focus on the knee joint and the hip joint.

1.3 Synovial joints

The synovial membrane or synovium (Figure 1.1) secretes and accommodates synovial fluid, which is required for lubricating the joint (Martini *et al.*, 2007). The synovium surrounds tendons and folds around ligaments, menisci and other internal structures within the diarthrodial joint, apart from the weight-bearing surfaces (Durward *et al.*, 1999). During movement these folds are permitted to extend to avoid damage to the synovium.

Synovial joints can be classified into six groups; plane (finger joint), pivot (ability to turn head left and right), condyloid (knuckles), saddle (thumb joint), hinge (wheel-like bone that fits into a trough-like bone, i.e. knee joint), and ball-and-socket (hemispherical head, which fits into a cup-shaped socket i.e. hip joint) (Marieb, 2004; Seely *et al.* 2005). Synovial joints experience nonaxial, uniaxial, biaxial, or multiaxial motions. Nonaxial movements only allow slipping motions, uniaxial allows movement in one plane, biaxial permits movement in two planes and, multiaxial allows movement in all three planes and axes (Marieb, 2004; Seely *et al.* 2005). The knee joint is a hinge joint, which has a single plane of directional movement. This uniaxial joint allows flexion and extension motion. The hip joint is a multiaxial ball-and-socket joint so that it can move in all axes and planes (Marieb, 2004).

1.4 Anatomy of the knee joint

As previously mentioned the knee joint is regarded as a 'hinge joint' and it has only one plane of directional movement, however, external and internal rotation is required for complete joint movement (Marieb, 2004). This joint is composed of the femur (thigh bone) which has a head at one end that fits into the hip joint and two 'wheel-like' femoral condyles at the opposite end, which articulate across the top of the tibia bone – the tibial

plateau (Figures 1.1 and 1.2). The condyles are separated by the patellar surface into medial and lateral condyles (Figure 1.2).

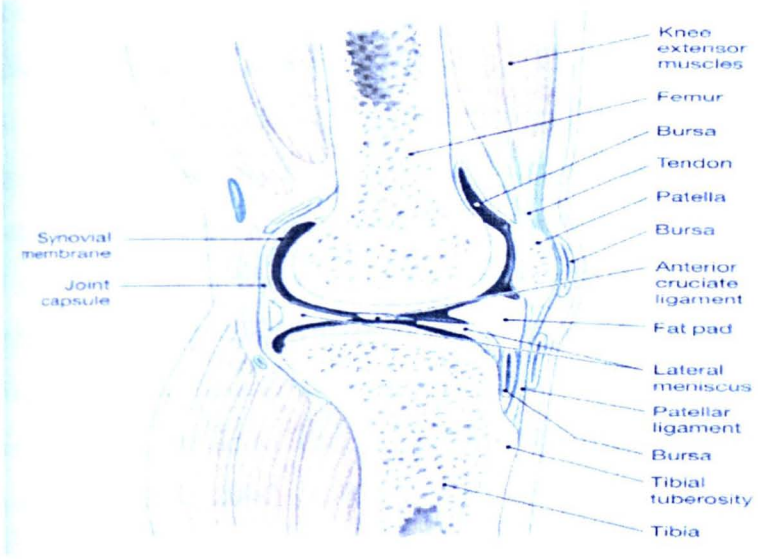

Figure 1.1 The lateral view of the human knee joint (Martini *et al.*, 2007)

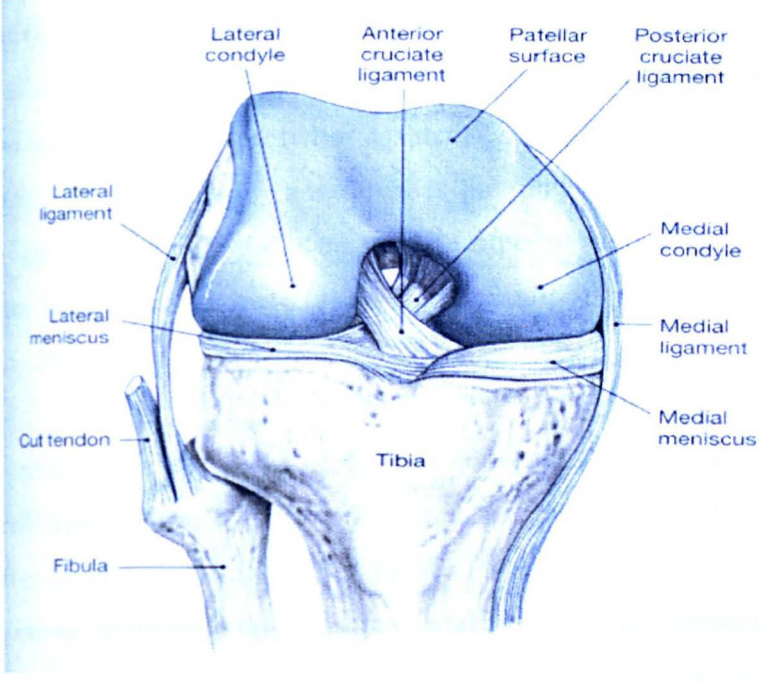

Figure 1.2 The flexed knee joint (Martini *et al.*, 2007)

Articular cartilage (AC) lines the ends of long bones (i.e. femur and tibia) to protect the underlying bone and acts as a cushion to support the loads experienced in the joint. AC is protected by two menisci (medial and lateral meniscus), which lie between the two opposing surfaces of the femoral condyles and tibial plateau (Figures 1.1 and 1.2). The two menisci are crescent-shaped fibrocartilage (fibrous cartilage) structures that cover the

surfaces leaving the middle section somewhat exposed for the internal ligaments; the anterior and posterior cruciate ligaments (Figures 1.1 and 1.2), which help to stabilise the joint (Porth and Kunert, 2002). The menisci, like AC act as cushions to distribute the applied load and thus, lessen the contact pressure. This contact pressure can increase three-fold in the absence of the menisci (Hall, 1999). The fibula is not part of the knee joint cavity but it aids joint stability via the attachment of ligaments and tendons (Figure 1.2). Fat pads protect the sides of the joint and help to decrease friction between the patella (knee cap) and opposing tissues (Figure 1.2). The patella tendon secures the patella superiorly and influences the muscles acting across the knee during movement, while the patella ligament secures the patella inferiorly by attaching to the tibial tuberosity (Marieb, 2004). The bursae (purse) are elongated fibrous sacs (Figure 1.1) containing a small amount of synovial fluid and aid to limit friction between the patella, patella ligament and other joint structures (Marieb, 2004).

Technically, the knee joint is a three-in-one joint consisting of the patella-femoral joint (true knee joint), the tibio-femoral joint and, the superior tibio-fibula joint. The patella-femoral joint allows the patella to glide across the patella groove. This action permits some rotation; however, the medial and lateral ligaments and the menisci prevent sided-to-side rocking (Figure 1.2). The tibio-femoral joint is the 'hinge joint' that allows the femoral condyles to glide and roll over the menisci. The superior tibio-fibula joint is not actually part of the true knee joint but, nevertheless is still an important part of the knee joint as a whole (Marieb, 2004).

During joint movement the point of contact constantly changes as the medial-medial condyle, lateral-lateral condyle and, patella-femur articulate (Figure 1.2). A normal knee joint allows for flexion (bending) and extension (straightening) motions accompanied by minimal adduction (movement towards body), and abduction (movement away from body) (Whittle, 1996). Furthermore, full extension of the joint permits a few degrees of rotation known as the automatic rotation mechanism (Whittle, 1996). In contrast, an injured or diseased joint will allow considerable rotation. The muscles and ligaments surrounding the joint are important as they contribute to the stability, strength, biomechanics and kinematics of the joint. The ligaments serve to control knee joint movement, stabilise the joint and, consequently provide support (Figures 1.1 and 1.2). Collectively, these ligaments limit excessive rotation, prevent dislocation and hyperextension within the joint (Table 1.1).

The knee extensor muscles (quadriceps), seen in Figure 1.1 extend the knee joint, while the hamstrings flex the knee (Whittle, 1996; Hall, 1999).

Table 1.1 Actions of ligaments in the knee joint

Ligament name	Action
Medial collateral ligament (MCL)	Prevents abduction (external rotation) of medial side of joint
Lateral collateral ligament (LCL)	Prevents adduction (internal rotation) of the lateral side joint
Anterior cruciate ligament (ACL)	Prevents anterior movement of tibia in relation to femur and restricts rotation
Posterior cruciate ligament (PCL)	Prevents posterior movement of tibia in relation to femur and limits rotation

1.4.1 Knee joint biomechanics

Muscles and ligaments account for the internal forces acting on joints, however, external forces also play a role. The body is in a state of equilibrium when standing because gravitational forces are applied to the body's mass. This leads to the body exerting a force on the ground (ground force reaction), leaving the body in a state of equilibrium (Whittle, 1996). Therefore, during movement, the ground force reaction and acceleration changes and alters equation 1.1,

$$\text{Force} = \text{Mass} \times \text{Acceleration} \qquad (1.1)$$

(Whittle, 1996; Stewart and Hall 2006)

The ground force reaction acts on all planes (horizontal, vertical, anterior, posterior, medial and lateral) and is crucial for locomotion. These external forces rely on the body's centre of gravity, which is an equal balance of weight (gravitational force on an object) and mass (amount of matter in an object). For example, to account for one foot being placed in front of the other during walking the centre of gravity has to change to maintain the balance (Whittle, 1996). The body's centre of gravity also plays a role in the range of motions within joints during daily activities.

Flexion is performed by the hamstrings in the knee joint and can reach an angle of 140° (degrees) when the hip is also flexed, however the angle decreases to 120° when the hip is extended (Palastanga *et al.* 2006). The quadriceps muscles are responsible for extending the knee joint, until the joint locks to prevent hyperextension. Moving the knee from extension to flexion; the condyles start to roll over the tibial plateau, followed by sliding and rolling of the condyles, then just before maximum flexion rolling stops but sliding continues (Palastanga *et al.* 2006). Tibia rotation in relation to the femur can reach 90° of flexion (to flex the knee joint) in the absence of load. Medial rotation (toes face towards each other) is an action of the hamstrings, which permits an angle of 30°. Lateral rotation can reach a 40° angle when the biceps femoris rotates the tibia so the toes point away from each other (Hall, 1999).

The knee joint experiences a range of contact stresses (pressures) due to applied load during daily activities. These stresses can vary between 0.5 to 20 times total bodyweight (BW) in the knee (Palastanga, *et* al., 2006). It is important to note that muscles and ligaments also play a role in forces that act on the joints, by bearing and transmitting the applied loads (Palastanga *et al.* 2006). Some of these loads during daily activities are indicated in Table 2.2.

Table 2.2 Loads in knee joint (information gathered from Hall, 1999 and Palastanga *et al.*, 2006)

Action	Tibiofemoral joint	Femoropatellar joint	Patellofemoral joint
Walking	>5x BW (usually between 2-4x BW)	0.5x BW	0.5x BW
Ascending ramps/stairs	4x BW	1.5-2x BW	>3x BW
Descending ramps/stairs	-	2.5-3x BW	-
Rising from a chair without arms	4x BW	3.5x BW	-
Jumping	24x BW	20x BW	-
Stance phase of walking	3x BW	-	-

The greatest contact area in the knee joint is possible when the joint is fully extended making the contact area position-dependent, and in turn the joint becomes load-dependent (Palastanga *et al.* 2006). The supporting load across the joint is unequal at low loads (below

500 Newton [N]), but at higher loads (>1500 N) it becomes equal (Palastanga *et al.* 2006). This is thought to be due to the unequal sizes of the condyles that result in different contact areas at low loads. The medial side of the tibia supports the majority of the load in the stance phase of walking, however, during swing phase the lateral side of the tibia supports the smaller loads (Hall, 1999). In the absence of the menisci the contact pressure doubles compared to pressure when the menisci are present. A nominal load of 1000 N to the knee joint gives a contact area of approximately 11.5 x 10^2 mm^2 in the presence of both menisci, resulting in a contact pressure of 3 MPa (Mega Pascals). However, in the absence of the menisci the contact area reduces to approximately 5.2 x 10^2 mm^2, and the contact pressure increases to 6 MPa (Palastanga *et al.* 2006).

1.5 Anatomy of the hip

The hip joint is a 'ball and socket' joint, which is able to move in all three planes of direction (multiaxial motion). The ball is the head of the femur, which securely fits into the socket or, acetabulum of the joint. The articular cartilage (AC) is thicker on the rim of the acetabulum which acts to stabilise the joint, preventing dislocation (Hall, 1999). The acetabulum (*vinegar cup)* is composed of three bones; the ilium, ischium and pubis (Figure 1.3). All three bones become fused to form a hemispherical shaped socket; the acetabulum (Figure 1.3). The ilium is a flared bone that attaches to the gluteal muscles and serves to transmit load from the spine to the pelvis. The lower side of the ischium is rough and thick to form the ischial tuberosity, which is the strongest of the hip bones as it carries the upper body weight in the seated position (Figure 1.3). The pelvis is then held together by the sacrotuberous ligament, which attaches to each ischial tuberosity. Finally, the pubis is found on the anterior side of the hip bone (Marieb, 2204). Functionally, the hip joint takes the weight of the upper body and conveys it to the lower limbs.

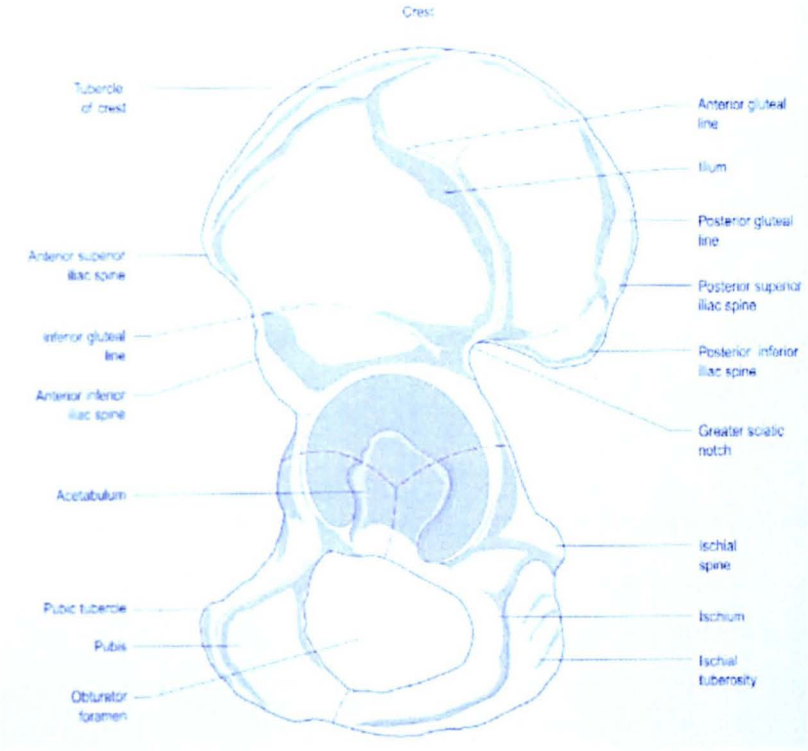

Figure 1.3 Lateral view of left side of the acetabulum. Red dotted lines indicate positioning of the ilium, ishium and pubis (Palastanga *et al.* 2006)

The fovea capitis (Figure 1.4) is a pit at the centre of the ball where the ligamentum teres attaches and extends to the acetabulum (Figure 1.3). This ligament functions to stabilise the joint and secures the head of the femur in the joint, it also contributes to the multiaxial motions with the help of a number of surrounding ligaments and muscles (Whittle, 1996; Marieb, 2004).

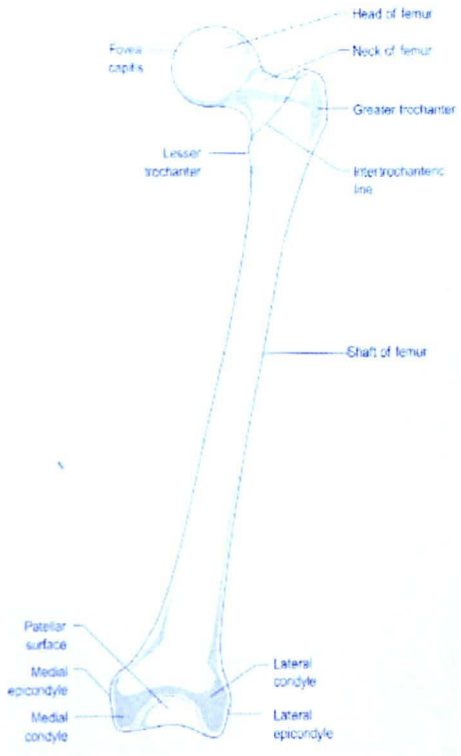

Figure 1.4 Front view of left femur (Palastanga *et al.* 2006)

1.5.1 Hip joint biomechanics

Flexion in the hip is performed by several muscles, in particular the iliopsoas and sartorius muscles (Hall, 1999). The degree of flexion in the hip is reduced if the knee is extended due to the tension in the hamstrings (Hall, 1999; Palastanga *et al.* 2006), and extension of the hip (an action of the hamstrings) does not reach beyond 30° (Palastanga *et al.* 2006). The degree of movement during adduction and abduction can reach 45° each (Palastanga *et al.* 2006), and the muscles responsible for abduction include the gluteus medius and gluteus minimus, which also contribute to joint stability during the support phase of walking (Hall, 1999). Adduction of the hip joint is performed by the adductor muscles (longus, brevis, magnus and gracilis), which act during the swing phase of walking (Hall, 1999). Rotation at the hip joint can be split into medial and lateral rotation, and the range of rotation is approximately 90° (Palastanga *et al.* 2006). The lateral rotators are estimated to be one-third stronger than the medial rotators because lower muscular forces are required for medial rotation (Hall, 1999). However, during level walking the range of motion is reduced and the hip joint is only required to move by 30° during flexion, 10° extension, 5° abduction/adduction, and 5° internal/external rotation (Callaghan *et al.*, 2007).

The average number of steps an individual takes per year is 2 million (Whittle, 1996). This equates to each leg undergoing 1 million cycles each at a frequency of 1 Hertz or 1 cycle per second (Whittle, 1996; Bellucci and Seedhom, 2001). Average loads acting at the hip are indicated in Table 1.3. These loads can range between 150 N (Newton) to 3200 N in the hip joint, which increases the contact area from 2470 to 2830 mm^2, resulting in contact stresses of 2-3 MPa (Palastanga, 2006).

Table 1.3 Loads acting on the hip joint (information gathered from Palastanga *et al.*, 2006 and Callagher *et al.*, 2007)

Action	Hip
Walking	2.1-3.3x BW
Support phase of walking	3-5x BW
Jogging	4.3-5.5x BW
One-legged stance	1.8-3x BW
Ascending stairs	1.5-5.5x BW
Descending stairs	1.6-5.1x BW
Standing up	1.8-2.2x BW

In a normal joint all tissue types experience compressive, tensile and shear stresses during daily activities, however, in a diseased or injured joint the tissues degenerate, which alters their mechanical properties leading to joint instability. Understandably, the stresses experienced by the damaged joint are overwhelming and therefore, lead to further destruction (diseased joints are discussed in Section 1.10).

1.6 Hyaline Articular Cartilage (AC)

Hyaline (gristle) AC is a highly specialised tissue with a glassy white appearance, which protects the ends of long bones, it is almost 'frictionless', and acts as a cushion to absorb compression. AC also viscoelastic, that is, it has viscous and elastic properties (Aigner *et al.*, 2006). Furthermore, this tissue is able to withstand loads several times body weight by resisting compressive and tensile forces. Hyaline cartilage is also a connective tissue, which is composed of fibres, cells and ground substance. The proteoglycans (large macromolecules), interstitial fluid, and cell adhesion proteins form the ground substance and the extracellular matrix is formed from the ground substance and collagen fibres (Marieb, 2004).

AC is an avascular tissue which relies upon diffusion of nutrients from the underlying bone or the surface amorphous layer (SAL) (Graindorge *et* al., 2005; Graindorge *et al.*, 2006). Nutrients diffuse through local blood vessels in the perichondrium (surrounds perimeter of AC within the joint) into the joint cavity. Diffusion also occurs within the ground substance due to the large amount of water, and the presence of collagen fibres, thus enabling the ground substance to act as a molecular filter (Marieb, 2004). The movement of fluid within cartilage helps to restore the tissues' original structure after being compressed. AC consists of four zones; superficial (tangential) zone, middle (transitional or intermediate) zone, deep (radial) zone and the calcified zone (Figure 1.5). However, the SAL extends from the superficial zone and is thought to play a role in the low frictional properties of cartilage, it is approximately 200 nm thick, but this can vary and the layer is not always continuous (Graindorge *et al.*, 2006). Graindorge *et al.* (2006) demonstrated that the SAL does not contain collagen fibres (a marked distinction from the superficial layer) but does contain other components, such as lipids, protein and glycosaminoglycans (GAGs) in equal concentrations.

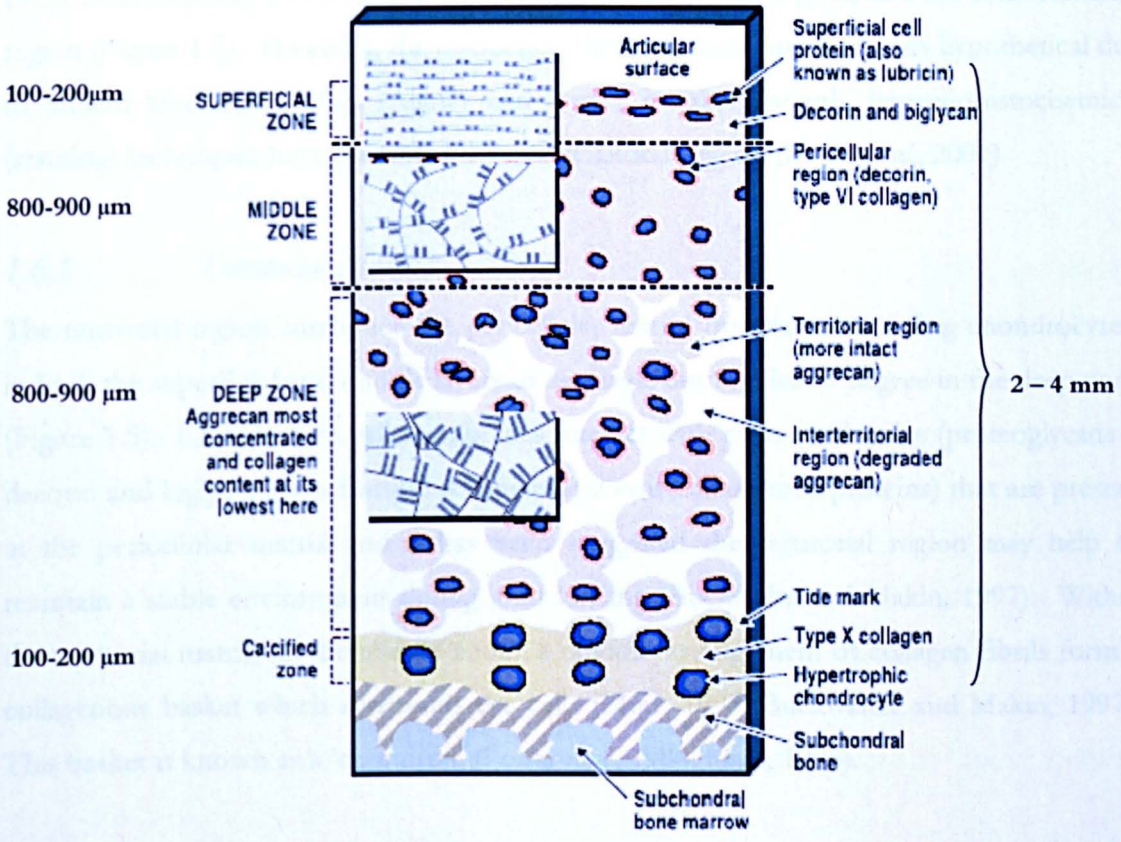

Figure 1.5 Adapted diagrammatic structure of adult human AC showing the different zones and regions. The insets show a comparative representation of the diameter and arrangement of collagen type II fibrils within each zone (Poole *et al.*, 2001).

AC is a biphasic material because it is composed of a solid phase (extracellular matrix) and a liquid phase (water). Cartilage is also hydrostatic, which enables the tissue to resist deformation because water binds strongly to the GAGs in the matrix (Freeman, 1979). This tissue is also capable of resisting stretch (due to its tensile strength), a property provided by the collagen fibres, though cartilage is unable to resist bending (Freeman, 1979). Although, AC is a viscoelastic material, tissue expansion is prevented by the presence of aggrecan aggregates (Aigner *et al.*, 2006). Therefore, the viscoelastic properties and tensile strength provided by components within cartilage contribute to the tissue's compressive stiffness (Aigner *et al.*, 2006).

The four zones of AC are shown in Figure 1.5. The superficial zone is 5-10% of the total thickness of AC, while the middle zone is 40-45% of the total thickness, the deep zone constitutes 40-45% of the total thickness, and the calcified zone makes up 5-10% of the total thickness (Freeman, 1979). All zones are comprised of collagen fibres, water, chondrocytes (cells characteristic of AC) and proteoglycans in varying concentrations. The ECM can essentially be divided into two areas; the territorial region, and the interterritorial region (Figure 1.5). However, the distinction between these areas remains hypothetical due to limited biochemical data (Aigner and Stove, 2003). Though, immunohistochemical (staining) techniques have identified the interterritorial region (Poole *et al.*, 2001).

1.6.1 Territorial Matrix

The territorial region surrounds the pericellular matrix (matrix surrounding chondrocytes) in both the superficial and middle layers of cartilage, but to a lesser degree in the deep zone (Figure 1.5). Chondrocyte cell membranes interact with macromolecules (proteoglycans – decorin and biglycan, non-fibrillar collagens and non-collagenous proteins) that are present in the pericellular matrix and it has been suggested the territorial region may help to maintain a stable environment during joint loading (Buckwalte and Makin, 1997). Within the territorial matrix (in the middle zone), a random arrangement of collagen fibrils form a collagenous basket which surrounds the cells (Muir, 1995; Buckwalter and Makin, 1997). This basket is known as a 'chondron' (Poole *et al.*, 1984; Muir, 1995).

1.6.2 Interterritorial Matrix

Degraded products of aggrecan are found in the interterritorial region (Figure 1.5). Aggrecan is thought to be degraded in the interterritorial matrix due to proteolysis (Poole *et*

al., 2001). There is an undefined boundary of the collagen fibre network that crosses the territorial and the interterritorial regions (Buckwalter and Makin, 1997). The orientation of this network becomes perpendicular to the subchondral bone as fibres move from the territorial region to the interterritorial region (Buckwalter and Makin, 1997). It has been reported that the mechanical properties of cartilage are governed by the interterritorial matrix (Buckwalter and Makin, 1997).

1.6.3 Chondrocytes

Chondrocytes, characteristic cells of articular cartilage (AC), function to maintain extracellular matrix homeostasis by secreting macromolecular components to maintain (collagens, proteoglycans, link protein and hyaluronic acid) and degrade (i.e. proteases) the extracellular matrix (Aigner and Stove, 2003; Mortellaro, 2003). Chondrocytes are also regulated by other anabolic cytokines and growth factors (i.e. transforming growth factor;, bone morphogenetic proteins and insulin-like growth factor 1 which stimulate the cells to produce the macromolecular components (Sandell and Aigner, 2001). Chondrocytes are active cells and under normal physiological conditions they synthesise their own catabolic (matrix degrading) enzymes for instance, matrix metalloproteinases (collagenases and stomelysin) and members of the ADAMTS (a disintegrin and metalloproteinase with thrombospondin) family i.e. aggrecanases (Aigner and Stove, 2003).

Chondrocytes are anchorage-dependent cells and produce mainly type II collagen, though other collagen types exist within the matrix i.e. types VI, IX, X, and XI. These cells are embedded in their own pericellular matrix (Figure 1.5) which is surrounded by extracellular matrix (Poole *et al.*, 2001). The existence of the pericellular matrix prevents cell-to-cell contact from occurring and may contribute to cell anchoring (Poole *et al.*, 2001). Collagen type VI is the main constituent collagen present in the pericelluar matrix and is thought to interact with both the chondrocytes and the extracellular matrix, particularly in the interterritorial region (Aigner and Stove, 2003). Chondrocytes contain rough endoplasmic reticulum and golgi apparatus which are necessary for matrix protein production. However, the activity of these cells varies depending on their location within cartilage (Aigner and Stove, 2003).

It has been shown that chondrocytes differ in their activity, morphology and size in the different zones of AC (Poole *et al.*, 2001). In the superficial zone the chondrocyte cell number is at its lowest and they are elongated and oval in shape (Buckwalter and Makin,

1997; Poole *et al.*, 2001). The cells can also form clusters of two or more cells with a diameter of 10-20 μm (Freeman, 1979). Chondrocytes in the transitional (middle) zone are rounder in shape (≥10μm) and slightly more active. In the radial (deep) zone the cells also adopt a round morphology but grow in vertical columns along the collagen fibres (Buckwalter and Makin, 1997). Chondrocyte number is increased in the deep zone and they are highly active compared to the other zones. Cells in the calcified zone secrete type X collagen to aid the production of a hypertrophic matrix which implies an increased level of activity, probably due to the high levels of alkaline phosphatase which is indicative of cell differentiation (Poole, 2003). Even though this region is calcified, it is more rigid than cartilage but not as strong as bone (Mente *et al.*, 1994). Essentially, the hypertrophic matrix is the mineralised or calcified form of the extracellular matrix (Poole *et al.*, 2001).

1.6.4 Collagen Network

Collagen and proteoglycans present in articular cartilage (AC) account for 20 to 40 per cent of the total wet weight (Buckwalter and Makin, 1997). Of this, collagens contribute up to 60 per cent of the dry weight (Buckwalter and Makin, 1997: Eyre, 2002), while 25 to 35 per cent can be attributed to proteoglycans, and non-collagenous proteins contribute 15 to 20 per cent of the dry weight (Buckwalter and Makin, 1997). As previously mentioned the extracellular matrix is mainly composed of type II collagen, however, other collagens do exist in the matrix and all have an apparent structural role to play. This structural role is aided by the ground substance in which the collagen fibres are encapsulated. The collagen fibres strengthen the tissue and limit the amount of diffusion that occurs (Marieb, 2004). Other collagens present in cartilage are types VI, IX, X, and XI and are highlighted in Table 1.4 (Buckwalter and Makin, 1997; Eyre, 2002; Aigner and Stove, 2003; Aigner *et al.*, 2006). All collagens are structurally very different from one another but do possess one common feature, and that is they consist of three α-chains which twist in a right-handed direction to form a triple helix (Gelse *et al.*, 2003).

Table 1.4 The different collagen types present in AC, indicating formation and function

Type	Composition	Matrix Formation	Function
II	$[\alpha 1(II)]_3$	Fibrillar	Provide tensile strength
VI	α1(VI),α2(VI),α3(VI)	Microfibrillar	Unclear
IX	α1(IX)α2(IX)α3(IX)	FACIT*	Control fibril diameter
X	$[\alpha 3(X)]_3$	Hexagonal network	Matrix calcification (?)**
XI	α1(XI)α2(XI)α3(XI)	Fibrillar	Control fibril diameter

** FACIT – Fibril-associated collagens with interrupted triple helices*

*** Type X collagen maybe associated with calcifying the matrix, though this has not been clarified*

In the superficial zone type II collagen fibres (Figure 1.5) align along the plane of the cartilage surface (Wilson *et al.*, 2005; Aigner *et al.*, 2006) accompanied by elongated chondrocytes (Buckwalter and Makin, 1997; Poole, 2003; Aigner *et al.*, 2006). Studies have shown that collagen fibrils increase in diameter throughout the tissue, the smallest fibres existing in the superficial zone (Figure 1.5), where they are typically 20 nm (Poole *et al.*, 2001; Eyre, 2002; Poole, 2003). Collagen and fibronectin (extracellular matrix protein) content is the highest compared to other zones in the superficial zone, while aggrecan content is the lowest (Buckwalter and Makin, 1997, Poole *et al.*, 2001; Aigner and Stove, 2003; Poole, 2003; Wilson *et al.*, 2005; Aigner *et al.*, 2006). Decorin (small proteoglycan) has been found to be associated with wide collagen fibrils (Figure 1.6), particularly collagen II and IX (Hansen *et al.*, 2006) and it is mostly concentrated in the superficial zone and pericellular matrix (Knudson and Knudson, 2001; Poole *et al.*, 2001). The role of decorin is to control the diameter of collagen type II fibres (Knudson and Knudson, 2001). This arch shaped protein fits securely round each fibre to control the diameter size (Figure 1.6). Another small proteoglycan, fibromodulin, is thought to be associated with regulating collagen fibre size (Figure 1.6) and collagen network formation (Kuettner, 1992; Poole *et al.*, 2001).

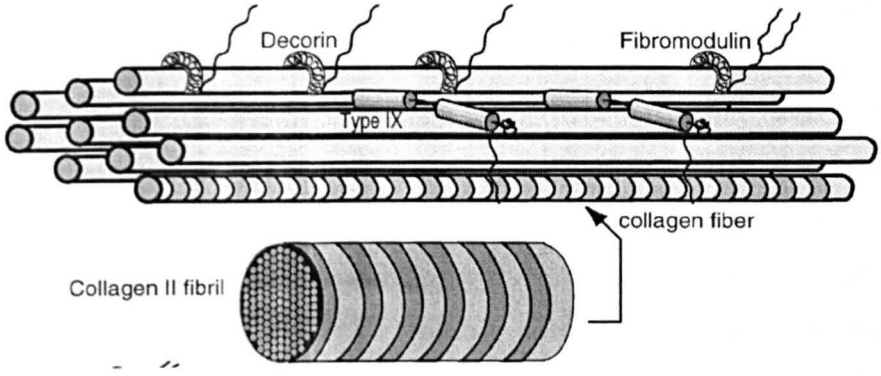

Figure 1.6 Schematic showing the binding arrangement of small proteoglycans and type IX collagen to collagen type II (Knudson and Knudson, 2001).

Type IX collagen forms anti-parallel heterotrimeric structures by cross-linking with collagen type II fibres (Poole *et al.*, 2001). It has been demonstrated that this stability enables the collagen fibres to resist the pressure of swelling exerted by proteoglycans under load (Mow *et al.*, 1992). Type XI collagen is also thought to be associated with regulating type II collagen fibre diameter to 15-50 nm (Gelse *et al.*, 2003; Wilson *et al.*, 2005).

The transitional (middle) zone (Figure 1.5) consists of less organised arrangements of collagen type II fibres (30 nm to 80 nm diameter) compared to the superficial zone (Freeman, 1979). This region has a reduction in collagen content compared to the superficial zone (Buckwalter and Makin, 1997; Poole, 2003; Wilson *et al.*, 2005). Collagen VI accounts for $\leq$ 1% (Eyre, 2002) and, it is associated with bonding to decorin and hyaluronan (Poole *et al.*, 2001), however, it is mostly concentrated in the pericellular matrix (Gelse *et al.*, 2003). The precise function of type VI collagen is still unclear, however, a number of studies have demonstrated its interaction with membrane-bound integrins present on chondrocytes though the mechanism has not been define (Soder *et al*, 2002). This network is predominantly in the pericellular matrix isolating the chondrocytes within the chondron to form a protective basket (Marcelino *et al.*, 1995). Type VI collagen has also been found in the interterritorial matrix and may play a role in cell-matrix interaction as the extended terminals appear inside and outside the cell (Gelse *et al.*, 2003).

The deep zone is where the largest collagen (type II) fibres exist, which are approximately 70 nm to 120 nm in diameter (Poole *et al.*, 2001) and align perpendicularly to the subchondral bone (Buckwalter and Makin, 1997; Poole *et al.*, 2001). This area has a further

reduction in collagen content (Buckwalter and Makin, 1997). In the calcified zone a tidemark (which is noncalcified) lies between the calcified layer and the subchondral bone. This separates the two tissues and the stability of the structures is provided by protruding collagen fibres that intersect the tidemark (Wilson *et al.*, 2005). The role of collagen type X is still unclear, although it has been proposed that it provides extra stability for the cells (of the growth plate) and type II collagen during the development of new matrix (Aspden, 1994). It is important to note, that when cartilage deteriorates, tissue repair expands into the deep zone creating additional tidemarks (Poole, 2003). It is assumed that these additional tidemarks lead to the tissue becoming more brittle due to the formation of a hypertrophic matrix. It has been suggested that the uneven tidemark separation line has a mechanical role in that it is able to withstand shear stresses (Mow *et al.*, 1974).

1.6.5 Proteoglycans

Proteoglycans (PGs) are high molecular weight hydrophilic macromolecules that function to withstand compression, thus they are in part, responsible for the stiffness of hyaline cartilage (Muir, 1981; Poole *et al.*, 2001). The macromolecular component of articular cartilage (AC) also consists of small (biglycan and decorin) and large proteoglycans. Aggrecan is the most dominant PG in AC. In the superficial zone aggrecan content is at its lowest (Buckwalter and Makin, 1997; Poole *et al.*, 2001; Aigner and Stove, 2003; Poole, 2003; Wilson *et al.*, 2005, Aigner *et al.*, 2006). The leucine-rich proteoglycans, decorin and biglycan attach to the collagen fibrils and are at their greatest concentration in this area of cartilage. Decorin has been found to be associated with collagen fibrils, particularly collagen II and XI (Hansen *et al.*, 2006) and it is mostly concentrated in the superficial zone and pericellular matrix (Knudson and Knudson, 2001; Poole *et* al., 2001). The middle zone has an increased concentration of aggrecan (Buckwalter and Makin, 1997; Poole, 2003; Wilson *et al.*, 2005), whereas the deep zone has the highest amount of aggrecan (Buckwalter and Makin, 1997), and the lowest amount of decorin and biglycan (Poole, 2003).

1.6.6 Structure of Aggrecan

The aggrecan protein (230 kDa) is composed of a core protein (Figure 1.7), in which three globular domains exist; G1, G2, and G3 (Knudson and Knudson, 2001). The G1 and G2 segments (Figure 1.7) are separated by a small interglobular domain (21 nm) at the amino-terminal end of the molecule (Kuettner, 1992; Knudson and Knudson, 2001). Between the G2 and G3 (carboxy-terminal end) domains glycosaminoglycan chains of keratin sulphate

(20-50 chains) and chondroitin sulphate (100 chains) are linked to the polypeptide chain (Figure 1.8) which extends to 260 nm in length (Kuettner, 1992). These sulphate groups are polysaccharides and constitute the glycosaminoglycan molecule, which in turn, aid to enhance the compressive properties of articular cartilage [AC] (Kuettner, 1992).

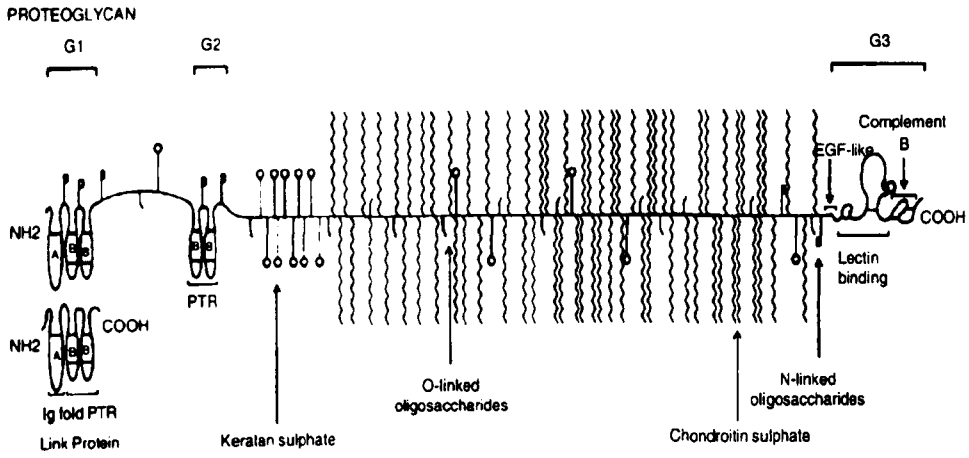

Figure 1.7 The aggrecan monomer showing G1 region (hyaluronan binding site), G2 region (role is unclear) and the G3 region (intracellular trafficking) (Muir, 1995). PTR, proteoglycan tandem repeats; NH_2, amino terminal end group; COOH, carboxy terminal end group; EGF-like, epidermal growth factor-like molecule.

Glycosaminoglycans (GAGs) are negatively charged and thus capable of holding water (Ge *et al.*, 2006). The water is trapped because GAGs are able to interlock, which can change the fluid to a viscous gel (Marieb, 2004). Therefore, the fluid or ground substance becomes more viscous with increasing concentrations of GAGs. Glycosaminoglycan chains, *N*- and *O*-linked oligosaccharides covalently bind to these domains on the core protein (Figure 1.7), and stick out exhibiting a 'bottle-brush' structure (Kuettner, 1992; Muir, 1995).

The N-terminus is within the G1 region and interacts with hyaluronan (an extracellular, high molecular weight GAG) via a non-covalently bound link protein (Kuettner, 1992; Muir, 1995; Knudson and Knudson, 2001). The G1 domain contains a triple looped structure, A, B and B`, which binds to disulfide chains forming double loop domains, known as proteoglycan tandem repeats, PTR (Muir, 1995; Knudson and Knudson, 2001). Both aggrecan and hyaluronan bind to sites in the PTR structures, called hyaluronan-binding region, HABR (Muir, 1995; Knudson and Knudson, 2001). The link protein (a 40-45 kDa glycoprotein) has a double loop formation which binds the G1 domain to

hyaluronan and acts as a stabilising component for hyaluronan and aggrecan (Neame *et al.*, 1999). A high number of aggrecan monomers (molecules) can bind to a single hyaluronan chain extracellularly to form aggregates (Kuettner, 1992; Poole *et al.*, 2001). The C-terminus appears in the G3 domain and is homologous to an epidermal growth factor (EGF) and a C-type lectin module (Muir, 1995; Knudson and Knudson, 2001).

1.6.7 Water

Water is found in high concentrations in articular cartilage (AC) and constitutes approximately 80% of the wet weight (Buckwalter and Makin, 1997). Water uptake swells cartilage and collagen fibres are pushed outwards against the surface of the tissue (Freeman, 1979). There is a balance between swelling pressure (due to negatively charged GAGs) in the tissue and tension of the collagen fibres, therefore cartilage is able to resist deformation (Freeman, 1979). The glycosaminoglycans (GAGs) which have an overall negative charge attract positive ions and increase the total number of ions within the tissue, and this leads to a pressure gradient known as the Donnan equilibrium (Mow and Hayes, 1997). Water content is highest in the superficial zone (85%) compared to other zonal regions (Buckwalter and Makin, 1997; Poole *et al.*, 2001; Aigner and Stove, 2003; Poole, 2003; Wilson *et al.*, 2005). The middle zone contains less water than the superficial zone (Buckwalter and Makin, 1997; Poole, 2003; Wilson *et al.*, 2005), and there is a further reduction of water in the deep zone to 60 per cent (Buckwalter and Makin, 1997).

1.6.8 Synovial Fluid

Synovial capillary walls act as a sieve to filter plasma to a high degree, and permit the diffusion of components < 10 kDa (Gerwin *et al.*, 2006). Synovial fluid differs from plasma because it contains hyaluronic acid (HA) and lubricin, whereas plasma also contains large proteins such as albumin and fibrinogen (Gerwin *et al.*, 2006). Synovial fluid is therefore an ultra filtered form of plasma consisting of polysaccharides, proteins, lipids and cells (Seely *et* al. 2005; Gerwin *et al.*, 2006). Synovial fluid is a transparent yellow viscous liquid that is encapsulated within the synovial membrane or synovium (Pascual *et al.*, 2005). As previously mentioned the synovium envelopes diarthrodial joints and is composed of two layers; the intima and subintima. The subintima differs from the intima layer because it is comprised of adipose, fibrous, or alveolar tissue (Gerwin *et al.*, 2006). Synovial membrane cells (type A and type B) are present in the intima layer and approximately one third of type A synoviocytes are macrophages, where as Type B synoviocytes are fibroblast-

like cells (Gerwin *et al.*, 2006). These fibroblast-like cells secrete HA (Gerwin *et al.*, 2006). HA and lubricin are present in synovial fluid and determine the fluid's viscosity therefore, playing a critical role in lubricating the joint. HA is a polysaccharide and a member of the glycosaminoglycan family, except HA is not sulphated (Gerwin *et al.*, 2006). HA has been reported to be essential nutrient for chondrocyte metabolism (Gerwin *et al.*, 2006).

Synovial fluid provides an excellent lubricating fluid for articulating joints and if failure of this system occurs lubrication of cartilage may rely upon the lipid layer (phospholipids in the superficial layer) (Ballantine and Stachowiack, 2002). It has been reported that exclusion of the lipid layer from joints accelerates wear, thus leading to the onset of osteoarthritis (Ballantine and Stachowiack, 2002). Chondrocytes along with synovial cells secrete the protein lubricin (or megakaryocyte stimulating factor), which has been suggested to be responsible for providing the almost frictionless environment within diarthrodial joints (Poole *et al.*, 2001; Poole, 2003). Many studies have been performed in order to mimic the properties of synovial fluid. As synovial fluid is unique to diarthrodial joints, this has not yet been achieved experimentally. HA provides nutrients to the cartilage and lubrication in order for the joint to function. It has been reported that if a high load is applied to the joint, the action of HA is an inefficient lubricant, and it is thought this is where lubricin may play a role in the lubricating system by interacting with surface-active phospholipids (Gerwin *et al.*, 2006).

1.7 Friction

Friction is described as the resistance to motion. The resistance that occurs when sliding is experienced by two surfaces in contact with each other is the measurement of friction (Hutchings, 1992). Molecular and mechanical factors contribute to the mechanism of friction in which force is required to shear and deform (adhesion and deformation) the sites of surface contact and the sliding of the two surfaces. There are two forms of friction; static and kinetic, the latter is also known as dynamic or sliding. During static friction, it is the force that causes the initial relative sliding of one surface across another. The force is dependent on the pressure between both surfaces when the surfaces are in contact. In order for sliding to continue force is required to sustain motion, this is kinetic friction. The force is also dependant on pressure and contact, and the lubrication mechanism (Hutchings, 1992). The coefficient of friction for AC is in the range of 0.002-0.3 but this is time dependent (Forster and Fisher, 1996). The friction values within

articulating joints are governed by the lubrication mechanisms that operate in the joint. Furthermore, friction can be utilised to identify the lubrication mechanism involved (Jin *et al.* 1996). It has also been reported that the surface morphology which can alter friction characteristics i.e. AC has a roughened surface, which influences friction since contact is reduced between the two joint surfaces (Forsey, 2004).

1.8 Lubrication

There are a number of lubrication mechanisms that operate within synovial joints. During fluid film lubrication (which includes hydrodynamic lubrication, elastohydrodynamic lubrication, and squeeze film lubrication), the opposing surfaces are separated by the fluid. In boundary lubrication (which includes mixed lubrication), surface molecules play an important role. Biphasic lubrication involves the components of the cartilage itself and what occurs within the tissue. No one lubrication mechanism is in action at all times within a weight bearing joint due to the varying loads in operation (Graindorge *et al.*, 2006).

When a normal load is applied to a joint, the articulating surfaces move towards each other and the synovial fluid flows sideways allowing the surfaces to approach further. The fluid flows towards a low pressure region, while cartilage deforms under the high pressure regions. Deformation of the cartilage tissue leads to an increase in hydrostatic pressure as the proteoglycans swell in the presence of water, but is eventually restricted by the tensile forces in the collagen network preventing further swelling (osmotic pressure of proteoglycan gel). At this point the fluid pressure within the cartilage and the hydrostatic pressure reach equilibrium. When the load is removed, cartilage is able to return to its original shape. This is because the internal hydrostatic pressure generated from tensile forces of the collagen network balance the proteoglycan gel osmotic pressure (Freeman, 1979).

The surface roughness of cartilage has been reported to measure between 1 μm and 2 μm (Maroudas, 1976), while the fluid thickness can be as low as 0.02-0.03 μm (Freeman, 1979). It has been well documented that cartilage wear is extremely low, as cartilage can survive cyclic loading over many decades. During compression articular cartilage is able to deform and consequently alter its surface roughness to permit lubrication with small volumes of synovial fluid; and in doing so maintaining a low friction coefficient.

1.8.1 *Fluid Film Lubrication*

Fluid film works optimally under certain conditions and maintains the space between two opposing surfaces; however, it is not efficient as a start-up lubricating regime after a long period of standing (Graindorge *et al.*, 2006). In order for the surfaces to remain separated (Figure 1.8) during fluid film lubrication the film needs to be thicker than the asperities on the bearing surfaces (Walker *et al.*, 1968). As the two bearing surfaces start to slide there is an initial resistance, which is enhanced by the viscosity of the fluid, therefore fluid is able to move into the space between the opposing surfaces (Graindorge *et al.*, 2006). Viscosity of the fluid is important because it assists with the resistance to movement (low speed), and has the ability to develop load-bearing pressures in the fluid, i.e. the lubricant supports the load. Therefore, wear of cartilage is at its lowest (Graindorge *et al.*, 2006).

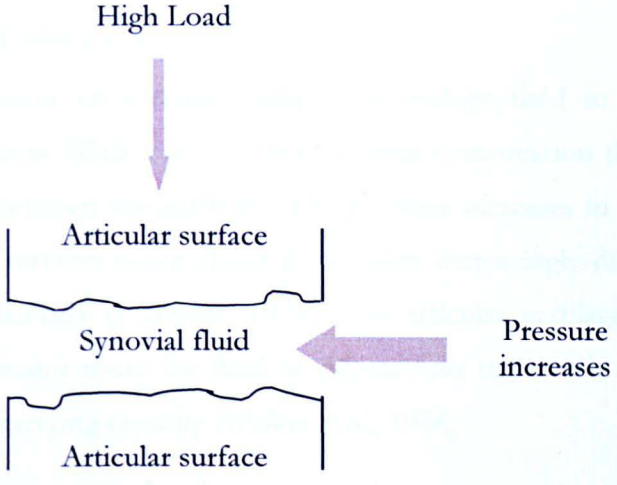

Figure 1.8 Schematic representation of fluid film lubrication. Opposing surfaces completely separated by fluid.

1.8.1.1 *Squeeze Film Lubrication*

Squeeze film lubrication (Figure 1.9) describes the movement of the upper surface towards the opposing surface in the normal direction, though surface contact only occurs after a significant period of time (Walker *et al.*, 1968). The upper surface squeezes fluid out, but viscous forces generate a resistance (Walker *et al.*, 1968). The fluid pressure increases causing the cartilage to deform and the lubricant to be forced out (Walker *et al.*, 1968). At this point the lubricant becomes less viscous and permits contact between the surfaces.

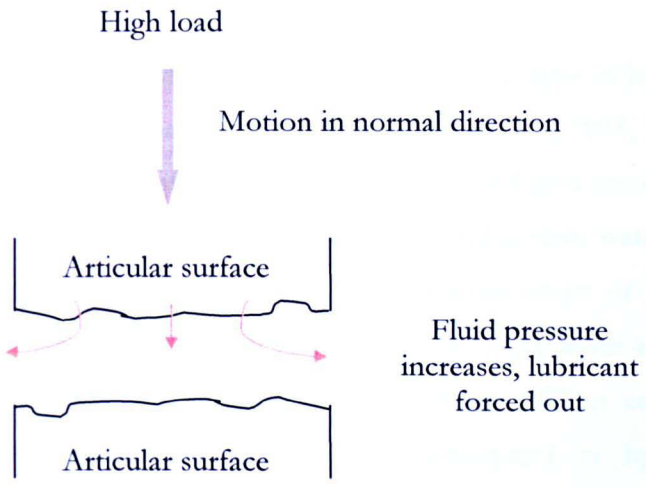

Figure 1.9 Schematic representation of squeeze film lubrication. Approaching surfaces squeeze out fluid.

1.8.1.2 Hydrostatic Lubrication

Hydrostatic lubrication requires an external pump to introduce fluid to the space in between two opposing surfaces (Walker *et al.*, 1968). Under compression the fluid flows laterally through the space between the surfaces. The pressure increases in order to hold the surfaces apart. As the surfaces move closer it becomes increasingly difficult for the fluid to continue flowing laterally (Freeman, 1979). As articular cartilage is a porous material, this becomes the major route for fluid to diffuse into the matrix (Figure 1.10), thereby decreasing the load-carrying capacity (Walker *et al.*, 1968).

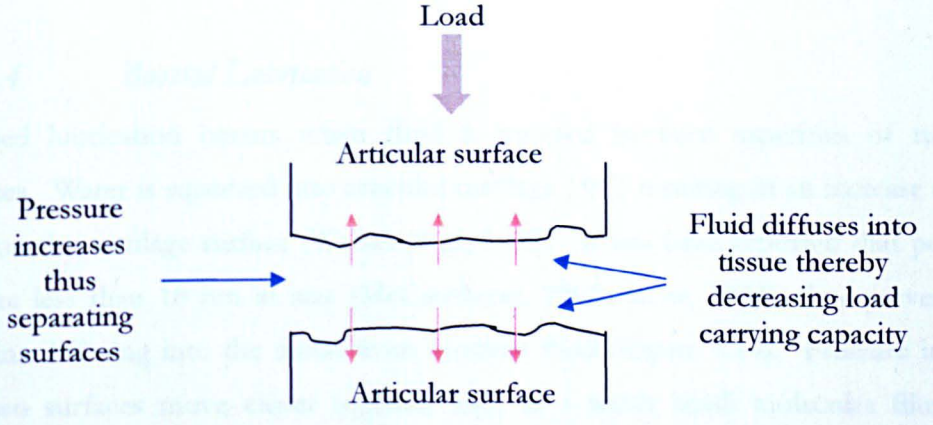

Figure 1.10 Schematic representation of hydrostatic lubrication. Fluid is squeezed through the porous matrix of AC.

1.8.1.3 Weeping Lubrication

Weeping lubrication was described by M^{c}Cutchen (1959, 1962). For this type of lubrication to exist, the bearing surfaces must be porous and deformable (M^{c}Cutchen, 1959, 1962). It is well documented that articular cartilage exhibits a porous matrix and to a certain extent cartilage is elastic in nature. The porous matrix of this tissue is filled with water and as cartilage can be deformed under various conditions, water carries most of the load (M^{c}Cutchen 1959, 1962). The extracellular matrix of cartilage prevents water exudation occurring parallel to the bearing surface (M^{c}Cutchen 1959, 1962). When cartilage is compressed, water 'weeps' out (M^{c}Cutchen, 1959), and participates in hydrostatic lubrication (Neu *et al.*, 2008). It is possible this lubrication regime may participate in cyclic loading and shear stresses (i.e. during normal walking), which could result in synovial fluid being diffused in and out of the cartilage tissue (Figure 1.11).

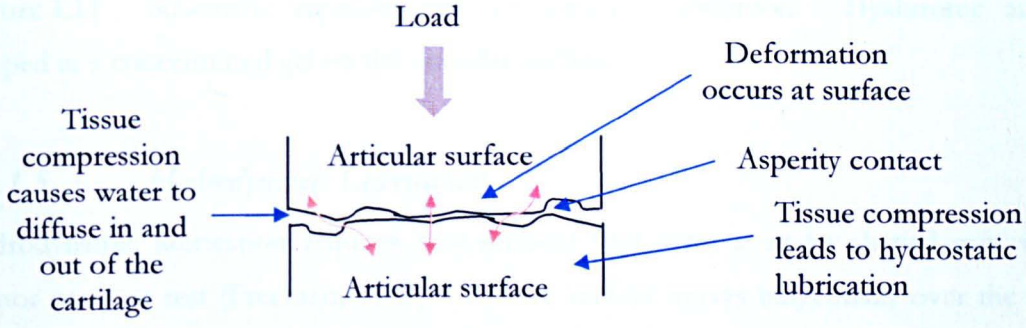

Figure 1.11 Schematic representation of weeping lubrication. When AC is compressed water exudates from the tissue.

1.8.1.4 Boosted Lubrication

Boosted lubrication occurs when fluid is trapped between asperities of two bearing surfaces. Water is squeezed into articular cartilage (AC) resulting in an increase of synovial fluid on the cartilage surface (Walker *et al.*, 1968). It has been reported that pores within AC are less than 10 nm in size (McCutcheon, 1962; Mow, 1984), thus preventing large proteins diffusing into the tissue from synovial fluid (Figure 1.14). Pressure increases as the two surfaces move closer together and, as a result small molecules filter into the extracellular matrix leaving hyaluronic acid (HA) on the surface of the cartilage; trapping concentrated pools of lubricant at the surface (Walker *et al.*, 1968). It has been proposed that HA is the lubricating body in this regime (Walker *et al.*, 1970), and that it forms a viscous gel on the cartilage surface, which may serve to 'boost' lubrication. This type of

lubrication may play a role in the load-bearing phase of joint movement (Walker *et al.*, 1968).

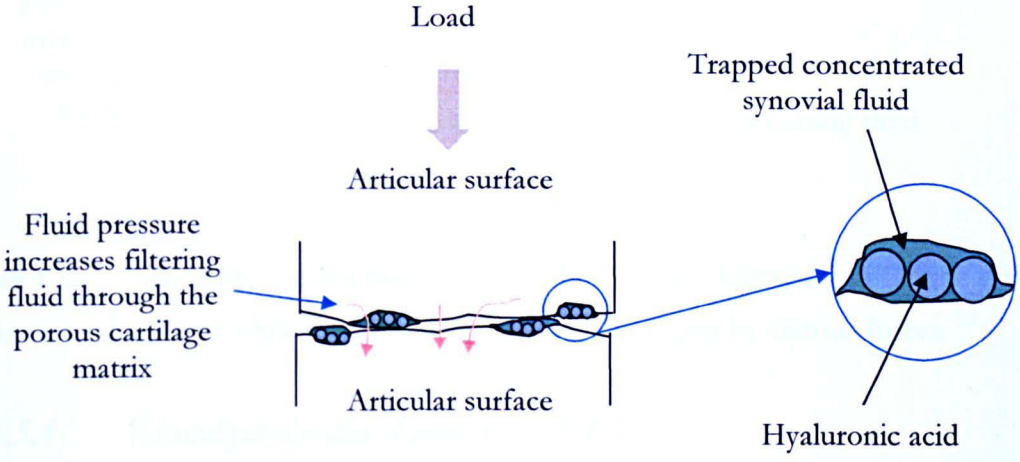

Figure 1.14 Schematic representation of boosted lubrication. Hyaluronic acid is trapped in a concentrated gel on the articular surface.

1.8.1.5 Hydrodynamic Lubrication

Hydrodynamic lubrication requires two surfaces that form a wedge-shaped gap, which cannot occur at rest (Freeman, 1979). As one surface moves tangentially over the other surface (Figure 1.12), an entraining fluid flows through the narrowing gap by viscous forces (Walker *et al.*, 1968), creating a hydrodynamic lift that forces the surfaces apart like a wedge (Neu *et al.*, 2008). The approaching surfaces slide at high speed and cause an increase in fluid pressure, as in squeeze film lubrication (Neu *et al.*, 2008). This film is reported to be < 15 μm thick (Mow *et al.*, 1992) preventing surface contact as the thickness of the fluid is higher than the asperities (Neu *et al.*, 2008), thus friction and wear is reduced (Mow *et al.*, 1992). Pressure within the fluid increases, to sufficiently support a transverse load (Walker *et al.*, 1968). This pressure is exerted on the loaded areas of the film and transferred to the neighbouring solid surfaces (Freeman, 1979), in which shear occurs at the interface (Tu and Fort, 2004).

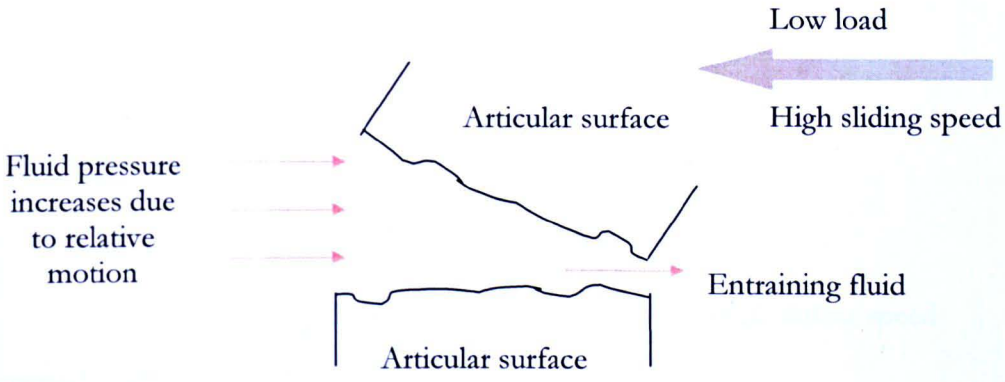

Figure 1.12 Schematic representation of hydrodynamic lubrication. Two surfaces forming a wedge shape while fluid is drawn into narrowing gap by viscous forces.

1.8.1.5.1 Elastohydrodynamic Lubrication (EHL)

EHL involves elastic deformation of the surfaces if the fluid pressure becomes too high (Walker *et al.*, 1968). This type of lubrication is based on a hydrodynamic regime but describes the deformation of the surface area (Figure 1.13). If deformation increases dramatically, the operating regime is said to be elastohydrodynamic (Freeman, 1979). A dramatic increase in film thickness can occur, due to the elastic surfaces because asperities essentially flatten due to localised loading; this type of lubrication is called micro-elastohydrodynamic lubrication (Dowson and Jin, 1992; Dowson, 1995), and this increase allows extra volumes of fluid to travel into the gap (Walker *et al.*, 1968). As the tissue deformation increases so does the film thickness, viscosity, sliding speed and elasticity of the bearing surfaces (Walker *et al.*, 1968). This lubrication regime operates at high loads and high speeds, thus preventing contact and wear, i.e. adhesive wear. However, deeper layers of articular cartilage can show signs of fatigue wear (Mow *et al.*, 1992).

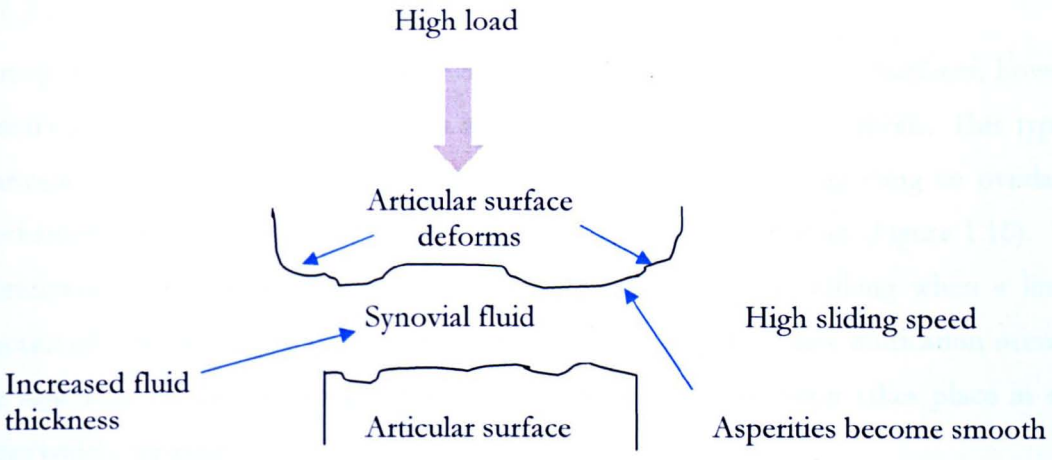

Figure 1.13 Schematic representation of elastohydrodynamic lubrication. Increased fluid pressure can cause elastic deformation to occur.

1.8.2 Boundary Lubrication

Boundary lubrication allows friction within the joint to remain low when contact is made between the two opposing surfaces of cartilage (Figure 1.15) due to components of synovial fluid which are able to adhere to opposing surface of the cartilage, forming a protective layer (Walker *et al.*, 1968). It is believed that hyaluronan and lubricin are responsible for creating this layer. This lubrication regime accommodates low speeds with high loads thus, reducing the film thickness due to the lack of fluid pressure (Mow *et al.*, 1992; Graindorge *et al.*, 2006). The high load forces the asperities to carry the load when they make contact leading to an increase in friction and in turn an increase in wear (Mow *et al.*, 1992; Graindorge *et al.*, 2006). The increased friction and wear (adhesive and abrasive) are due to the breaking of asperities via a stick-slip action, however, wear is somewhat limited by the protective layer. Boundary lubrication operates following long periods of standing or low speeds but is highly undesirable as a continuous lubrication regime.

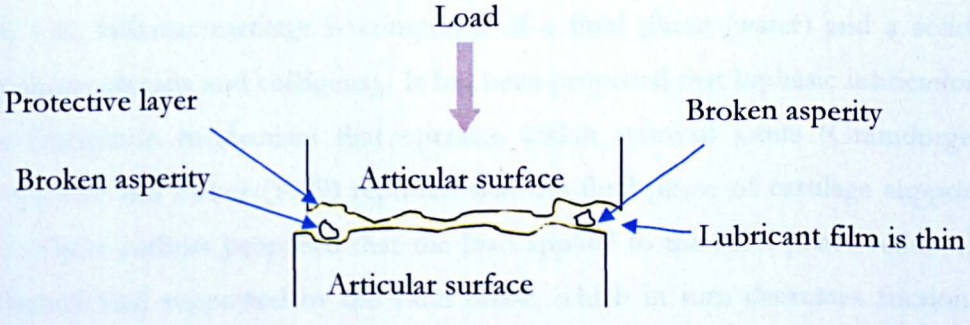

Figure 1.15 Schematic representation of boundary lubrication. Proteins adhere to the cartilage surface preventing surfaces from touching.

1.8.2.1 *Mixed Lubrication*

During mixed lubrication there is an element of separation between the surfaces, however, contact is made between the surfaces at the points where asperities meet. This type of lubrication is a mixture of boundary and fluid film lubrication, suggesting an overlap of mechanisms during transition from one lubricating regime to another (Figure 1.16). This lubrication regime possibly occurs during the stance phase of walking when a limited amount of fluid would be apparent between the asperities. Boundary lubrication occurs at the asperities on the opposing surfaces, while fluid film lubrication takes place in areas more widely separated.

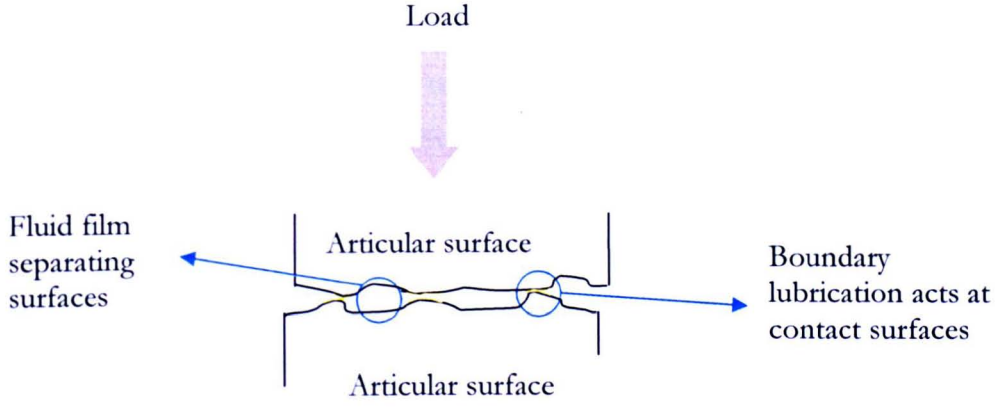

Figure 1.16 Schematic representation of mixed lubrication. Boundary lubrication occurs at asperities on cartilage surface and fluid film takes places in areas more widely separated.

1.8.3 *Biphasic Lubrication*

Biphasic lubrication involves the fluid and solid components of articular cartilage (AC) which is responsible for the biphasic properties of the tissue. As previously mentioned (Section 1.6), articular cartilage is composed of a fluid phase (water) and a solid phase (namely proteoglycans and collagens). It has been proposed that biphasic lubrication is the primary lubrication mechanism that operates within synovial joints (Graindorge *et al.*, 2006). Forster and Fisher (1999) reported that the fluid phase of cartilage supports load initially. These authors proposed that the load applied to the solid phase reduces due to the increased load supported by the fluid phase, which in turn decreases friction. This separation of load support between phases is time dependent, suggesting that loading and unloading cartilage determines the coefficient of friction (Forster and Fisher, 1999). It is

known that when a load is applied to cartilage, this results in the exudation of water from loaded to unloaded areas (M'Cutchen, 1959; M'Cutchen, 1962). After the load is removed cartilage is able to imbibe the fluid (Forster and Fisher, 1999).

Forster and Fisher (1996) demonstrated that the coefficient of friction for AC increases when left stationary for a period of loading, followed by continuous sliding, possibly due to the biphasic properties of the tissue. *In vitro* studies have investigated the frictional properties of AC and in turn, highlighted the biphasic nature of AC. Northwood *et al.* (2007) investigated the friction between bovine osteochondral plugs against stainless steel plates and AC plates. Coefficient of friction results were initially low (<0.05) at the start of the test but gradually increased (>0.35) for the cartilage against stainless steel. The authors suggested that fluid was released from the cartilage plug due to the constant load applied. The constant load prevented the pin from rehydrating, which increased friction and also wear. In contrast, the coefficient of friction for cartilage against cartilage sustained a constant low value (0.04) throughout the test. The constant low friction result for cartilage against cartilage was due to the reciprocating mechanism of the test and was suggested that the unloaded area of the cartilage plate was able to rehydrate, so when the area was reloaded both the cartilage plug and plate were able to maintain fluid load support and replace lost fluid. Furthermore, after testing there were no significant differences in the surface roughness (plug and plate) compared to untested controls (Northwood *et al.*, 2007). The diameter of the plug played an important role in the lubrication and friction when reciprocated against the AC plate, for example a reciprocating length of 10 mm with a 9 mm diameter plug would allow the plate to rehydrate and maintain low friction. However, the same reciprocating length with a 10 mm diameter plug would not allow the plate to rehydrate and thus, friction would increase.

1.9 Wear Particles of Natural Cartilage

It is to be expected that hyaline cartilage releases wear particles as a result of friction due to applied load. However, the damage progression of cartilage is significantly enhanced by the release of wear particles, leading to degenerative joint disease (Van den Berg, 1999). Furthermore, cartilage releases wear particles which initiate inflammation in the synovium in the latter stages of ostearthritis (Van den Berg, 1999). There are several studies describing the natural wear characteristics of articular cartilage. Loading and friction are involved in the wear of joints, but the actual behaviour of these two factors has not been

fully explored with regards to the generation of wear particles. It is important to note there are different types of wear mechanisms including adhesive, abrasive and fatigue wear.

Adhesive wear involve asperities contacting each other, which adhere under load. For joint movement to occur the adhered asperities undergo a shearing effect and are pulled away from the surfaces (Freeman, 1979), resulting in flake-like particles and pitting (Gallagher *et al.*, 2007). However, it is possible for asperities to be transferred from one surface to another (Freeman, 1979). There are two types of abrasive wear; two-body wear and three-body wear. Two-body wear occurs when asperities on one surface detach asperities from the opposing surface. These detached particles are essentially 'free' and can remove asperities from one or both surfaces; this is three-body wear (Freeman, 1979). Abrasive wear can be further divided into microploughing, microcutting, microcracking and microfatigue (Gallagher *et al.*, 2007). Cyclic loading can result in cyclic stresses that vary with load and movement (Freeman, 1979), causing microcracks which can lead to pitting and delamination (Gallagher *et al.*, 2007). However, these stresses can lead to fatigue fractures on the surface, increasing the likelihood of wear debris; this is known as *fatigue wear* (Freeman, 1979). Surface fatigue wear can occur in situations where solid contacts solid during sliding and rolling motions. Furthermore, all three wear mechanisms can act during sliding and rolling motions despite the presence of wear debris (Gallagher *et al.*, 2007).

1.10 Cartilage Degradation and Diseases of the Joint

There has been much speculation about the cause of articular cartilage (AC) destruction and the onset of joint diseases. It has been proposed that one of the first signs of cartilage disease is the degradation of aggrecans (Monfort *et al.*, 2006). However, some investigators believe that the first sign of cartilage disease is surface abrasion of the tissue, while others believe abnormal metabolism of the subchondral bone is responsible for cartilage damage and thus progression of disease. Aggrecan degrades as it is cleaved between the G1 and G2 regions within the interglobular domain [Figure 1.8] (Arner, 2002). The aggrecanases responsible have been identified as, 'A Disintegrin and Metalloproteinase Family with Thrombospondin Motifs' (ADAMTS); aggrecanase-1 (ADAMTS-4) and aggrecanase-2 (ADAMTS-5) which are members of the (Arner, 2002). This enzymatic process releases cleaved aggrecan monomers and creates an unstable environment in which cartilage is

unable to resist compressive load (Arner, 2002). Hence, the mechanical properties of the tissue become impaired.

It is important to note that articular cartilage (AC) damage does not necessarily correspond to the initial onset of end-stage diseases, as most cases of osteoarthritis (OA) [or primary OA] have no known cause of joint damage (Aigner *et al.*, 2006; Ge *et al.*, 2006). However, with regards to secondary OA, studies of the pathogenesis of the disease, or disease group, have revealed many different physiological mechanisms (Aigner *et al.*, 2006; Ge *et al.*, 2006). The pathogenesis of rheumatoid arthritis, however, has been identified and involves inflammatory mediators that activate chondrocytes to release cytokines and destructive proteases which breakdown the surrounding matrix (Miller *et al.*, 2004). The changes observed with cartilage breakdown in OA are fibrillation resulting in roughening of the surface, crack formation through the tissue and ulceration, reduced thickness, discolouration and softening of the tissue (Mortellaro, 2003). These changes also occur during OA, and both diseases may include osteophyte formation and subchondral cysts (Ge *et al.*, 2006). Even though the pathological processes of OA have not been fully elucidated, the identification of various cytokines, growth factors and matrix metalloproteases have been studied.

There are a number of cytokines that act on chondrocytes in either a destructive (catabolic), regulatory (inhibitory) or enhancing (anabolic) manner. As already mentioned chondrocytes also produce their own anabolic and catabolic cytokines. Under pathological conditions chondrocytes continue to synthesise anabolic and catabolic molecules, however, anabolic molecule production may be inhibited or catabolic molecules up-regulated causing an imbalance and thus compromising the functional integrity of AC (Aiger *et al.*, 2003). Furthermore, during osteoarthritis this balance is compromised and usually leads to an increase in catabolic cytokines (Sandell and Aigner, 2001). It is generally believed this up-regulation of degrading and enhancing cytokines cause chondrocytes to become 'activated' and therefore, change phenotype. This change in phenotype results in chondrocytes producing regulatory (transforming growth factor-beta; TGF-β, bone morphogenetic proteins; BMPs and insulin growth factor-I; IGF-1), and catabolic (interleukin-1; IL-1β, and tumour necrosis factor; TNF-α) factors they would not normally secrete (Sandell and Aigner, 2001). Under pathological conditions the synovium also produces and secretes these cytokines, which lead to the destruction of cartilage (Sandell and Aigner, 2001). It is

important to note that the metabolic reactions which take place during OA are initiated by both destructive and enhancing cytokines (as a whole) and not by individual cytokines acting alone (Sandell and Aigner, 2001). This review will focus on the cytokines involved in osteoarthritis. Catabolic cytokines [interleukin-1 (IL-1), IL-6, IL-8, tumour necrosis factor-alpha (TNF-α), leukaemia inhibitory factor (LIF), IL-17 and IL-18], Inhibitory cytokines [IL-4, IL-10, IL-11, IL-13, and interleukin receptor antagonist (IL-ra)] and, Anabolic cytokines [insulin-like growth factor-1 (IGF-1), transforming growth factor-beta (TGF-β), bone morphogenetic proteins [BMP, such as BMP-2, and BMP-7)] are described in Table1.5

Table 1.5 Actions of cytokines and growth factors

Name	Released by	Action
	Catabolic cytokines (pro-inflammatory)	
IL-1β	Chondrocytes, activated macrophages and the synovium (Miller *et al.*, 2004)	IL-1 is a 17kDa protein (Choy *et al.*, 2001) and inhibits the production of type II collagen, proteoglycans and mediates the release of matrix metalloproteases from chondrocytes which leads to cartilage degradation (Van den Berg, 1999; Choy *et al.*, 2001; Aigner *et al.*, 2003). IL-1 has been found to stimulate the release of IL-6 (Van Snick, 1990), type II collagen and proteoglycan production (Van den Berg, 1999; Choy *et al.*, 2001; Aigner *et al.*, 2003).
IL-6	Monocytes, macrophages, T-cells, synovial fibroblasts (Choy *et al.*, 2001), mast cells and endothelial cells (Van Snick, 1990).	Chondrocyte proliferation is increased by IL-6 though the formation of proteoglycans is prevented (Martel-Pelletier *et al.*, 1999). Tissue inhibitor of metalloproteinases (TIMP) are destructive to cartilage (Van den Berg, 1999; Westacott and Sharif, 1996), however, IL-β, and TNF-α up-regulates IL-1ra. Inhibition of IL-1β and TNF-α inhibits the production of IL-8 (Raman *et al.*, 2003).
IL-8	Monocytes, macrophages and chondrocytes (Martel-Pelletier *et al.*, 1999)	This cytokine stimulates the infiltration of leukocytes to the site of inflammation and induces neutrophils to secrete superoxides and proteases (Raman *et al.*, 2003).
TNF-α	Chondrocytes, activated macrophages and the synovium and can act as an autocrine or paracrine stimulator (Aigner *et al.*, 2003). Present in the chondrocyte cell	*In vitro* studies have shown TNF-α to be involved in the destruction of cartilage but its effect is less than that of IL-1 (Van den Berg, 1999). TNF-α enhances release of IL-1, IL-6 and IL-8 (Choy *et al.*, 2001), but inhibits type II collagen formation (Aigner *et al.*, 2003).

	membrane during synthesis (Choy *et al.*, 2001)	
LIF	Chondrocytes, activated macrophages, synovium (Miller *et al.*, 2004), osteoblasts and T-cells (Hui *et al.*, 1998)	LIF is associated with the degradation of proteoglycans by preventing proteoglycan synthesis. High concentrations of LIF have been identified in the joints of arthritic patients (Hui *et al.*, 1998; Grimaud *et al.*, 2002; Fan *et al.*, 2004). LIF enhances the release of MMP-13 (Collagenase 3), IL-1 and IL-6 (Hui *et al.*, 1998; Grimaud *et al.*, 2002; Fan *et al.*, 2004).
IL-17	T-cells and activated macrophages (Jovanovic *et al.*, 1998; Van den Berg, 1999)	A recent study demonstrated that inflammation and cartilage damage was initiated when IL-17 was introduced into joints (Dudler *et al.*, 2000), and it has been found in the synovium of patients with rheumatoid arthritis (Bessis *et al.*, 2001). IL-17 stimulates synovial cells to release LIF and induces chondrocytes to release IL-6 and nitric oxide; LIF also activates macrophages to synthesise TNF-α, IL-1, IL-6, IL-12 and prostaglandin E-2 (Jovanovic *et al.*, 1998).
IL-18	Activated macrophages, lymphocytes, osteoblasts, keratinocytes, dendritic cells and chondrocytes (Bessis *et al.*, 2001)	IL-18 is associated with cartilage breakdown and increases the release of glycosaminoglycans (Park *et al.*, 2001). IL-18 has been identified in the synovium of patients with rheumatoid arthritis, and it has been reported to initiate its own synthesis, production of nitric oxide, nitric oxide synthase, IL-6 and MMP-3 (Stromelysin 1) (Bessis *et al.*, 2001; Park *et al.*, 2001). IL-18 stimulates angiogenesis (Park *et al.*, 2001), and promotes T-cells to release interferon gamma (Bessis *et al.*, 2001), which may have a role in osteoarthritis (Muir, 1995).
	Inhibitory cytokines (anti-inflammatory)	
IL-4	CD4+ T cells, TH2 cells, basophils and mast cells (Seder and Paul, 1994)	IL-4 is capable of controlling inhibitors of IL-1 (i.e. IL-1ra), IL-6, IL-8 and scavenger receptors of both IL-1 and TNF-α (Van den Berg, 1999). IL-4 generates nitric oxide and it

		has been demonstrated that high levels of nitric oxide is generated when chondrocytes are stimulated with IL-1 or TNF-α, which induce cell death (Lotz *et al.*, 1999).
IL-10	T cells (Raman, 2003)	Controls inhibitors of IL-1 (i.e. IL-1ra), IL-6, IL-8 and scavenger receptors of both IL-1 and TNF-α (Van den Berg, 1999) have been identified in the synovial fluid of individuals with rheumatoid arthritis and is produced by T-cells, B-cells, monocytes and macrophages (Van den Berg, 1999). Prevents the release of IL-1 and TNF-α by chondrocytes and macrophages (Van den berg, 1999). Inhibitory effect on cartilage degradation (Van Roon *et al.*, 1995; Van Roon *et al.*, 1996).
IL-13	Helper T cells (Zlotnik and Moore, 1991)	IL-13 controls inhibitors of IL-1 (i.e. IL-1ra), IL-6, IL-8 and scavenger receptors of both IL-1 and TNF-α (Van den Berg, 1999). It has been reported that lipopolysaccharide-induced IL-6 secretion can be inhibited by IL-13 (Zlotnik & Moore, 1991). IL13 inhibits the release of IL-1 and TNF-α by chondrocytes and activated macrophages and inhibits the catabolic activity of IL-1 and TNF-α (Van den Berg, 1999). IL-13 can increase the synthesis of IL-1ra (Etter, 1998).
IL-1ra	Monocytes and activated macrophages (Eisenberg *et al.*, 1990)	IL-1ra has been found in high quantities in the synovium of patients with rheumatoid arthritis but the concentration does not exceed that of IL-1 (Eisenberg *et al.*, 1990). Experiments have been conducted on arthritic models showing that anti-IL-1 antibodies and IL-1 receptor antagonist (IL-1ra) limit the progress of arthritis (Van de Loo *et al.*, 1995; Joosten *et al.*, 1996). IL-1ra blocks IL-1 receptors and prevents activation by IL-1, however, the binding of the antagonist does not activate the IL-1 receptor (Eisenberg *et al.*, 1990).

	Anabolic cytokines	
IGF-1	Produced in the liver and cells throughout the body (Daughaday & Rotwein, 1989; Westacott and Sharif, 1996)	IGF-1 enhances cartilage production, and therefore, can prevent degradation of the tissue (Westacott and Sharif, 1996). In the presence of IL-1 and TNF-α, IGF-1 is also capable of promoting proteoglycan production (Westacott and Sharif, 1996). In the presence of IL-1β, IGF-1 inhibits proteoglycan synthesis (Van den Berg, 1999). IGF-1 increases the expression of IGF receptors on chondrocytes and prevents IL-1 activity and possibly inhibits the IL-1 receptor (Westacott and Sharif, 1996).
TGF-β	Fibroblasts, endothelial cells, monocytes and macrophages (Ozbilgin *et al.*, 2003)	Chondrocytes change their phenotype due to over exposure and become more responsive to TGF-β (Van den Berg, 1999). TGF-β counteracts the catabolic action of IL-1, prolonged exposure of TGF-β produces osteophytes (outgrowth of bone) in the periosteal layers (Van den Berg, 1999).
BMP-2	Could potentially be synthesised by chondrocytes within osteoarthritic cartilage. Healthy adult cartilage has been shown to contain negligible BMP-2 (Nakase *et al.*, 2003)	BMP-2 induces cartilage and bone formation and over exposure leads to proteoglycan synthesis (Westacott and Sharif, 1996). Over exposure of BMP-2 prevents IL-1 interaction, possibly due to inhibition of IL-1 receptors (Westacott and Sharif, 1996).
BMP-7	Chondrocytes (Sandell and Aigner, 2001)	BMP-7 increases proliferation and maturation of chondrocytes and osteoblasts, as well as stimulating matrix formation (Sandell and Aigner, 2001). BMP-7 enhances the expression of aggrecan and collagen type II mRNA in chondrocytes. BMP-7 has an effect on osteoarthritic cartilage by enhancing proteoglycan production (Stove *et al.*, 2006).

Understanding the mechanisms of osteoarthritis (OA) and cartilage degradation will give a greater insight to the patho-physiological processes involved. Thus far, the cause of proteoglycan breakdown is not fully understood. However, it is known that OA involves the interaction of matrix metalloproteases (MMPs), which are activated by IL-1β (Miller *et al.*, 2004). MMPs are known to be involved in the breakdown of cartilage (Caterson *et al.*, 2000). They are associated particularly with the digestion of collagen and aggrecan core protein, thus releasing glycosaminoglycans [GAGs] (Caterson *et al.*, 2000). These released GAGs, such as chondroitin sulphate and keratan sulphate, are no longer trapped within the matrix and thus, allow the influx of water into the cartilage, which leads to a loss of mechanical properties of the tissue (Caterson *et al.*, 2000). A number of MMPs have been identified, MMP-13 (Collagenase 3) being the most important regarding the breakdown of cartilage during osteoarthritis (Monfort *et al.*, 2006).

Monfort and others (2006) subjected small leucine-rich proteoglycans contained within normal and diseased (i.e. OA) cartilage samples to MMP-13. MMP-13 cleaved biglycan, decorin, fibromodulin and lumican (matrix molecule that regulates the formation of macrofibrils), though to differing degrees. They found that cleavage of biglycan and fibromodulin were favoured over decorin and lumican by MMP-13. Moreover, excluding fibromodulin, the other SLRPs were digested in a similar way for normal and OA cartilage. Increased cartilage degradation related to an increase in the level of fibromodulin breakdown (Monfort *et al.*, 2006). This study concluded that the collagen network could be disturbed by exposing the MMP-13 cleavage site and, both biglycan and fibromodulin may be used to identify early signs of cartilage destruction during OA (Monfort *et al.*, 2006).

A previous study compared chondrocyte gene expression between advanced and minimal OA cartilage samples (Yagi *et al.*, 2005). Immunological staining of the samples showed that minimal OA cartilage had higher chondroitin sulphate (proteoglycan) content, with an even distribution of chondrocytes throughout the tissue compared to advanced OA cartilage, which had fewer visible cells with an uneven distribution. The advanced OA cartilage also showed signs of fissures extending to the deep zone and no visible signs of fissures were in the superficial zone. It was apparent that advanced OA cartilage had signs of chondrocyte proliferation; an attempt of tissue repair, however, proteoglycan and GAG content was significantly lower than in the minimal OA cartilage. Surprisingly, collagen content did not change to any great extent, as hydroxyproline content was assessed.

Hydroxyproline can be used as a marker of collagenous content, though it cannot be used to differentiate between collagen types. Gene expression also differed between both diseased tissues. Aggrecan and link protein mRNA were significantly lower in advanced OA cartilage, however, collagen type II and MMP-13 gene expression varied between samples. However, there was a slight increase in expression of markers for apoptosis Bcl-2 (B-cell lymphoma 2) and Sox9 (transcription factor). MMP-3 (Stromelysin 1) and MMP-9 (Gelatinase B) expression decreased in advanced OA cartilage compared to minimal OA cartilage. These findings indicated that chondrocytes may change phenotype at different stages of OA, with chondrocytes exhibiting decreased expression of aggrecan and link protein but an increased expression of osteopontin with advanced disease (Yagi *et al.*, 2005).

The onset of OA results from mechanical, physical and chemical alterations within the joint leaving AC unable to withstand compression (Aigner *et al.*, 2006). It is not only cartilage that is affected by these failures but the disease also has a direct effect on other surrounding connective tissues (including the synovial membrane), muscles and nervous system (Aigner *et al.*, 2006). The damage leads to the individual experiencing pain, inflammation, stiffening of the joint (capsular fibrosis) and swelling (Aigner *et al.*, 2006). As the disease progresses cartilage is destroyed further until the subchondral bone is exposed. If the condition is left untreated the mobility of the diseased joint reduces dramatically for the individual, often resulting in disability and hence, a severe lifestyle impairment.

1.11 Current Treatments for Cartilage Repair

Many procedures are performed to treat diseased or injured joints. Cartilage anomalies in these joints are usually referred to as cartilage lesions or cartilage defects; these two terms can be sub-divided to define whether the anomaly is a chondral or osteochondral defect/lesion. Again these terms can be divided further into full thickness and partial thickness chondral defects/lesions to describe damage down to the subchondral bone or, cartilage flap, respectively. Osteochondral defects/lesions are full thickness, which cross the tidemark and into the subchondral bone (Bhosale and Richardson, 2008). Non-surgical treatments include oral pharmacological agents, weight loss, exercise and, injections (i.e. corticosteroids). However, if the disease or trauma is too severe or the above approaches fail to work then surgical intervention is the next stage of treatment (Pylawka *et al.*, 2006).

Surgical treatments are subdivided into palliative (arthroscopic debridement), reparative (microfracture, abrasion arthroscopy, subchondral drilling) and restorative treatments (tissue engineering and osteochondral grafting). Palliative treatments are usually the first choice of surgical treatment for defects < 2 cm^2 in size (Pylawka *et al.*, 2006). Reparative treatments are typically performed on active patients with small defects (< 2cm^2) or less active patients with large defects (> 2 cm^2). Restorative treatments such as autologous chondrocyte implantation are used for medium to large defects (> 2 cm^2), osteochondral autografts are used to treat small defects, which are less than 2 cm^2 in size, and osteochondral allografts are used to treat larger defects(> 2 cm^2), which other methods cannot treat (Pylawka *et al.*, 2006).

Arthroscopic debridement involves a technique that removes debris, cytokines and proteases from the joint cavity (Pylawka *et al.*, 2006). This treatment is often followed by marrow stimulation techniques, whereby the subchondral bone is drilled (subchondral drilling) to release mesenchymal stem cells in order to encourage new tissue growth (Bhosale and Richardson, 2008). During this procedure it is not possible to smooth or stabilise the cartilage surface (Pylawka *et al.*, 2006).

Bone Marrow Stimulation is one of the early treatments for cartilage repair. A hole is drilled into the subchondral bone in order to stimulate the influx of pluripotent stem cells (Polster and Recht, 2005). It was initially believed that the stem cells would differentiate into chondrocytes and produce matrix to fill the void. However, the matrix formed in these areas has been shown to be fibrocartilage, which does not exhibit the same mechanical properties as native tissue (Polster and Recht, 2005). The bone marrow stimulation technique also includes abrasion arthroscopy and microfracture, discussed below.

Abrasion Arthroplasty is a technique in which the cartilage defect is debrided until healthy tissue is exposed. The fibrin clot forms a provisional matrix for new matrix development. This method does present a disadvantage because cell death occurs due to the heat caused by the abrasion burr used (Polster and Recht, 2005).

Microfracture requires a series of fractures to be produced in the defective area in an attempt to initiate the influx of stem cells (Polster and Recht, 2005). However, like bone

marrow stimulation, fibrocartilage is produced rendering the newly formed tissue mechanically inferior. No heat is produced with this technique; an advantage over abrasion arthroscopy.

Mosaicplasty (autologous osteochondral transplant) can be performed with allografts or autografts. Autografts are the preferred choice because the method uses the patient's own tissue and prevents the risk of an immune response and/or infection. This technique uses osteochondral plugs from low weight-bearing areas of the joint and implants then into the defective areas. However, problems occur with this method because of the mismatched size of the plug to the defect causing apoptosis, lack of integration and only a small amount of donor cartilage is available from the patient (Polster and Recht, 2005). Other disadvantages include donor site morbidity and cell viability of allografts as the plugs can be stored frozen (Pylawka *et al.*, 2006).

Autologous Chondrocyte Implantation, ACI (the earliest type of tissue engineering) is a technique in which a biopsy of healthy cartilage (300-500 mg) is removed from a low weight-bearing area of the joint i.e. patella or upper medial femoral condyle (Polster and Recht, 2005; Pylawka *et al.*, 2006). The cells are expanded *in vitro* under aseptic conditions then injected into the defect under a periosteal patch. The neocartilage is thought to be like hyaline cartilage with superior biomechanical properties compared to fibrocartilage (Pylawka *et al.*, 2006). However, this technique is extremely invasive and the post-operative rehabilitation is over a period of months with restriction to weight bearing activities. The ability to expand cells *in vitro* is an advantage over the mosaicplasty method (Polster and Recht, 2005).

Matrix-induced Autologous Chondrocyte Implantation, MACI is an improved version of the ACI procedure and developed in order to avoid donor-site morbidity (Gibson *et al.*, 2006). In this technique, the chondrocytes are expanded in the same way as ACI, however, the cells are seeded onto a I/III collagen matrix membrane. In ACI the cells are injected and it is thought that the cells will be a more evenly distributed when seeded onto a matrix (Gibson *et al.*, 2006). The chondrocytes maintain their phenotype and remain viable within the collagen matrix (Zheng *et al.*, 2004). The matrix is positioned into the defect and secured with fibrin (Gibson *et al.*, 2006).

Osteotomy (bone cutting) is a procedure in which the knee joint is realigned due to advanced disease or mechanical overload (Ge *et al.*, 2006; Malviya *et al.*, 2006). The load is distributed to the undamaged areas of cartilage in order to reduce the load applied on the most severely damaged areas (Malviya *et al.*, 2006). Cartilage in the offloaded area begins to repair but produces fibrocartilage (Malviya *et al.*, 2006). Over time the individual experiences pain again and exhibits signs of disease progression (Buckwalter and Makin, 1997), due to the degeneration of the fibrocartilage (Malviya *et al.*, 2006).

Paste Grafting requires the removal of healthy cartilage which is ground into a paste and is replaced back into the defect of the patient. This technique is not particularly popular due to certain areas of the knee being hard to reach arthroscopically, such as the posterior femoral and posterior tibial regions. There are also no available instruments to graft patellar lesions (Stone *et al.*, 2006).

Tissue Engineering of cartilage requires healthy tissue to be removed and the cells extracted from this to be expanded *in vitro*. The cells are seeded on to scaffolds (i.e. synthetic natural scaffolds, acellular animal/human scaffolds) and cultured for a period of time in order for the cells to produce matrix and eventually form tissue, before being placed into the defect area of the joint. However, this technique poses several problems; scaffold detachment, synovitis, arthofibrosis, and cell death if perfusion of the new tissue is not permitted. This area is under extensive investigation and is a possible future treatment (Ge *et al.*, 2006).

Unicondylar arthroplasty (uni-compartmental arthroplasty) uses a prosthesis to surface a single part of a joint i.e. the medial or lateral side of the tibia or femur in order to regain joint mechanics. This method has advantages over total joint replacements in that less bone is removed and the procedure is less invasive (Carlsson *et al.*, 2006). As a single part of the joint is artificial this gives rise to a bearing surface and thus, wear of the material is initiated potentially leading to osteolysis, loosening and bone loss (Springer *et al.*, 2006).

Hemiarthroplasty removes one part of the joint i.e. the femoral head in the hip joint, and replaces it with an artificial head (metal or ceramic prosthesis) but leaves the opposing counterface in its natural state. Like uniarthroplasty, this procedure does not remove a large amount of bone from the joint. Patients that do not qualify for osteotomy or

uniarthroplasty (i.e. obese patients) or are too young and agile for total joint replacments, tend to be considered for hemiarthroplastic surgery (Springer *et al.*, 2006).

Total Joint Replacement (TJR) replaces both sides of the joint with an artificial prosthesis. In the knee, the condyles of the femur and the tibial plateau are removed and replaced with prostheses. The prostheses are designed with the same shape of the knee joint, the femoral prosthesis has naturally shaped condyles, while the tibial prosthesis has a stem and is shaped like the natural tibial plateau. These are implanted into the femur and tibia to recreate the knee joint. In the hip, the acetabular cup and femoral head are removed and replaced with prostheses. These prostheses have been designed with the same shape as the native acetabular cup and femoral head in order to rebuild the hip joint.

This technique has several disadvantages; the main ones involve generation of wear particles and aseptic loosening. Wear particle generation is associated with load and friction exerted on implantable materials, more commonly with biomaterials inserted in articulating areas. This includes total joint replacement prostheses and other materials implanted for surface defects, i.e. cartilage surface deformations. Aseptic loosening applies to a series of cellular and chemical events that occur post-surgery, that is, this phenomenon is not caused by infection. This has been shown by many investigators; as the development and improvement of methods such as cell staining, immunocytochemistry, biochemical and molecular biological techniques in recent years, has given great insight into the involvement of various cell types, mediators and enzymes, without signs of infection (Bellemans *et al.*, 2005; Malviya *et al.*, 2006).

Currently, there is extensive literature concerning both metal and polyethylene wear debris. Surprisingly, the literature severely lacks information relating to wear particles derived from more recently employed biomaterials such as hydrogels and other cartilage substitution materials. Therefore, there is a general deficiency of knowledge in this area which necessitates further investigation.

Currently, the National Institute for Health and Clinical Excellence (NICE) have given full guidance for arthroscopic debridement, mosaicplasty and total joint replacements (mini-incision surgery for total knee replacement and minimally invasive total hip replacement) to be performed by the NHS. Microfracture is not considered as a Standard clinical

procedure because there is a lack of efficacy and safety information. Autologous chondrocyte implantation is not recommended by NICE for treatment of articular cartilage defects except in clinical studies. In NICE guidelines, all other procedures mentioned above were not cited.

1.12 Novel Therapies for Cartilage Substitution

This review focuses on elastomeric polymers and hydrogels as cartilage substitution biomaterials. The hard polymers include polyurethane and the hydrogels include polyvinyl alcohol (PVA). It is important to note that limited information is available on these materials; not all of these materials have been used clinically as cartilage substitution biomaterials as yet.

1.12.1 Polyurethanes (PU)

PU has been used in clinical applications and has been found to have extremely good mechanical properties (Santerre *et al.*, 2005). In a polar environment PU can be manufactured to expose the hard segment at the interface or expose the soft segments in a non-polar environment (Santerre *et al.*, 2005). PU is a polymer (Figure 1.17) consisting of three parts; a hard segment, a soft segment and a chain extender. The soft segment (polyol) is an oligomeric macromonomer which includes a chain that has a hydroxyl terminal (Santerre *et al.*, 2005). The chain extender has a small hydroxyl or amine group. The third part is a low molecular weight molecule, diisocyanate, and can interact with either the soft segment or the chain extender. When the chain extender and the diisocyanate interact they form the 'hard segment' of the molecule (Santerre *et al.*, 2005). The ratio of hard and soft segments alters the composition of the polymer and this gives rise to many different forms of PU, however, the rate of degradation is determined by the ratio of soft and hard segments (Santerre *et al.*, 2005). Polyurethanes are cured during their production forming crosslinks, therefore the process can determine the level of crosslinking. The hard segment is essentially embedded in a soft flexible matrix and is an elastomer. At increased temperatures the soft segment flows but when cooled the material returns to demonstrate elastomeric properties.

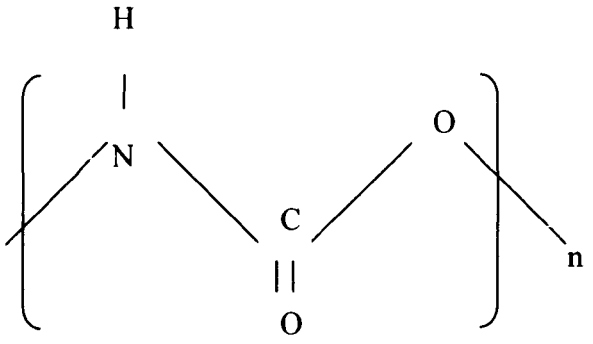

Figure 1.17 Generic structure of polyurethane

PUs are long chain polymers with side groups attached to the long backbone, which is composed of $NHCO^2$ groups (carbamate groups). PUs contain a diisocyanate (OCN-R-NCO; hard segment), which reacts with a chain extender and a diol, or polyol (HO-R-OH; soft segment), leaving an active alcohol group (OH) at one side of the molecule and a reactive isocyanate (NCO) at the other. These compounds are then free to react with other active groups, such as ester groups. Common isocyanates include toluene diisocyanate (TDI) and methylene diphenyl diisocyante (MDI); these aromatic compounds are responsible for the chain stiffness due to the presence of benzene rings. Generally, MDIs are highly active and produce PUs with better physical properties. MDIs also crystallises in the solid, whereas TDIs do not. Crystallisation occurs with increasing symmetry of the isocyanate, thus increasing the physical properties of the PU i.e. phase separation, modulus, hardness and abrasion resistance. In contrast, aliphatic isocyantes such as hexamethylene diisocyanate and methylene bis (p-cyclohexyl isocyanate (H_{12}MDI) produce less stiff chains with a low melting point giving rise to low elastic, soft polyurethanes. However, aliphatic isocyanates are extremely light stable an advantage over MDIs, and are more hydrolytically and thermally resistant (Lamba *et al.*, 1998).

Polyols possess high molecular weights and are available in a range of viscosities; these include polyether polyols and polyester polyols. Polyesters and polyethers are more commonly used and are low in molecular weight (400-5000), though polycarbonates are also utilised. Polyethers are highly viscous thereby producing hydrolytically stable polyurethanes with excellent tensile, abrasion, and flexing properties. In contrast, polyesters are prone to cleavage at the ester links making them hydrolytically unstable; however, they are mechanically superior to polyethers. With increasing molecular weight of the polyol, the glass temperature falls while the tensile properties increase. Chain

extenders such as hydroxyl amines, glycols or diamines also have low MWs but are used to increase the MW of the hard segment (Lamba *et al.*, 1998).

Chain extenders can affect the soft and hard segments by altering the modulus of the PU. The choice of chain extender can also influence the mechanical properties, for example aromatic extenders synthesise harder polyurethanes than aliphatic extenders. Crystallisation is also an important factor as it provides greater physical properties, while the number of carbons in the chain extender can determine the degree of crystallisation. The most frequently used chain extenders are 1, 4-butanediol, ethylene diamine, ethylene glycol and hexanediol, which are primarily used to lengthen the hard segment and thus, increase the molecular weight (Lamba *et al.*, 1998).

1.12.2 Hydrogels

Hydrogels can be natural (collagen, chitosan) or synthetic polymers such as polyvinyl alcohol [PVA] (Cheung *et al.*, 2007). PVA hydrogels are known for their excellent mechanical properties, good biocompatibility, chemical stability and superior hydrophilicity. These hydrogels are composed of strong hydrogen bonds resulting in inadequate lubricating properties (Zheng *et al.*, 2008). The insufficient lubrication of PVA hydrogels can be improved by the addition of other compounds e.g. hydrogels such as polyvinyl pyrrolidone (PVP), are soluble in water and have good biocompatibility (Zheng *et al.*, 2008).

These materials are extremely hydrophilic and can be crosslinked to provide extra stability (Hoffman, 2002). PVA hydrogels have weak mechanical properties and, so are crosslinked to improve their stability. Different methods are used to crosslink hydrogels ranging from formaldehyde to gamma irradiation. However, chemical crosslinking tends to lead to toxicity and, therefore is unsuitable for biomedical applications. The preferred technique for crosslinking is the freeze/thaw method; freezing at -20°C and thawing at room temperature. Repeated cycles of freezing and thawing of PVA hydrogels, increases the degree of crystallinity and thus improves the mechanical properties. The degree of crystallinity, process time, molecular weight and PVA concentration can all be manipulated to determine the properties of the final hydrogel (Pilaszkiewicz *et al.*, 2005). Addition of other molecules such as polyvinyl pyrrolidone (PVP) can also be used to improve the mechanical properties of these gels. Due to their hydrated composition these materials

have been likened to native articular cartilage [AC] (Cheung *et al.*, 2007). Hydrogels pose a number of advantages, which include physical properties (similar to AC), good biocompatibility and good transport systems for nutrients and waste products (Fray *et* al., 2007). These materials are capable of swelling in the presence of water and can maintain large quantities of fluid (Rosiak, *et al.*, 1999; Darwis *et al.*, 2002; Hoffman, 2002). Hydrogels swell until equilibrium is achieved, which can be up to thousands of times their dry weight (Rosiak, *et al.*, 1999; Hoffman, 2002). The structure of the hydrogels is very important and conveys their ability to hold such large quantities of fluid - it is this property that maintains their three dimensional structure (Hoffman, 2002).

Water molecules bind to hydrophilic domains (primary bound water, via ionic or H-bonding) within these structures, which expand the three dimensional shape to expose hydrophobic sites (Rosiak, *et al.*, 1999; Hoffman, 2002). The hydrophobic domains within hydrogels also attract water molecules to bind (hydrophobic interactions) within the structure – secondary bound water (Rosiak, *et al.*, 1999; Hoffman, 2002). The term 'total bound water' refers to combined binding of both primary and secondary bound water (Rosiak, *et al.*, 1999; Hoffman, 2002). Additional water can still infiltrate these three dimensional structures even after all possible binding sites have been accommodated (Rosiak, *et al.*, 1999). This is because hydrogels expand and create voids within the structure. Water ('free' or 'bulk' water) enters the voids until equilibrium is achieved (Rosiak, *et al.*, 1999).

Hydrogels are currently being utilised for biomedical (such as spinal implants; Prosthetic Disc Nucleus, Aquarelle and NeuDisc, for detailed reviews, see Carl *et al.*, 2004; Goins *et al.*, 2005) and pharmacological applications. They have also been used in various applications from scaffolds in cartilage replacement to reconstruction. These materials are ideal drug delivery systems because they do not dissolve in water due to their hydrophilic nature. Their hydrophilicity however, can be altered by incorporating different degrees of crosslinking of various chemical bonds (such as hydrogen bonding and ionic interaction), and this in turn determines their rate of degradation. Hydrogels are very compliant and are able to 'remember' their original shape. This property is therefore useful and hydrogels are now being considered for cartilage substitution biomaterials. These materials have only recently been investigated for use as cartilage substitution biomaterials hence information

regarding their frictional and wear properties is limited (Rosiak, *et al.*, 1999; Hoffman, 2002).

Hydrogel mixes are common and one of the most studied is the PVA/PVP blend. PVA hydrogels are of research interest because of their excellent hydrophilic, biocompatible and mechanical properties. The lubrication properties of PVA hydrogels are poor due to their chemistry; however, the addition of PVP greatly improves this property. PVP also has excellent biocompatible properties, it is soluble in water and its active surface provides this material with lubrication properties (Zheng *et al.*, 2008).

1.13 Overview

This literature review has discussed the components of human articular cartilage (AC) and their importance to the function of the joint. The components contribute to the tissues stiffness, friction, lubrication and wear. The destruction or loss of any one component can lead to disastrous events resulting in cartilage loss which can lead to degenerative diseases. The onset of inflammation can enhance the destruction of cartilage and the underlying bone. The cell types involved in the process of inflammation can contribute to implant loosening and the release of cytokines from these cells can also contribute to further tissue destruction. Therefore, a balance between destructive, regulatory and inhibitory cytokines is required to reduce the inflammatory process. It is important to understand friction and wear properties of AC and cartilage substitution biomaterials to develop novel treatments for degenerative joint diseases.

1.14 Rationale

There are increasing numbers of patients with arthritis in load bearing joints, who traditionally have been treated with major surgery and total joint replacements. Developments in advanced imaging and diagnosis, coupled with technological developments in minimally invasive and image-guided surgery are enabling early intervention and repair of small cartilage defects prior to more widespread joint degeneration. The replacement of cartilage and underlying bone defects with substitution biomaterials or scaffolds, which regenerate *in vivo*, is an alternative approach to treatment. Hydrogels have attracted substantial attention as potential cartilage substitution biomaterials as well as other applications such as drug delivery systems and tissue engineering (Hoffman, 2002). Materials such as hydrogels eliminate the requirement for

bone removal essential for total joint replacements, and studies have shown that hydrogels reduce friction and wear when exposed to natural cartilage (Northwood *et al.*, 2007). The need for alternative, less destructive treatments has arisen due to the younger age of patients that present with symptoms of these debilitating diseases. Cartilage substitution therapies are less destructive to the joint, however, the relationship between the wear particles produced and their physiological effects are unclear. Therefore, preclinical evaluation of cartilage substitution biomaterials will provide essential and much needed information.

Determining the volume of wear debris and particle characteristics that the materials produce and understanding the effects of the wear particles on macrophages could lead to the development of cartilage substitution biomaterials that release limited volumes and/or critical size wear particles and exhibit low friction rates (to both synthetic biomaterials and natural cartilage). The longevity of these devices would be extended dramatically, and this has the potential to delay the time when a total joint replacement will be required.

1.15 Aims and objectives

The aims of this thesis are to investigate friction, wear, wear debris and functional biocompatibility of natural articular cartilage (AC) and substitution biomaterials (hydrogels and polyurethanes) to be used as cartilage substitution therapies in the hip and knee.

The main objectives of this project are to:-

- Determine the friction characteristics of polyvinyl alcohol/polyvinyl pyrrolidone hydrogels, polyurethane and natural AC utilising a reciprocating pin-on-plate single station friction rig.

- Determine the wear characteristics of these materials utilising a multi-directional single station pin-on-plate wear rig, in order to produce wear particles from the natural and substitution materials which will be isolated and cultured with cells to determine biocompatibility.

- Determine volumetric wear loss by three dimensional geometrical measurements such as contacting Form Talysurf, non-contacting white light interferometry.

- Develop a method to isolate particles from natural cartilage and substitution biomaterials and characterise these particles (in terms of size and volumetric conc. as a function of particle size). Visually assess wear particles and characterise by means of field emission gun environmental scanning electron microscopy and ImagePro plus computer software.

- Establish the biological response to wear particles from cartilage substitution biomaterials at a range of volume doses i.e. $10\mu m^3$l:1 and $100\mu m^3$:1 by culturing wear particles with macrophages using an agarose gel method and assessing their biocompatibility by measuring cytokine release using enzyme-linked immunosorbent assay.

Chapter Two

Materials and Methods

2.1 Introduction

This chapter will describe the chemicals, equipment, materials and experimental procedures used throughout this thesis.

2.2 Materials

For all materials and equipment used throughout this thesis see Appendix I, Table I.i and Table I-ii, respectively for suppliers.

2.2.1 Pyrogen-free ultrapure sterile water

Pyrogen-free ultrapure water was obtained from Fresenius Kabi, Warrington, USA and stored at room temperature until required.

2.2.2 Phosphate buffered saline (PBS)

PBS was obtained from Oxoid Ltd, Hampshire, U.K. One PBS tablet was dissolved in 100 mL pyrogen-free ultrapure water (Section 2.2.1) as stated by the manufacturer and stored at room temperature until required. The solution was adjusted to pH 7.4.

2.2.3 Foetal bovine serum (FBS)

FBS (mycoplasma and virus screened) was obtained from Lonza, Basel, Switzerland. FBS was heat inactivated for 1 hour at 56°C, aliquoted and stored at -20 °C until required (thawed at 37°C).

2.2.4 Phosphate buffered saline (PBS) + 25% (v/v) foetal bovine serum (FBS) lubricant

FBS (Section 2.2.3) was added to PBS (Section 2.2.2) solution to a final concentration of 25% (v/v) just prior to use.

2.2.5 Rosslyn Park Memorial Institute 1640 medium (RPMI)

RPMI 1640 culture medium (R0883) was obtained from Sigma-Aldrich Company Ltd., Poole, Dorset, UK. The media was stored at 4°C until required.

2.2.6 Penicillin/streptomycin

Penicillin/streptomycin was obtained from Invitrogen Life Technologies Ltd., Paisley, UK. The stock concentration was 5000 U ml^{-1} of penicillin and 5000 U ml^{-1} of streptomycin which was dispensed into 5 ml aliquots and stored at -20°C until required (thawed at 37°C).

2.2.7 HEPES (N-(2-hydroxyethyl) piperazine-N'-(2-ethanesulfonic acid)

HEPES was obtained from Sigma-Aldrich Ltd., Dorset, UK. The 1 M stock solution was stored at room temperature until required.

2.2.8 Transport medium

Transport medium consisted of Rosslyn Park Memorial Institute 1640 medium (Section 2.2.5) 1640, 100 $U.ml^{-1}$ penicillin, 100 $mg.ml^{-1}$ streptomycin (Section 2.2.6) and, 20 mM HEPES (N-(2-hydroxyethyl) piperazine-N'-(2-ethanesulfonic acid) [Section 2.2.7]. The medium was stored at 4°C until required, for a maximum of one week.

2.2.9 L-Glutamine

L-Glutamine was obtained from Invitrogen Life Techonologies Ltd., Paisley, UK. The stock concentration was 200 mM ml^{-1} which was dispensed into 5 ml aliquots and stored at -20°C until required (thawed at 37°C).

2.2.10 *Culture medium*

Cell culture medium consisted of RPMI (Section 2.2.5) 1640, 10% (v/v) FBS (Section 2.2.3), 100 $U.ml^{-1}$ penicillin, 100 $mg.ml^{-1}$ streptomycin (Section 2.2.6) and 2 mM L-glutamine (Section 2.2.9). Culture medium (Section 2.2.10) was then stored at 4°C until required for a maximum of one week.

2.2.11 *Lymphoprep®*

Lymphoprep® was obtained from Nycomed UK Ltd., Birmingham, UK and stored at 4°C until required.

2.2.12 *Microbiological culture plates and broth*

Nutrient broth, heated blood agar , nutrient agar and saboraud dextrose agar were obtained from Media Laboratory, Institute of Molecular and Cell Biology, University Of Leeds, UK. All were stored at 4°C until required.

2.2.13 *Agarose gel*

Agaorse was obtained from Helena Biosciences Europe, Gateshead, UK and stired at room temperature until required. Agarose gel was prepared by adding 2% (w/v) agarose to Rosslyn Park Memorial Institute 1640 medium (Section 2.2.5), which was sterilised by autoclaving at 121°C for 20 minutes at 15 pounds per square inch (psi). The agarose gel was stored at 4°C until required. When required the agarose gel was heated in a microwave at medium power for two minutes to dissolve.

2.2.14 *Silica gel*

Silica gel (0.7 % w/v) was obtained from Merck, Darmstadt, Germany and stored at room temperature until required. Silica gel was incubated at 160°C for 1 h until a colour change was achieved from blue to brown. A blue colour indicated the silica gel was hydrated and brown indicated dehydration.

2.2.15 *Enzyme-Linked Immunosorbant Assay (ELISA) kits*

Tumour necrosis factor alpha (TNFa), interleukin-1 beta (IL-1β), interleukin-6 (IL-6), interleukin-8 (IL-8) ELISA kits were obtained from IDS, Michigan, USA. The ELISA kits were stored at 4°C until required.

2.2.15.1 Tween 20

Tween 20 was obtained from Sigma-Aldrich Company Ltd., Poole, Dorset, UK and stored in a dark container at room temperature.

2.2.15.2 Wash buffer

Wash buffer contained 0.05% (v/v) Tween 20 (Section 2.2.15.1) in phosphate buffered saline (Section 2.2.2). The solution was adjusted to pH 7.4.

2.2.15.3 Bovine serum albumin

Bovine serum albumin was obtained from Sigma-Aldrich Ltd., Dorset, UK and stored at 4°C until required.

2.2.15.4 Saturation buffer

Saturation buffer contained 5% (w/v) bovine serum albumin (Section 2.2.15.3) in phosphate buffered saline (Section 2.2.2). The solution was adjusted to pH 7.4.

2.2.15.5 Standard diluent buffer

Standard diluents buffer contained 1% (w/v) bovine serum albumin (Section 2.2.15.3) in phosphate buffered saline (Section 2.2.2). The solution was adjusted to pH 7.4.

2.2.15.6 Horse radish peroxidase-streptavidin diluent buffer

HRP-Streptavidin diluent buffer contained 0.1% (v/v) Tween 20 (Section 2.2.15.1), 1% (w/v) bovine serum albumin (Section 2.2.15.3) in phosphate buffered saline (Section 2.2.2). The solution was adjusted to pH 7.4.

2.3 Materials tested

2.3.1 Preparation of bovine femurs

Bovine femurs were obtained from John Penny & Company, Rawden, Leeds, UK. The femurs were obtained from 18 month old skeletally mature animals. Articular cartilage pins (9 mm diameter) and plates (20 mm x 25 mm) were extracted from the patellofemoral grooves of each joint. The electric drill, metal plate, screws, drill corer, holding bath and 9 mm diameter corers were manufactured in the School of Mechanical Engineering, University of Leeds, UK (Appendix I).

2.3.2 Preparation of bovine femurs

Clamps were attached to a metal plate on a table with screws at the front and the back (Figure 2.1). All pieces of equipment were manufactured in the School of Mechanical Engineering, University of Leeds, UK., unless otherwise stated (see Appendix I).

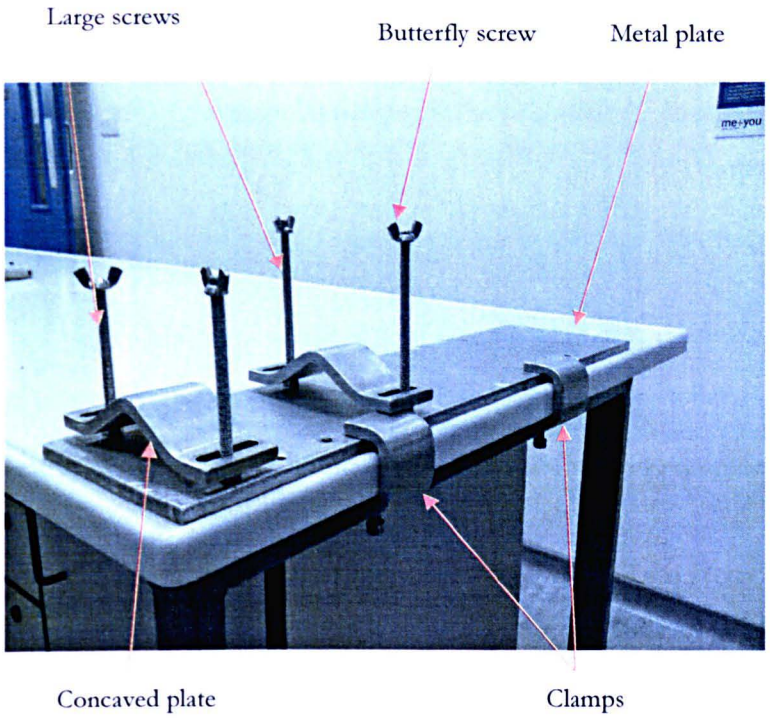

Figure 2.1 Equipment to stabilise bovine femurs

Two concave plates were placed on top of the femur and screwed into place with butterfly screws to secure the joint, ensuring the femoral condyles were positioned over the table (Figure 2.2).

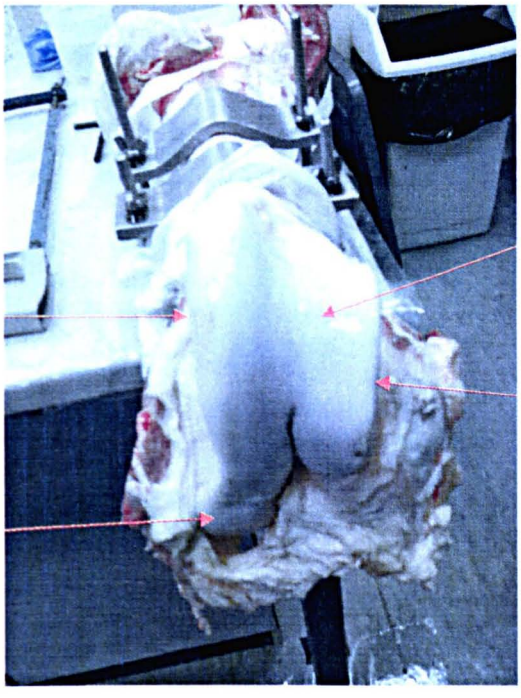

Figure 2.2 Bovine joint assembled in stabilisation equipment

All bovine femurs had previously been stripped of any excess tissue from the bone at the abattoir. Using a scalpel blade the knee joint cavity was carefully exposed, ensuring the cartilage surface was not damaged by the blade. The cartilage surface was also inspected for any other signs of damage or disease, and if found the femur was disposed of. Phosphate buffered saline (Section 2.2.2) was used to wash away traces of synovial fluid and used regularly to keep the tissue hydrated during pin and plate retrieval. All pins and plates were removed from the patella groove, as this area was large in size with flat regions. This ensured a flat counterface of the retrieved osteochondral samples.

2.3.2.1 Osteochondral pin and plate retrieval

The medial and lateral edges of the patella groove were removed using a hack saw (Figure 2.3), and sections of the cartilage tissue were marked using a scalpel blade to identify areas to extract osteochondral pins with a flat surface.

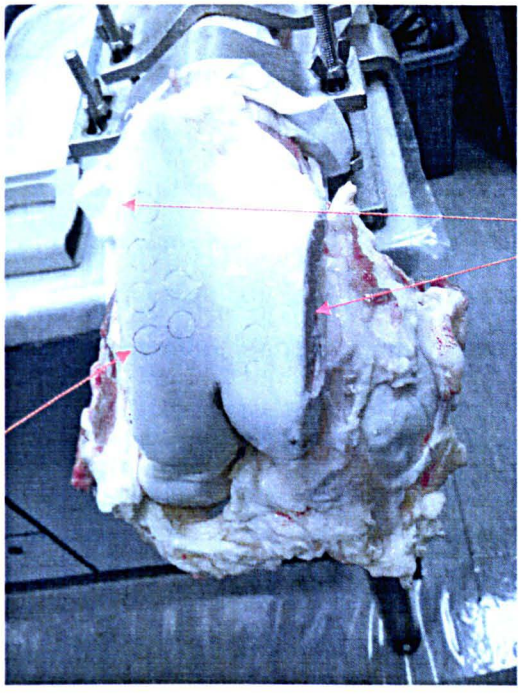

Figure 2.3 Pin sectioning in cartilage tissue

Pre-defined holes were made in the cartilage surface by pushing a 9 mm diameter corer (Figure 2.4) directly into the tissue until the subchondral bone was reached (Figure 2.3).

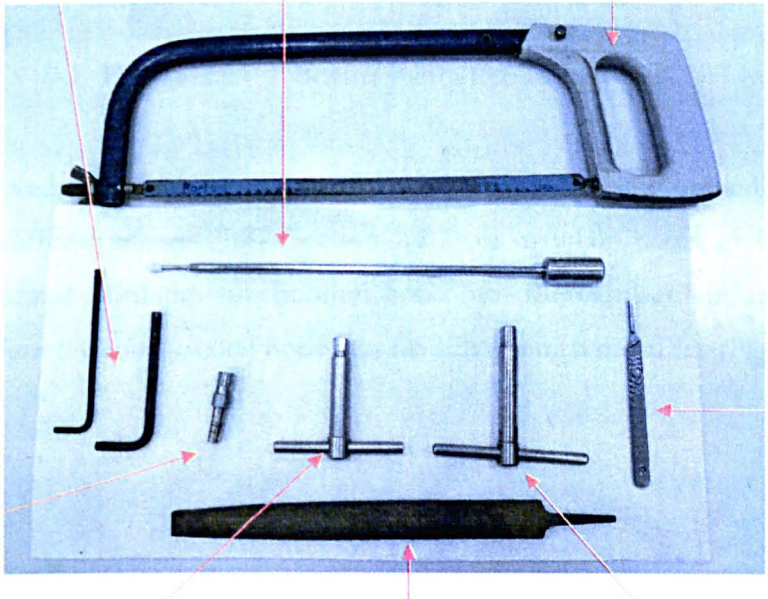

Figure 2.4 Dissection equipment

Exaggerated impressions were prepared in the cartilage surface using a 9 mm diameter serrated corer (Figure 2.4) in the pre-defined holes. This was to ensure an even cut around the circumference of the cartilage pins and prevent tissue damage due to sliding of the 9 mm drill bit (Figure 2.4) across the cartilage surface. The cartilage pin sections were drilled to approximately 10 mm in depth using the 9 mm diameter drill bit and an electric hand drill at a moderate speed to prevent tissue burning. The osteochondral pins were removed from the joint by snapping the subchondral bone using the 9 mm corer (Figure 2.5).

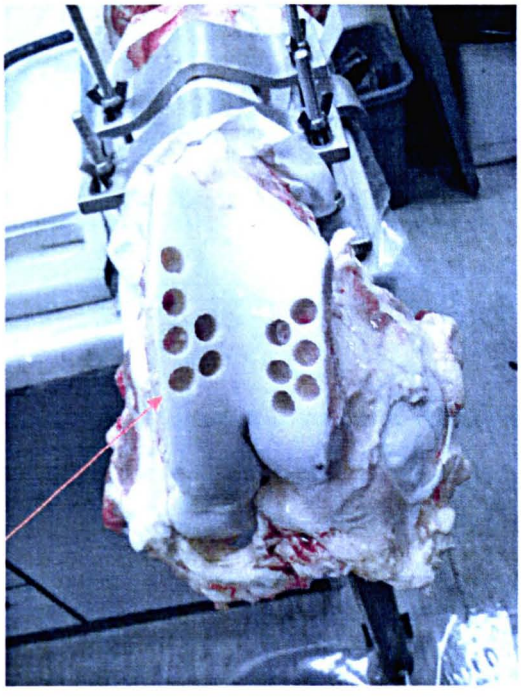

Pin retrieval

Figure 2.5 Bovine joint after pin retrieval

Pins were removed from the corer using a plunger (Figure 2.4) and immediately immersed in phosphate buffered saline [PBS] (Section 2.2.2) to maintain tissue hydration. Excess debris was removed from the subchondral bone (not the cartilage surface) of each pin (Figure 2.6) before the subchondral bone was filed flat using a metal file (Figure 2.4).

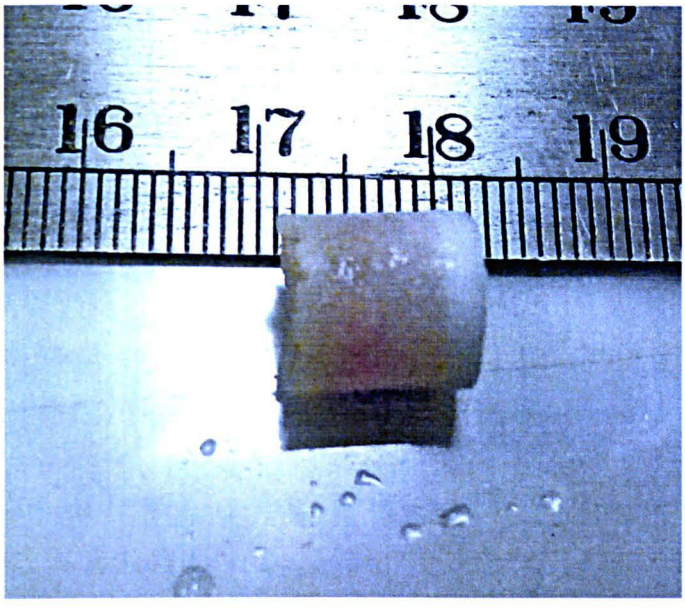

Figure 2.6 Retrieved osteochondral pin

Each pin was placed on PBS (Section 2.2.2) soaked tissue paper in separate containers before being stored at -20°C until required for testing (maximum storage was one month). A nick was made with a scalpel blade in the tissue to mark the position of the plates (approx. 25mm x 25mm) to be retrieved. The nick was used as a guide to prevent the saw from slipping and scratching the surface of the tissue. The surface of the tissue was checked to ensure it was flat before marking the positions of the plates to be cut. The joint was cut directly down the middle of the patella groove (cut 3 in Figure 2.7) using a hack saw (Figure 2.4), and then cut across the groove in several places (cut 4, 5 and 6) marking out the plates (Figure 2.7).

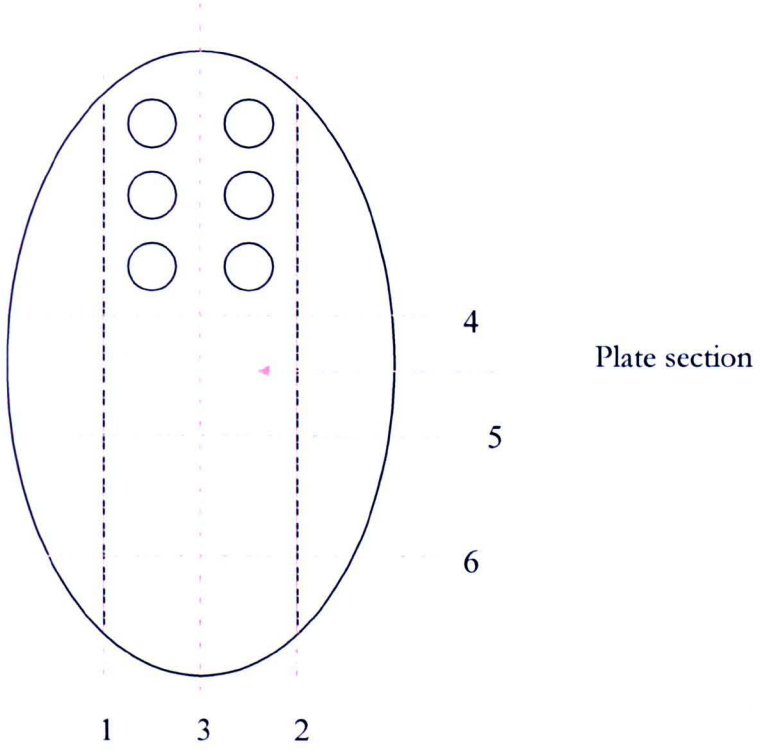

Figure 2.7 Schematic representation of a knee joint, showing the patella groove. The red dashed lines indicate the cutting of the joint with the hacksaw. Lines 1 and 2 indicate the cutting of the joint lips. Line 3 indicates cutting down the middle of the patella groove to separate the plates. Lines 4, 5 and 6 represent cutting the plate sections. The smaller circles also represent the drilling of the pin sections.

The plates were finally released from the knee joint by cutting into the subchondral bone (a depth of 10-20mm). The plates were immersed in fresh PBS (Section 2.2.2) to maintain hydration before adjusting the depth of the plates to approximately 7 mm using a hacksaw and a custom made jig (Figure 2.8).

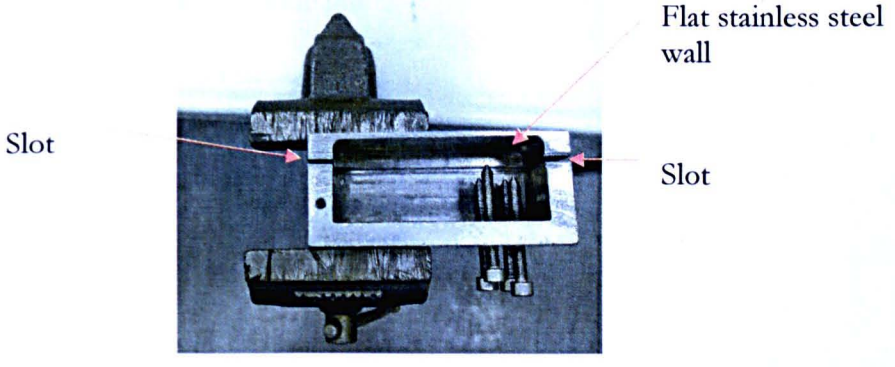

Figure 2.8 Custom made jig for adjusting the depth of articular cartilage plates

The cartilage surface of the plates was placed against the flat stainless steel wall of the jig (Figure 2.8), and secured by tightening the screws. The blade of the hacksaw was placed between the slots of the jig and the excess bone was cut.

2.3.4 Thermoset polyurethanes

The thermoset polyurethanes used throughout this thesis were Diprane D50 (53 series) and Chemtura A90 (LF blend) which were obtained from PPL Polyurethane Products Ltd., Retford, UK (see Appendix I). Diprane 53, an ester based material comprising methylene diphenol diisocyanate polyurethane had a shore hardness of D50, and Chemtura (LF blend), an ether based material comprising toluene diisocyanate polyurethane had a shore hardness of A90. Pins (Figure 2.9 A and B) were machined (in the School of Mechanical Engineering, University of Leeds, UK) from sheets to be 12 mm in diameter and 7 mm in depth with a 9 mm truncated head (Figure 2.9) and, plates were cut 87 mm x 26 mm x 7 mm (Figure 2.10). Two holes were drilled in the plates to allow them to be screwed into the bath of the friction and wear rigs (Sections 2.4.5 and 2.4.11).

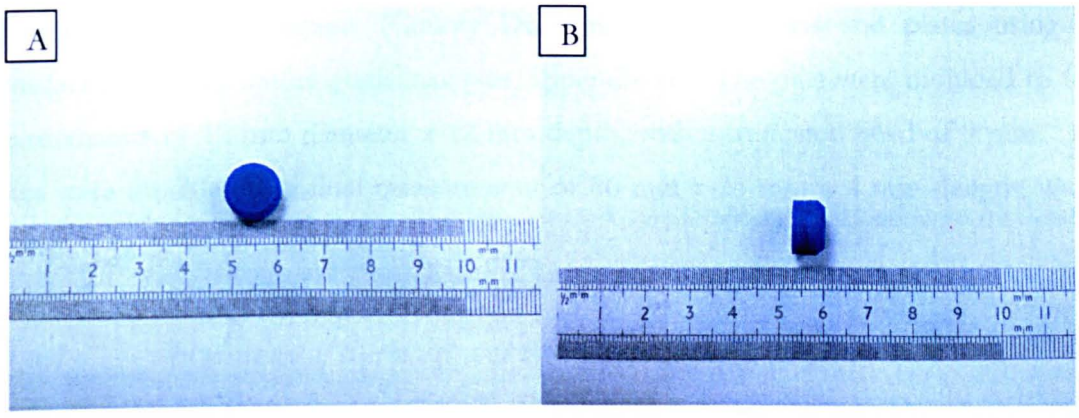

Figure 2.9 A) aerial view of a Diprane D50 (53 series) polyurethane pin and B) lateral view of a D50 Diprane 53 polyurethane pin

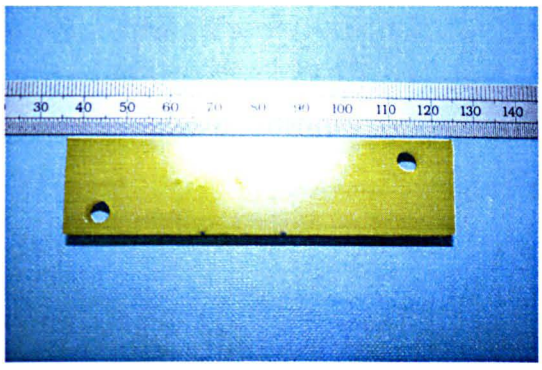

Figure 2.10 Chemtura A90 (LF Blend) polyurethane plate

2.3.5 Thermoplastic polyurethanes

Tecoflex® (obtained from Thermedics™, USA, see Appendix I) is an aliphatic polyether polyurethane and shore hardnesses of D51 and A94 were used throughout this thesis. Corethane (shore hardness D55) was obtained from Corvita Corporation, USA (see Appendix I) and is an aromatic polycarbonate polyurethane and has been researched extensively due to its excellent physical and biocompatible properties. These thermoplastic polyurethanes were injection moulded according to our own specifications by RW Injection Moulding Company (County Durham, UK) into pins and plates using the manufacturer's temperature guidelines (see Appendix II). The pins were moulded to final measurements of 12 mm diameter x 12 mm depth, with a truncated head of 9 mm. The plates were moulded to a final measurement of 86 mm x 25 mm x 4 mm (length, width, depth).

2.3.5.1 Hydration of thermoset and thermoplastic polyurethanes

Polyurethanes are hygroscopic materials in that they attract and hold water. These materials are able to absorb moisture from the environment in which they are situated i.e. fluid or air. The hygroscopic nature of these materials made it extremely difficult to gravimetrically measure (Section 2.3.5.1.1) the polyurethanes as they could only be weighed to three decimal places as opposed to six decimal places due to vast fluctuations even after exposure to an ion generator to eliminate static After the polyurethanes were soaked (minimum of 16 days) in pyrogen-free ultrapure water (Section 2.2.1) or phosphate buffered saline (Section 2.2.2) then placed in a controlled humidity room to acclimatise before being tested, they increased in weight (indicated at three decimal places). However, when the materials were acclimatised to 50°C for 4 h (in a dessicator containing silica gel

[Section 2.2.14]), a gravimetrical measurement (Section 2.3.5.1.1) to six decimal places was achieved.

The polyurethane materials were then soaked in pyrogen-free ultra pure water (Section 2.2.1) for a minimum of 16 days, washed in household detergent then placed in 70% (v/v) isopropanol (Appendix I) and sonicated (ultra sonication bath, see Appendix I) for a minimum of 10 minutes to remove any particulate debris. All polyurethane materials were stored in pyrogen-free ultrapure water (Section 2.2.1) until required for wear testing. After testing, the pins were left for 4 h at 50°C (in a dessicator containing silica gel [Section 2.2.14]) to acclimatise before being gravimetrically measured three times as described in (Section 2.3.5.1.1).

2.3.5.1.1 Mettler Toledo Analytical Balance

All samples were measured gravimetrically using a six-figure Mettler Toledo analytical balance (AT21 comparator, European Instruments, Oxford, UK) to an accuracy of ±5 μg after stabilisation in a temperature and humidity controlled environment in the School of Mechanical Engineering, University of Leeds, UK. Each pin and plate was gravimetrically measured three times to obtain an average weight.

2.3.5.2 Sterilisation of thermoset and thermoplastic polyurethanes

Both thermoset (Diprane 50D polyurethane and Chemtura 90A, [Section 2.3.4]) and thermoplastic (Corethane 55D, Tecoflex 51D and Tecoflex 94A, [Section 2.3.5]) polyurethanes were soaked in pyrogen-free ultrapure water (Section 2.2.1) and washed as described in Section 2.3.5.1. The pins used to generate aseptic wear particles (Chapter 6) were immersed and agitated in sodium hypochlorite (concentrated bleach) solution for 10 minutes before being placed in nutrient broth (Section 2.2.12) using aseptic technique (i.e. flaming a platinum loop and the top of the nutrient broth container) for a minimum of 48 h to determine sterility. Pins that were not completely sterile were not used in tests and therefore, the above process was repeated until sterilisation was achieved. After testing the pins were washed in sterile pyrogen-free ultra pure water (Section 2.2.1), acclimatised and gravimetrically weighed (Sections 2.3.5.1 and 2.3.5.1.1).

2.3.6 Ultra high molecular weight polyethylene

Ultra high molecular weight polyethylene GUR1120 was obtained from Hoechst, Germany (Appendix I). The ram extruded bar stock was machined into pins (12 mm in depth x 12

mm in diameter with a truncated head of 8 mm, Figure 2.11) in the School of Mechanical Engineering, University of Leeds, UK.

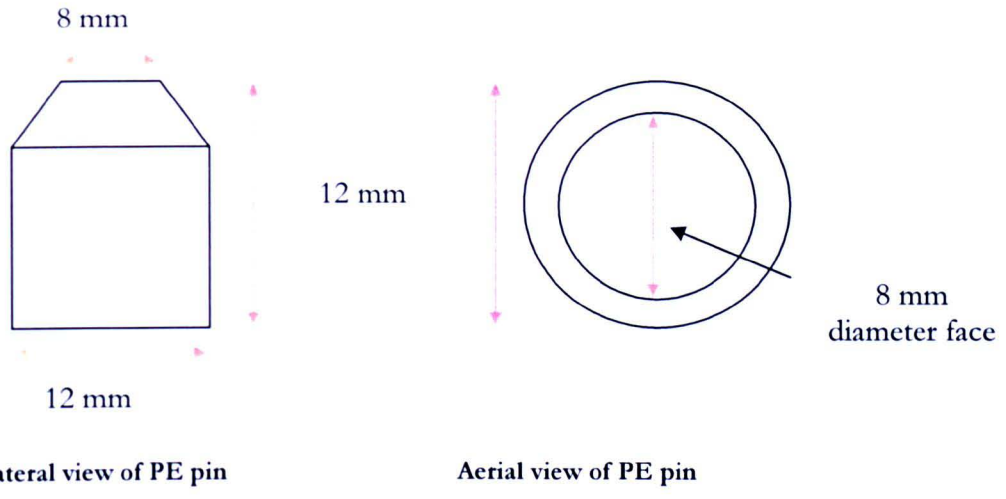

Figure 2.11 Schematics showing the dimensions of PE pins

2.3.6.1 Hydration of ultra high molecular weight polyethylene

The polyethylene pins were immersed in pyrogen-free ultrapure water (Section 2.2.1) for a minimum of 14 days then acclimatised at room temperature for 48 h in a controlled humidity environment followed by gravimetrical measurement (Section 2.3.5.1.1). Polymer pins were eliminated of static particles using an ion generator before being measured gravimetrically three times as described in Section 2.3.5.1.1 (unless otherwise stated). The pins were pre-washed with household detergent to remove any surface particles, placed in 70% (v/v) isopropanol and sonicated (ultra sonication bath, see Appendix I) for a minimum of 10 min. All pins were stored in pyrogen-free ultrapure water (Section 2.2.1) until required for testing. After testing the pins were washed with household detergent and left for 48 h in a controlled humidity environment (at room temperature) to acclimatise (at room temperature) before being gravimetrically measured three times as described in (Section 2.3.5.1.1).

2.3.6.2 Sterilisation of ultra high molecular weight polyethylene

Polyethylene pins were soaked in pyrogen-free ultrapure water (Section 2.2.1) and washed as described in Section 2.3.5.1. The pins used to generate aseptic wear particles (Chapter 6) were immersed and agitated in sodium hypochlorite (concentrated bleach) solution for 10 minutes before being placed in nutrient broth (Section 2.2.12) using aseptic technique (i.e.

flaming a platinum loop and the top of the nutrient broth container) for a minimum of 48 h to determine sterility. Pins that were not completely sterile were not used in tests and therefore, the above process was repeated until sterilisation was achieved. After testing the pins were washed in sterile pyrogen-free ultra pure water (Section 2.2.1), acclimatised (at room temperature) and gravimetrically weighed (Section 2.3.5.1.1).

2.3.7 Polyvinyl alcohol/polyvinyl pyrrolidone (PVA/PVP) hydrogels

The PVA/PVP hydrogels (H1B, H2B and H2A) used throughout this thesis provided by Dr. Wojciech Swieszkowski from Warsaw University, Poland (Appendix 1). The pins were produced to measure 12 mm in depth x 9 mm in diameter (Figure 2.12 A and B).

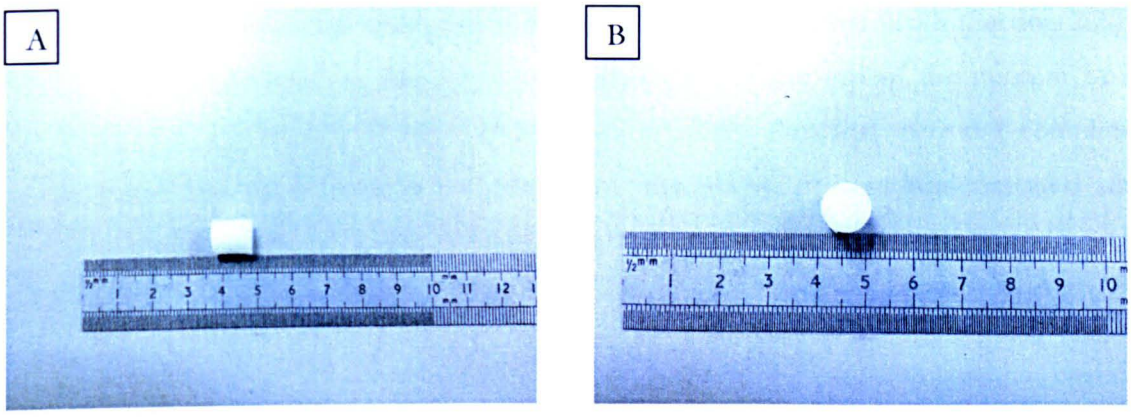

Figure 2.12 A) aerial view of a PVA/PVP hydrogel pin and, B) lateral view of a PVA/PVP hydrogel pin

The PVA/PVP hydrogels were a blend of polyvinyl alcohol (PVA) and polyvinyl pyrrolidone (PVP). H1B contained 25% (w/v) PVA with 7% (v/v) gluconic acid, H2B contained 28% (w/v) PVA and 7% (v/v) gluconic acid and, H2A contained 28% (w/v) PVA. Before receiving the PVA/PVP hydrogels, they were subjected to freeze/thaw cycles to increase crosslinking within the hydrogel network (Hickey and Peppas, 1995). This required the PVA/PVP hydrogels to be repeatedly frozen at -20°C and thawed at room temperature. The incorporation of gluconic acid was to increase internal porosity.

2.3.7.1 Hydration of polyvinyl alcohol/polyvinyl pyrrolidone (PVA/PVP) hydrogels

The hydrogel pins were washed in household detergent and acclimatised in a controlled humidity environment room for 48 h (room temperature) before being gravimetrically

measured three times as described in Section 2.3.5.1.1. The PVA/PVP hydrogels were then placed in pyrogen-free ultrapure water (Section 2.2.1) for a minimum of four days before testing. After testing the PVA/PVP hydrogels were washed with household detergent and left for 48 h at room temperature to acclimatise before being gravimetrically measured (Section 2.3.5.1.1).

2.3.7.2 Sterilisation of polyvinyl alcohol/polyvinyl pyrrolidone (PVA/PVP) hydrogels

PVA/PVP hydrogel pins were washed as described in Sections 2.3.5.1 then soaked in sterile pyrogen-free ultra pure water (Section 2.2.1) in sterile containers. The pins used to generate aseptic wear particles (Chapter 6) were not immersed in sodium hypochlorite (to prevent damage to the materials), but were placed in sterile nutrient broth (Section 2.2.12) using aseptic technique (i.e. flaming a platinum loop and the top of the nutrient broth container) for a minimum of 48 h to determine sterility. Pins that were not completely sterile were not used in tests and therefore, the above process was repeated until sterilisation was achieved. After testing the pins were washed in pyrogen-free ultra pure water (Section 2.2.1), acclimatised (at room temperature) and gravimetrically measured (Sections 2.3.5.1.1).

2.3.9 Stainless steel plates

Medical grade 316L stainless steel was used throughout this thesis, as it does not corrode when autoclaved. All plate specimens were marked with an identification code. The plates were prepared by the School of Mechanical Engineering (University of Leeds, UK) with a roughness between Ra = 0.07 μm - 0.08 μm (rough plates) or a smooth finish between Ra = 0.01 μm - 0.03 μm. Ra is internationally recognised and the most common roughness parameter used. The dimensions of the stainless steel plates can be seen in Figure 4.13.

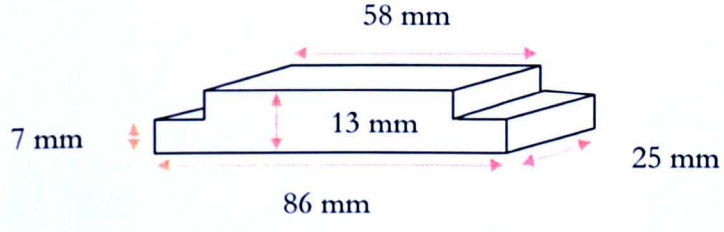

Figure 2.13 Dimensions of the stainless steel plates

2.3.9.1 Stainless steel pins

Medical grade 316 stainless steel pins were polished to a Ra of 0.01 - 0.03 μm (Section 2.2.3), and were machined to final dimensions of 12 mm high x 9 mm diameter. Two pin geometries were produced, one with a radius head (100°) and one with a 9 mm truncated head.

2.3.9.2 Cleaning of stainless steel pins and plates

Before testing the pins and plates were washed in household detergent (Appendix I) to remove any debris, then soaked in Trigene for a minimum of 10 minutes, rinsed in deionised water and sonicated (ultra sonication bath, see Appendix I) for 30 min in 70% (v/v) isopropanol to further remove any remaining debris. Plates were dried and wrapped in soft tissue paper before and after testing to prevent scratching to the bearing surface.

2.4 Experimental methods

2.4.1 Shore hardness measurements - Durometer

A durometer D7900 (obtained from Zwick, Ulm, Germany) was used to measure the resistance to indentation in terms of Shore hardness (see Chapter 3) of the polyvinyl alcohol/polyvinyl pyrrolidone (PVA/PVP) hydrogels (Section 2.37), thermoset (Section 2.34) and thermoplastic (Section 2.35) polyurethane pins. Pins (n=3 for each material) were placed on the stage of the durometer after revealing the indenter by moving the presser foot (Figure 2.14). The PVA/PVP hydrogel pins were placed inside a collet before each measurement to obtain an accurate reading; due to the softness of these materials deformation occurred under the pressure of the indenter without use of a collet. The handle was held down to allow the indenter to contact the surface of the pins (Figure 2.14).

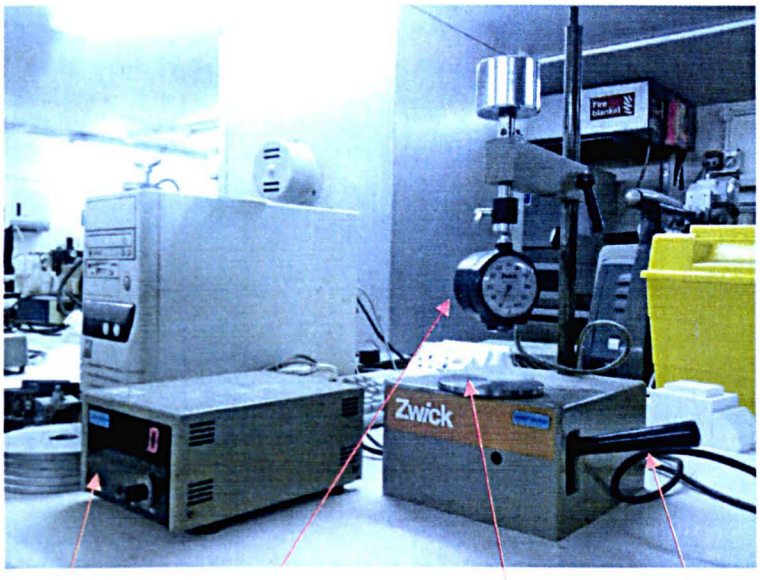

Figure 2.14 Durometer with digital reader

Upon contact, an alarm sounded to indicate the measurement had been taken, which gave a reading on the digital display (Figure 2.14), and this was recorded. The indicator hand on the dial indicator (Figure 2.15) also measured the hardness, however, the digital reader (obtained from Zwick, Ulm, Germany) displayed readings to one decimal place and, thus presented a precise measurement.

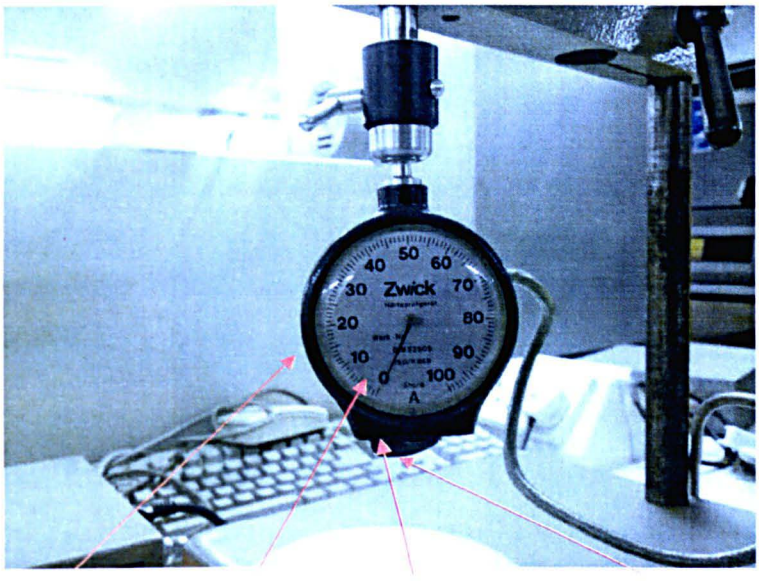

Figure 2.15 Shore A dial indicator

The shore hardness of the softer materials (PVA/PVP hydrogels, Tecoflex 94A and Chemtura 90A) was measured with a Shore A dial indicator (Figure 2.15). A Shore D dial indicator (contained a stiffer spring) was used to measure the harder materials (Corethane 55D, Diprane 50D and Tecoflex 51D).

2.4.2 Tensile measurements - Instron

Tensile properties of the thermoset (Section 2.34) and thermoplastic (Section 2.35) polyurethanes (Chapter 3) were assessed using an Instron tensile tester 3365, which was obtained from Instron Service UK, High Wycombe, UK (Appendix I). The data was stored in Bluehill software (Instron Service UK, High Wycombe, UK). The Instron (Figure 2.16) consisted of a crosshead in which a 5 kN (kilo Newton) load cell was attached and, connected to a pneumatic clamp.

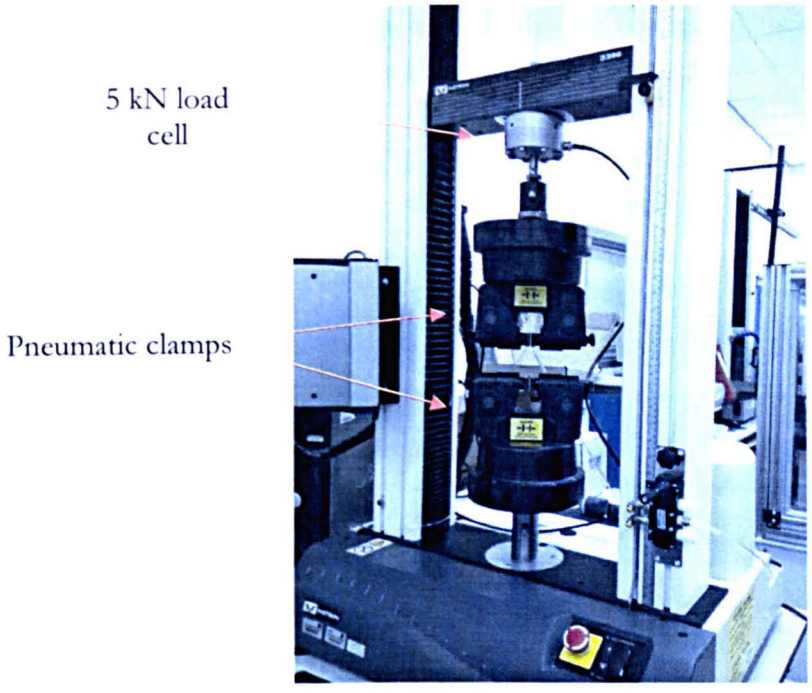

Figure 2.16 Instron assembled with pneumatic clamps

Each thermoset (Section 2.34) and thermoplastic polyurethane plate (Section 2.3.5) was secured by the pneumatic clamp on the crosshead and the pneumatic clamp connected to the base of the Instron (Figure 3.4). Emory paper was placed between the clamps and the polyurethane plate to prevent slipping of the materials. An air supply was fixed to both clamps in order to hold and release the polyurethane plates and, was operated by a foot pedal. The gauge length and load were balanced by resetting to zero using Bluehill software before the commencement of each test. A 500 $mm.min^{-1}$ crosshead speed was applied to the plates until failure was achieved. Data were stored on an attached PC.

2.4.3 Material deformation measurements - Indentation rig

Material deformation (Forster and Fisher, 1996) was investigated using an in-house custom built indentation rig (School of Mechanical Engineering, University of Leeds, UK), which utilised Labview 9 software (National Instruments Ltd., Berkshire, UK) [Appendix I].

The indentation rig consisted of three parts; the main shaft, load cell and small shaft (Figure 2.17). Deformation of articular cartilage (Section 2.3.1), polyvinyl alcohol/polyvinyl pyrrolidone (PVA/PVP) hydrogel (Section 2.37), thermoset (Section 2.34) and thermoplastic polyurethane (Section 2.35) pins was determined using the

indentation rig. The bottom of the main shaft was connected to a 3 mm diameter flat indenter in order to measure deformation of each pin sample.

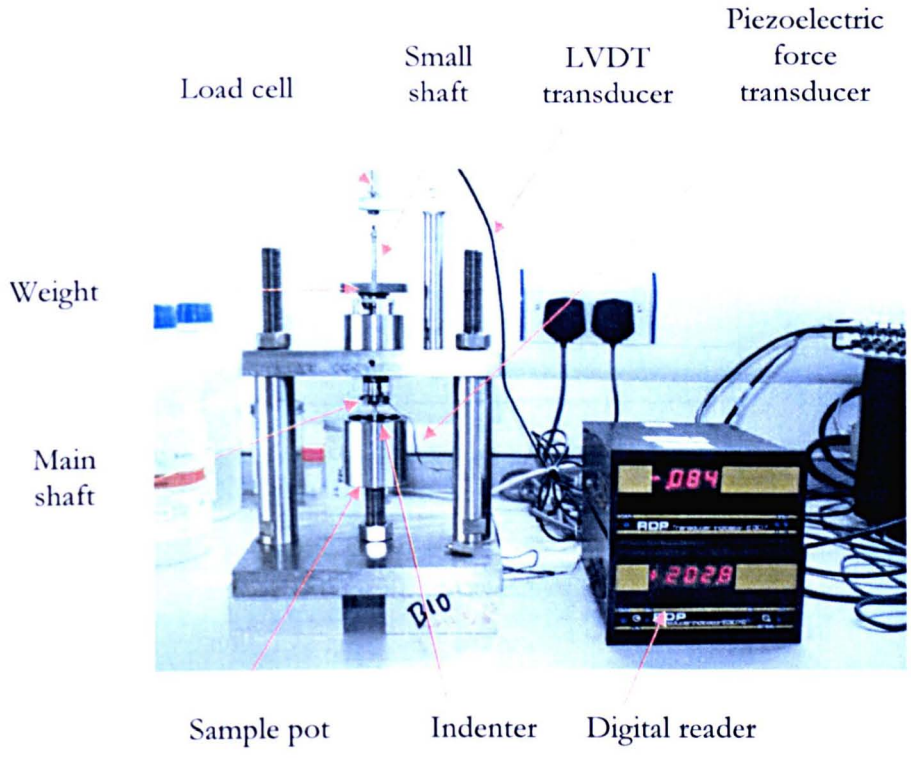

Figure 2.17 Assembled indention rig

Connected to the top of the main shaft was a small shaft, which extended to a load cell. Attached to the load cell was an LVDT (Linear Variable Differential Transformer) transducer (RDP D5-200H; 2 mV/V/0.001" sensitivity), which recorded the displacement of the whole shaft. A piezoelectric force transducer was connected to the main shaft and, data from both transducers were converted from analogue to digital measurements at a sampling frequency of 5 Hertz (Hz), when measuring deformation. The data was automatically saved to a PC via Labview 9 software (Appendix I). Measurements were recorded every 0.2 seconds and the deformation was calculated for the time points stated in Table 2.1.

Table 2.1 Time at which deformation was calculated for each material

Time (Minutes)
0
0.08
0.1
0.2
0.4
0.5
1
2
4
5
10 – 60 (measurement every 10 minutes)

The sample holder was screwed into the base of the indentation rig to the required height and tightened with a locking nut. A pin sample was then placed into a holding pot which contained a collet to secure the pin, and then slotted into a hole at the base of the sample holder. The sample holder was filled with phosphate buffered saline (Section 2.2.2) until the surface of the pin was immersed in the fluid in order to prevent dehydration. It was not possible to apply a contact pressure (to represent physiological loading) of 2.5 MPa to the polyurethane and osteochondral pins (Section 2.3.1) and, 1.26 MPa to the PVA/PVP hydrogels due to the limited space for weight attachment on the small shaft. Therefore, 10% (upper limit of the machine) of the above stated contact pressures (0.25 MPa and 0.126 MPa) was used during deformation measurements and, this was performed by attaching lead weights to the small shaft of the indentation rig. The loads applied to the pin samples generated by the main shaft (52 grams), load cell (15 g) and small shaft (3 g) were taken into account when attaching the lead weights to the rig. A latch behind the main shaft was released to allow the indenter to contact the pin sample surface.

2.4.4 Contact angle measurements - Microdrop analyser

A microdrop analyser with Build 306 software was obtained from First Ten Angstroms, Portsmouth, VA, USA (Appenix I). The microdrop analyser (Appendix I) was used to determine the contact angles (Θ) of the thermoset (Section 2.34) and thermoplastic

polyurethanes (Section 2.35). The system was primed with deionised water three times to flush out any possible contaminants to prevent interference with the results. A dry polyurethane plate was placed on the stage and the stage was adjusted to be in view of the attached video camera (Figure 2.18).

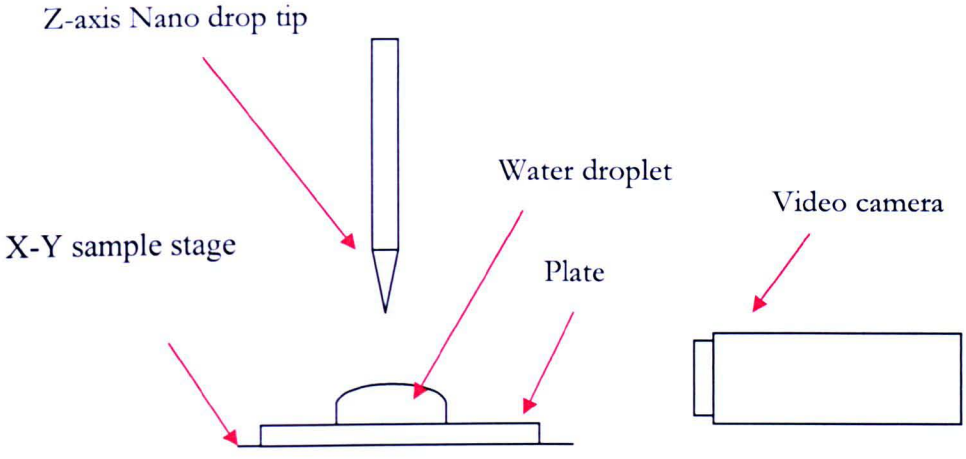

Figure 2.18 Microdrop analyser

The image was transmitted to an attached computer and the tip was lowered towards the plate. A drop of deionised water was expelled on to the surface of the plate, which was recorded as the static contact angle. A spherical fit was fitted to the water droplet on the screen with the baseline at the interface of the water droplet and the plate (Figure 2.19). Data was analysed using Build 306 software (Appendix I).

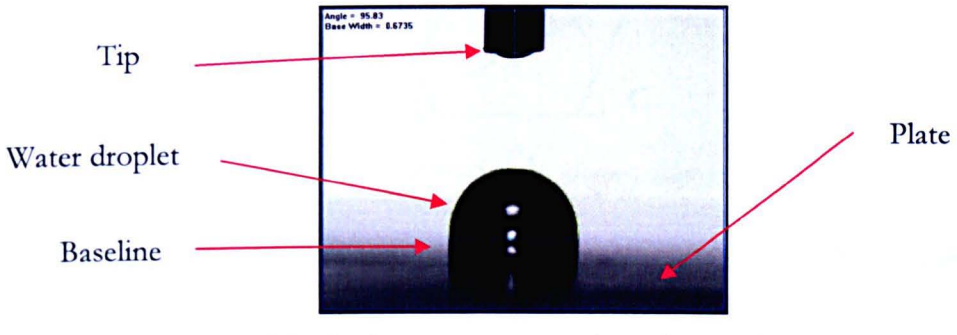

Figure 2.19 A drop of deionised water on a polyurethane plate with the baseline identified at the interface.

The tip was lowered to contact the water droplet and on commencement of withdrawing the water via the tip, a measurement was taken when the baseline started to reduce and the droplet began to recede across the surface; dynamic receding angle. In contrast, as the

water droplet was expelled and the baseline of the droplet proceeded to advance across the surface, a measurement was taken and recorded the dynamic advancing angle. Static and dynamic measurements were repeated six times along the length of each plate.

The geometric measurement of the static and dynamic angles considered phase boundaries; where the solid, liquid and gas phase intersect. Materials with a Θ equal to zero implied that the material was completely hydrophilic due to complete wetting of the surface; however, a Θ equal to 90° suggested the material was hydrophobic (Figure 2.20 A).

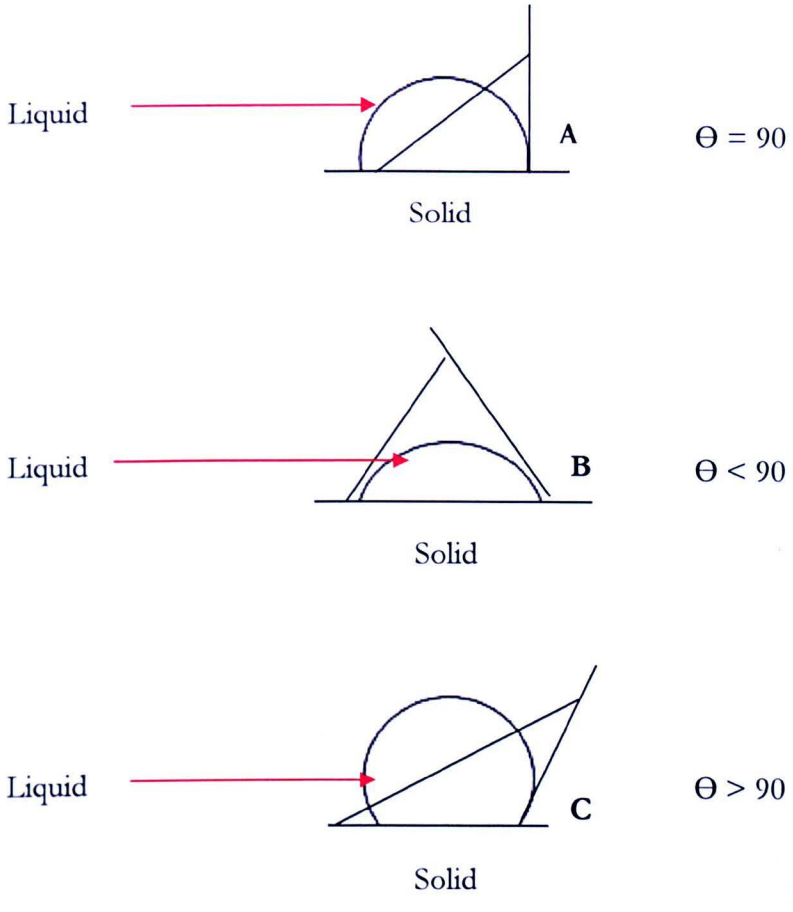

Figure 2.20 Schematic showing contact angles of a drop of liquid at 90° (A), less than 90° (B) and, over 90° (C).

In contrast a material with Θ < 90° (Figure 2.20 B), was hydrophilic due to the liquid advancing tangentially on the surface. However, a Θ > 90° (Figure 2.20 C), indicating a material was hydrophobic because the liquid did not easily advance tangentially across the surface.

2.4.5 *Wear particle generation*

2.4.5.1 *Six station multidirectional pin-on-plate wear rig*

A six-station multidirectional wear pin-on-plate rig (and related pieces, Figure 2.21) was custom built in the School of Mechanical Engineering, University of Leeds, UK (Appendix I) and was used to generate wear particles (Galvin *et* al., 2005) and to determine the recovery rates of polyurethanes (Sections 2.3.4 and 2.3.5), polyvinyl alcohol/polyvinyl pyrrolidone (PVA/PVP) hydrogels (Section 2.37) and articular cartilage (Section 2.3.1) pins after deformation. All equipment used in the set up of the six station wear rig are shown in Figure 2.21.

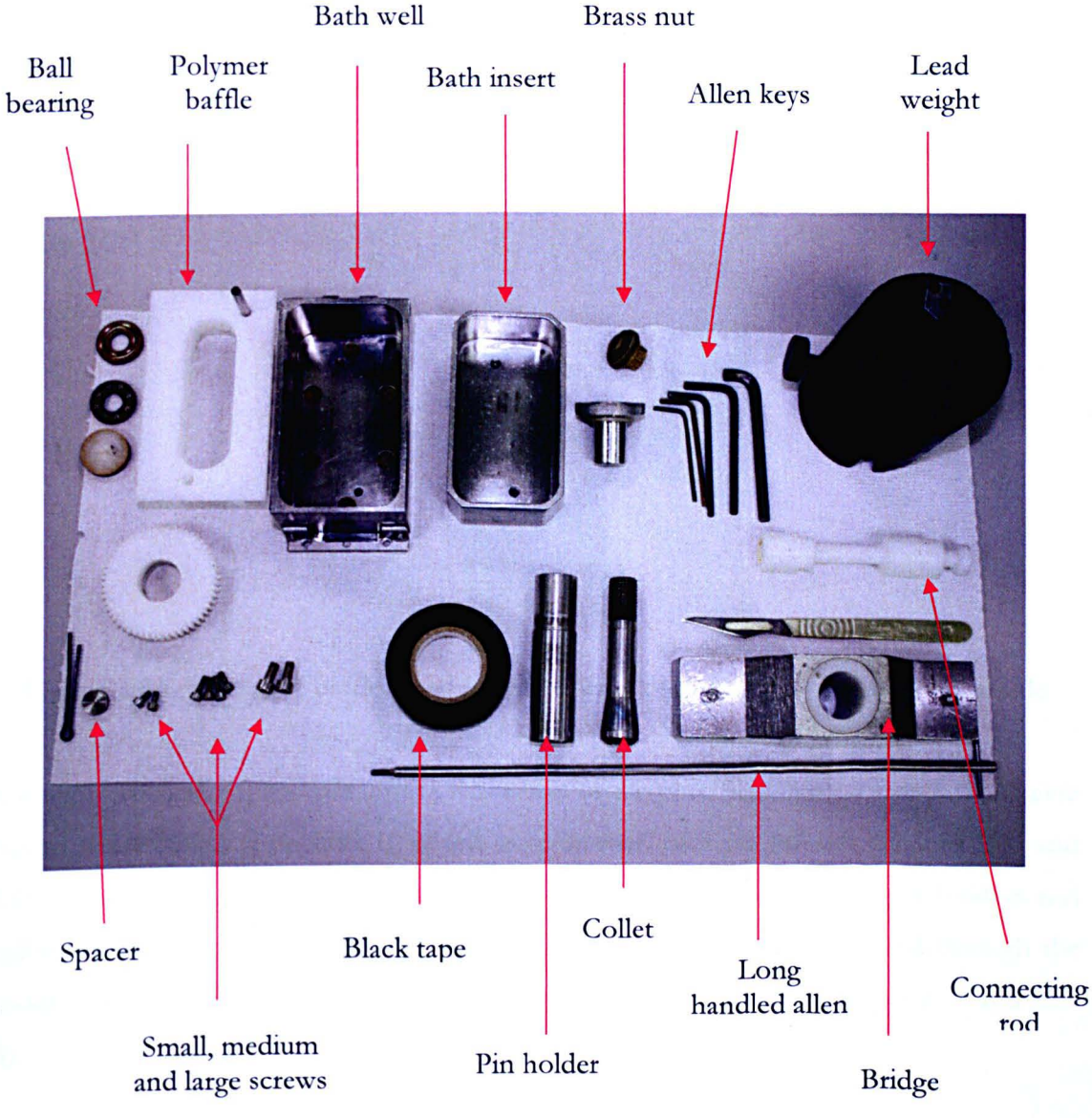

Figure 2.21 Equipment pieces for 6-station pin-on-plate multidirectional wear rig

Bath inserts (Appendix I) were placed into bath wells (Figure 2.22) before screwing stainless steel plates into place.

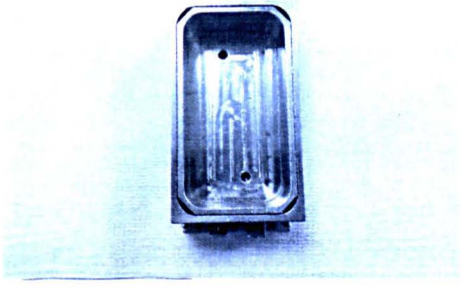

Figure 2.22 Bath insert and bath well

Polymer baffles (Appendix I) were placed inside the bath inserts and black tape was used to seal round the edges to prevent leaking (Figure 2.23). Stainless steel toothed racks (Appendix I) were then attached to one side of the bath wells with small screws (Figure 2.21). Brass nuts were screwed into the back of the bath wells to secure the bath inserts (Figure 2.21).

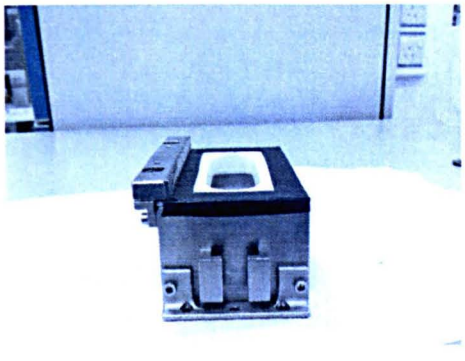

Figure 2.23 Polymer baffle taped into bath with a toothed rack secured on the side

A spacer (Appendix I) and pin (after preparation of the pins, Sections 2.3.2 to 2.3.7.2) were placed inside collets (Appendix I), which were inserted into pin holders (Figures 2.21 and 2.24 A). Polymer gear wheels (Appendix I) were then pushed onto the pin holders and tightened with an allen key, the pin holders (Appendix I) were then pushed through the middle section of the bridge before being tightened with a large nut (Figures 2.21 and 2.24 B).

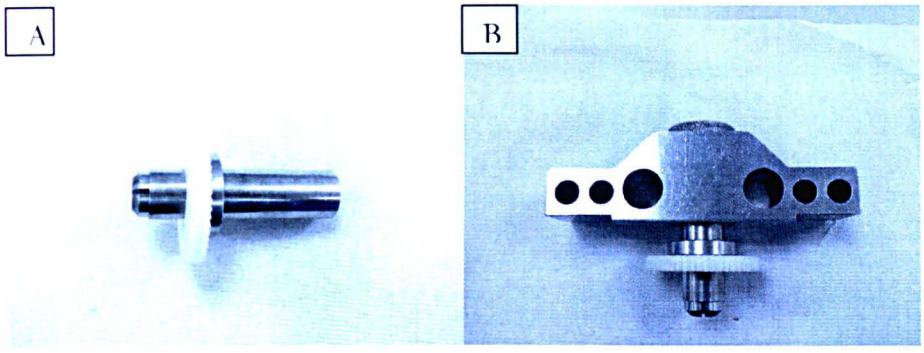

Figure 2.24 A) Polymer gear wheel slotted through a pin holder and B) A pin holder with polymer gear wheel slotted through a bridge

The bridges (Appendix I) were slotted into the corresponding stations of the rig so that the pin faces were in contact with the plates and the teeth on the polymer gear wheels (Appendix I) fitted between those of the stainless steel toothed racks (Appendix I), which were attached to the baths (Figure 2.25).

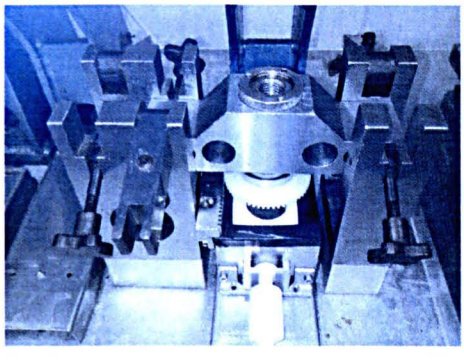

Figure 2.25 Bath and pin holder in corresponding station

Connecting rods (Appendix I) were attached from the scotch yoke mechanism to the bath to ensure reciprocal motion and ball bearings (Figure 2.21) were placed on top of the threaded nuts of the pin holder and the load arms connected (Figure 2.26).

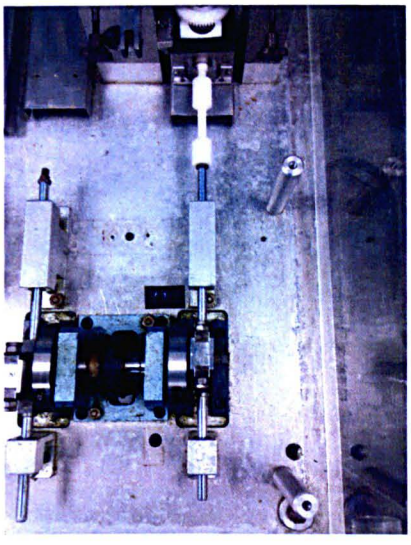

Figure 2.26 Connecting rods attached to the scotch yoke mechanism and the bath

Each bath well (Appendix I) was then placed onto the corresponding tray of the six-station wear rig (Figure 2.27) and secured with medium sized screws using a long handled allen key (Figure 2.21).

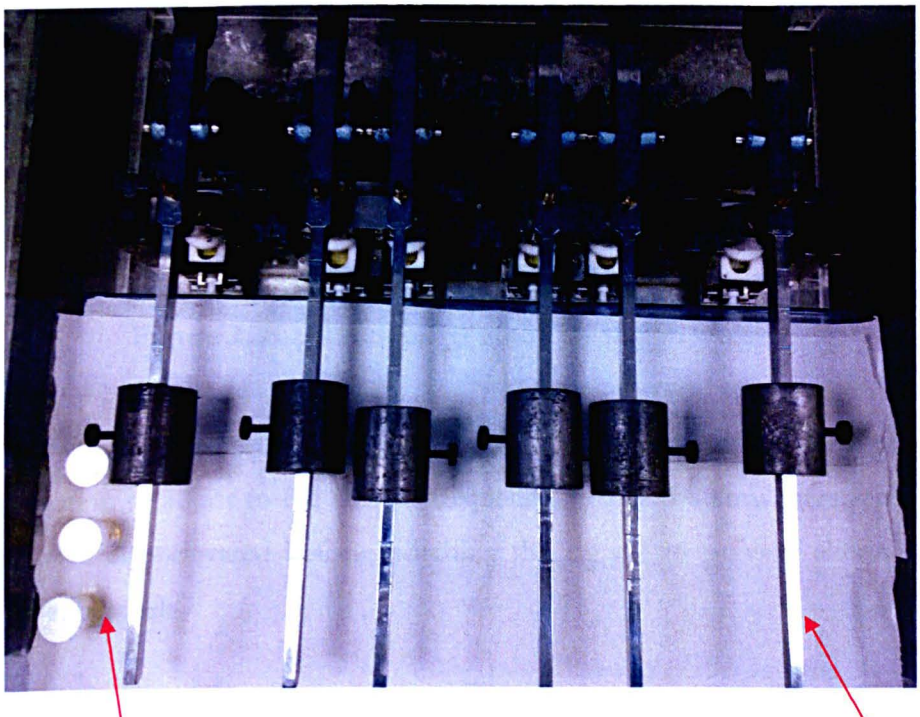

Figure 2.27 Six station multidirectional wear rig

Phosphate buffered saline [PBS] (Section 2.2.2) lubricant (40 ml) was aliquoted into each bath and the pin holders (Appendix I) lifted to allow lubricant between the pins and plates. Control pins for each material were placed in pots with the same volume of lubricant for the test period. Load arms (Appendix I) were attached to each station and lead weights (Appendix I) were connected to each arm, the resulting loads, number of cycles and contact pressures are highlighted in Sections 2.4.5.1.2 and 2.4.5.1.3. Each wear test was set to operate at 1 Hz (Hertz) using the dial on the front panel and the number of cycles were recorded (Figure 2.28).

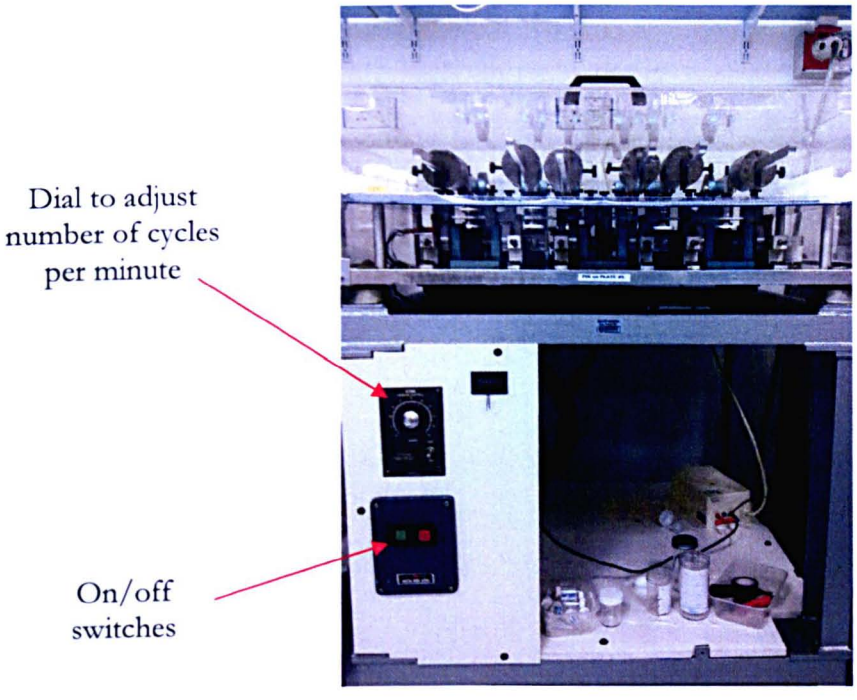

Figure 2.28 Front panel of the six station wear rig

The load arms (Appendix I) were elevated when the rig was switched on to allow the reciprocal motion to adjust to the correct frequency, before the arms were replaced. The load arms were also elevated before switching the rig off to prevent altering the wear factors of the materials.

2.4.5.1.1 Calibration

A calibrated load cell was placed under the loading point and lead weights were place on the loading arm at the relevant load. The lead weight (Appendix I) was adjusted along the arm until the required load was reached and the position was recorded. The number of

cycles were counted and adjusted to 60 cycles per minute corresponding to a frequency of 1 Hz, which represented the speed of walking.

2.4.5.1.2 Generation of wear particles

The six station pin-on-plate multidirectional wear rig (Appendix I) was assembled as described in Chapter 2 (Section 2.4.5). To determine the wear of the materials a load of 160 N [Newton] (thermoplastic polyurethanes, Section 2.35) and 80 N (polyvinyl alcohol/polyvinyl pyrrolidone hydrogels, Section 2.37) was used and the stroke length was set to 28 mm at a frequency of 1 Hertz in polyvinyl alcohol/polyvinyl pyrrolidone (Section 2.2.2) lubricant. Four pins of each material were used in the tests; two pins of each material were reciprocated against smooth stainless steel plates (Ra = 0.01 – 0.03 μm), and two were reciprocated against rough stainless steel plates (Ra = 0.07 - 0.09 μm). Therefore, each pin was reciprocated twice against the relevant stainless steel plate to obtain four lubricant samples. It was thought that the PVA/PVP hydrogels and the thermoplastic polyurethane (Section 2.35) pins would wear quickly, so the tests were not run overnight. Due to the measurement difficulties (Sections 2.3.5.1) and time constraints the pins were acclimatised (Sections 2.3.5.1, 2.3.6.1, 2.3.7.1) and gravimetrically measured (Section 2.3.5.1.1) at the end of the total test period. Control pins for each material were also used and the uptake of water was accounted for by subtracting the weight changes of the control pins from the test pins. The PVA/PVP hydrogel tests were stopped early because they had worn quickly.

The particles generated against both smooth and rough stainless steel plates were filtered (a volume of 1 mm^3; see Sections 2.4.7 and 2.4.8 for calculations) from the phosphate buffered saline lubricant through a series of filters (10 μm, 1 μm and 0.015 μm pore-sized filters; Appendix I for supplier) described in Section 2.4.6 to isolate the particles. A volume of 1 mm^3 of particles (Sections 2.47 and 2.48 for calculations) of the same lubricants were spiked with 25% foetal bovine serum (FBS, Section 2.2.3) in order to determine whether the same volume of particles could be retrieved after an alkaline digestion (Section 2.4.6) and filtered through a series of 10 μm, 1 μm and 0.015 μm pore-sized filters (Appendix I). Digestion was not required for the particles in PBS lubricant as no serum. The particles generated in PBS were compared to those spiked with serum in terms of size and area (Sections 2.4.9.2 and 2.4.9.3) in order to determine whether the digestion protocol had any adverse effects on the generated particles.

2.4.5.1.3 Deformation and recovery tests

A six station multidirectional pin-on-plate wear rig (Appendix I) was assembled as described Section 2.4.5.1, however, the rig was not switched on as the pins (osteochondral, polyvinyl alcohol/polyvinyl pyrrolidone hydrogels, thermoset and thermoplastic) were only subjected to loading for 1 hour (h), in order to deform the materials, and from this the recovery rates were determined. A 160 N load was applied to the osteochondral pins, thermoset and thermoplastic polyurethane pins, resulting in a contact pressure of 2.5 MPa. As the polyvinyl alcohol/polyvinyl pyrrolidone hydrogel pins were much softer, an 80 N load was applied giving a contact pressure of 1.26 MPa. Three pins of each material were used in the tests and phosphate buffered saline (Section 2.2.2) was used as a lubricant to keep the samples hydrated. The heights of all pins were measured using a TRIMOS vernier scale (Section 2.4.5.1.3.1) before and after testing. The height of the articular cartilage on the osteochondral pins was also measured before and after testing using a Nikon profile projector (Section 2.4.5.1.3.2).

2.4.5.1.3.1 Height measurements – TRIMOS vernier scale

A TRIMOS height vernier scale with a resolution of 1 μm attached to a 10 μm resolution dial indicator was obtained from Draper Expert, Middlesex, UK. Before loading the pins in the six station multidirectional pin-on-plate wear rig (Section 2.4.5.1), the depth of all pins was measured using the TRIMOS height vernier scale (Figure 2.29).

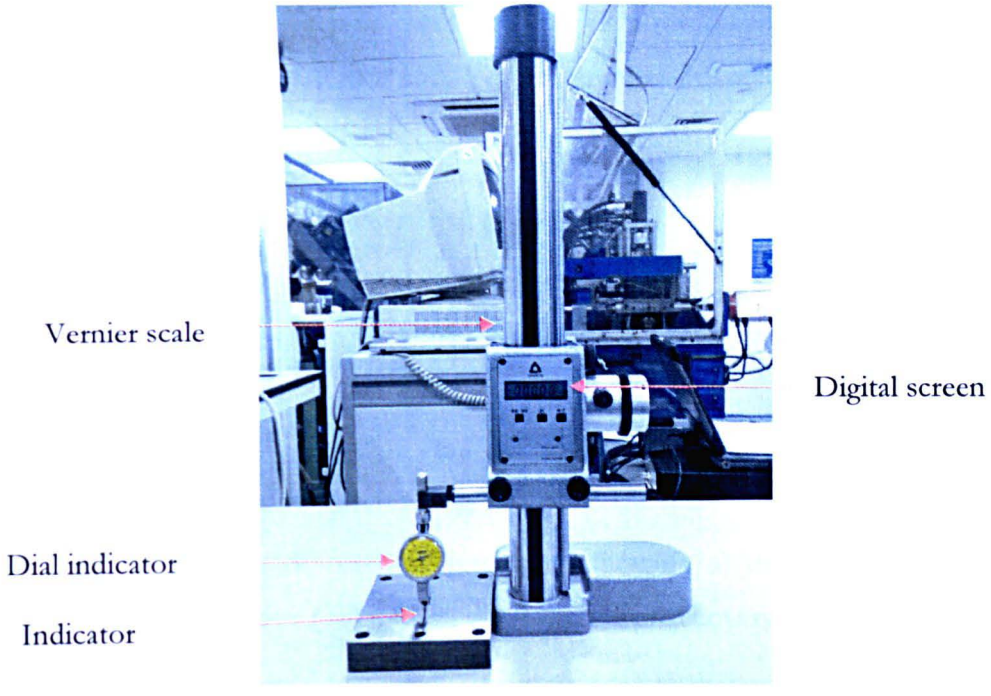

Figure 2.29 TRIMOS vernier scale with attached dial indicator

Each pin was placed on a metal block and the dial indictor was lowered so that the indicator (Figure 2.29) contacted the pin surface. Three measurements were performed round the circumference of each pin and readings were recorded on the digital screen (Figure 2.29). Between each pin measurement the level on the dial indicator was lowered to contact the metal block so the device could be reset to zero. The pins were loaded for 1 h as described in Section 4.3.2.

After loading the depth of each pin was measured (n=3) at regular intervals between time zero and 60 minutes. During measurements all pins were hydrated in phosphate buffered saline (Section 2.2.2), to prevent dehydration. The percentage reduction, percentage recovery and percentage permanent deformation (Katta *et* al., 2009), were calculated from the measurements (equations 2.1 – 2.3).

$$\text{Percentage reduction} = \frac{Tb - Ta}{Tb} \times 100 \qquad (2.1)$$

$$\text{Percentage recovery} = \frac{Teq}{Tb} \times 100 \qquad (2.2)$$

$$\text{Percentage permanent deformation} = \frac{Tb - (Ta + Teq)}{Tb} \times 100 \qquad (2.3)$$

Where, *Ta* represented the measurement immediately after loading (time zero), *Tb* was the measurement taken before the test and, *Teq* represented the recovery equilibrium (Figure 2.30).

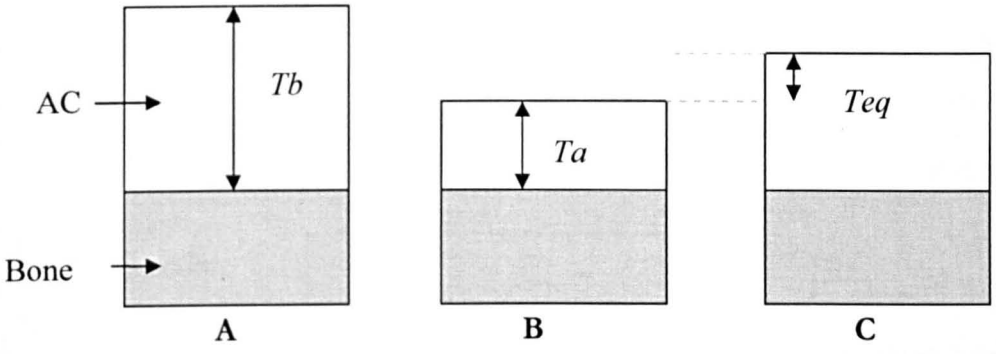

Figure 2.30 Schematic of osteochondral pins showing a) depth before test (*Tb*), b) depth immediately after test (*Ta*) and, c) depth at which recovery had reached equilibrium (*Teq*).

The total depth of the osteochondral pins (Section 2.3.1) was measured using a vernier scale, however, the depth of the articular cartilage was measured using a Nikon profile projector (see Section 4.3.4) to calculate (Equations 2.1 to 2.3) cartilage depth only. Ta, Tb and Teq (Equations 2.1 to 2.3) were calculated from the complete heights of all other pins.

2.4.5.1.3.2 Height measurements - Nikon Profile Projector

A Nikon profile projector (model V -16D) was obtained from Nippon Kogaku K. K., Tokyo, Japan (Appendix I). The osteochondral pins were placed on the stage of the Nikon profile projector and a white light source was applied to the top of the osteochondral pin. This cast a silhouette on the screen and the focus was adjusted using the focus handle (Figure 2.31). The tidemark separating the cartilage and underlying bone could be clearly visualised.

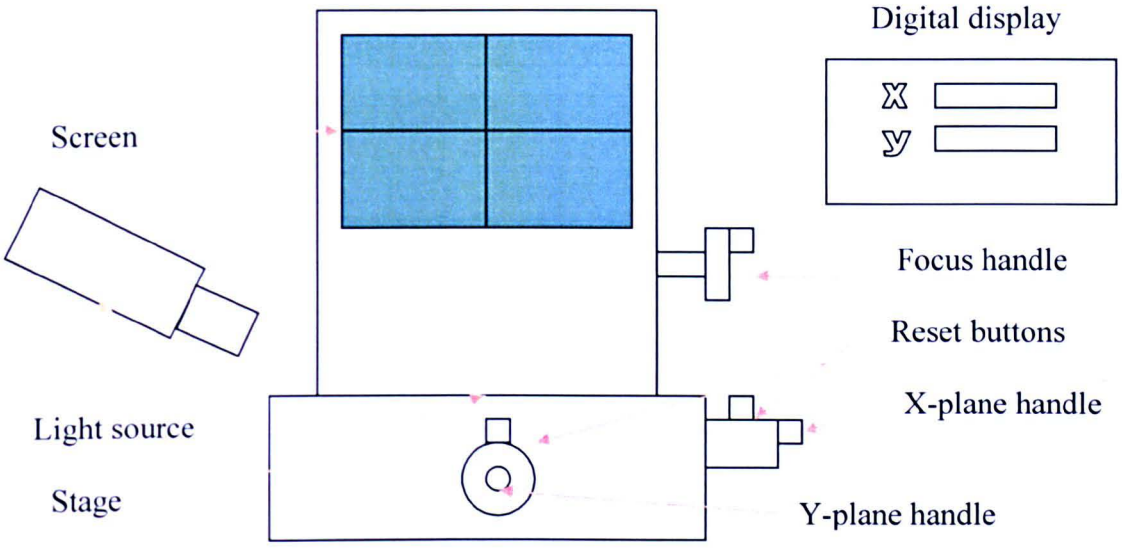

Figure 2.31 Diagram representing the Nikon Profile Projector.

The bottom of the tidemark was aligned along the centre x-axis line shown on the screen (Figure 2.32). The reset button on the x-axis handle was reset so that the reading on the digital display was zero.

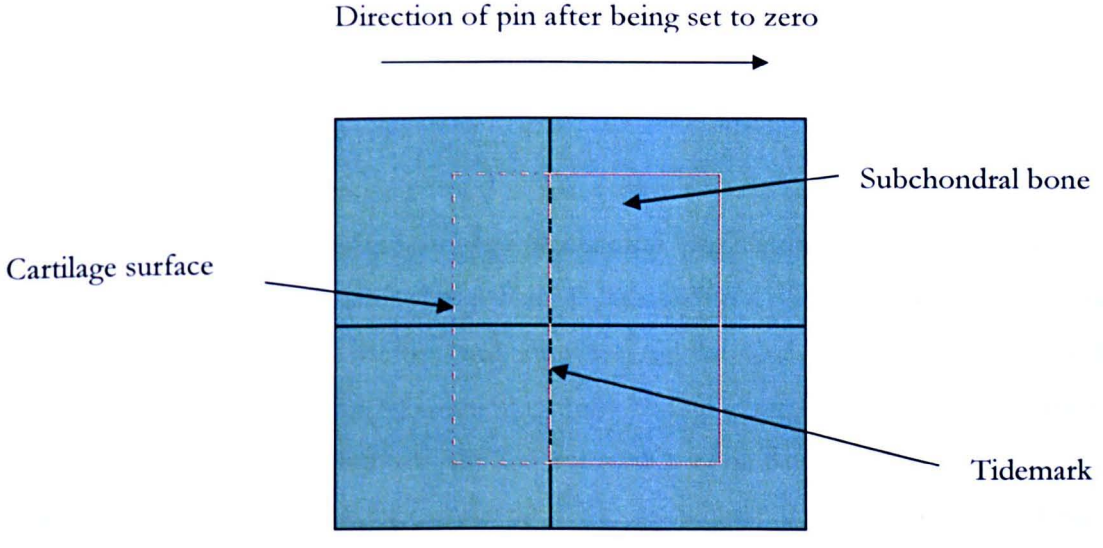

Figure 2.32 Representation of the profile projector screen. The tidemark was positioned to the x-axis centre line.

Using the x-axis handle, the osteochondral pins were positioned so that the surface of the cartilage surface was level with the x-axis line (Figure 2.33).

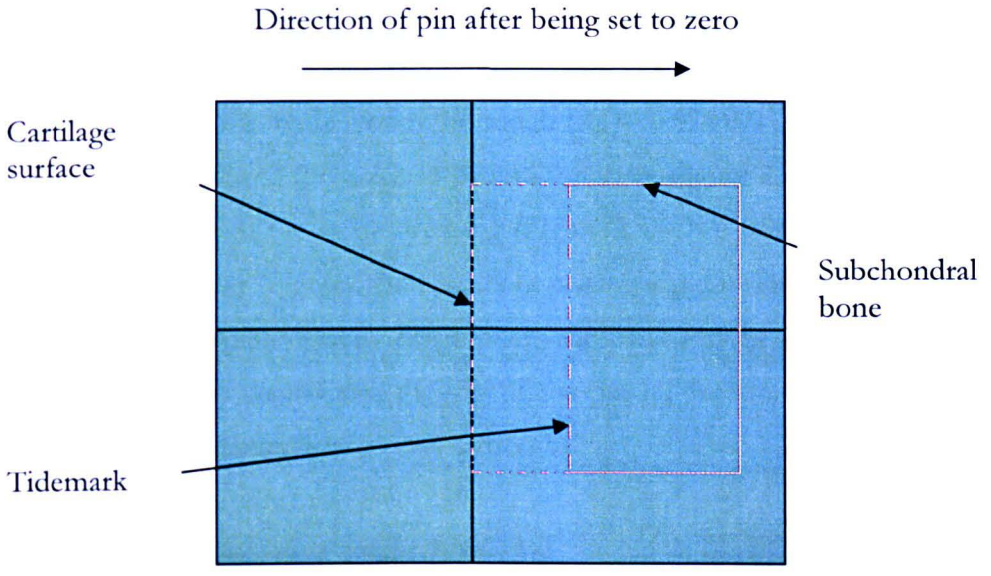

Figure 2.33 Representation of the profile projector screen. The height of the osteochondral pin was measured by aligning the cartilage surface with the x-axis centre line.

The reading on the digital display was recorded. Each measurement was carried out three times in the x- and y-axis and the readings recorded.

2.4.5.2 Assembly of single station pin-on-plate multidirectional aseptic wear rig and generation of wear particle

A single station multidirectional pin-on-plate aseptic wear rig (and related pieces, Figure 2.34) was custom built in the School of Mechanical Engineering (University of Leeds, UK). The aseptic wear rig was housed in a Class II laminar flow hood and aseptic technique was used throughout setup. Before and after testing the Class II laminar flow hood was cleaned with 1% (w/v) Virkon solution (Sigma-Aldrich Company Ltd., Poole, Dorset, UK) followed by 70% (v/v) ethanol (VWR, Poole, UK). The day before each test (and at the end of each test) a UV light (inside the Class II laminar flow hood) switched on for a minimum of 4 h after cleaning. The Class II laminar flow hood was cleaned again with Virkon and ethanol just before commencing the experiment. The wear rig components (i.e. bath, plates, pin holder, screws and allen keys) were washed with household detergent, soaked in 1% (w/v) Virkon (minimum of 10 minutes) and sonicated (ultra sonication bath, see Appendix I) in 70% (v/v) isopropanol for a minimum of 30 minutes. The stainless steel components of the wear rig were sterilised in a dry heat oven at 190°C for 4 h. The

thermoset (Section 2.34), thermoplastic polyurethane (Section 2.35) and PE (polyethylene) pins were soaked, acclimatised (see Sections 2.3.2 and 2.3.3) and gravimetrically measured (Section 2.3.5.1.1). Using sterile gloves the rough (Ra = 0.07-0.08 μm) stainless steel plate (Figure 2.34 A) was screwed (Figure 2.34 B) into the bath (Figure 2.34 A) and the bath was screwed onto the stage of the sterile wear rig (Figure 2.35). A spacer was placed into the bottom of the pin holder (Figure 2.34 C) before placing a pin inside. The grub screw was tightened to secure the pin in place. The washers and ball bearings (Figure 2.34 D, in order from left to right) were placed into the top of the pin holder after being lubricated with sterile Vasoline (dry heat sterilised at 190°C for 4 h).

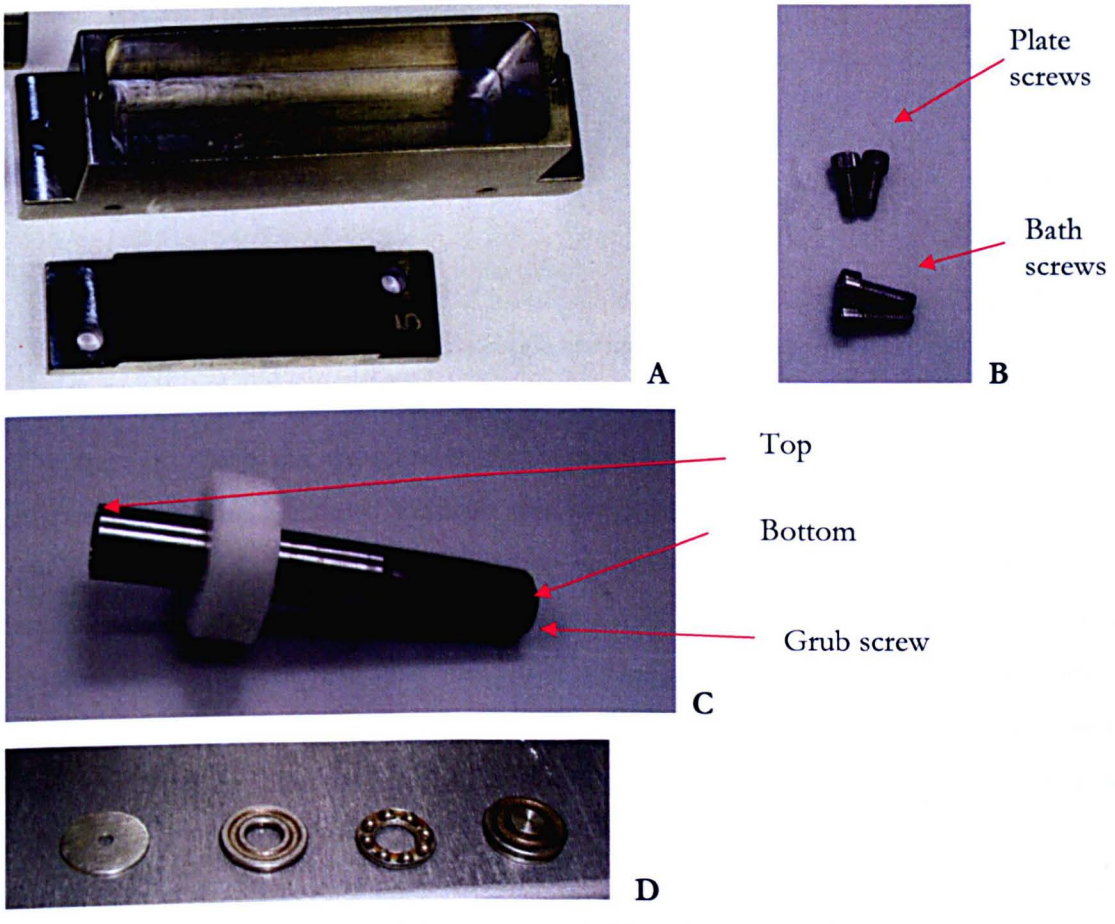

Figure 2.34 Components of the sterile multidirectional wear rig A) bath and plate, B) screws, C) pin holder and, D) ball bearings and washers (placed in order from left to right)

Approximately 25 ml of lubricant (Rosslyn Park Memorial Institute 1640 medium + 25% (v/v) foetal bovine serum (see Sections 2.2.3 and 2.2.5) was aliquoted into the bath before the pin holder was placed through the bridge of the sterile wear rig (Figure 2.35) until the pin contacted the plate. The load arm was lowered and a weight was placed on the arm at

160 to represent 160 N, which resulted in a contact stress of 2.5 MPa and operated at a frequency of 1 Hz per second (60 cycles/minute). The stroke length was set to 28 mm.

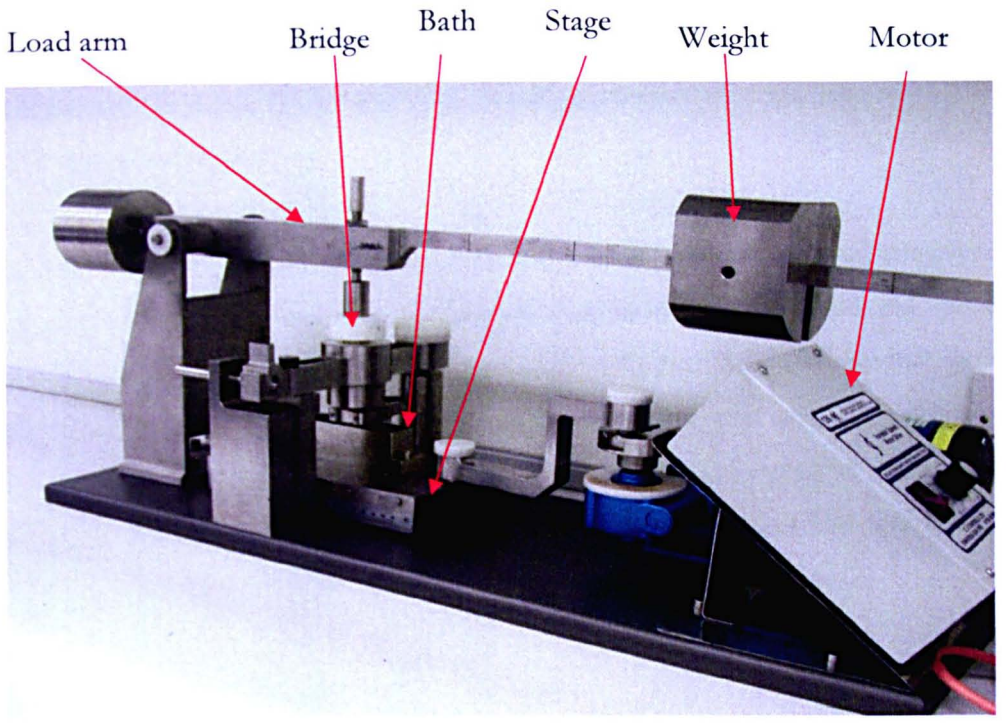

Figure 2.35 Sterile single station multidirectional wear rig

The time at which the experiment commenced and ended was recorded. To prevent evaporation of the lubricant, the bath was topped up with sterile pyrogen-free ultrapure water (Section 2.2.1) twice a day (morning and evening) throughout the duration of the experiment. At the same time that the lubricant was topped up, the experiment was stopped by lifting the load arm (time recorded), a 1-2 ml aliquot of the lubricant was removed (using a sterile syringe) and dispensed into a sterile bijoux for microbial testing (Section 2.4.5.2.1). The load arm was lowered [time recorded] and the experiment was restarted.

At the end of the experiment the speed controller was turned down to zero and the motor was switched off. The load was removed and the arm was lifted in order to disassemble the pin holder. The lubricant was removed from the bath using a sterile syringe, and dispensed into a sterile universal. Approximately 10 ml pyrogen-free ultrapure water (Section 2.2.1) was aliquoted into the bath to obtain any remaining polymer particles. The liquid was added to the same sterile universal containing wear debris/lubricant and was stored at -20°C until required for cell culture (see Section 2.4.10.1) and particle isolation

(Section 2.4.6). All components were disassembled, cleaned and sterilised as described earlier in this Section. The cabinet was thoroughly cleaned with detergent followed by Virkon and then 70% (v/v) ethanol as described earlier in this section. The pins were immersed in household detergent, then wiped clean to remove any particulate debris before being acclimatised (Sections 2.3.5.1 and 2.3.6.1) and gravimetrically measured three times as described in Section 2.3.5.1.1.

A volume of 1 mm^3 of particles (Sections 2.47 and 2.48 for calculations) of the lubricants was digested (Section 2.4.6) and filtered through a series of 10 μm, 1 μm and 0.015 μm pore-sized filters (Appendix I) in order to determine whether the same volume could be retrieved. The particles were characterised, in terms of size and shape as described in Sections 2.4.9.2 and 2.4.9.3) and compared to particles in generated in the six-station multidirectional pin-on-plate wear rig in PBS lubricant (Section 2.4.5.2) and the serum spiked lubricants (Section 2.4.5.2).

2.4.5.2.1 Microbial Testing

Heat blood (HBA), nutrient (NA) and Saboraud dextrose agar (SAB) plates (Section 2.2.12) were inverted in a plate drying room for 20-30 minutes at 36°C. A sample of the aseptic lubricants were plated onto each plate using aseptic technique i.e. flaming a platinum loop and the top of the bijoux, each time the loop was dipped into the lubricant. The lubricant was spread over the plates in a series of standard lines (Figure 2.36).

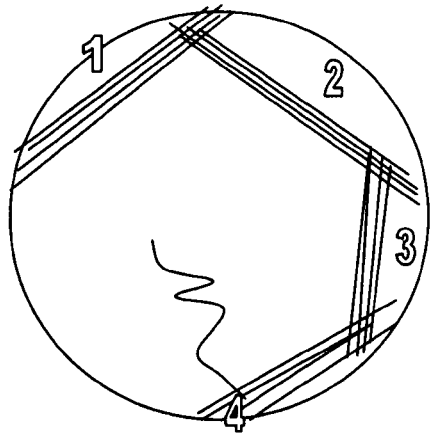

Figure 2.36 Standard method of plating out lubricant on to bacterial growth plates.

For each plate the platinum loop was only immersed into the lubricant for the first line to be traced. The loop was then flame sterilised and the second line was traced from the first line, and so on. The fourth line ends by tracing the lubricant into the middle of the plate. The HBA and NA plates were incubated at 37°C, while the SAB plates were incubated at 30°C for 48 h. For contaminated wear debris/lubricants the microbes colonised along the lines after incubation and became diluted the further away they were from the first line of lubricant plated. These contaminated wear debris/lubricants were not used for cell culture purposes.

2.4.6 Alkali digestion of lubricants

Particles generated in the six station multidirectional pin-on-plate wear rig (Section2.4.5.1.2) and the single station multidirectional pin-on-plate aseptic wear rig (Section 2.4.5.2.1) were digested and isolated using an adapted method (Richards, 2008) from Tipper *et al.*, (2000). A 10 μm, 1 μm and 0.015 μm polycarbonate filter paper (Appendix I) were dried and gravimetrically weighed (Section 2.3.5.1.1) for each material sample. Filters used for the isolation of the polyethylene (Section 2.3.6) samples were dried for a minimum of 4 h using an infra red lamp before and after filtering. However, for isolation of the polyurethane samples the filters were placed in an airtight dessicator containing silica gel (Section 2.2.14) for 24 h before and after filtering, due to the hygroscopic nature of the polyurethane particles. It was envisaged that drying these wear particles under infra red light may have alter the size and shape. Each filter containing particles was gravimetrically measured (Section 2.3.5.1.1) after drying before to determine the weight of the particles.

Potassium hydroxide (KOH; Fisher Scientific, Loughborough, Leicestershire, UK) was added to clean glass universals (6.25 g per 10 ml of lubricant) containing a volume of 1 mm^3 (Sections 2.4.7 and 2.4.8) of wear particles from each sample. Lubricant containing serum were dispensed into each universal and then placed in a 60°C waterbath for 3 – 5 days until the serum had digested (clear liquid). During this time the universals were mixed regularly to aid digestion. Each sample was then placed at 4°C for a minimum of 30 minutes before transferring 10 mL aliquots of each sample to fresh glass universals and adding 10 mL choloform:methanol (2:1 ratio) and mixing. The samples were left to incubate at room temperature for 48 h before being centrifuged at 2000 rpm (revolutions per minute) for 20 minutes. Centrifugation was used to separate the lipids from the

solution. The addition of chloroform:methanol, incubation and centrifugation were repeated until the top layer of solution was clear.

Ice cold (-20°C) absolute ethanol was added to each sample before centrifugation at 1000 RCF (4°C) for 10 minutes. The supernatants were transferred to fresh glass bottles and equal volumes of pyrogen-free ultra pure water were added. Each sample was magnetically stirred overnight at 4°C to precipitate any proteins. The supernatants were transferred to sterile Sorvall dry spin centrifuge bottles (Appendix I) and centrifuged in a high speed Sorvall Evolution RC centrifuge (Appendix I) at 14 000 rpm for 2 h at 4°C. Again the supernatants were transferred to fresh glass bottles, before being filtered (inside a Class I laminar flow hood) through a series (10 μm, 1 μm and 0.015 μm) of polycarbonate filter papers. The filter papers containing the particles were dried as described above and gravimetrically weighed (Section 2.3.5.1.1). All filters containing particles were stored at room temperature in air-tight box containing silica gel (Section 2.2.14) until required for analysis.

2.4.6.1 Validation of digestion method

In preliminary tests, four thermoset polyurethane pins (Diprane 50D and Chemtura 90A, see Section 2.34) were used to generate aseptic wear particles (Section 2.4.5.2.1). However, only one pin of the polyethylene (Section 2.3.6) and thermoplastic polyurethanes (Section 2.35) were used to generate aseptic wear particles (Section 2.4.5.2.1). The wear factor of each material was calculated (Section 2.4.7) is order to determine a volume of 1 mm^3 (Section 2.4.8). The 1 mm^3 volume of particles (Section 2.4.8) from each lubricant was digested to remove traces of foetal bovine serum before the particles were isolated and filtered through the series of (pre-weighed) filters. The filters were dried and re-weighed to determine whether the same volume of particles could be retrieved. The remaining sterile particle/lubricant mixtures were stored at -20°C until required for biocompatibility testing (Chapter 6).

2.4.7 Wear factor calculation

The total experimental time, frequency, and distance travelled by the polymer pins were used to determine the sliding distance (Equation 2.4):

Sliding distance (m) = Experimental time (h) X distance travelled by pin in one cycle X frequency of motion X 60 in one cycle (2.4)

The volume of wear was determined using Equation 2.5:

Volume lost (mm^3) = Weight loss of polymer pin (g) / Density (g/ mm^3) (2.5)

This was followed by calculating the wear factor (Equation 2.6):

Wear factor (mm^3/Nm) = Volume lost (mm^3) / Sliding distance (m) X Load applied (N) (2.6)

2.4.8 Conversion of Particle Volume (μm^3) to a Mass Equivalent

The mass of wear particles used to stimulate macrophages was calculated for each culture experiment as described below in Equation 2.7.

- Density = mass/volume (2.7)
- Assuming a volume of 1 mm^3 of material = 1 mg
- 1 mm^3 = 10^9 μm^3, therefore, 1 μm^3 of material = $1x10^{-9}$ mg
- Particle volumes (μm^3) to macrophage number ratios 10 μm^3:1 and 100 μm^3:1 were investigated
- If 1.125×10^5 cells were seeded per well at the highest particle volume (μm^3) to cell number ratio (i.e. 100μm^3:1), a particle volume of $1.125x10^7$ μm^3 would be required. Since 1 μm^3 weighs $1x10^{-9}$ mg, $1.125x10^7$ μm^3 weighs ($1.125x10^7$) x ($1x10^{-9}$) mg, therefore, the mass of particles required per well = 0.01125 mg = 11.25 μg

The density of the materials was taken into account and Table 2.2 shows the density of the polyethylene (Section 2.3.6) and polyurethanes used in this study.

Table 2.2 Density of Corethane 55D, Tecoflex 51D and 94A, Diprane 50D and Chemtura 90A

Material	Density (g/cm^3)
Corethane 55D	1.21
Tecoflex 51D	1.09
Tecoflex 94A	1.09
Diprane D50	1.22
Chemtura A90	1.22
Polyethylene	0.934

2.4.9 Characterisation of wear particles

2.4.9.1 Field emission gun scanning electron microscope (FEGSEM)

The LEO 1530 field FEGSEM(was obtained from LEO Electron Microscopy Limited, Cambridge, UK; see Appendix 1) was a high resolution microscope in which high resolution images of the particles were captured. Sections of each filter paper were analysed using a LEO FEGSEM (Appendix I). Each section of the filter papers were taped to aluminium stubs using double sided carbon adhesive tape (Appendix I). The stubs were then sputter coated with 3 nm platinum/palladium before being viewed in the chamber of the FEGSEM under vacuum. Electrons (3 kv) were fired at the samples and an in-lens detector formed a surface image which was visualised on a PC. The brightness was set to 50% and the working distance was set to 3 mm. Five images were taken of each pore-sized filter at various magnifications as shown in Table 2.3

Table 2.3 Images taken of particles per pore sized filter

Filter	Magnification
10 μm	0-4 K
	4-10 K
	10-15 K
1 μm	0-10 K
	10-20 K
	20-30 K
	30-40 K
0.015 μm	0-35 K
	50-65 K
	65-100 K

Each image was taken at random to eliminate bias and to characterise the generated wear particles using Image-Pro® Plus.

2.4.9.2 Field emission gun environmental scanning electron microscope (FEGESEM)

Due to the high demand of the LEO FEGSEM (Appendix I), it was decided a QUANTA™ FEGESEM (obtained from FEI, Hanover, Germany; see Appendix I), should be used to capture the images of the particles. This microscope was also high resolution but had a lens inside the chamber unlike the LEO FEGSEM (Appendix I) which had an in lens detector. The filter paper sections were taped to aluminium stubs using adhesive carbon tape then sputter coated with 1.5 nm platinum. (In preliminary experiments, samples were coated with platinum to a thickness of 2 nm, 2.5 nm, 3nm, and 4 nm but visually it appeared the coating was extremely thick. At 1 nm thickness there was evidence that the particles were charging). The aluminium stubs were placed inside the chamber of the microscope and a vacuum was created before firing electrons towards the sample. The in chamber detector formed an image of the surface which was visualised on a PC.

Many problems were encountered trying to visualise the polyurethane samples. In order to visualise polymer particles a beam deceleration mode was used, by attaching a back scatter detector (BSD) inside the chamber. An electron beam of 7 kV was fired at the samples,

however, the landing energy was only 3 kV when using the BSD. The beam deceleration mode only worked well at very high magnifications (> 100 K) with the polyurethane samples, giving poor images at lower magnifications. However, using the BSD without the beam deceleration mode appeared beneficial at lower magnifications (< 100 K) and this method was used throughout. An electron beam of 5 kV was used but the working distance and brightness varied unlike the LEO FEGSEM (Section 2.4.9.1).

2.4.9.2.1 Validation of the field emission gun environmental scanning electron microscope (FEGESEM)

Initially, particles were imaged using the LEO FEGSEM (Section 2.4.9.1, Appendix I for supplier). However, due to the popular use of the LEO FEGSEM (Section 2.4.9.1, Appendix I for supplier) and time constraints it was necessary to switch and use the Quanta™ FEGESEM (Section 2.4.9.2, Appendix I for supplier). The thermoset polyurethane (Section 2.34) wear particles had already been imaged using the LEO FEGSEM (Section 2.4.9.1, Appendix I for supplier). Therefore, the use of the Quanta™ FEGESEM (Section 2.4.9.2, Appendix I for supplier) was compared to the LEO FEGSEM (Section 2.4.9.1, Appendix I for supplier). A fresh volume (1 mm^3) of Chemtura 90A particles were filtered through 10, 1 and 0.015 μm filers (as described in Section 2.4.6) and images were taken at each magnification listed in Table 2.3. The particles from each material were sized using Image-Pro® Plus (Section 2.4.9.3, Appendix I for supplier). The results were comparable (Chapter 5) and therefore, the Quanta™ FEGESEM was used.

2.4.9.3 Image-Pro® Plus

Image-Pro® Plus (Appendix I for supplier), a software program was used to image and size the wear particles from each material. The particles were sized (Mrs Sha Zhang is acknowledged with sizing particles for five samples) by tracing around the perimeter and the software program calculated the area, aspect ratio, perimeter and size (in length and width). Image-Pro® Plus was used to determine a number of physical properties (Figure 2.37) such as area of the particle, roundness (values range from zero to one, one being an exact circle. $R = (4Area)/(\pi d_{max}^2)$, where d_{max} is the greatest diameter), aspect ratio (calculates the shape of the particle which is the longest straight line [major diameter] between any two points on the outline of the particle and the longest line that is at a right angle [minor diameter] to the major diameter. $AR = d_{max}/d_{min}$), and size in length and width (Podsiadlo *et al.*, 1997).

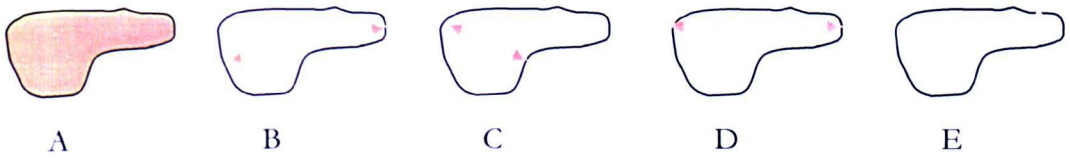

Figure 2.37 A – area of particle; B – Maximum diameter (d_{max}) length of longest line through centre of particle; C – Minumum diameter (d_{min}) of length of shortest line through particle centre; D – Size of length (Feret diameter) along the major axis and, E – Size of width (Feret diameter) along minor axis.

A minimum of 150 particles were sized, however, >500 particles were generally sized. Aggregated particles and silicon were not sized and therefore not included in the final analyses. Control lubricants (lubricants without material particles) were filtered through the series of filters and any other 'unknown' particles imaged were also disregarded from final analyses. Each particle measurement was saved in Microsoft Excel to determine the size ranges of wear particles and the area of the particles in each size range. Images which contained no particles were also included in the analysis. Particles were categorised into the following size ranges; < 0.1 μm, 0.1 – 1.0 μm, 1.0 – 10 μm and, > 10 μm.

An average of the parameters (Section 2.4.9.3) was determined from all the particles sized (per material) over the different magnification ranges (Table 2.3) to give a value for the four different size ranges (< 0.1 μm, 0.1 – 1.0 μm, 1.0 – 10 μm and, > 10 μm). For each material, four lubricants containing particles were generated in the six station multidirectional pin-on-plate wear rig. The particles in each lubricant should have isolated and characterised to determine the variance. However, due to time constraints the duplicate lubricants were pooled, so any variances and significant differences were unable to be determined.

2.4.10 Biological response to generated aseptic wear particles

2.4.10.1 Isolation of Primary Human Peripheral Blood Mononuclear cells

Primary human peripheral blood mononuclear cells (PBMNC) were obtained from healthy volunteers by venepuncture. All material (Lymphoprep®, Trypan blue solution [0.2% v/v], foetal bovine serum, latex beads) suppliers are described in Appendix I. To collect blood

from healthy volunteers ethical approval (reference number R1307) was obtained from the Faculty of Biological Sciences, Ethics Committee, University of Leeds, UK.

All work was carried out in a Class II laminar flow hood using aseptic technique throughout Section 2.4.10.1 to Section 2.4.10.1.3. Approximately 50 ml blood was collected from each volunteer (Donor 1, male, aged 20-30; Donor 2, female, aged 30-40; Donor 3, male, aged 30-40), using a 21G needle into heparinised universals., which were inverted to mix the contents. The blood was diluted 1:1 with transport medium (RTM) as described in Section 2.2.8. To each tube, 7 ml of blood was added drop-wise into 3 ml Lymphoprep® (Section 2.2.11), so the blood cells could slowly separate from the solution. The layered blood and Lymphoprep® solution was centrifuged at 800 x g for 30 minutes. A band of PBMNC was apparent at the interface between the Lymphoprep® and plasma.

The PBMNC layer was carefully removed and dispensed into separate tubes. Fresh RTM (Section 2.2.8) was then added to the PBMNC fractions up to a 20 ml volume. Centrifugation was repeated at 800 x g for 30 minutes. This was repeated if the supernatant appeared cloudy and to remove any traces of Lymphoprep® (Section 2.2.11). The cells from a given donor were pooled together in 5 ml fresh RTM (Section 2.2.8), and a total cell count was performed three times, using a haemocytometer.

The total number of cells per milliliter was calculated (Equation 2.8) using the following equation:

Number of cells x number of squares counted in 25 squares x dilution factor (2.8)

For example, 214 cells counted in 6 squares:-

$$214 \times \frac{25}{6} \times 10^4$$

$$= 8.92 \times 10^6 \text{ cells in 1 ml}$$

$$= 4.46 \times 10^7 \text{ cells in 5 ml (total cell suspension)}$$

Trypan blue exclusion assay was used to assess cell viability (1:10, trypan blue:cell suspension). A volume of 20 µl of the 1:10 dilution was added to a haemocytometer and covered with a coverslip. The cells were viewed under a microscope and the proportion of cells that were stained with the trypan blue (dead cells) and the total number of cells was

counted. Approximately 100 cells were counted within 25 squares on the haemocytometer and >98% cell viability was expected. The concentration of viable cells was then calculated (Equation 2.9):

$$\frac{Dead}{Total} \times 100 \qquad (2.9)$$

A latex bead (Appendix I) assay was performed using 100 µl of the cell suspension. The remaining cells were cultured with wear particles.

2.4.10.1.1 Estimation of Monocytes (Latex bead assay)

To 100 µl of cell suspension in a microcentrifuge tube 15 µl of foetal bovine serum and 50 µl of Latex beads were added. The contents were gently mixed by 'flicking' the microcentrifuge tube followed by incubation at 37°C for 30 minutes. Latex beads that had not been ingested by the cells were carefully separated by slowly dispensing 100 µl FBS under the cell suspension. The cell suspension was then centrifuged at 100 x g for 1 min. The supernatant was removed and the pellet was resuspended in 100 µl culture medium (Section 2.2.10). A 50 µl volume of cell suspension was added to a microscope slide and a coverslip was placed on top. The cells were observed using a 40 x objective under a light microscope to determine the percentage of cells that had ingested the latex beads. This represented the percentage of monocytes in cell suspension (Equation 2.10).

$$\text{Percentage number of monocytes} = \frac{\text{Number of cells with ingested latex beads}}{\text{number of total cells}} \times 100 \qquad (2.10)$$

The average percentage of monocytes per blood sample ranged between 5 and 11%.

The number of monocytes was therefore,

$$\textbf{Proportion of monocytes } \left(\frac{x}{100}\right) \qquad (2.11)$$

2.4.10.1.2 Agarose gel preparation

Prior to assembly of the particle agarose gels (Section 2.2.13), wear particle lubricants were sonicated (ultra sonication bath, see Appendix I) for a minimum of 30 min to separate any aggregated particles. The 2% (w/v) agarose gel was removed from 4°C and placed in a microwave for 2 minutes at medium power to melt back into a solution. For the positive

and negative controls 1 ml of 2% (w/v) agarose (Section 2.2.13) and 1 ml of transport medium (Section 2.2.8) were mixed before 200 µl of the solution was aliquoted into 8 wells (of a 48-well culture plate) for the negative and positive controls.

For the wells containing wear particles, a 1.5 ml volume of 2% (w/v) agarose (Section 2.2.13) was added to the 1.5 ml wear particles and transport medium (Section 2.2.8). The volume of particles to be added to the agarose gel (Section 2.2.13) was determined using the equation in Section 6.2.7 to give concentrations of 10 μm^3 particles per cell and 100 μm^3 particles per cell. The volume of transport medium (Section 2.2.8) added was determined by the volume of wear particles added, however, the final volume (of agarose [Section 2.2.13], wear particles and transport medium [Section 2.2.8]) was 3 ml. A 200 µl volume of 10 μm^3 particles per cell (of each material) and 100 μm^3 particles per cell/agarose solutions were then dispensed into wells to give four replicates of each. The plate was centrifuged on a plate spinner at 800 x g to allow a superficial layer of wear particles to form at the surface of the agarose gel as the gel set. The plates were taped to prevent evaporation and stored at 4°C overnight.

2.4.10.1.3 Culture of monocytes with wear particles

Each well (of the 48-well plate) containing agarose gel/particle gels was washed four times with transport medium (Section 2.2.8) and seeded with 1.125 x 10^5 monocytes (determined from Equation 2.11). Culture medium (Section 2.2.10) was dispensed into each well, to make up to a volume of 1000 µl. The positive control (no polymer particles) was 0.2 µm sized polystyrene FluoSpheres™ (see Appendix I for supplier) added to 1.125 x 10^5 cells at a concentration of 100 μm^3 per cell. Previous studies by Richards (2008) had shown that 0.2 µm FluoSpheres stimulated a significant increase in tumour necrosis factor alpha (TNF-alpha), interleukin-1 beta (IL-1β), and interleukins-6 and -8 (IL-6, IL-8) from peripheral blood mononuclear cells in comparison to the cells only negative control. The 10 μm^3 and 100 μm^3 particle per cell concentrations were calculated as Richards (2008) and are shown in Appendix III.

The negative controls contained 1.125 x 10^5 cells in a 1ml volume with no particle stimulus. The plates were incubated for 12 and 24 h in an atmosphere of 5% (v/v) CO_2 in air. The supernatant was removed aseptically at each time point and stored at -20°C in 48-well polycarbonate plates until required for cytokine analysis and an MTT [3-(4,5-

dimethylthiazol-2-yl)-2,5-diphenyltetrazolium bromide] assay was performed on the remaining cells.

2.4.10.2 MTT [3-(4,5-dimethylthiazol-2-yl)-2,5-diphenyltetrazolium bromide] cell viability assay

The cell viability of primary human peripheral blood monocytes (on agarose gels) was measured using the MTT assay. This was a colorimetric assay in which the yellow tetrazolium salt, MTT was reduced to formazan changing colour from yellow to purple in metabolically active cells. A solution of MTT was prepared by adding 5 mg. ml^{-1} of MTT to phosphate buffered saline (stored at -20°C in 100 µl aliquots, wrapped in foil). Sodium dodecyl sulphate (25g) was dissolved in 247.5 ml distilled water and 2.5 ml of 1 M hydrochloric acid (SDS-HCl) and stored at 4°C.

Aliquots of MTT were thawed and SDS was warmed at 37°C before the assay. To each well of the 48-well plate containing agarose/cells, 100 µl of fresh culture medium (Section 2.2.10) was added followed by 10 µl of MTT solution. The plates were incubated at 37°C in 5% (v/v) CO_2 in air for 4 h. A volume of 100 µl of SDS-HCl was added to each well before wrapping the plates in foil and incubating at 37°C overnight. The supernatants were transferred to a 96-well plate (100 µl of sample per well) and the absorbance was then measured at 570 nm.

2.4.10.3 Enzyme-Linked Immunosorbent Assay kits

Tumour necrosis factor alpha (TNF-α), interleukin-1 beta (IL-1β), interleukin-6 (IL-6) and, interleukin-8 (IL-8) standards, capture antibody (monoclonal mouse anti-human TNF-α, IL-1β, IL-6 and IL-8), detection biotinylated antibody (monoclonal anti-human TNF-α, IL-1β, IL-6 and IL-8), horse-radish peroxidise (HRP)-streptavidin D, and ready-to-use tetramethylbenzidine were stored at 4°C until required (see Appendix I for suppliers). Phosphate buffered saline was prepared as described in Section 2.2.2. Wash buffer, saturation buffer, standard diluent buffer and HRP-streptavidin diluent buffer were prepared as described in Sections 2.2.15.2 and 2.2.15.4 to 2.2.15.6.

2.4.10.3.1 Enzyme-Linked Immunosorbent Assay (ELISA)

All ELISAs were performed as per manufacturer's instructions. Capture antibody was used to coat the wells of a plate in order to 'capture' a sample containing antigen. A biotin-

conjugated secondary antibody was then added which was antigen specific. Streptavidin-horse radish peroxidase was added to allow a colour change to occur when tetramethylbenzidine was added (Figure 2.38).

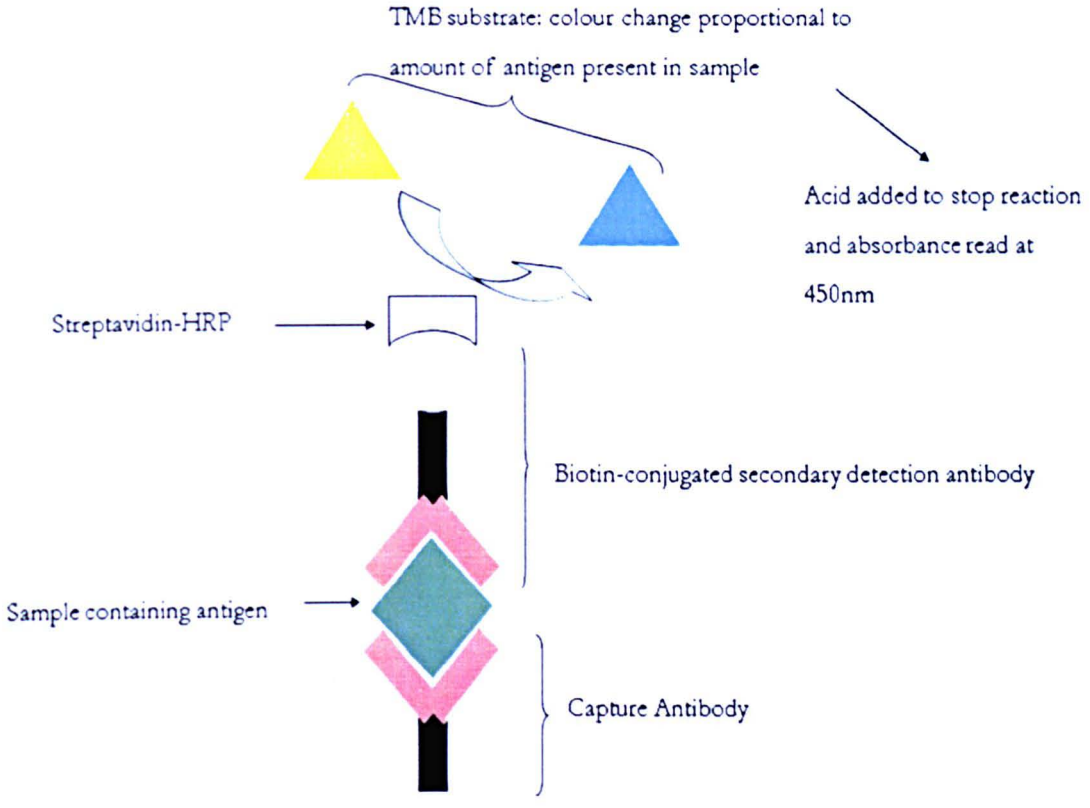

Figure 2.38 Schematic of the ELISA method

2.4.10.3.2 Preparation of Maxisorb ELISA Plates

I) To 10 ml PBS (Section 2.2.2), 100 µl of capture antibody was added for TNF-α ELISAs
II) To 10 ml PBS (Section 2.2.2), 100 µl of capture antibody was added for IL-1β ELISAs
III) To 10 ml PBS (Section 2.2.2), 50 µl of capture antibody was added for IL-6 ELISAs
IV) To 10 ml PBS (Section 2.2.2), 50 µl of capture antibody was added for IL-8 ELISAs

A 100 µl volume of the diluted capture antibody was dispensed into each well of a 96-well polystyrene plate. The plate was wrapped in foil and stored at 4°C overnight. The contents of the 96-well plate were expelled and the wells were washed twice with 400 µl wash buffer (Section 2.2.15.2). The wells were blocked with 250 µl saturation buffer (Section 2.2.15.4) and incubated for 2 h at room temperature. Again the contents of the wells were expelled and the plate was dabbed on tissue paper to remove excess fluid. The plate was left to dry

for 24 hours at room temperature. At this stage the plate could be wrapped and stored at 4°C for up to two weeks.

2.4.10.3.3 Preparation of Standards and Samples

I) A 800 pg TNF-α standard was reconstituted with 1.18 ml of RPMI 1640 and serially diluted 2-fold to 25 pg. ml^{-1}.

II) A 500 pg IL-1β standard was reconstituted with 1.03 ml of RPMI 1640 and serially diluted 2-fold to 15.6 pg. ml^{-1}.

III) A 200 pg IL-6 standard was reconstituted with 1.58 ml of RPMI 1640 and serially diluted 2-fold to 6.25 pg. ml^{-1}.

IV) A 800 pg IL-8 standard was reconstituted with 0.90 ml of RPMI 1640 and serially diluted 2-fold to 25 pg. ml^{-1}.

To each well 100 µl of each standard was dispensed in duplicate into the wells. The blank wells contained 100 µl RPMI 1640 to the wells in duplicate. The unknown samples were dispensed (100 µl) into duplicate wells. The relevant biotinylated detection antibody (anti-TNF-α, anti-IL-1β, anti-IL-6, or anti-IL-8) was diluted with 0.55 ml of distilled water then diluted further to 1:50 with standard diluent buffer (100 µl in 5 ml). A 50 µl volume of this solution was aliquoted into each well of the 96-well plate followed by incubation at room temperature (3 hours for TNF-α and IL-1β ELISAs and 1 h for IL-6 and IL-8). The contents were expelled and the wells were washed three times with 400 µl wash buffer (Section 2.2.15.2).

2.4.10.3.4 Quantification of TNF-a, IL-1β, IL-6 and IL-8

A volume of 5 µl of streptavidin-horse radish peroxidise (HRP) was diluted with 500 µl HRP-streptavidin diluent buffer (Section 2.2.15.6). The solution was further diluted by adding 150 µl to 10 ml of HRP-streptavidin diluent buffer (Section 2.2.15.6). To each well, 100 µl was dispensed and the plate was incubated for 20 min at room temperature. The contents were removed and the wells were washed three times with 400 µl with wash buffer (Section 2.2.15.2). Tetramethylbenzidine was added to each well in 100 µl aliquots and the plate was wrapped in foil and left for 15min to allow the colour to develop. The reaction was brought to an end by aliquoting 100 µl 1M H_2SO_4 to each well. The plate was read with an absorbance of 450 nm and a 570 nm reference filter. The absorbance values obtained from the standards were used to construct a standard curve and the concentration

of each cytokine from each sample was interpolated from the standard curve as pg. ml^{-1} (minus the blank). The results were stored in Microsoft Excel and the values were converted from pg. ml^{-1} to ng. ml^{-1}.

2.4.11 Friction characteristics

2.4.11.1 Assembly of the single station multidirectional pin-on-plate friction rig

A single station multidirectional (however, all tests were performed in unidirectional motion) pin-on-plate friction rig (and related pieces, Figure 2.39) was manufactured in the School of Mechanical Engineering, University of Leeds, UK. . Plates (stainless steel plates with an Ra of 0.01 - 0.03 μm or polyurethane plates) were screwed into a bath. While, articular cartilage plates were secured to an aluminium plate using double-sided adhesive tape and placed on top of a stainless steel plate in the bath, before being clamped in the bath (Figure 2.39).

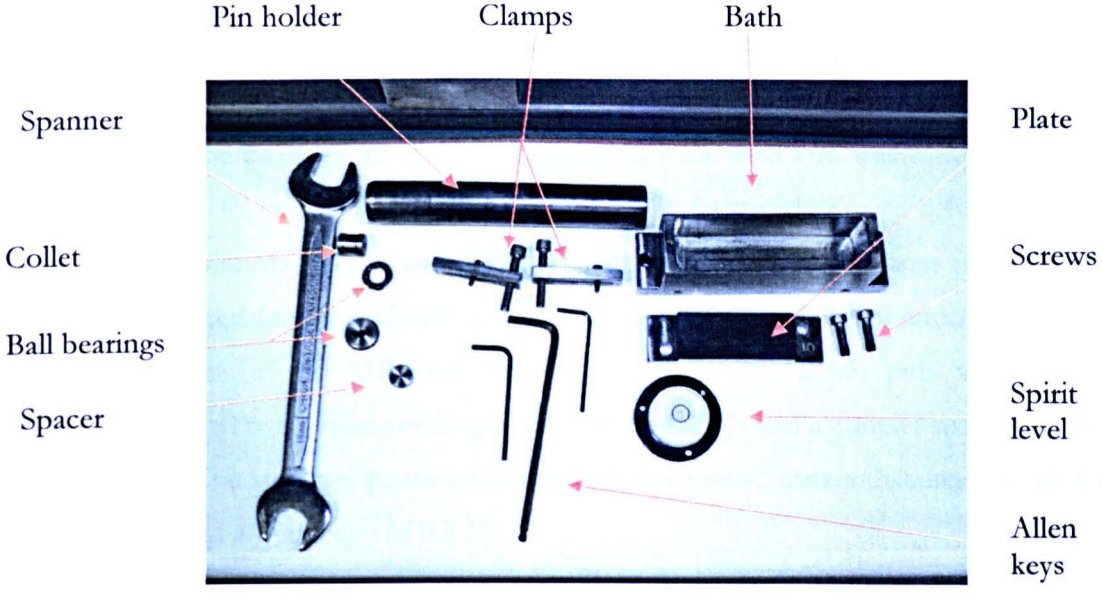

Figure 2.39 Equipment for single station friction rig

A spacer and collet were slotted into the pin holder before placing the pin inside and tightening (Figure 2.39). The bath was screwed to a reciprocating stage on the friction rig and approximately 25 ml of lubricant was added to the bath (in order to keep the plate hydrated) before the pin holder was then slotted through the bridge of the friction rig (Figure 2.40).

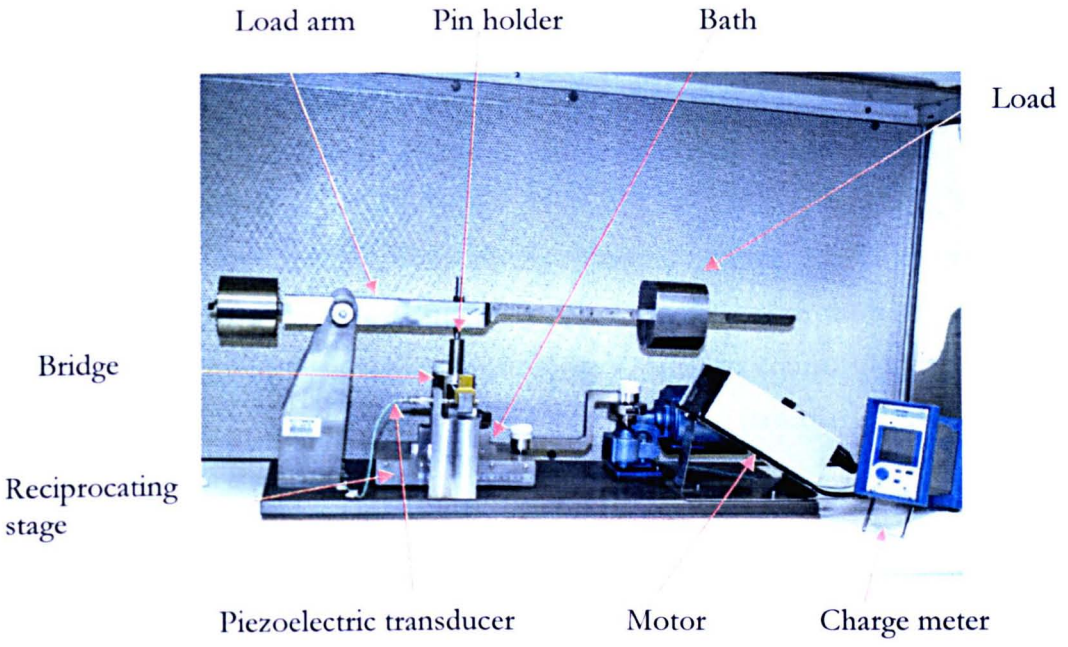

Figure 2.40 Single station multidirectional pin-on-plate friction rig

After placing the bearings on top of the pin holder the load arm was lowered and a spirit level was used to ensure the arm was horizontally balanced (Figure 2.40). The charge amplifier was reset to zero when no load was applied to zero the settings (Figure 2.40). A weight was placed on the load arm corresponding to a load of 160 N which, represented a contact pressure of 2.5 MPa for all (Sections 2.3.1 and 2.3.6) pins while, polyvinyl alcohol/polyvinyl pyrrolidone hydrogel pins (Section 2.37) had a contact stress of 1.26 MPa (80 N load). The stage reciprocated at a speed of 4 $mm.s^{-1}$ over a distance (stroke length) of 10 mm and at a frequency of 0.5 Hz.

The charge amplifier (Figure 2.40) was set to 'operate' and the motor was switched on to commence reciprocal motion. The load arm and the load were lowered onto the pin holder at the same time the test was started. A piezoelectric transducer connected to the friction rig also attached to a data acquistion unit which, converted the frictional force (between the pin and plate) into volts and relayed to the charge amplifier and stored the information on the attached PC. Labview 9 (Appendix I) computer software was used to record the data in volts from which the coefficient of friction was calculated using the gradient of the slope from a calibration curve. Six repeats were performed for all tests unless otherwise stated. Short-term tests had a time period of 1 h while, long-term tests

had a 3 h period. Long term tests were performed on the material combinations where the coefficient of friction continued to increase at the 1 h time point.

The coefficient of friction was measured for articular cartilage (Section 2.3.1), thermoplastic polyurethanes (Section 2.35), thermoset polyurethanes (Section 2.34), PVA/PVP hydrogels and polyethylene (Section 2.3.6) pins reciprocating against articular cartilage plates and stainless steel plates. Articular cartilage pins reciprocated against thermoset and thermoplastic polyurethane plates to determine the coefficient of friction. All material combinations were compared to a negative control (articular cartilage pins against articular cartilage plates) and, a positive control (articular cartilage pins against a smooth stainless steel plates).

2.4.11.1.1 Calibration

Calibrations were performed to ensure the optimum performance of the single station multidirectional pin-on-plate friction rig. A wheel was attached to the side of the apparatus, in order to tie a length of thread around the pin holder and positioned in the groove of the wheel (Figure 2.41). The thread was then attached to a weight holder and the charge amplifier was set to zero.

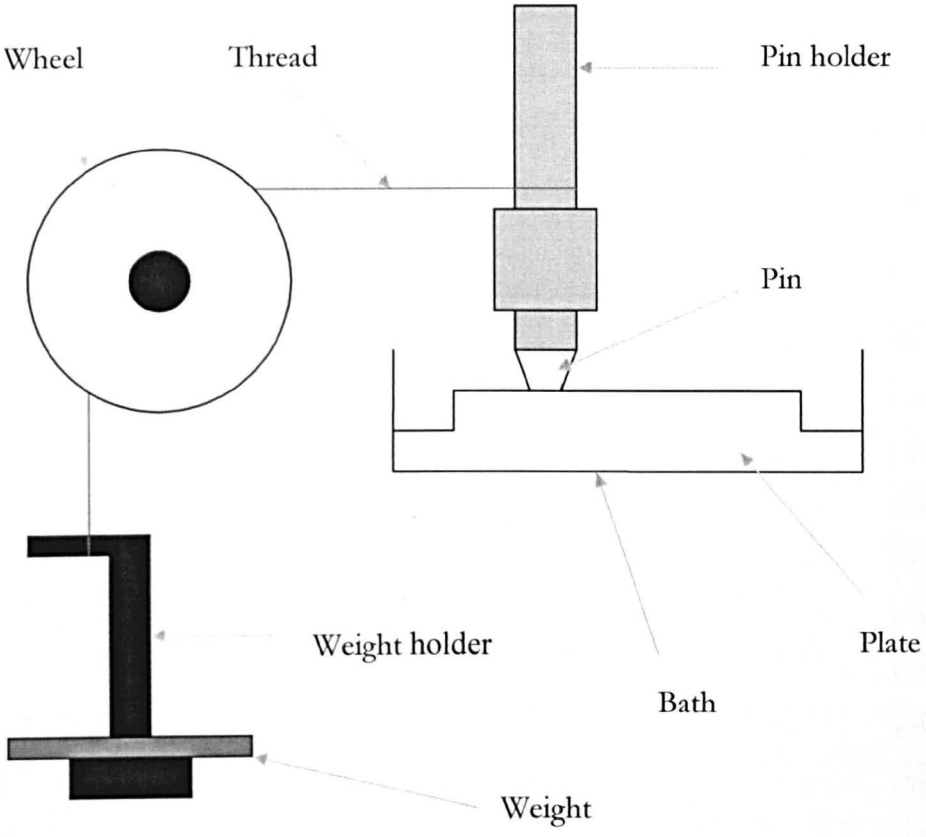

Figure 2.41 Schematic of the single station friction rig calibration set up

Each weight was gravimetrically measured (Section 2.3.5.1.1) before being added to the weight holder to obtain a 'known' weight and the charge amplifier was switched to 'operate'. A 50 g weight was attached every 80 seconds until a load of 650 g was achieved, before removing each weight every 80 seconds. Three readings were recorded within each 80 second interval. The calibration procedure was repeated three times and a calibration curve was produced from the results. The readings were tabulated and a calibration curve was plotted; average readings against weight. The coefficient of friction from each test and frictional force were used to calculate a calibration factor from the slope of the calibration curve.

2.4.11.1.2 Validation

The friction rig was validated by determining the coefficient of friction from a polyethylene (Section 2.3.6) pin which reciprocated against a stainless steel plate (Ra = 0.01 - 0.03 μm) in phosphate buffered saline. A 30 Newton load was used and the results were compared to those from other users. The data is not shown here but they were within range of previous results.

2.4.11.1.3 Materials used in friction measurements

The specific combinations of the articular cartilage, polyethylene (Section 2.3.6), polyurethane and polyvinyl alcohol/polyvinyl pyrrolidone (PVA/PVP) hydrogel pins against articular cartilage plates are highlighted in Table 2.4.

Table 2.4 Pins reciprocated against articular cartilage plates (n=6)

Pin	Plate	Lubricant
Articular cartilage	Articular cartilage	PBS*
Polyethylene (GUR1120)	Articular cartilage	PBS*
Chemtura 90A	Articular cartilage	PBS*
Diprane 50D	Articular cartilage	PBS*
Corethane 55D	Articular cartilage	PBS*
Tecoflex 51D	Articular cartilage	PBS*
Tecoflex 94A	Articular cartilage	PBS*
H1B	Articular cartilage	PBS*
H2B	Articular cartilage	PBS*
H2A	Articular cartilage	PBS*

* phosphate buffered saline (PBS)

All tests with an articular cartilage sample (pin or plate) were performed using PBS (Section 2.2.2) as the lubricant. Preliminary friction tests showed no significant differences between tests using PBS alone and PBS + 25% (v/v) foetal bovine serum (FBS, Section 2.2.4) when used as a lubricant in the presence of articular cartilage (results not shown). Therefore, PBS was chosen as the lubricant of choice for these particular material combinations. For material combinations in the absence of articular cartilage (Section 2.3.1) PBS + 25% (v/v) FBS (Section 2.2.4) was the lubricant of choice because the materials did not have surface proteins to aid with lubrication, unlike the articular cartilage samples. Articular cartilage, polyethylene (Section 2.3.6), polyurethane and PVA/PVP hydrogel pins (Section 2.37) were reciprocated against stainless steel (Ra = 0.01 – 0.03 μm) plates, which can be seen in Table 2.5.

Table 2.5 Pins reciprocated against stainless steel plates (n=6)

Pin	Plate	Lubricant
Articular cartilage	Stainless steel	PBS
Polyethylene (GUR1120)	Stainless steel	PBS + 25% (v/v) FBS
Chemtura 90A	Stainless steel	PBS + 25% (v/v) FBS
Diprane 50D	Stainless steel	PBS + 25% (v/v) FBS
Corethane 55D	Stainless steel	PBS + 25% (v/v) FBS
Tecoflex 51D	Stainless steel	PBS + 25% (v/v) FBS
Tecoflex 94A	Stainless steel	PBS + 25% (v/v) FBS
H1B	Stainless steel	PBS + 25% (v/v) FBS
H2B	Stainless steel	PBS + 25% (v/v) FBS
H2A	Stainless steel	PBS + 25% (v/v) FBS

The friction characteristics of articular cartilage pins (Section 2.3.1) against polyurethane plates (Sections 2.3.4 and 2.3.5) were also tested. Chemtura 90A and Diprane 50D pins were reciprocated against Chemtura 90A and Diprane 50D plates (respectively) in PBS lubricant (Table 2.6).

Table 2.6 Pins reciprocated against polyurethane plates (n=6)

Pin	Plate	Lubricant
Articular cartilage	Chemtura 90A	PBS
Chemtura 90A	Chemtura 90A	PBS + 25% (v/v) FBS
Articular cartilage	Diprane 50D	PBS
Diprane 50D	Diprane 50D	PBS + 25% (v/v) FBS
Articular cartilage	Corethane 55D	PBS
Articular cartilage	Tecoflex 51D	PBS
Articular cartilage	Tecoflex 94A	PBS

It was not possible to test the thermoplastic polyurethanes against the corresponding plates, as the friction was too high, resulting in loosening of equipment parts on the friction rig. Measurements were recorded and automatically saved to a computer via Labview 9 software. The measurements were recorded every 0.25 seconds to 5 minutes, then every 5 minutes to the 60 minute time point (see Table 2.1).

2.4.12 Surface topography measurements

2.4.12.1 Contacting form talysurf profilometer

The contacting form talysurf profilometer 120L was obtained from Taylor Hobson Ltd, Leicester, UK (Appendix I). The machine's specifications are indicated in Table 2.7.

Table 2.7 Contacting form talysurf profilometer specifications

Measurement	Specifications
Straightness of trace	Within 0.5 μm over 120 mm
Trace speed	5.0 mm/s ± 5%
Vertical resolution	20 nm @ 20 mm range
Diamond tip radius	2.5 μm
Applied vertical force	0.85 mN
Cut-off filter	Gaussian 0.8 mm

The contacting form talysurf profilometer 120L (Appendix I) was used to measure the surface roughness (Ra) of articular cartilage (Section 2.3.1), polyethylene (Section 2.3.6) and PVA/PVP hydrogel (Section 2.37) samples. Osteochondral and PVA/PVP hydrogel samples were measured using the talysurf profilometer (Figure 2.42) as this technique was faster than the White Light Interferometer [WLI] (Appendix I) thus, preventing the samples from dehydrating.

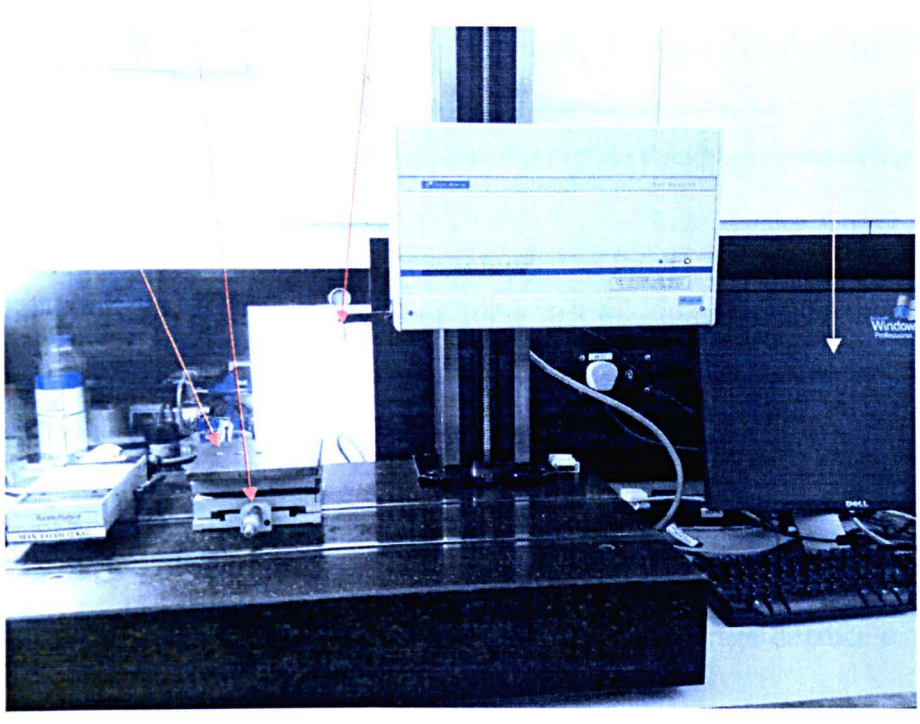

Figure 2.42 Contacting Form Talysurf Profilometer

Also, both the articular cartilage and PVA/PVP hydrogel samples had a low refractive index thus, making it difficult to visualise using the WLI (Appendix I). All polyurethane samples were measured using the WLI (Appendix I), however, some thermoplastic polyurethane samples were measured using the Talysurf (Appendix I) in order to compare the surface roughness to datasets from the WLI (Appendix I). Samples were placed on the stage and the diamond tip stylus was lowered towards the centre of the sample surface before a measurement was conducted (Figure 2.42). A micrometer situated on the stage was used to centre the sample under the stylus (Figure 2.42). On commencement of each trace the stylus was set to automatically contact the surface of the sample and trace along the pre-defined assessment length.

Electrical signals were recorded as the stylus traversed across the surface of a specimen in the Z axis; these signals displayed (on the PC) a surface profile with the required surface roughness parameters (Figure 2.43 and Table 2.8) after being converted to a digital measurement.

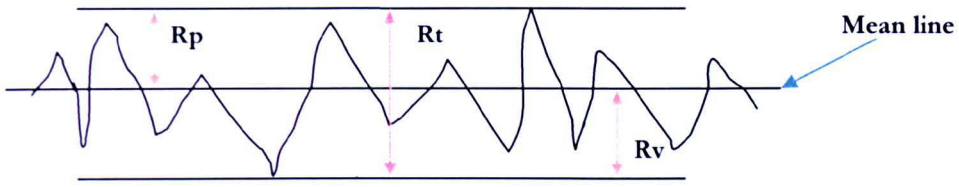

Figure 2.43 Schematic showing various roughness parameters

Surface roughness measurements were then recorded as Ra, Rt, Rv, Rp, and Rpm (Figure 2.14) at a 5 x 0.8 mm cut-off at a ratio of 100:1 (0.8 mm upper cut-off to 8 μm lower bandwidth cut-off) using a Gaussian filter. Roughness parameters are explained in Table 2.5.

Table 2.8 Description of roughness parameters

Parameter	Description
Ra	International parameter of roughness. It is the average distance to the mean line
Rt	the maximum (total) peak to valley height
Rv	depth of the deepest valley below the mean line
Rp	the maximum height of the highest peak above the mean line
Rpm	average peak to average height, or average value of five highest peaks above the mean line in five successive sample lengths

The number of traces measured for pins and plates are discussed in Sections 2.4.12.1.1 and 2.4.12.1.2.

2.4.12.1.1 Surface topography measurements of stainless steel plates

Before testing, measurements were taken every 5 x 0.25 mm over the assessment length of the plate. Surface measurements of each plate were performed before and after each test. The measurements of the surface roughness were then recorded as Ra, Rt, Rv, Rp, and Rpm at a 5 x 0.8 mm cut-off at a ratio of 100:1 (see Section 2.2.6). However, a cut-off of 20 x 0.25 mm was used if large amounts of waviness (more widely spaced irregularities across the assessment length compared to those of the surface roughness) were present.

After testing, surface roughness measurements were performed on the visible worn areas of the plates. For example, plates with discrete scratches were measured in the same way as

plates before testing to identify background roughness and each scratch was measured perpendicularly to the wear surface

2.4.12.1.2 Surface topography measurements of osteochondral plates

The wear scars of the osteochondral plates were 9 mm in the Y axis and 10 mm in X axis when worn against 9 mm diameter pins (osteochondral and hydrogel [Section 2.37]), and 8 mm in the Y axis and 10 mm in the X axis for PE (polyethylene) pins. Three 14 mm traces at 3 mm intervals were measured across the width of each wear scar, with an additional trace which was measured outside of the wear scar (Figure 2.44). Two 14 mm traces at 3 mm intervals were measured across the length of the wear scar (Figure 2.44). The surface roughness measurements were then recorded as Ra, Rt, Rv, Rp, and Rpm at a 5 x 0.8 mm cut-off (100:1) using a Gaussian filter.

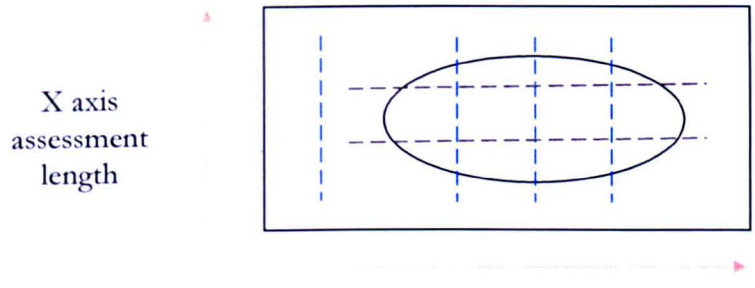

Figure 2.44 Schematic showing X (– –) and Y (– –) axis measurement traces (14 mm at 3 mm intervals) in blue

2.4.12.1.3 Surface topography measurements of pins

Two 8 mm perpendicular traces were measured on all pin samples [7 mm for PE pins] (Figure 2.45). The measurements of the surface roughness were then recorded as Ra, Rt, Rv, Rp, and Rpm at a 5 x 0.8 mm cut-off (100:1) using a Gaussian filter.

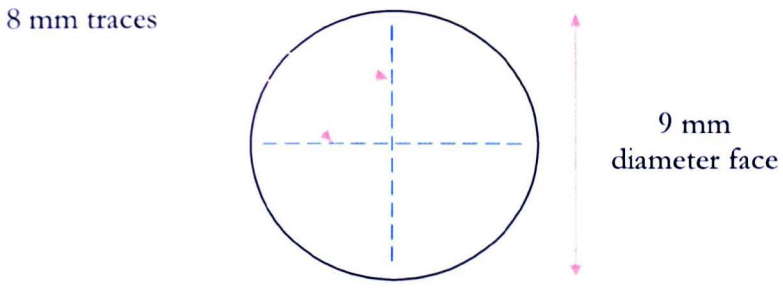

Figure 2.45 Schematic showing X (– –) and Y (– – ·) axis pin measurement traces (8 mm) in blue

2. 4.12.1.4 Software analysis

Taylor-Hobson Ultra software programme was used to analyse each trace by excluding the form fit to exclude unnecessary data from the analysis (Figure 2.46).

Figure 2.46 Diagram showing form fit exclusion. Data behind the black lines (indicated by the arrows) are excluded from the measurements

A Least Square (LS) measurement was completed on all datasets to level the traces (Figure 2.47 A and B). Analyses for plate measurements were set to a LS arc (due to the generated wear scar) profile and a primary measurement was performed. Pin measurements were set to a LS line (flat surface) and a roughness measurement was performed.

Figure 2.47 Diagram showing two identical traces (A) without Least Square levelling and (B) including Least Square levelling

2.4.12.15 Calibration

Calibration involved measuring the condition of the stylus using a ball calibrator (Figure 2.48, Appendix I).

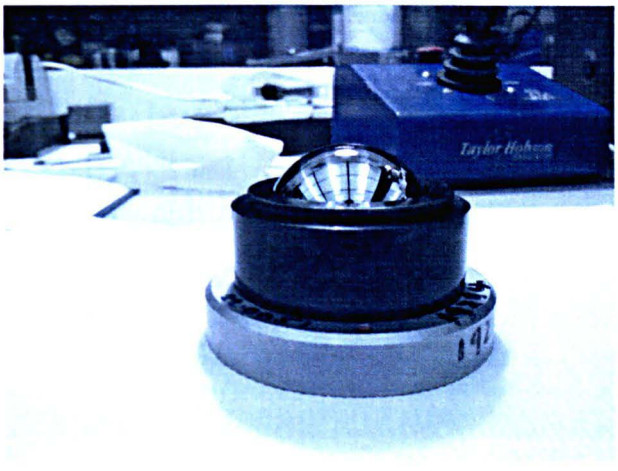

Figure 2.48 Ball calibrator

To determine the precision and accuracy of the stylus a measurement of 22.0051 mm radius for the ball calibrator (Appendix I) should be demonstrated (Figure 2.49). The stylus was set to measure the radius of the ball calibrator (Appendix I) in the same way as described in Section 2.4.12.1.

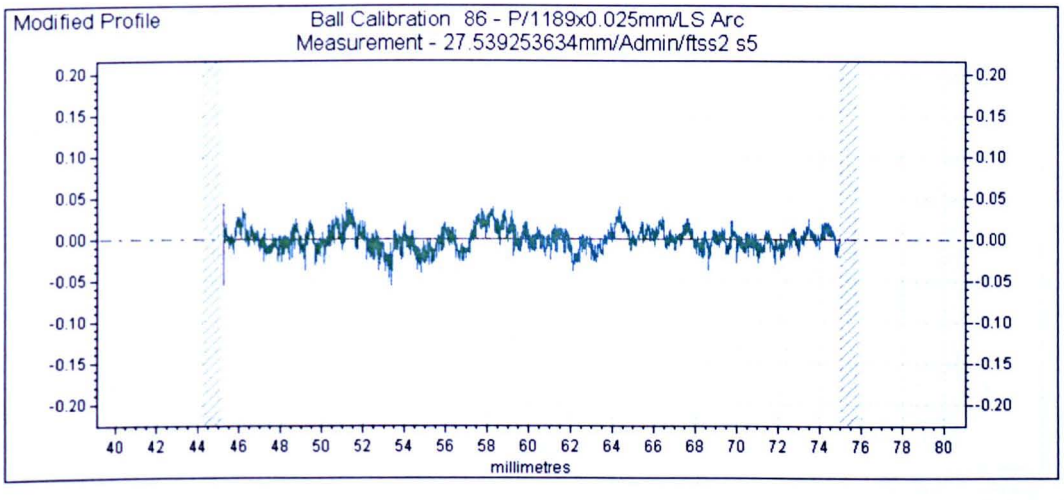

Pt	0.0997	µm	Radius	22.0051	mm	Range	6	mm
Z1	0.98873		Z2	0.004094		Z3	0.0000054	
X1	-0.44338		X2	0.009959		X3	-0.0000745	

Figure 2.49 Example of calibration trace after measuring ball calibrator. Data under graph shows a measured radius of 22.0051 mm

A Roughness Standard (Figure 2.50, Appendix I) was also used to calibrate the machine, which consisted of an 8 μm Ra measurement line and a 0.04 μm (depth) 3-square step measurement line.

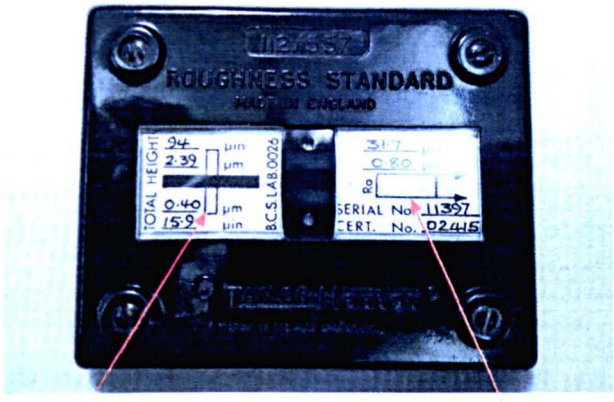

0.4 μm 3-square step measurement line 8 μm Ra measurement line

Figure 2.50 Ra Standard

The stylus was set to measure (as mentioned in Section 2.4.12.1) the lines indicated in Figure 2.51 to obtain a surface roughness of approximately 0.8 μm Ra (Figure 2.51) and a 0.4 μm 3-square step profile (Figure 2.52).

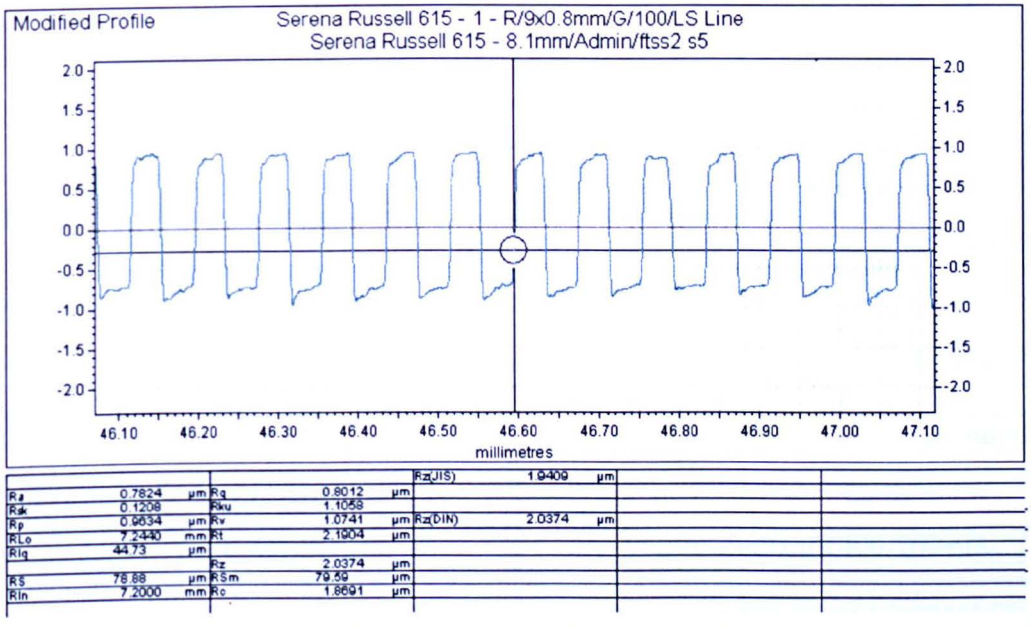

Figure 2.51 Example of calibration trace after measuring 0.8 μm Ra Roughness Standard. Data shows surface roughness values for typical roughness parameters

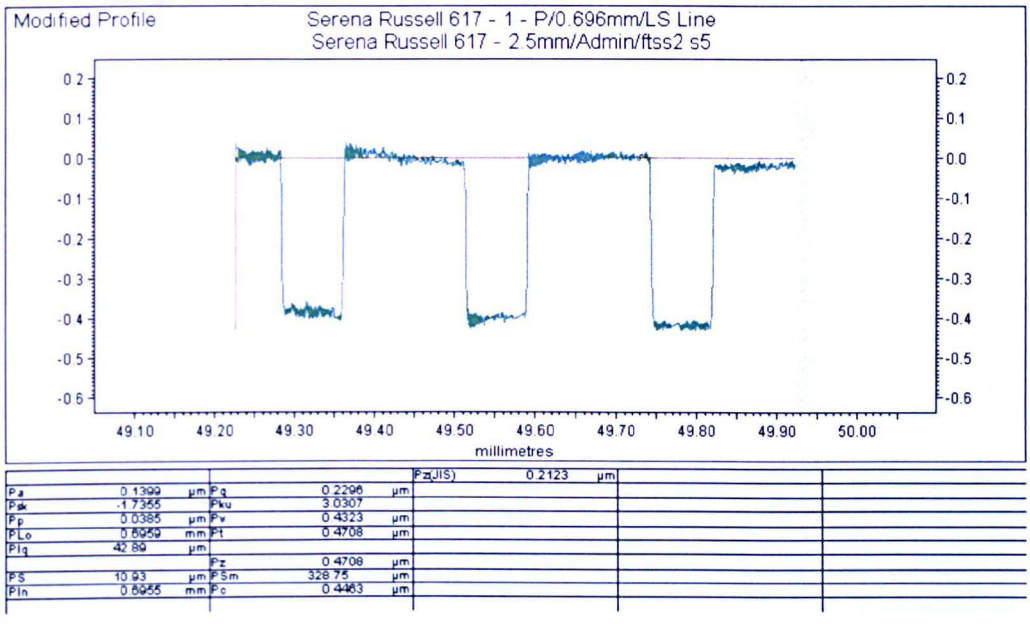

Figure 2.52 Example of calibration trace after measuring 0.4 µm 3 step square surface profile. Data shows the surface profile of the 0.4 µm 3-step surface with profile values

Measurements of the ball calibrator (Appendix I), 8 µm Ra Standard (Appendix I) and 0.4 µm 3-square step were analysed using a Gaussian filter with a 0.8 mm upper cut-off and a 8 µm lower cut-off (100:1). A LS arc was used on data retrieved from the ball calibrator and a LS line was used for the Ra Standard (Appendix I).

2.4.12.2 Non-contacting White Light Interferometer

The non-contacting white light interferometer (WLI) NT 33005 was obtained from Veeco, MA, USA. The machine's specifications are shown in Table 2.9.

Table 2.9 Non-contacting white light interferometer specifications

Measurement	Specifications
Vertical range	2 mm
Vertical resolution	3 nm
Accuracy	Surface and magnification dependent
Area of focus	Dependent on magnification
Light source wavelength	Visible spectrum 400-700 nm

The WLI was used to measure the surface roughness of the thermoset and thermoplastic samples (described in Section 2.2.7). The surface roughness of thermoset and thermoplastic pins and plates were measured by placing them on the stage of the WLI (Figure 2.53). A X10 magnification lens and a white light source were used to visualise each sample using Vision 32 software.

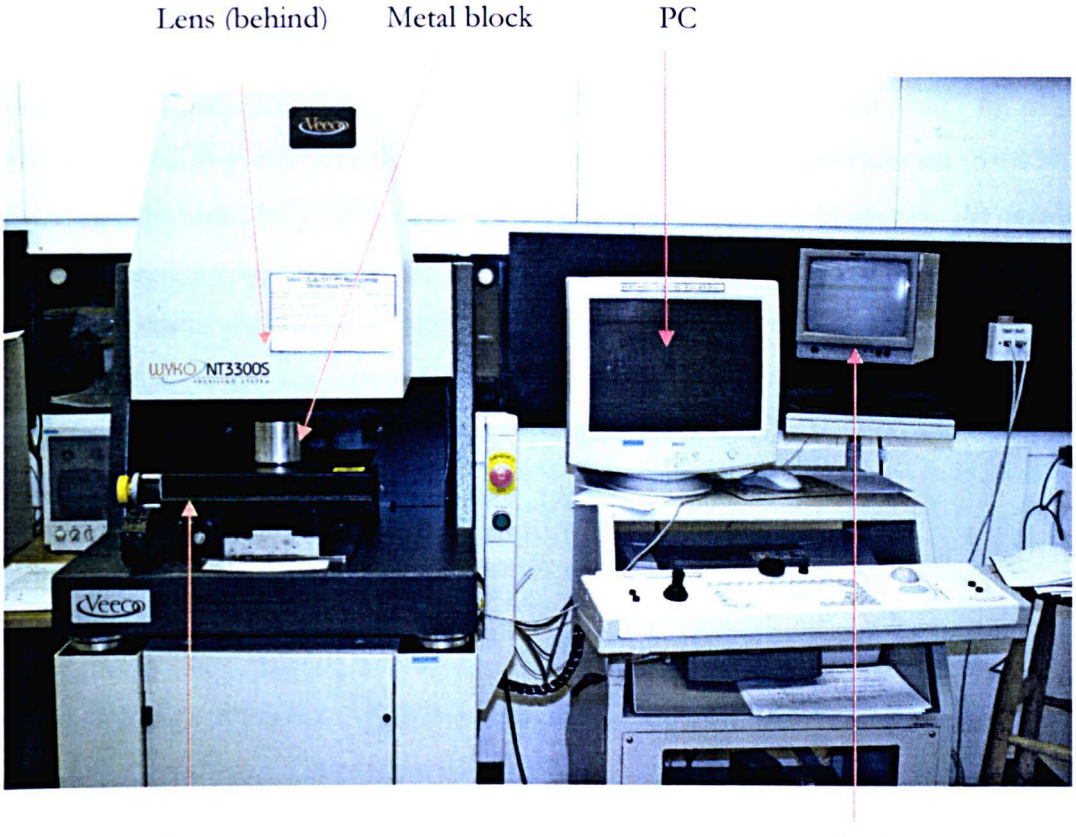

Figure 2.53 Non-contacting White Light Interferometer

The WLI works by dividing a white light source by a beamsplitter which, then recombines to generate an interference pattern on the sample. The intensity of light varies on each sample and the beam interferes at different wavelengths causing 'fringes', which appear as light and dark alternating bands that can be seen on the monitor. Groups of fringes have different wavelengths and the spacing of the bands is dependent on these wavelengths.

For pin and plate measurements the magnification lens was set to backscan before each measurement (minimum of 15 μm) in order to focus on the sample from the top of the highest peak to the bottom of the lowest valley. This resulted in the image on the monitor

moving in and out of focus. The data was translated to the Vision 32 software. All measurements were performed using the VSI (vertical scanning interferometry) mode.

2.4.12.2.1 Surface topography measurements of polyurethane plates

The width of the wear scars were too long to measure in full so 'stitching' was required to obtain a complete measurement (Figure 2.54). The X axis was measured at 0.15 mm and stitched to the 11 mm measured in the Y axis (NOTE: during volume loss analysis the data was multiplied accordingly to account for the volume of the full wear scar). An overlap of 1% was required to calculate the best fit. The modulation threshold was set to 0.1%, which increased the sensitivity of the camera during measurement. However, the modulation threshold had to be increased to 5% for thermoplastic polyurethanes (Section 2.35) to decrease camera sensitivity. This may have been because the thermoplastic polyurethanes (Section 2.35) were less opaque than the thermoset polyurethanes (Section 2.34) and therefore, high camera sensitivity was not required.

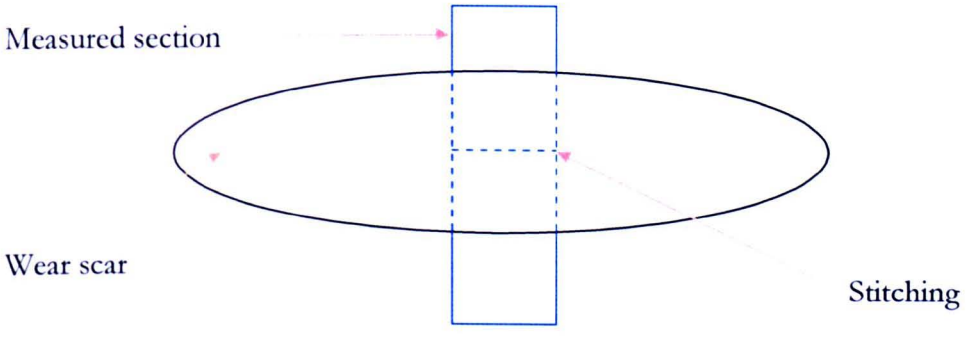

Figure 2.54 Diagram of a small measured 'stitched' section of a wear scar

2.4.12.2.2 Surface topography measurements of polyurethane pins

Pin measurements also required stitching in the X and Y axes (Figure 2.55), to determine the average Ra in both the X and Y axes. Measurements were taken 4 mm in each direction, which overlapped by 25% at a modulation threshold of 1%. Measurements were taken before and after each test.

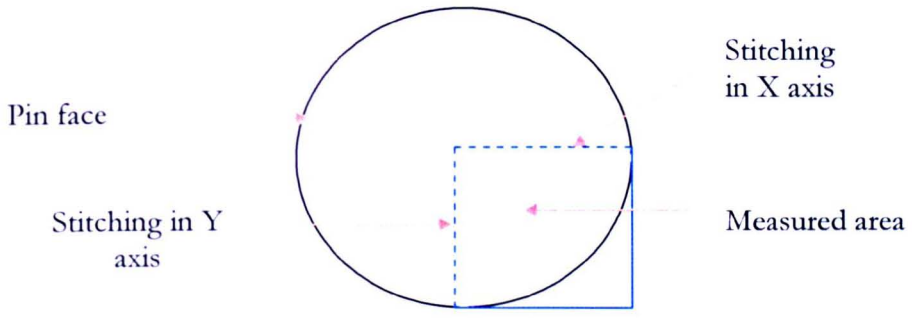

Figure 2.55 Diagram of a measured and 'stitched' section of a pin face

2.4.12.2.3 Software analysis

The datasets from the pin and plate measurements were saved as .OPD files and analysis was performed on these. A Least Squares line was performed on each dataset excluding the form fit. Vision 32 software was used to determine the width, depth, volume and 3-dimensional image (Figures 2.56 to 2.59) of the wear scar for each plate, while the average surface roughness was determined from the X and Y axes of the pins.

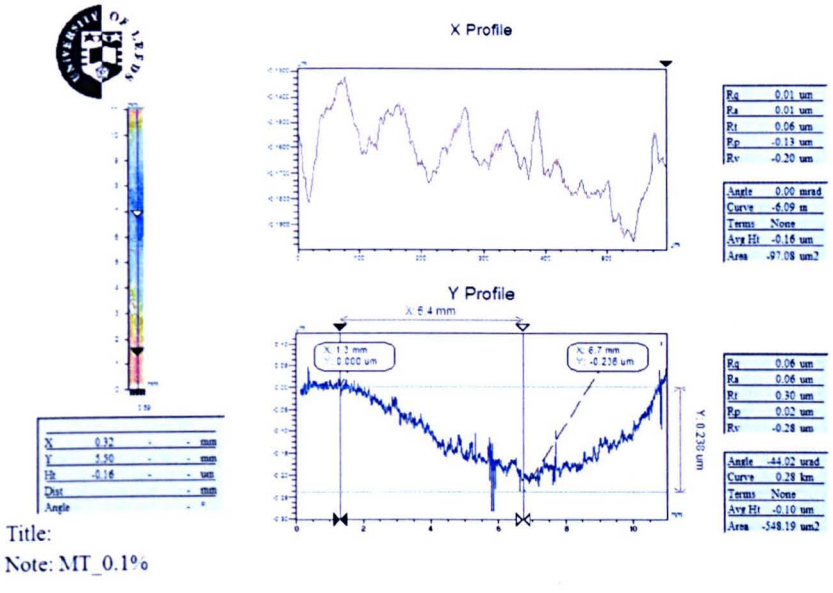

Figure 2.56 Example of data showing depth of wear scar on a plate. The depth of the wear scar is indicated on the Y profile and average surface roughness values are shown for typical roughness parameters

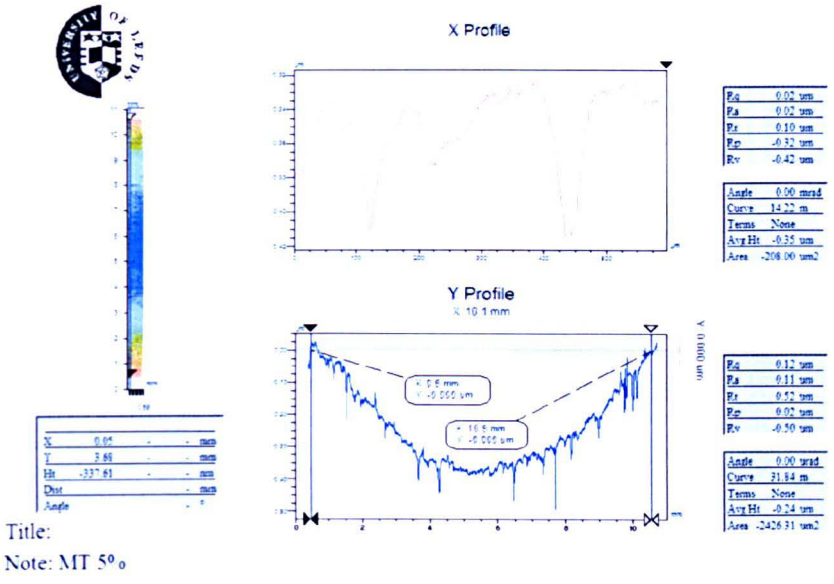

Figure 2.57 Example of data showing width of wear scar on a plate. The width of the wear scar is indicated on the Y profile and average surface roughness values are shown for typical roughness parameters

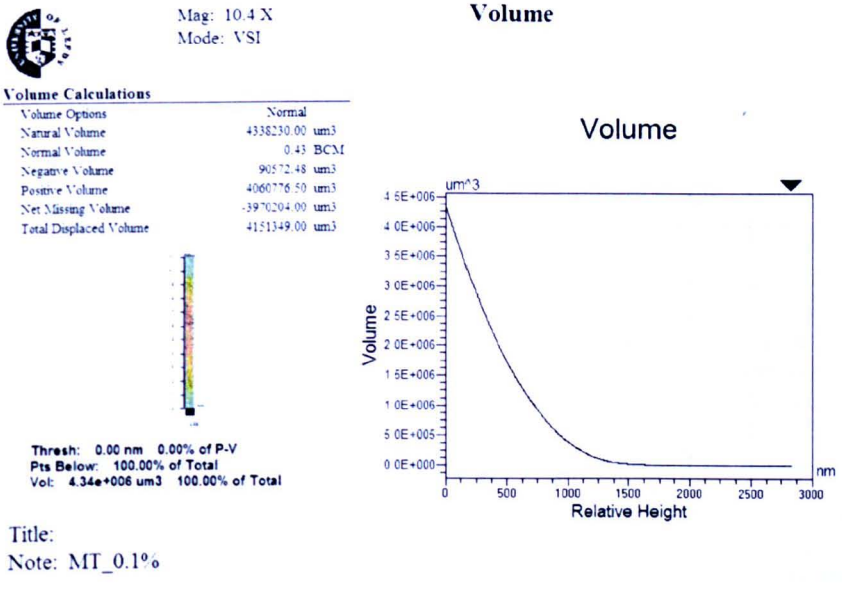

Figure 2.58 Example of data showing volume of wear scar. The volume of the wear scar is shown in the chart and average values are included in the calculation section. NOTE: the volume is multiplied to account for full wear scar and thus, full volume loss.

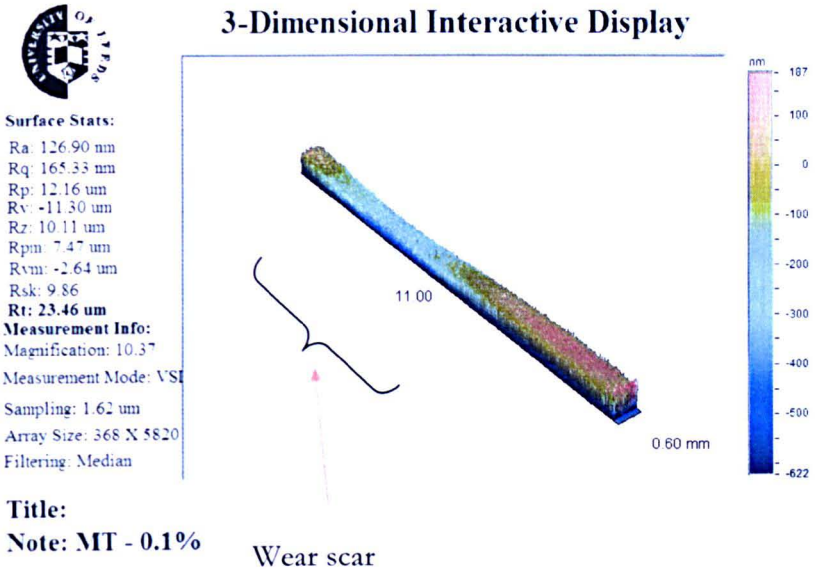

Figure 2.59 Three dimensional image showing area of wear scar on a plate. The wear scar can be seen in a narrow section of a measured sample, with surface roughness values indicated for typical roughness parameters

Analysis was performed in the X and Y axes for each dataset to a length of 0.25 mm cut-off using a Gaussian external filter and shortwave length of 25 μm using a Gaussian filter; a ratio of 100 to 1. Five sample lengths were taken for every dataset to ensure an accurate measurement. Measurements were analysed in the same way for pin datasets, however, 0.8 mm was the cut-off value and the short wave length was 8 μm resulting in a ratio of 100 to 1.

2.4.12.2.4 Calibration

A glass calibration specimen with a 'WYKO' engraving was used to calibrate the machine. The glass was handled with cotton gloves in order to avoid transfer of particulates. The X10 objective lens was lowered to the glass specimen and the light intensity was set to approximately 50%. Fringes were observed and set perpendicular to the main features on the glass specimen, which were located by moving the lens out of focus. The objective lens was set to backscan 5 μm (no stitching involved) at a modulation threshold of 5%, so the camera sensitivity was at its lowest. Analysis was performed to attain an average Ra of approximately 10.07 μm (Figure 2.66).

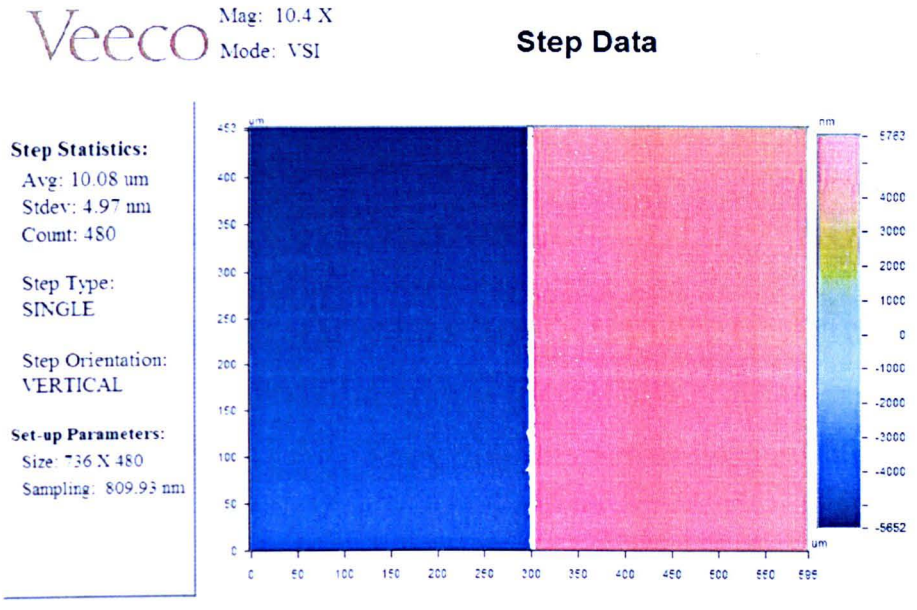

Note: MT 0.1

Figure 2.60 Example of calibration data from a WYCO glass specimen, measuring 10.08 μm. Step data showing the measured surface roughness

2.4.12.3 Talymap Gold

Talymap Gold, is a computer software program was obtained from Taylor Hobson Ltd, Leicester, UK. Talymap Gold software program was used to analyse the surface roughness and profile data of samples measured by white light interferometry and to allow comparison of the surface roughness data measured by the contacting form talysurf profilometer. The .OPD files from WLI were used to analyse each dataset. Levelling was performed on each dataset, which was equivalent to Least Squares (analysis on Talysurf), followed by excluding the form fit. The profile was extracted from the data to convert into a series of measurements and measurements of the surface roughness were recorded as Ra, Rt, Rv, and Rp at a 5 x 0.8 mm (pins) or 0.25 mm (plates) cut-off using a Gaussian filter.

Chapter Three

Mechanical Properties of thermoset and thermoplastic polyurethanes

3.1 Introduction

Three thermoplastic polyurethanes were used in this study; Corethane 55D (an aromatic polycarbonate), Tecoflex 51D and 94A (aliphatic polyethers). Two thermoset polyurethanes, Diprane 50D (polyether) and Chemtura 90A (polyester) were also used (Table 2.2 for suppliers). As previously mentioned in Chapter 1, polyurethanes are composed of a diisocyanate, a chain extender (collectively forming the hard segment) and a polyol (soft segment). The mechanical and physical properties of some materials can be manipulated (Brook and Hatton, 1998), this is also true for polyurethanes (PUs), which are dependent on the type and concentration of all three components, hence, the large variety of available PUs (Lambda *et al.*, 1989). Compositions of the PUs used in this study are stated in Table 3.1.

Table 3.1 Thermoplastic and thermoset PU components

Material	Diisocyanate	Chain extender	Macrodiol (polyol)
Tecoflex 94A	H_{12}MDI	BD	PTMEG
Tecoflex 51D	H_{12}MDI	BD	PTMEG
Corethane 55D	MDI	BD	PC
Chemtura 90A	TDI	unknown	polyether
Diprane 50D	MDI	unknown	polyester

H_{12}MDI, 4, 4'-dicyclohexylmethane diisocyanate; MDI, 4,4'-diphenyl methane diisocyanate; BD, 1,4-butane diol;, PTMEG, polytetramethylene ether; PC, polycarbonate; TDI, toluene diisocyanate; MDI, 4,4'-diphenyl methane diisocyanate.

The polyvinyl alcohol/polyvinyl pyrrolidone (PVA/PVP) hydrogels used in this study were named H2A (28% (w/v) PVA), H1B (25% (w/v) PVA + 7% (v/v) gluconic acid) and, H2B (28% (w/v) PVA + 7% (v/v) gluconic acid) [Table 2.2 for supplier]. The incorporation of gluconic acid increased the porosity of the hydrogel network (Fray *et al.*, 2007).

Polymers are able to oppose indentation, and this resistance can be measured in terms of 'hardness'. The most commonly used polymers fall into two categories of hardness; namely Shore hardness A and Shore hardness D. Generally, soft polymers are within a range of Shore hardness 10 - 100A, while harder polymers fall within a range of Shore hardness 6 - 58D.

For an elastic plastic material, determining a materials response to stress (by performing a tensile test) can provide a great insight to other mechanical properties the material possesses. For example, producing a stress-strain curve (by applying stress to a material in order to cause fracture), Young's modulus (refers to material stiffness), ultimate elongation (percentage increase in original length at the time of failure after applying a tensile stress) and, ultimate tensile strength (maximum tensile stress experienced prior to fracture) can be determined. An example of a stress-strain relationship curve is shown in Figure 3.1. The linear portion of the curve extending to the proportional limit is known as the elastic region. This is when a material undergoes elastic deformation, and begins to elongate. Most materials adopt this linear trend that describes Hooke's law (equation 3.1) which, states the stress applied to a material is proportional to the strain, therefore as stress increases so does strain.

$$\delta = E\,\epsilon \qquad (3.1)$$

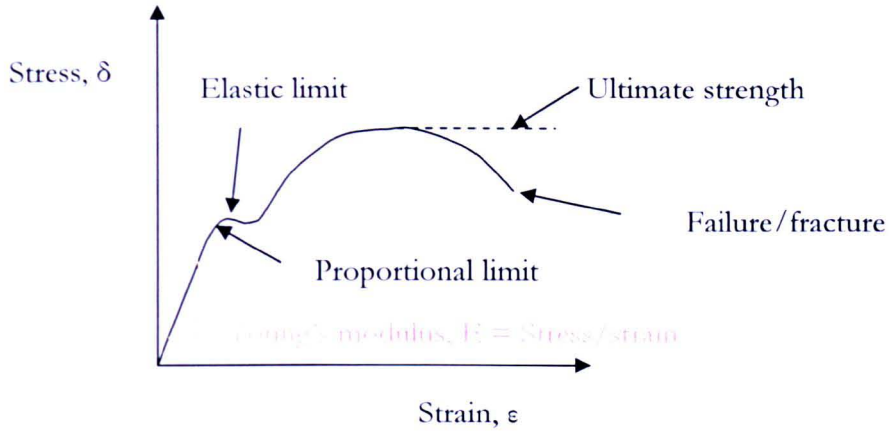

Figure 3.1 Example of a stress-strain relationship curve

Where, δ refers to the applied stress, E is the Young's modulus, and ε is the strain experienced by the material. The Young's modulus (or elastic modulus) can be determined from the gradient of the slope in the elastic region (linear portion of the curve) and is the ratio of stress divided by the strain (equation 3.2) giving an indication of the stiffness of the material.

$$E = \frac{\delta}{\varepsilon} \qquad (3.2)$$

Where, E is the Young's modulus, δ is the applied stress and, ε is the strain experienced by the material. When materials reach the elastic limit (Figure 3.1) and the stress is removed they no longer return to the original dimensions, however, upon removal of stress before this point, the material will return to its original dimensions. Beyond the elastic limit the curve continues in a nonlinear manner known as the plastic region. This is when the material undergoes plastic deformation and, hence looses the ability to return to its original dimensions. During plastic deformation the material continues to elongate, however, the cross sectional area reduces until the material breaks or fractures (Figure 3.1). Ultimate tensile strength is experienced by the material, where a maximum amount of stress is applied before failure of the material occurs.

The aim of this chapter was to determine the mechanical properties (Shore hardness and tensile) of the thermoplastic and thermoset PUs and compare them to the information stated by the manufacturers and to the literature where possible. Unfortunately, the tensile properties of the PVA/PVP hydrogels were not investigated because it was difficult to cut these materials while trying to preserve a uniform surface, thus a uniform cross sectional area was not achievable. Therefore, it was envisaged that

the results would not be a true representation of the tensile properties. However, due to the lack of mechanical testing of the PVA/PVP hydrogels at Warsaw University a comparison was not possible. Only the Shore hardness of the PVA/PVP hydrogels was investigated in this chapter.

3.2 Materials and Methods

A durometer (Section 2.4.1; Appendix I for supplier) was used to determine the Shore hardness of the polyvinyl alcohol/polyvinyl pyrrolidone hydrogels pins (Sections 2.3.7; Appendix I for supplier) and the thermoset (Diprane 50D and Chemtura 90A) and thermoplastic (Corethane 55D, Tecoflex 51D and Tecoflex 94A) polyurethane pins (Sections 2.3.5 and 2.3.4; Appendix I for suppliers). To investigate the tensile properties of the thermoset and thermoplastic polyurethanes an Instron (Section 2.4.2; Appendix I for supplier) was used.

3.3 Results

3.3.1 Shore hardness - Durometer

The Shore hardness of the polyvinyl alcohol/polyvinyl pyrrolidone hydrogels was determined, however, this property was not investigated by Dr. Wojciech Swieszkowski (Warsaw University, Poland) and, therefore, could not be compared. Chemtura 90A and Tecoflex 94A were not significantly different to the manufacturer's data but, the Shore hardness D polyurethanes (PUs) were significantly different (Table 3.2).

Table 3.2 Experimental data versus Manufacture's data

Material	Manufacturer's data	Mean Shore hardness (experimental data n = 3)	95% confidence interval (±)
Chemtura	90A	87.0 A	5.8
Tecoflex	94A	92.6 A	6.0
H1B hydrogel	-	31.2 A	2.0
H2B hydrogel	-	34.6 A	3.2
H2A hydrogel	-	34.4 A	4.5
Diprane	50D	37.0 D	0.6
Corethane	55D	52.3 D	1.3
Tecoflex	51D	53.7 D	1.5

3.3.2 Tensile properties of thermoplastic polyurethanes (TPUs)

The tensile properties for the TPUs are shown in Figure 3.2. Each material exhibited an initial significant increase in tensile stress at low strain during elastic deformation. This was followed by a significant increase in tensile strain, prior to failure of the materials when the cross sectional area decreased and elongation increased during plastic deformation. The thermoplastic Shore hardness D polyurethanes failed before Tecoflex 94A, suggesting that Tecoflex 94A was more ductile, because tensile strain was higher.

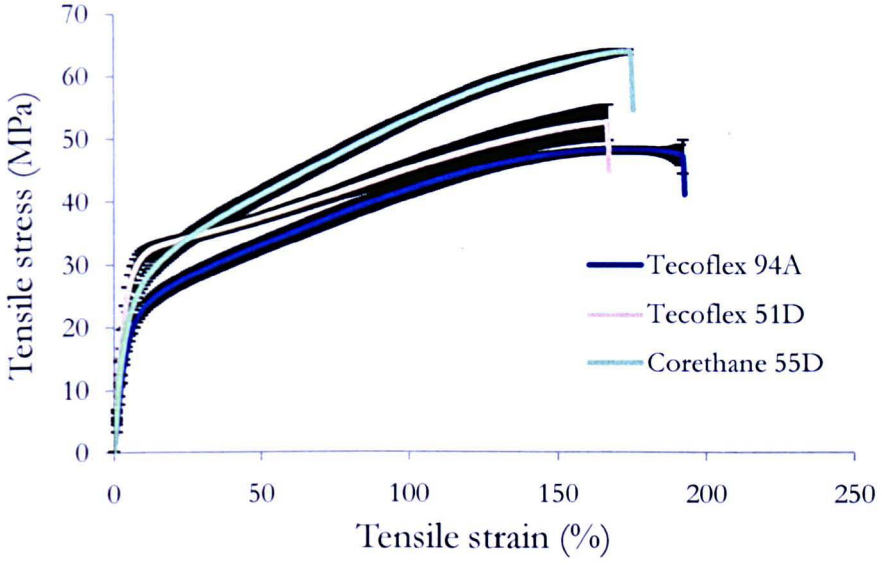

Figure 3.2 Stress- strain relationship curves for TPUs (n=3)

The tensile strain was measured as a percentage when a tensile stress (MPa) was applied to Tecoflex, 94A, Tecoflex 51D and, Corethane 55D (n = 3).

A higher ultimate tensile stress was required to fracture Corethane 55D compared to Tecoflex 94A and 51D (Table 3.3). However, Tecoflex 94A had the highest increase of original length compared to the other two materials. As stress increased so did strain, when tensile stress at 50% and 100% elongation was compared. Furthermore, the stiffness of Tecoflex 51D indicated by the Young's modulus was greater than the other two materials; Tecoflex 94A had the lowest Young's modulus and therefore, was less stiff.

Table 3.3 Mechanical properties of TPUs (n=3)

	Tecoflex 94A	Tecoflex 51D	Corethane 55D
Ultimate strength (stress), MPa	41	45	55
Ultimate elongation %	193	167	175
Tensile stress (MPa)			
at 50% elongation	33	37	41
at 100% elongation	42	45	53
Young's modulus (MPa)	4.8	7.8	6.2

3.3.3 Tensile properties of thermoset polyurethanes (PUs)

The stress-strain relationship curves for the thermoset PUs exhibited a similar trend (Figure 3.3). During elastic deformation an initial increase in tensile stress at low strain was seen before a dramatic increase in tensile strain (consistent with an increased length). Prior to failure a decrease in tensile stress can be seen, possibly due to the PUs slipping between the clamps. During plastic deformation the cross sectional area had decreased before the material fractured.

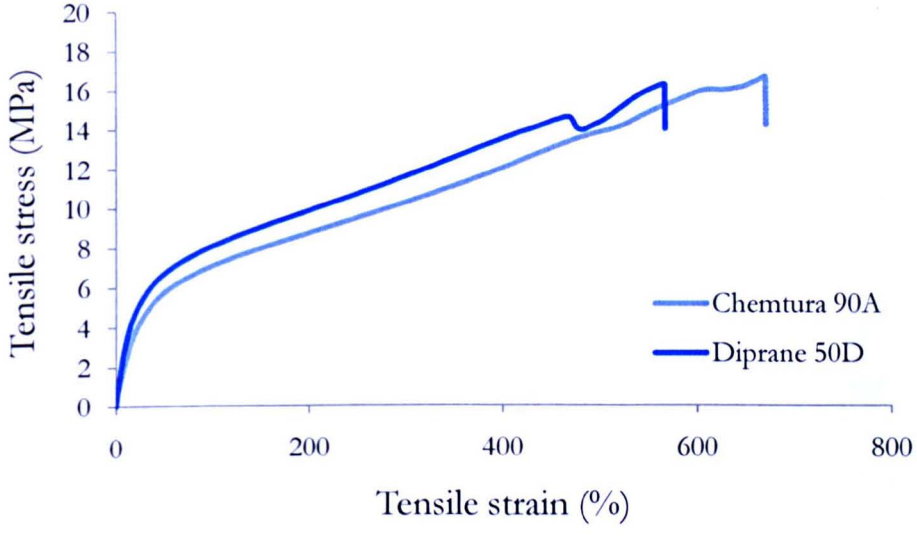

Figure 3.3 Stress- strain relationship curves for thermoset PUs. The tensile strain was measured as a percentage when a tensile stress (MPa) was applied to Chemtura 90A and Diprane 50D (n = 3).

Although, ultimate tensile stress was similar for both PUs, there was a difference in ultimate elongation (Table 3.4). As with the thermoplastic Shore hardness D PUs,

Diprane 50D failed before Chemtura 90A indicating that Chemtura 90A was more ductile. Stress was proportional to strain for both thermoset PUs when percentage elongation was compared.

Table 3.4 Mechanical properties of thermoset PUs (n=3)

	Chemtura 90A	Diprane 50D
Ultimate strength (stress), MPa	17	18
Ultimate elongation %	671	567
Tensile strength, MPa		
at 50% elongation	6	7
at 100% elongation	7	8
at 200% elongation	9	10
at 300% elongation	10	12
Young's modulus	0.3	0.4

The Young's modulus was plotted against the Shore hardness of the materials (Figure 3.4) from the data in Tables 3.2 and 3.3 which clearly shows the differences in material stiffness between the thermoset PUs and TPUs.

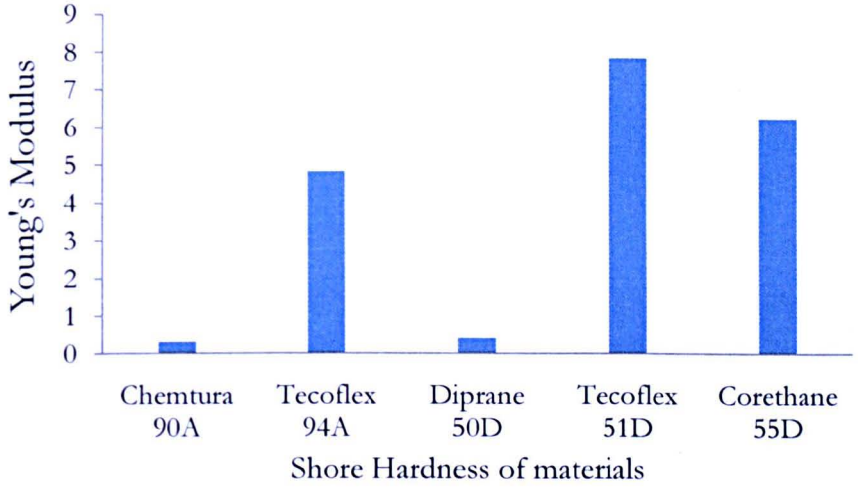

Figure 3.4 Mean Young's modulus for the thermoset PUs and TPUs (n=3)

3.4 Discussion

The Shore hardness A polyurethanes (PUs) were similar to those specified by the manufacturers, however, the Shore hardness D PUs differed. Diprane 50D was found to be much lower, suggesting that the material was softer than stated by the

manufacturer. This could be due to the high hardness values overlapping between Shore hardness A and D; so a 90A PU can exhibit a similar hardness to a 50D PU (Lambda *et al.*, 1989). Tecoflex 51D and Corethane 55D had significantly higher Shore hardness than Diprane 50D indicating they were harder materials.

The stress-strain relationships of the thermoplastic and thermoset PUs appeared to comply with Hooke's law during elastic deformation, in which the atoms with each material began to rearrange (Lambda *et al.*, 1989). At low stress and low strain the PUs acted as linear elastic solids as the chemical bonds within the PUs were being stretched (Lambda *et al.*, 1989). The area under each curve (Figure 3.5) also suggested that thermoplastic polyurethanes (TPUs) were tougher than the thermoset PUs, because the area under each curve was larger (Lambda *et al.*, 1989). The thermoset PUs adopted a stress-strain curve typical of elastomers (Lambda *et al.*, 1989), and the differences seen between both types of PUs could have been due to age. It was initially thought that temperature had contributed to the differences, because the tests in this study were performed at 21°C, however, the manufacturers and literature tests were performed at 23°C following the American Society for Testing and Materials (ASTM) D412 and British Standards ISO 2782, respectively. The ISO 2782 stated testing at room temperature and referred to BS ISO 23529 for correct temperature. This standard stated that normal laboratory temperature was 23°C in temperate countries (i.e. UK), ± 2°C. Therefore, the temperature at which the materials were tested in this study was within range and did not contribute to the differences seen.

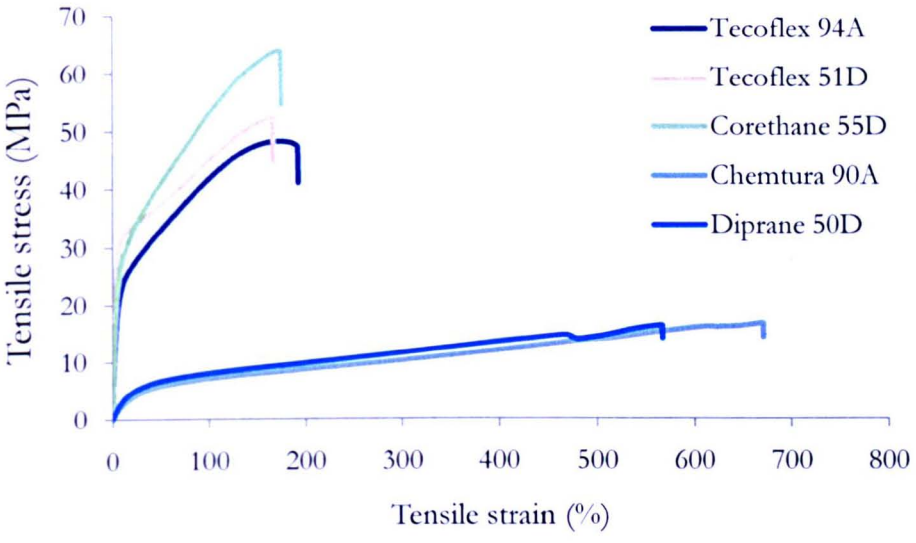

Figure 3.5 Stress-strain relationship curves for both thermoset and thermoplastic PUs (n = 3)

Beyond the elastic limit the PUs had permanently deformed (Figure 3.8). Tecoflex 94A and Chemtura 90A PUs had a higher percentage elongation (evident by an extended plastic region), suggesting they were more ductile compared to the other PUs. These larger plastic regions were indicative of softer materials (Lambda *et al.*, 1989). Diprane 50D also had a large plastic region suggesting the material was softer than the other D Shore hardness PUs, which correlated with the low Shore hardness measurement of 37D. The thermoset PUs experienced a decrease in tensile stress which, may have been due to the materials slipping between the pneumatic clamps before failure.

The Young's modulus results confirmed the TPUs were stiffer than the thermoset polyurethanes. During plastic deformation the atoms within the materials had rearranged due to the increasing stress with increasing elongation (strain). The Young's modulus results of the PUs were compared to the literature as seen in Table 3.5 and the experimental data did not correlate to the data from the literature.

Table 3.5 Literature and manufacturer's comparison of Young's modulus

Material	Young's Modulus (literature)	Young's Modulus
Tecoflex 94A	11.5 (†)	4.8
Tecoflex 51D	15 (††)	7.8
Corethane 55D	11.7-13.8 (††)	6.2
Diprane 50D	?	0.4
Chemtura 90A	?	0.3

† - Quigley *et al.*, 2002, †† - Lambda *et al.*, 1989

The reduced Young's modulus suggested a lack of stiffness in the PUs used in this study. The age of the PUs used in this study appeared to be a contributing factor of the reduced Young's modulus. Consequently, Young's modulus decreases as age of the materials increases. These materials were housed for some time in the School of Mechanical Engineering (University of Leeds) before being utilised in this study. Obtaining fresh material for this study was extremely difficult as well as acquiring confidentiality agreements.

The ultimate tensile strength (stress) of the thermoplastic and thermoset PUs were compared to those obtained from the literature and manufacturer's datasheets (Table 3.6). Even though the Young's modulus of the TPUs did not correlate with the literature, the ultimate tensile strength was very similar in comparison, suggesting a similar stress was applied to each material. Diprane 50D exhibited the same ultimate tensile strength as stated in the literature, however, there was almost a three-fold difference seen for Chemtura 90A.

Table 3.6 Literature and manufacturer's comparison of ultimate tensile strength

Material	Ultimate tensile strength (MPa) (literature)	Ultimate tensile strength (MPa) (experimental)
Tecoflex 94A	38 †, 56 ‡	41
Tecoflex 51D	42 ††, 57 ‡	45
Corethane 55D	48.2-58.6 ††, 60 ‡	55
Diprane D50	18 ‡	18
Chemtura A90	49.6 ‡	17

† - Quigley *et al.*, 2002, ‡ - Manufacturer's datasheets (see Appendix I), †† - Lambda *et al.*, 1989

The tensile stress applied to the PUs at various elongations (% strain) were not comparable to the manufacturer's data; stress being >three-fold higher for TPUs, >four-fold higher for Diprane 50D, however, Chemtura 90A had a closer relationship (albeit less applied stress) to the manufacturer's data (Table 3.7). The fact that an increased tensile stress was required to elongate the PUs (except Chemtura 90A) to 50%, 100% and 300% strain, suggested these materials were not particularly ductile.

Table 3.7 Manufacturer's comparison of tensile strength at different percentage strains

Material	Tensile strength at (manufacturer's information)	Tensile strength (experimental data)
Tecoflex 94A	11 at 100% strain	42 at 100% strain
Tecoflex 51D	12 at 100% strain	45 at 100% strain
Corethane 55D	12 at 50% strain 17 at 100% strain	41 at 50% strain 53 at 100% strain
Diprane D50	1.4 at 100% strain 2.6 at 300% strain	8 at 100% strain 11.5 at 300% strain
Chemtura A90	8.3 at 100% strain 10.3 at 200% strain 15.2 at 300% strain	7 at 100% strain 9 at 200% strain 10 at 300% strain

Experimental data for Young's modulus and stress at 50% and 100% strain were approximately two-fold higher than the data seen in Table 3.8, suggesting that the Tecoflex 94A used in this study was stiffer at higher strains. In comparison a higher stress was required to elongate the PU used in this study. As previously mentioned, the age of the Tecoflex 94A used in this study could account for the differences.

Table 3.8 Literature and experimental comparison of tensile stress and elongation for Tecoflex 94A

Material	Tecoflex 94A (Quigley *et al.*, 2002)	Tecoflex 94A (experimental)
Ultimate stress MPa	38.14	41
Ultimate elongation %	405	193
E modulus at 50% strain	20.49	40.19
E modulus at 100% strain	13.34	24.71
Stress at 50% strain	10.24	33
Stress at 100% strain	15.34	42

The ultimate elongation data for the TPUs were almost two-fold lower than the manufacturer's data, suggesting the materials used in this study were less ductile and thus, harder because ultimate elongation was lower (Table 3.9). Diprane 50D had a lower ultimate elongation compared to the manufacturer's stated value suggesting that it was less ductile. The Chemtura 90A PU was more ductile than stated by the manufacturer.

Table 3.9 Manufacturer's comparison of percentage ultimate elongation

Material	Ultimate elongation (%) (Manufacturer's data)	Ultimate elongation (%) (experimental data)
Tecoflex 94A	370	193
Tecoflex 51D	360	167
Corethane 55D	365	175
Diprane D50	700	567
Chemtura A90	525	671

As discussed earlier in this chapter, the composition of the PUs can alter mechanical and physical properties of the materials. It has been reported that aromatic isocyanates can increase the stiffness of polymer chains, while aliphatic isocyanates decrease the mechanical properties of a material (Lambda *et al.*, 1989). The diisocyanate, MDI (4,4'-diphenyl methane diisocyanate) is known to increase the physical properties of PUs, as do polyester polyols (Lambda *et al.*, 1989). However, PUs containing PTMEG (polytetramethylene ether) possess the greatest physical properties and have equivalent

mechanical properties to PUs containing polyester (Lambda *et al.*, 1989). Furthermore, aliphatic chain extenders have been used to develop softer PUs (Lambda *et al.*, 1989). It was not possible to find information regarding the concentration of each component and, therefore, relating the mechanical differences to the components was not feasible.

3.5 Conclusions

Thermoplastic polyurethanes had a higher stiffness than the thermoset polyurethanes, possibly due to the age of the materials or type of processing. However, the thermoplastic polyurethanes were less stiff and less ductile compared to results from manufacturer's data sheets and literature, indicating these polyurethanes lose their mechanical properties over time.

Chapter Four

Friction Characteristics of Articular Cartilage and Cartilage Substitution Biomaterials

4.1 Introduction

The coefficient of friction for articular cartilage (AC) has been investigated for many years, because of the low friction environment that exists between the two bearing surfaces within diarthrodial joints. It has been reported that articular cartilage exhibits a coefficient of friction between 0.002-0.3, which is time- and load-dependent (Forster and Fisher, 1996). Friction is defined by Amonton's law (see equation 4.1) which explains that friction force is relative to the applied load but, does not rely on the contact area, and dynamic friction does not depend on the sliding speed (velocity) (Bhushan, 2002).

$$F = \frac{\mu}{N} \tag{4.1}$$

Where, F is the frictional force, N is normal load and, μ is the coefficient of friction. However, Amonton's law does not account for lubricated surfaces and only applies to dry friction. Addition of a lubricant significantly changes the tribology of a material. The load- and time-dependent response of cartilage comes from the biphasic and viscoelastic properties of articular cartilage. Collagen fibers are viscoelastic in nature (Stoltz, 2004) and, play a dominant role in the viscoelastic shear modulus of cartilage (Hayes and Bodine, 1978), while proteoglycans have an elastic role within the tissue structure (Stoltz, 2004). The elastic modulus (also known as the aggregate modulus) is also an important property of articular cartilage, which is related to viscoelasticity; the initial elastic modulus is exhibited by the initial resistance to compression by the fluid phase when load is applied,

however, the depth-dependent share of its stiffness is governed by the equilibrium modulus (McCredie *et al.*, 2009).

Polyurethanes (PUs) have previously been used in clinical applications and exhibit extremely good mechanical and biocompatible properties (Santerre *et al.*, 2005). These materials are composed of a diisocyanate, a chain extender (collectively forming the hard segment) and a polyol (soft segment). The hard segments are dispersed within a soft segment matrix, which is somewhat mobile (Lambda *et al.*, 1998). The hard and soft segments of PUs can be exposed to the material surface depending on the environment at the interface. Therefore, the surface arrangements of these segments can determine the host response to the material (Santerre *et al.*, 2005), and possibly affect friction characteristics. Hydrogels are currently being utilised for biomedical and pharmacological applications. They have also been used in various applications from scaffolds in cartilage replacement to reconstruction. Polyvinyl alcohol (PVA) hydrogels are known for their good biocompatibility, chemical stability and superior hydrophilicity. These materials contain strong hydrogen bonds resulting in inadequate lubricating properties, however, this can be significantly improved by the addition of other compounds or hydrogels such as polyvinyl pyrrolidone (PVP), which is soluble in water and has good biocompatible properties (Zheng *et al.*, 2008). Pure PVA hydrogels have weak mechanical properties, and so are crosslinked to improve their stability, and addition of PVP can improve the mechanical properties of these gels (Katta *et al.*, 2006). The swelling ability of hydrogels allows them to hold large amounts of water and therefore they have been likened to native articular cartilage (Cheung *et al.*, 2007).

Similar to articular cartilage, PUs and hydrogels are viscoelastic materials, which owe this property to the components within their structure. Hydrogels and articular cartilage are biphasic materials (fluid phase and solid phase), which hold large amounts of water. Water accounts for 60-80% of AC (Buckwalter *et al.*, 1997) and 65-72% of hydrogels (Fray *et al.*, 2007) [used in the present study]. PUs are hygroscopic materials but do not hold the same amount of water as AC or hydrogels. However, the dispersed hard segments in the somewhat mobile soft segment matrix may be considered as 'biphasic'. As previously mentioned, lubrication can alter the tribological properties of a material and the mode of lubrication can be determined from the coefficient of friction as a function of the Hersey number in the Stribeck curve (Gleghorn and Bonassar, 2008). The Stribeck curve

represents the dependence of friction coefficient to the Hersey number; $\eta\upsilon/p$ (applied load p [MPa], sliding velocity υ [rpm], and the viscosity of the lubricant η [Pa s]). However, the sliding velocity has a direct affect on the friction of the two surfaces by increasing the thickness of the fluid film as load increases, as can be seen in Figure 4.1 (Gleghorn and Bonassar, 2008).

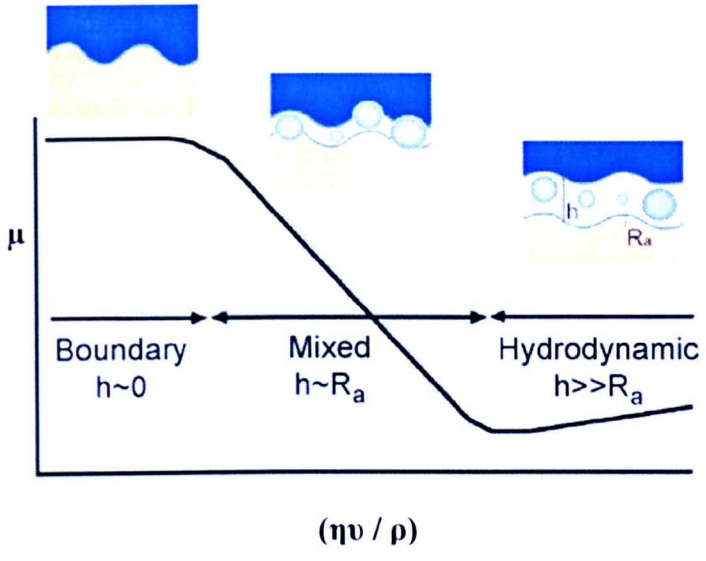

Figure 4.1 Stribeck curve indicating the relationship between coefficient of friction, normal load speed and viscosity of the lubricant (Gleghorn and Bonassar, 2008).

The slope at zero indicates boundary lubrication in which the surface asperities meet (increasing friction thus wear) due to the lack of fluid film. The slope begins to decline as friction decreases in a mixed lubrication system because the fluid film is the same thickness (h) as the surface roughness (Ra) of the opposing surfaces, however, a little asperity contact still exists. Hydrodynamic lubrication exists when the fluid thickness is higher than the Ra due to the complete separation of surfaces thereby, maintaining low friction (Tu and Fort, 2004; Gleghorn and Bonassar, 2008).

The aim of this chapter was to investigate the friction characteristics of thermoset (Diprane 50D a polyether and Chemtura 90A a polyester) and TPUs (Corethane 55D, Tecoflex 51D and Tecoflex 94A). The friction characteristics of three hydrogels were also evaluated; H2A (28% (w/v) PVA), H1B (25% (w/v) PVA + (v/v) 7% gluconic acid) and, H2B (28% (w/v) PVA + 7% (v/v) gluconic acid). The hydrogels were composed of a PVA/PVP

mixture and the incorporation of gluconic acid increased the porosity of the hydrogel network (Fray *et al.*, 2007). All materials were compared to native articular cartilage (negative control) and ultra high molecular weight polyethylene (positive control). Many research groups have explored the tribological properties of ultra high molecular weight polyethylene, thus this was an appropriate material to use as a comparative control.

4.2 Materials and Methods

A single station multidirectional pin-on-plate friction rig (however, unidirectional motion was used throughout this chapter) was used as described in Section 2.4.11, to determine the frictional characteristics of the Polyvinyl alcohol/polyvinyl pyrrolidone hydrogel pins (Sections 2.3.7; Appendix I for supplier), native articular cartilage pins and plates (Section 2.3.1), thermoset (Diprane 50D and Chemtura 90A), and thermoplastic (Corethane 55D, Tecoflex 51D and Tecoflex 94A) polyurethane (PU) pins and plates (Sections 2.3.5 and 2.3.4; Appendix I for suppliers). All pins were reciprocated against articular cartilage plates and smooth (Ra = 0.01 - 0.03 μm) stainless steel plates (Section 2.3.9), however, stainless steel pins (Section 2.3.9.1) and PUs plates were used in some tests. All friction tests (refer to Tables 2.4 to 2.6) with an articular cartilage sample (pin or plate) were performed using phosphate buffered saline (PBS) as the lubricant (Section 2.2.2). For material combinations (refer to Tables 2.5 to 2.6) in the absence of articular cartilage (Section 2.3.1) PBS + 25% (v/v) FBS (Section 2.2.4) was the lubricant of choice because the materials did not have surface proteins to aid with lubrication, unlike the articular cartilage samples.

An indentation rig (Section 2.4.3) was utilised to establish the deformation of the materials, while the recovery rate of all materials was investigated by loading the pins in a six station multidirectional pin-on-plate wear rig (as described in Sections 2.4.5.1. and 2.4.5.1.3) using PBS as a lubricant (Section 2.2.2). The contact angles of the PUs were established using a Microdrop Analyser (Section 2.4.4). The surface roughness of the pins and plates were measured using a contacting talysurf profilometer (Sections 2.4.12.1 to 2.4.12.15) and a non-contacting white light interferometer (Sections 2.4.12.2 to 2.4.12.3).

4.3 Results

4.4.1 Deformation of materials

Articular cartilage (AC) pins were indented with a 3 mm diameter flat indentor (in PBS), resulting in a contact pressure of 0.25 MPa. The deformation was determined by the difference between time zero (the point at which the indentor had contacted the surface of the pins) and 1 h (hour). The cartilage deformed quickly at the start of the test until steady state was achieved at approximately 40 minutes (Figure 4.2). The average deformation was 0.30 mm over a time period of 1 h.

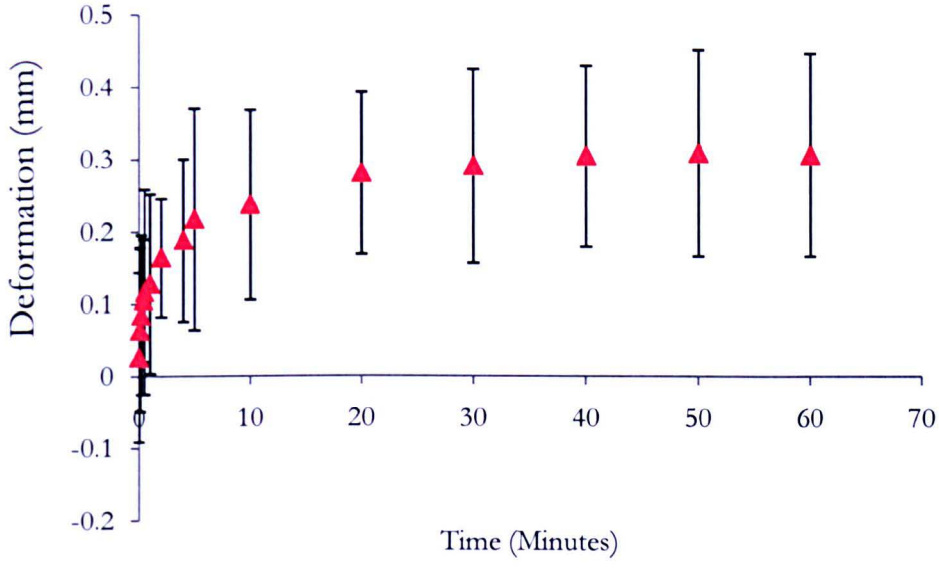

Figure 4.2 Deformation of AC (n=3) over 1 h in PBS. Error bars: 95% confidence limits.

A contact pressure of 0.25 MPa was applied to the thermoset and AC pins (n=3) using a 3 mm diameter flat indentor for 1 h in PBS. The deformation of the thermoset polyurethanes (PUs) appeared to occur at the beginning of the test while, cartilage deformation continued for a longer period (Figure 4.3). The average deformation of Diprane 50D and Chemtura 90A were 0.02 mm and 0.02 (respectively) compared to an average deformation of 0.3 mm for AC. The deformation of AC was significantly higher than Diprane 50D and Chemtura 90A between 1 minute to 60 minutes ($p < 0.05$; ANOVA).

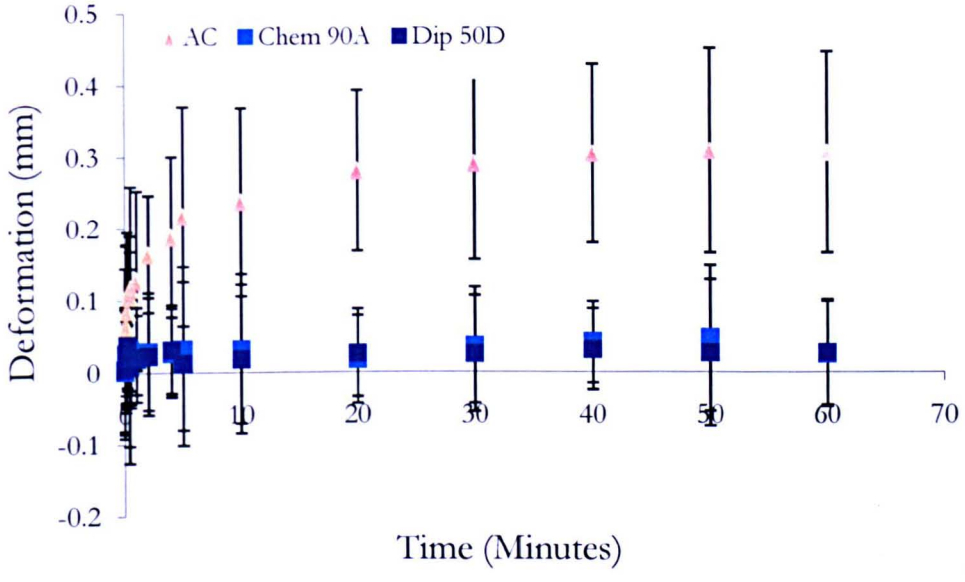

Figure 4.3 Comparison of deformation between Diprane 50D (Dip 50D), Chemtura 90A (Chem 90A) and articular cartilage (AC), over 1 h in PBS. Data was analysed by ANOVA which revealed a significant difference ($p < 0.05$) between articular cartilage and the other materials at 1 to 60 minutes. Data is expressed as mean (n=3) ± 95% confidence limits.

A contact pressure of 0.25 MPa was applied to thermoplastic pins (immersed in PBS) with a 3 mm diameter flat indentor for 1 h. The deformation of AC was significantly higher than the thermoplastic PUs between 2 to 60 minutes [$p < 0.05$; ANOVA] (Figure 4.4). However, as with the thermoset PUs, the thermoplastic PUs deformed quickly at the start of the test. The thermoplastic PUs had an average deformation of 0.04 mm (Corethane 55D), 0.06 mm (Tecoflex 94A) and, 0.12 mm (tecoflex 51D), all of which were lower than articular cartilage (0.3 mm).

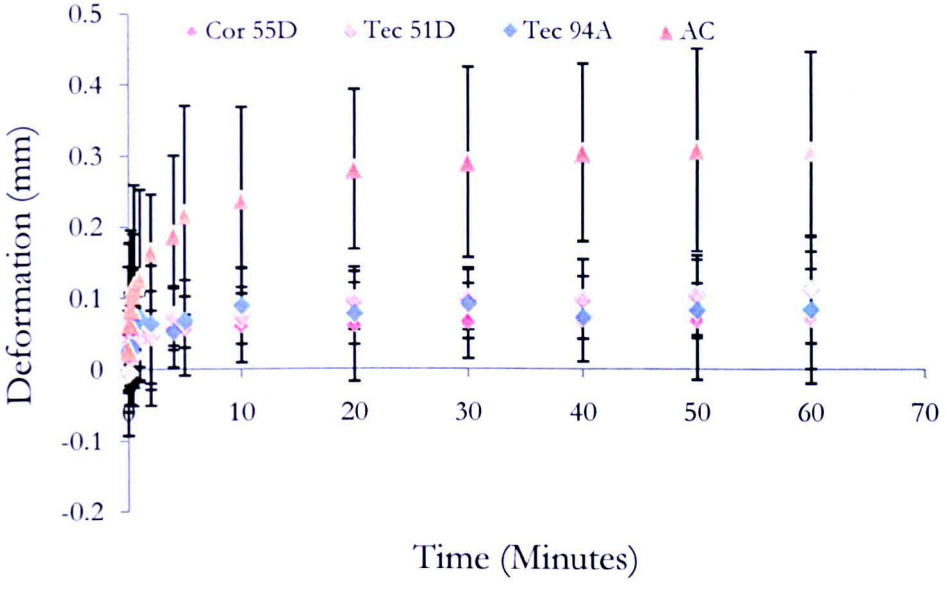

Figure 4.4 Comparison of deformation between Corethane 55D (Cor 55D), Tecoflex 51D (Tec 51D), Tecoflex 94A (Tec 94A) and articular catilage (AC), over 1 h in PBS. Data was analysed by ANOVA which revealed a significant difference ($p < 0.05$) between articular cartilage and the other materials at 2 to 60 minutes. Data is expressed as mean (n=3) ± 95% confidence limits.

The applied contact pressure for AC pins was 0.25 MPa, while a contact pressure of 0.126 MPa was applied to the PVA/PVP hydrogels. All pins were immersed in PBS throughout the 1 hour period. No significant differences ($p > 0.05$; ANOVA) were seen between the PVA/PVP hydrogels and AC (Figure 4.5). However, the average deformation of the PVA/PVP hydrogels was 0.19 mm for H1B, 0.17 mm for H2B and, 0.20 mm for H2A over a period of 1 h, compared to 0.30 mm for articular cartilage.

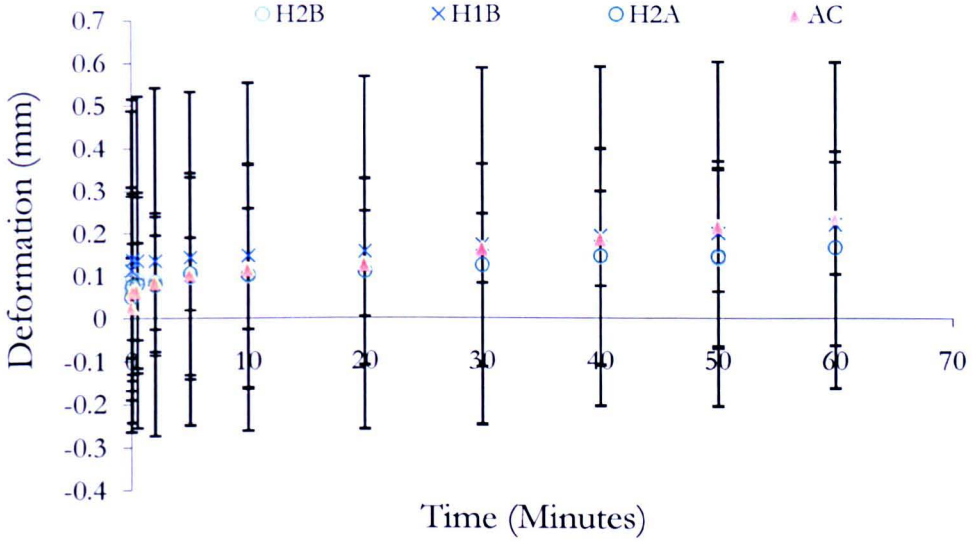

Figure 4.5 Comparison of deformation between hydrogels H1B, H2B, H2A and articular cartilage (AC), over 1h in PBS. ANOVA ($p > 0.05$) revealed no differences.

4.4.2 *Material deformation and recovery measurements*

The average depth of the articular cartilage (AC) was 1.24 mm (n = 3, ± 0.18, 95% CL), before testing. The percentage change in depth of the AC (n = 3) in terms of reduction, recovery and permanent deformation is shown in Figure 4.6. After 1 h of loading in PBS at 160 N (2.5 MPa contact pressure) the mean reduction in depth was 53.66% (± 2.98), however, the AC recovered by 46.98% (± 6.62) of the original depth, 1 h after the removal of the load. This resulted in a permanent deformation of 6.34% (± 7.6) of the AC that did not fully recover.

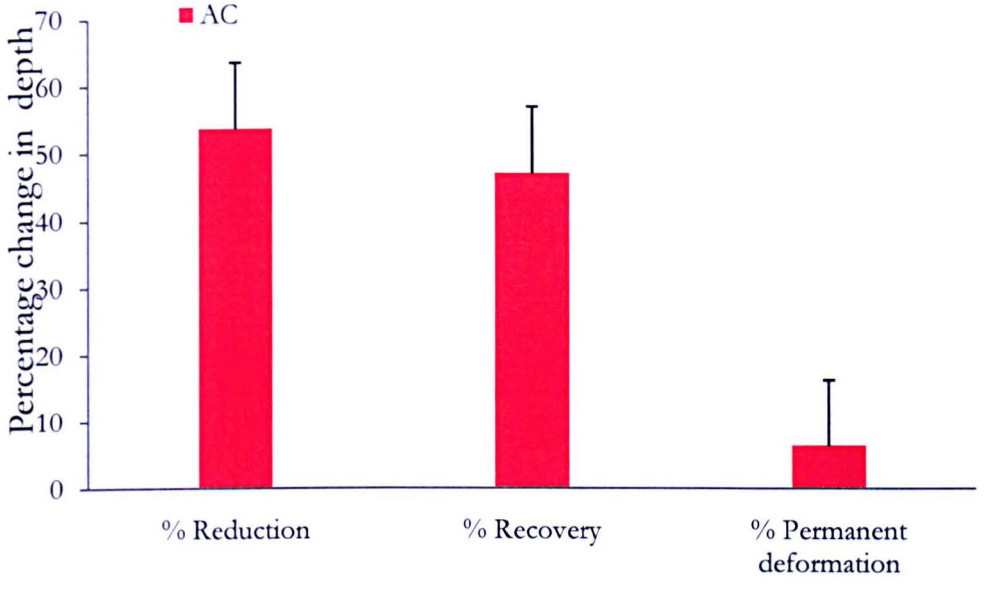

Figure 4.6 Average percentage change of articular cartilage depth in terms of reduction, recovery and permanent deformation after 1 h of loading at a contact stress of 2.5 MPa. Data is expressed as mean (n=3) ± 95% confidence limits.

The average depth of the thermoset polyurethanes (PUs) before the test was 12.29 mm ± 0.01 (n = 3, 95% CL) for Corethane 55D pins, 12.28 mm ± 0.07 (n = 3) for Tecoflex 94A pins and, 12.29 mm ± 0.01 (n = 3) for Tecoflex 51D pins (Figure 4.7). The percentage reduction after 1 h of loading in PBS with 160 N load (2.5 MPa contact stress) for Corethane 55D, Tecoflex 94A and Tecoflex 51D was 0.41% (± 0.31), 0.45% (± 1.18) and, 1.50% (± 1.10), respectively. The thermoplastic polyurethanes (TPUs) were allowed to recover over a 1 h period after removal of the load, which resulted in 0.24% (± 0.21) recovery for Corethane 55D, 0.45% (± 0.73) for Tecoflex 94A and, 1.23% (± 0.73) recovery for Tecoflex 51D. The permanent deformation for Corethane 55D was 0.16% (± 0.30), Tecoflex 94A was 0.12% (± 0.10) and Tecoflex 51D had a permanent deformation of 0.29% (±0.40). There were no significant differences between the TPUs for percentage reduction, recovery or permanent deformation ($p > 0.05$; ANOVA).

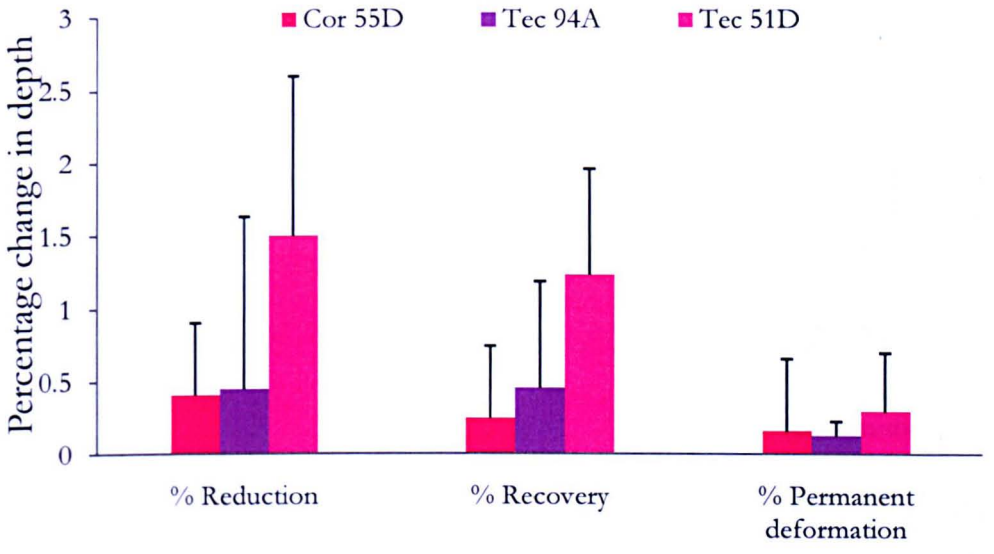

Figure 4.7 Average percentage change of TPU depth in terms of reduction, recovery and permanent deformation after 1 h of loading at a contact stress of 2.5 MPa. AC, articular cartilage; Cor 55D, Corethane 55D; Tec 94A, Tecoflex 94A; Tec 51D, Tecoflex 51D. ANOVA ($p > 0.05$) revealed no differences. Data is expressed as mean (n=3) ± 95% confidence limits.

The average depth of the thermoset PUs before the test were 7.04 mm (n = 3, ± 0.16) for Diprane 50D pins and, 6.98 mm (n = 3, ± 0.02) for Chemtura 90A pins. Loading the thermoset PUs for 1 h in PBS at 160 N (2.5 MPa contact stress) reduced the depth of Diprane 50D and Chemtura 90A by 0.54 (± 1.68%) and 0.33 (± 0.62%), respectively (Figure 4.8). Upon removal of the load, Diprane 50D and Chemtura 90A had recovered over a period of 1 h by 0.27 ± 0.67% and 0.44 ± 0.63% (respectively) of the original depth. Diprane 50D had permanently deformed by 0.85 (± 1.08%) while, Chemtura 90A had deformed permanently by 0.65 (± 0.58%). No significant differences were found between the thermoset polyurethanes for percentage reduction, recovery or permanent deformation ($p > 0.05$; ANOVA).

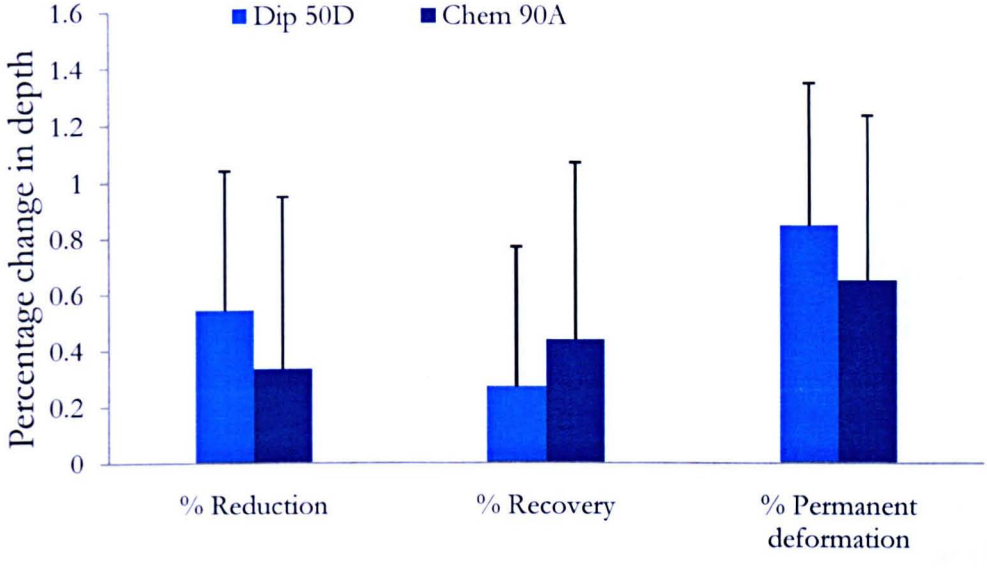

Figure 4.8 Percentage change of thermoset polyurethane depth in terms of reduction, recovery and permanent deformation after 1 h of loading at a contact stress of 2.5 MPa. Dip 50D, Diprane 50D; Chem 90A, Chemtura 90A. ANOVA ($p > 0.05$) revealed no differences. Data is expressed as mean (n=3) ± 95% confidence limits.

The average depth of the PVA/PVP hydrogels before each test was 10.41 mm ± 0.22 (n = 3) for H1B, 9.94 mm ± 2.03 (n = 3) for H2B and, 10.56 mm (n = 3, ± 0.64) for H2A. After 1 h of loading in PBS with a load of 80 N (1.26 MPa contact stress) H1B had reduced by 3.14 (± 4.60%), H2B had reduced by 3.07 (± 4.30%), and H2A had reduced by 3.71 (± 1.10%). After removing the load, H1B, H2B and H2A had recovered by 2.06% ± 3.36, 0.53% ± 1.21, and 1.4% ± 1.34 (respectively) of the original depth (Figure 4.9). While the permanent deformation was 1.36 (± 0.37%) for H1B, 2.52 (± 4.64%) for H2B and, 2.33 (± 1.94%) for H2A. There were no significant differences between the PVA/PVP hydrogels for percentage reduction, recovery or permanent deformation ($p > 0.05$; ANOVA).

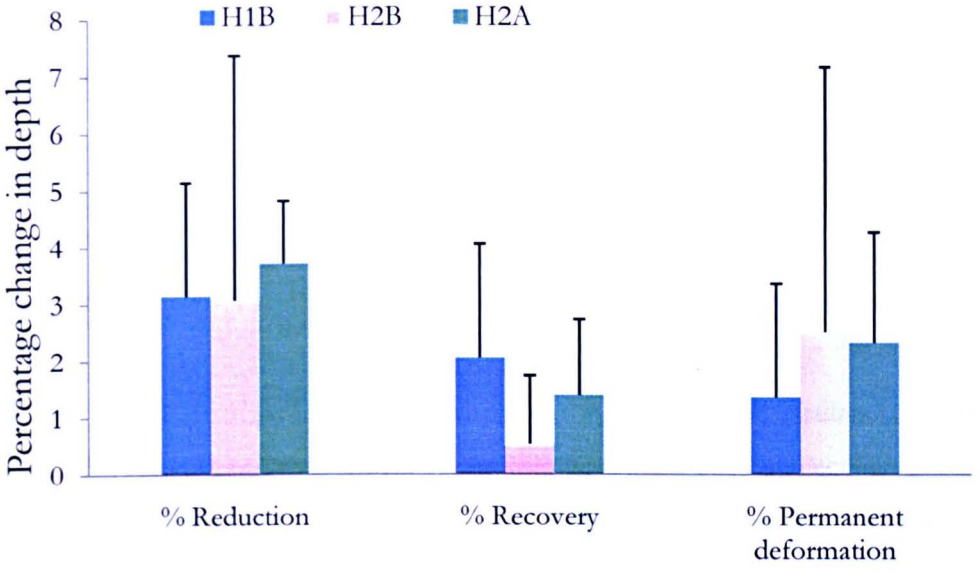

Figure 4.9 Percentage change of PVA/PVP hydrogel depth in terms of reduction, recovery and permanent deformation after 1 h of loading at a contact stress of 1.26 MPa. ANOVA ($p > 0.05$) revealed no differences. Data is expressed as mean (n=3) ± 95% confidence limits.

The permanent deformation of all the materials was normalised to the full pin height (i.e. the full height of the AC pin including the underlying bone). The AC pin had a significantly higher permanent deformation compared to all other materials and PVA/PVP hydrogel, H1B was significantly higher than Chemtura 90A. H2A had a significantly higher normalised permanent deformation compared to Diprane 50D, Chemtura 90A, Corethane 55D and Tecoflex 94A (Figure 4.10).

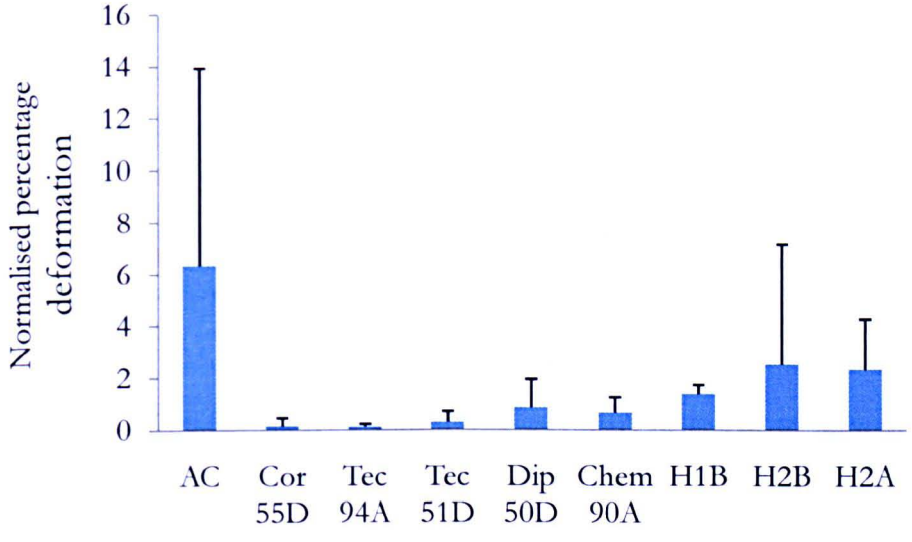

Figure 4.10 Normalised percentage deformation for AC (articular cartilage), Chem 90A (Chemtura 90A), Dip 50D (Diprane 50D), Cor 55D (Corethane 55D), Tec 94A (Tecoflex 94A), Tec 51D (Tecoflex 51D), and PVA/PVP hydrogels (H1B, H1B and H2A) after 1 h loading in PBS. Data was analysed by ANOVA ($p < 0.05$) which revealed differences between articular cartilage and all other groups, H1B between Chemtura 90A and H2A between Diprane 50D, Chemtura 90A, Corethane 55D and Tecoflex 94A. Data is expressed as mean (n=3) ± 95% confidence limits.

4.4.3 Coefficient of friction

4.4.3.1 Short term tests – articular cartilage counterfaces

Thermoset polyurethane (PU) pins were reciprocated against articular cartilage (AC) plates in phosphate buffered saline (PBS), for 1 h with a 160 N load resulting in a contact stress of 2.5 MPa (Figure 4.11). An initial increase in friction was seen (Figure 4.11) before steady state was reached for all groups except the negative control (AC pin on AC plate; AC-AC). The friction coefficient of polyethylene (PE) pins (positive control) was significantly higher than the negative control ($p<0.05$; ANOVA). The coefficient of friction for Diprane 50D was significantly higher than AC-AC for the first 25 minutes ($p < 0.05$; ANOVA), while the coefficient of friction for Chemtura 90A was significantly higher than AC-AC between 1.75 and 25 minutes [$p > 0.05$; ANOVA] (inclusive). Throughout the 1 h test no significant variations were found between the coefficient of friction for Diprane 50D, PE and Chemtura 90A.

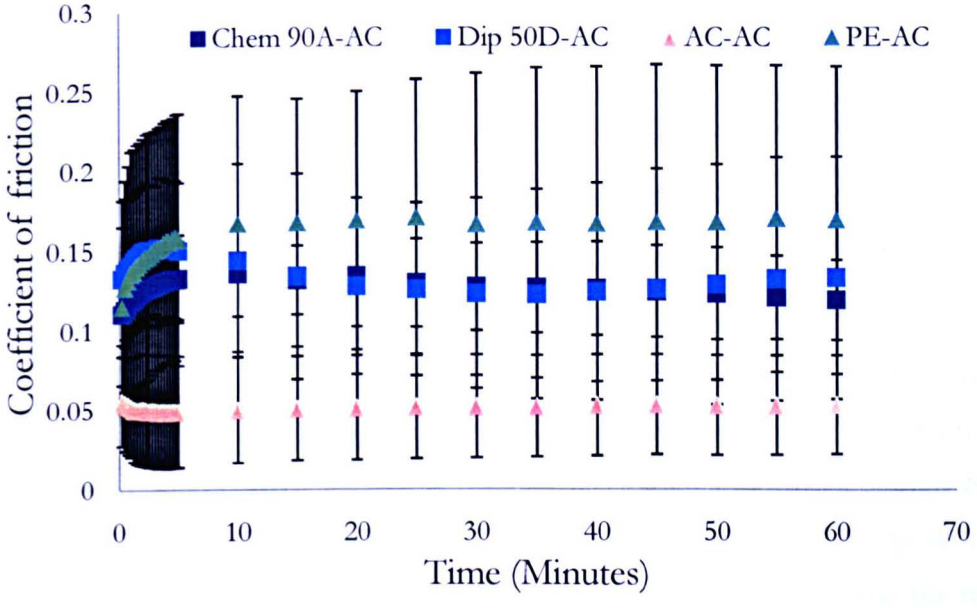

Figure 4.11 Polyethylene, PE (positive control), articular cartilage, AC (negative control), Chemtura 90A (Chem 90A) and, Diprane 50D (Dip 50D) pins reciprocated against articular cartilage plates over a sliding distance of 10 mm at 4 mm s^{-1} for 1 h in PBS at a contact stress of 2.5 MPa. Data was analysed by ANOVA which revealed a significant difference ($p < 0.05$) between articular cartilage and Diprane 50D at 0.25 to 25 minutes, and Chemtura 90A at 1.75 to 25 minutes. Data is expressed as mean (n=6) ± 95% confidence limits.

Thermoplastic polyurethane (TPU) pins were articulated against AC plates for 1 h in PBS with a 160 N load resulting in a contact stress of 2.5 MPa (Figure 4.12). The coefficients of friction for the TPUs followed the same trend as the negative control (AC-AC) and were not significantly different to the negative control. However, the friction coefficient of the positive control (PE-AC) was significantly higher than negative control, Corethane 55D-AC and, Tecoflex 94A-AC throughout the 1 h test. Furthermore, friction of the positive control was significantly higher than Tecoflex 51D-AC between 3 and 25 minutes (inclusive). There were no significant differences in friction between the TPUs against AC plates.

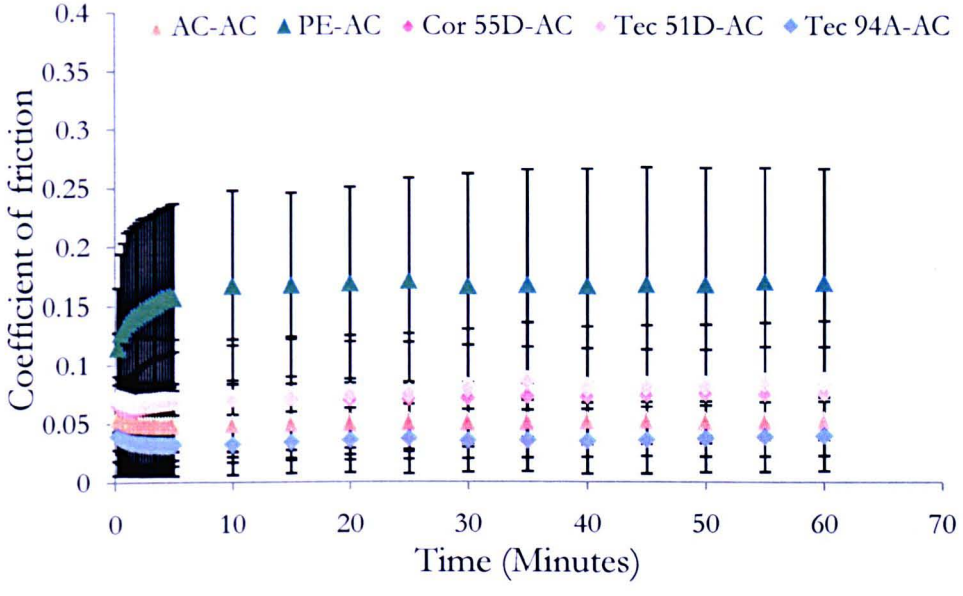

Figure 4.12 Polyethylene, PE (positive control), articular cartilage, AC (negative control), Corethane 55D (Cor 55D) Tecoflex 51D (Tec 51D) and, Tecoflex 94A (Tec 94A) pins reciprocated against articular cartilage plates over a sliding distance of 10 mm at 4 mm s^{-1} for 1 h in PBS at a contact stress of 2.5 MPa. Data was analysed by ANOVA which revealed a significant difference ($p < 0.05$) between the positive control and the negative control at 0.25 to 60 minutes, Tecoflex 51D-AC at 3 to 25 minutes. Data is expressed as mean (n=6) ± 95% confidence limits.

All PVA/PVP hydrogel pins (n = 3) were reciprocated against AC plates in PBS under an 80 N load (contact stress was 1.26 MPa), for 1 h and compared to the negative control and positive control, which were reciprocated against AC plates for a period of 1 h in PBS under a 160 N load (Figure 4.13). Although the coefficient of friction for the PVA/PVP hydrogels was higher than AC-AC (negative control), no significant differences in the friction of the PVA/PVP hydrogels were evident when compared to each other and to the positive and negative controls ($p > 0.05$; ANOVA).

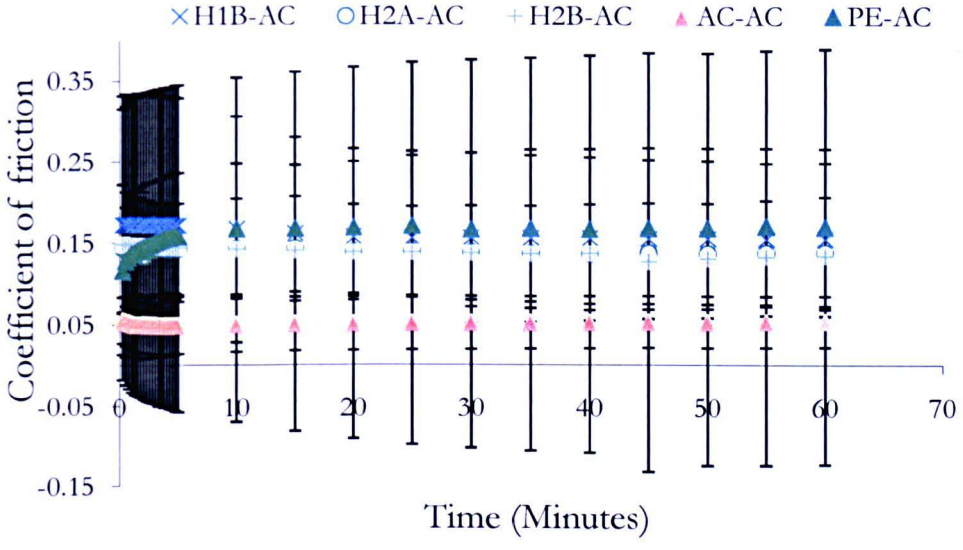

Figure 4.13 Polyethylene, PE (positive control), articular cartilage, AC (negative control), H1B, H2B and H2A pins reciprocated against articular cartilage plates over a sliding distance of 10 mm at 4 mm s^{-1} for 1 h in PBS at a contact stress of 1.26 MPa (2.5 MPa for AC-AC and PE-AC). ANOVA ($p < 0.05$) revealed no differences. Data is expressed as mean (n=3) ± 95% confidence limits.

4.4.3.2 *Short term tests – Stainless steel counterfaces*

Thermoset polyurethanes (PUs) , articular cartilage (AC) and polyethylene (PE) pins (n = 6) were reciprocated against smooth stainless steel (SS) plates (Ra = 0.01-0.03 μm) under a 160 N load (contact stress was 2.5 MPa) for 1 h in PBS (Figure 4.14). The thermoset polyurethanes (PUs) increased in friction at the start of the test before reaching steady state friction, however, Diprane 50D-SS reached steady state friction before Chemtura 90A-SS. The coefficient of friction for Diprane 50D-SS was significantly higher than that of Chemtura 90A-SS for the first half of the test period (to 30 minutes) [$p < 0.05$; ANOVA]. The negative control (AC-SS) continued to increase in friction throughout the test period while, the positive control (PE-SS) reached steady state early in the test (from 10 minutes). The coefficients of friction for Chemtura 90A-SS and Diprane 50D-SS were significantly higher ($p < 0.05$; ANOVA) than the positive and negative controls throughout the 1 h period. The negative control (AC-SS) was significantly higher than positive control (PE-SS) from 35 minutes until the end of the test period.

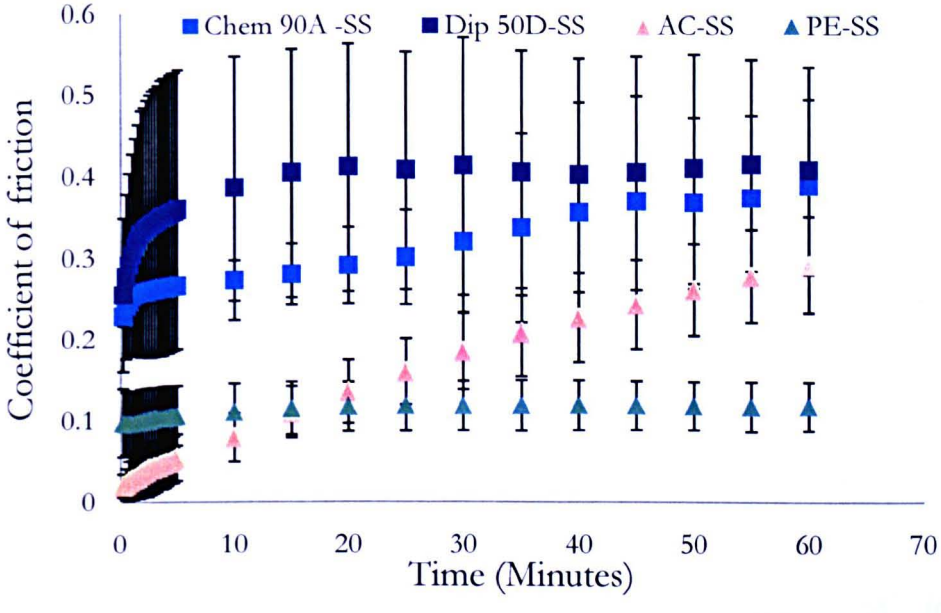

Figure 4.14 Polyethylene, PE (positive control), articular cartilage, AC (negative control), Chemtura 90A (Chem 90A) and, Diprane 50D (Dip 50D) pins reciprocated against stainless steel (SS) plates over a sliding distance of 10 mm at 4 mm s^{-1} for 1 h in PBS + 25% (v/v) FBS at a contact stress of 2.5 MPa. Data was analysed by ANOVA which revealed a significant difference ($p < 0.05$) between Diprane 50D-SS and Chemtura 90A-SS at 0.25 to 30 minutes, between the thermoset polyurethanes and the PE and AC at 0.25 to 60 minutes and between articular cartilage and PE at 35 to 60 minutes. Data is expressed as mean (n=6) ± 95% confidence limits.

AC pins were reciprocated against smooth stainless steel plates (Ra = 0.01–0.03 μm) with a 160 N load (contact stress was 2.5 MPa), for 1 h in PBS (Figure 4.15). PE and thermoplastic polyurethanes (TPU) pins were reciprocated against smooth stainless steel plates in PBS + (v/v) 25% foetal bovine serum (FBS) under a load of 160 N. The coefficient of friction for negative control (AC-SS) became significantly higher than Tecoflex 51D-SS, Tecoflex 94A-SS and positive control (PE-SS) from 35 minutes to the end of the test period, while the negative control (AC-SS) friction was only significantly higher than Corethane 55D-SS for the last 10 minutes of the test. The coefficient of friction for Corethane 55D-SS was significantly higher than the positive control (PE-SS) for the first 3.25 minutes while the coefficient of friction for Tecoflex 51D-SS and Tecoflex 94A-SS were higher than the positive control for the first 1.25 minutes of the test period. However, the coefficients of friction for the TPUs were significantly higher than the negative control for the first 10 minutes of the 1 h period. No significant differences were seen between the coefficient of friction for TPUs.

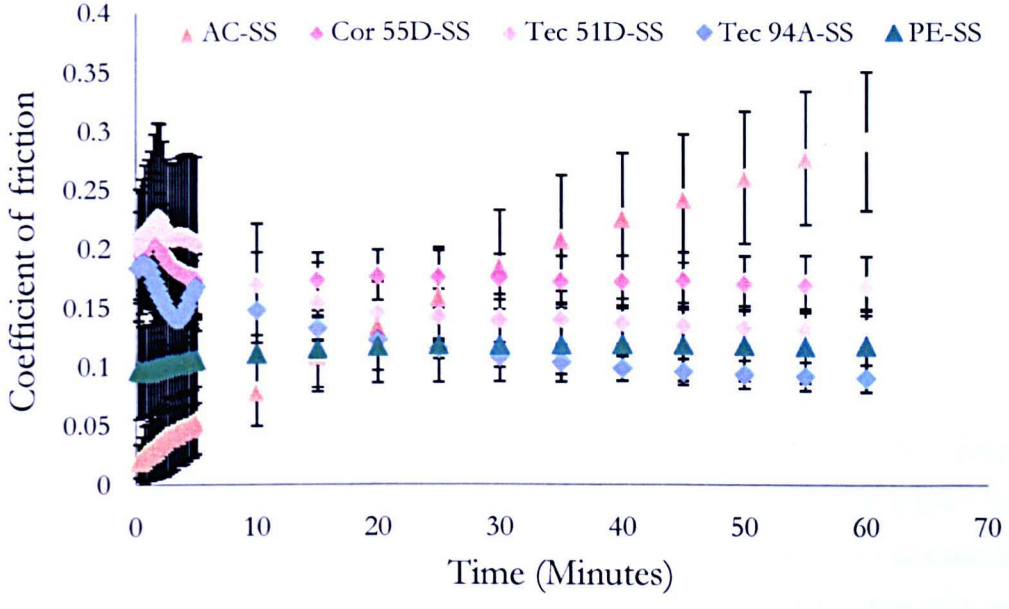

Figure 4.15 Polyethylene, PE (positive control), articular cartilage, AC (negative control), Corethane 55D (Cor 55D) Tecoflex 51D (Tec 51D) and, Tecoflex 94A (Tec 94A) pins reciprocated against stainless steel (SS) plates over a sliding distance of 10 mm at 4 mm s^{-1} for 1 h in PBS + 25% (v/v) FBS at a contact stress of 2.5 MPa. Data was analysed by ANOVA which revealed a significant difference ($p < 0.05$) between the articular cartilage and Tecoflex 51D, Tecoflex 94A and PE at 35 to 60 minutes, between AC and Corethane 55D at 50 to 60 minutes. Data is expressed as mean (n=6) ± 95% confidence limits.

All the hydrogel pins (n = 3) were articulated against smooth stainless steel plates (Ra = 0.01-0.03 μm) in PBS under an 80 N load (contact stress was 1.26 MPa), for 1 h. AC and PE pins (n = 6) were reciprocated against smooth stainless steel plates (Ra = 0.01-0.03 μm) for a period of 1 h in PBS under a 160 N load (Figure 4.16). When compared to the negative and positive controls no significant differences were evident. However, the coefficient of friction of H2B-SS was significantly higher than H1B-SS for the first 5 minutes and H2A-SS throughout the test period. The coefficient of friction of H1B-SS was significantly higher than H2A-SS for the full duration of the test and higher than H2B-SS between 10 and 60 minutes.

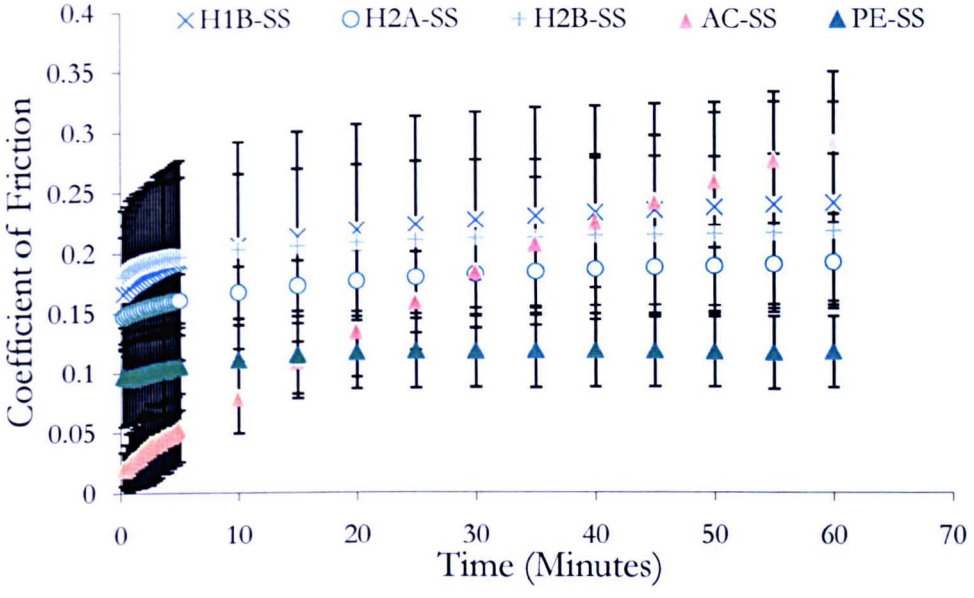

Figure 4.16 Polyethylene, PE (positive control), articular cartilage, AC (negative control), H1B, H2B and H2A pins reciprocated against stainless steel (SS) plates over a sliding distance of 10 mm at 4 mm s^{-1} for 1 h in PBS + 25% (v/v) FBS . at a contact stress of 1.26 MPa (2.5 MPa for AC-SS and PE-SS). Data was analysed by ANOVA which revealed a significant difference ($p < 0.05$) between the H2B and the H1B at 0.25 to 5 minutes, H2A at 0.25 to 60 minutes and between H1B and H2A at 0.25 to 60 minutes, and H2B at 10 to 60 minutes. Data is expressed as mean (n=3) ± 95% confidence limits.

4.4.3.4 Short term friction tests – polyurethane counterfaces

Articular cartilage pins were reciprocated against thermoset and TPU plates and compared to the positive control (AC-SS) and negative control (AC-AC). All tests were performed in

PBS with a 160 N load (contact stress was 2.5 MPa), for 1 h. All groups increased in friction throughout the test (Figure 4.17). The coefficient of friction for AC-Corethane 55D was significantly higher than AC-Chemtura 90A, AC-Diprane 50D and AC-SS for the first 0.5 minutes. The coefficient of friction for Tecoflex 94A was significantly higher than Chemtura 90A and Diprane 50D the first 2 minutes and 0.5 minutes, respectively. Tecoflex 94A was also significantly higher in friction than the positive control (AC-SS) for the first 0.5 minutes. The coefficient of friction for AC-SS (positive control) and AC-Chemtura 90A was significantly higher than the negative control (AC-AC) from 10 and 20 minutes (respectively) to 60 minutes. However, between 15 and 60 minutes, all the other groups exhibited significantly higher friction than the negative control (AC-AC).

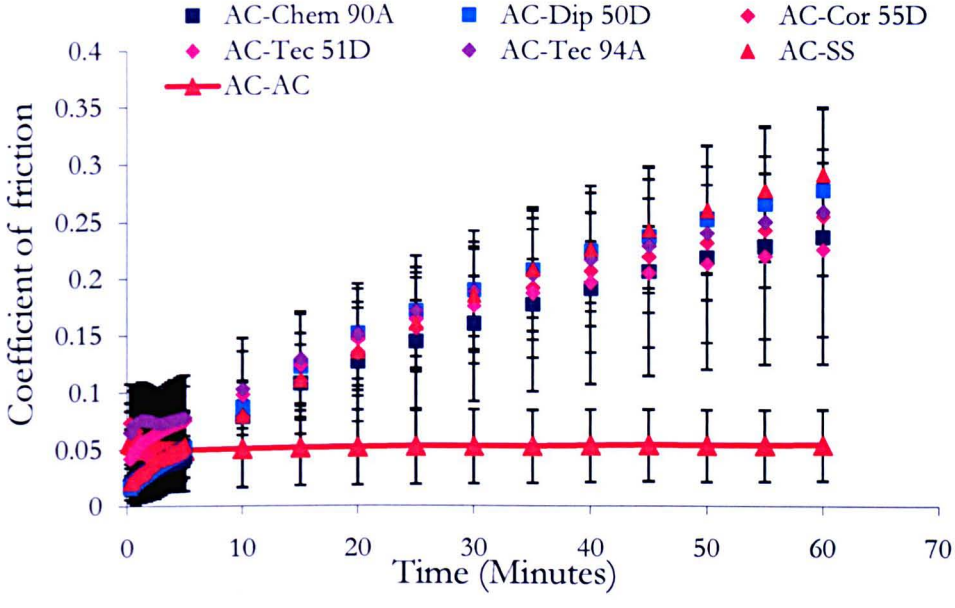

Figure 4.17 Articular cartilage (AC) pins reciprocated against Chemtura 90A (Chem 90A) and, Diprane 50D (Dip 50D), Corethane 55D (Cor 55D) Tecoflex 51D (Tec 51D) and, Tecoflex 94A (Tec 94A), articular cartilage and stainless steel (SS) plates, over a sliding distance of 10 mm at 4 mm s^{-1} for 1 h in PBS at a contact stress of 2.5 MPa. Data was analysed by ANOVA which revealed a significant difference ($p < 0.05$) between AC-Corethane 55D and AC-Chemtura 90A, AC-Diprane 50D and AC-SS at 0.25 to 0.5 minutes, between AC-Tecoflex 94A and AC-Chemtura 90A and AC-Diprane 50D at 2 to 0.5 minutes, between Tecoflex 94A and AC-SS at 0.25 to 0.5 minutes, between AC-SS, AC-Chemtura 90A and AC-AC at 10 and 20 minutes(respectively) to 60 minutes, and between AC-AC and all other groups at 15 to 60 minutes . Data is expressed as mean (n=6) ± 95% confidence limits.

Chemtura 90A and Diprane 50D pins were reciprocated against corresponding PU plates in PBS + 25% (v/v) FBS and compared to AC pins against AC plates (negative control) in PBS (Figure 4.18). Diprane 50D-Diprane 50D increased in friction at the start of the test before reaching steady state (at 40 minutes) and friction was significantly higher than Chemtura 90A-Chemtura 90A and the negative control (AC-AC). Chemtura 90A-Chemtura 90A increased in friction at the start of the test before reaching steady state (at 20 minutes) earlier than Diprane 50D-Diprane 50D, however, the coefficient of friction for Chemtura 90A-Chemtura 90A and the negative control were not significantly different from each other.

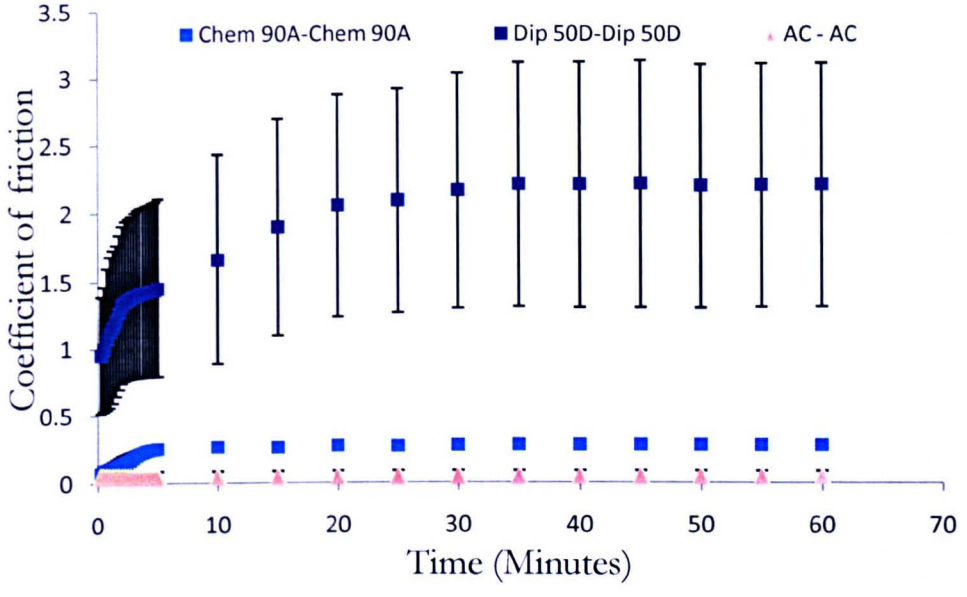

Figure 4.18 Chemtura 90A (Chem 90A) and Diprane 50D (Dip 50D) pins reciprocated against corresponding plates and articular cartilage, AC pins against articular cartilage plates, over a sliding distance of 10 mm at 4 mm s^{-1} for 1 h in PBS at a contact stress of 2.5 MPa. Data was analysed by ANOVA which revealed a significant difference ($p < 0.05$) between Diprane 50D-Diprane 50D and Chemtura 90A-Chemtura 90A and AC-AC at 0.25 to 60 minutes. Data is expressed as mean (n=3) ± 95% confidence limits.

The same corresponding thermoset pins and plates were also compared to the positive control (AC pins against stainless steel plates). There were no significant differences between Chemtura 90A-Chemtura 90A and the positive control (Figure 4.19). However, the coefficient of friction for Diprane 50D-Diprane 50D was significantly higher than both Chemtura 90A-Chemtura 90A and the positive control (AC-SS).

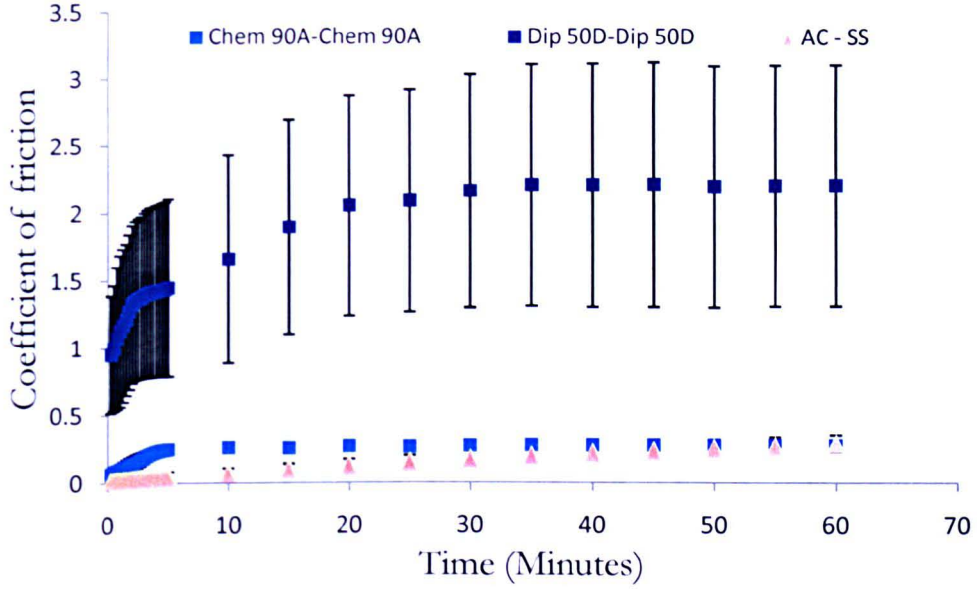

Figure 4.19 Chemtura 90A (Chem 90A) and Diprane 50D (Dip 50D) pins reciprocated against corresponding plates and articular cartilage, AC pins against stainless steel (SS) plates, over a sliding distance of 10 mm at 4 mm s^{-1} for 1 h in PBS at a contact stress of 2.5 MPa. Data was analysed by ANOVA which revealed a significant difference ($p < 0.05$) between Diprane 50D-Diprane 50D and the other groups at 0.25 to 60 minutes. Data is expressed as mean (n=3) ± 95% confidence limits.

4.4.3.5 *Long term friction tests*

When articular cartilage pins articulated against polyurethane and stainless steel plates the coefficient of friction gradually increased during the 1 h test period (Figure 4.17). For this reason, the tests were repeated and the time period was extended to 3 h to determine when the coefficient of friction reached equilibrium (Figure 4.20). All groups reached steady state at approximately 150 minutes and no significant differences were evident between any of the materials tested.

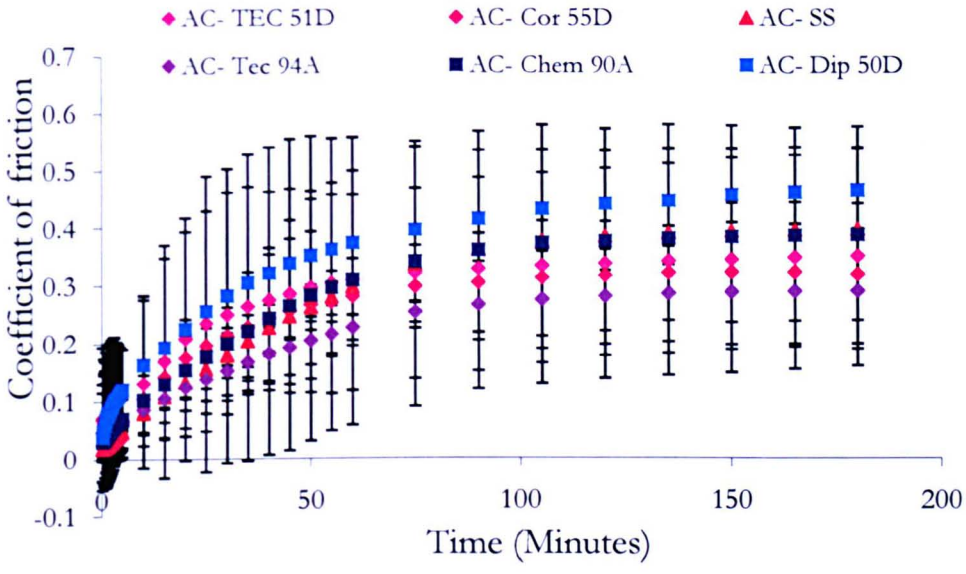

Figure 4.20 Articular cartilage pins (n=3) reciprocated against Corethane 55D (Cor 55D), Tecoflex 94A, (Tec 94A), Tecoflex 51D (Tec 51D) Chemtura 90A (Chem 90A), Diprane 50D (Dip 50D) and stainless steel (SS) plates over a sliding distance of 10 mm at 4 mm s^{-1} for 3 h in PBS at a contact stress of 2.5 MPa. ANOVA ($p < 0.05$) revealed no differences. Data is expressed as mean (n=3) ± 95% confidence limits.

4.4.4 *Surface roughness*

The surface roughness (Ra) of the pins and plates used in the short term friction tests was measured before and after testing. Ten articular cartilage (AC) pins were measured (using the talysurf profilometer) before testing and the average was used as a comparison. Both, H2A and H1B hydrogel pins had a significantly higher Ra after testing against stainless steel plates compared to before the test (Figure 4.21). While the H2B hydrogels were signifcantly smoother (lower Ra) after testing. There were no signicant differences in Ra between any of the polyurethane, AC and PE (polyethylene) pins after testing. The stainless steel plates were also measured and no significant diffferences were seen (results not shown). Before testing only H2B pins had a significantly higher Ra than the AC pins.

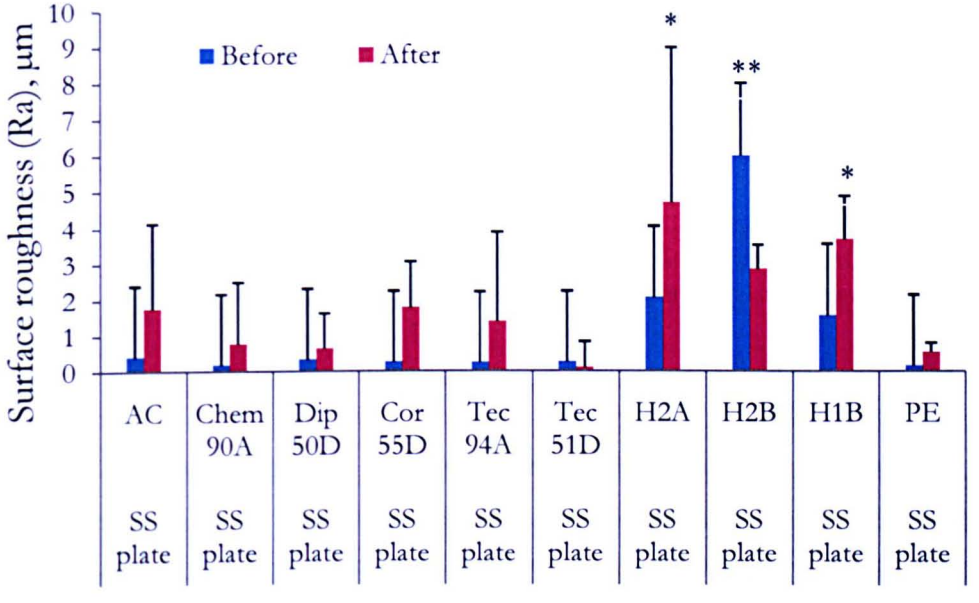

Figure 4.21 Surface roughness of various pins before and after reciprocating against stainless steel plates in PBS (AC,articular cartilage) or PBS + 25%FBS (all other pins). AC (n=10 before, n=3 after); Chem 90A, Chemtura 90A (n=3); Dip 50D, Diprane 50D (n=3); Cor 55D, Corethane 55D (n=3); Tec 94A, Tecoflex 94A (n=3); Tec 51D, Tecoflex, 51D (n=3); PE, polyethylene (n=3). ANOVA, $p < 0.05$; error bars 95% confidence limits, * $p < 0.05$ statistically higher than before testing and, ** $p < 0.05$ statistically lower than before testing.

The Ra of H2A and H1B pins were significantly higher after testing against AC plates, indicating the opposing AC plate had an adverse affect on the Ra of these polyvinyl alcohol/polyvinyl pyrrolidone (PVA/PVP) hydrogels. In contrast, the Ra of the H2B pins was significantly higher (before the test) than after testing (Figure 4.22). This suggested that the pins had minimal damage and thus, minimal wear. No significant differences were found before and after testing for the other pins.

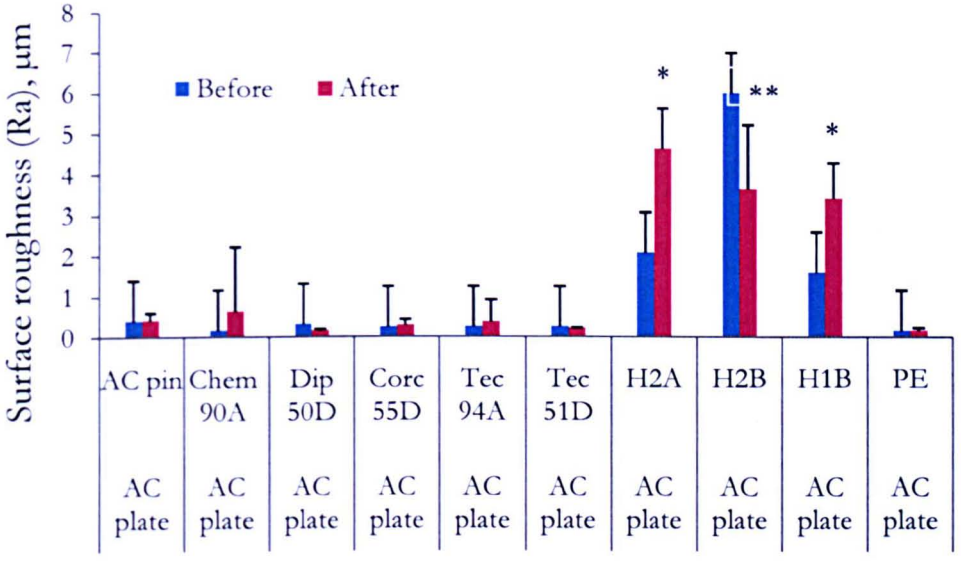

Figure 4.22 Surface roughness of various pins before and after reciprocating against articular cartilage plates in PBS. AC, articular cartilage (n=10 before, n=3 after); Chem 90A, Chemtura 90A (n=3); Dip 50D, Diprane 50D (n=3); Cor 55D, Corethane 55D (n=3); Tec 94A, Tecoflex 94A (n=3); Tec 51D, Tecoflex, 51D (n=3); PE, polyethylene (n=3). ANOVA, $p < 0.05$; error bars: 95% confidence limits, * $p < 0.05$ statistically higher than before testing and, ** $p < 0.05$ statistically lower than before testing.

Ten AC plates were measured before testing and the average was used for comparisions. Chemtura 90A, Diprane 50D, Corethane 55D, Tecoflex 51D and PE pins caused the Ra of the opposing AC plates to increase signifcantly after testing (Figure 4.23). There was no change in Ra for the AC plate of the negative control (AC-AC). Tecoflex 94A and the hydrogel pins showed no signifcant differences in Ra before and after testing AC plates (Figure 4.23).

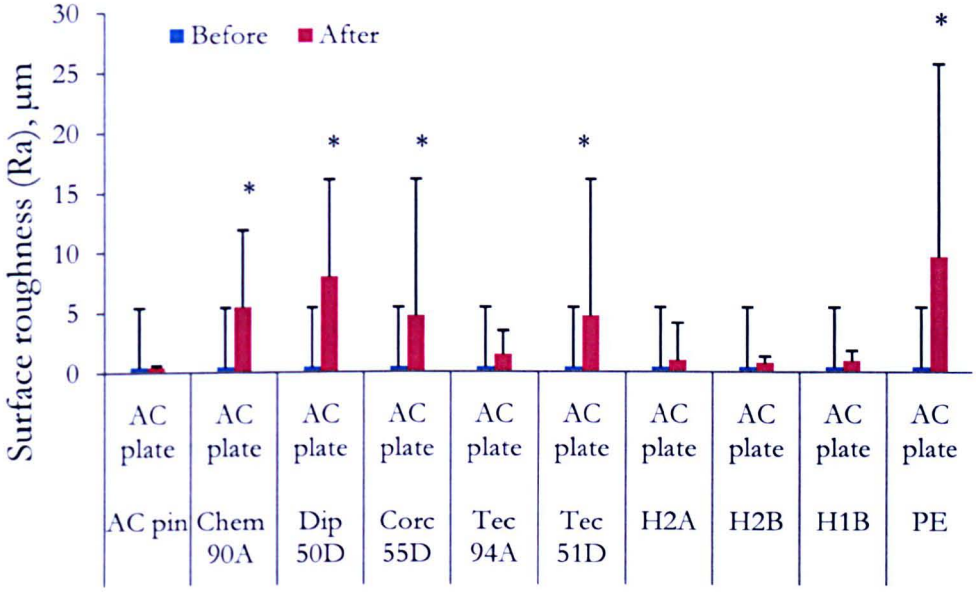

Figure 4.23 Surface roughness of coressponding articular cartilage plates to pins (Figure 4.22) before and after reciprocation in PBS. AC, articular cartilage (n=10 before, n=3 after); Chem 90A, Chemtura 90A (n=3); Dip 50D, Diprane 50D (n=3); Cor 55D, Corethane 55D (n=3); Tec 94A, Tecoflex 94A (n=3); Tec 51D, Tecoflex, 51D (n=3); PE, polyethylene (n=3). ANOVA, $p < 0.05$; error bars: 95% confidence limits, * $p < 0.05$ statistically higher than before testing.

AC pins were reciprocated against thermoset polyurethane (PU) plates and the Ra of both the AC pins and PU plates is shown in Figure 4.24. There were no significant differences in Ra before and after testing for any of the materials.

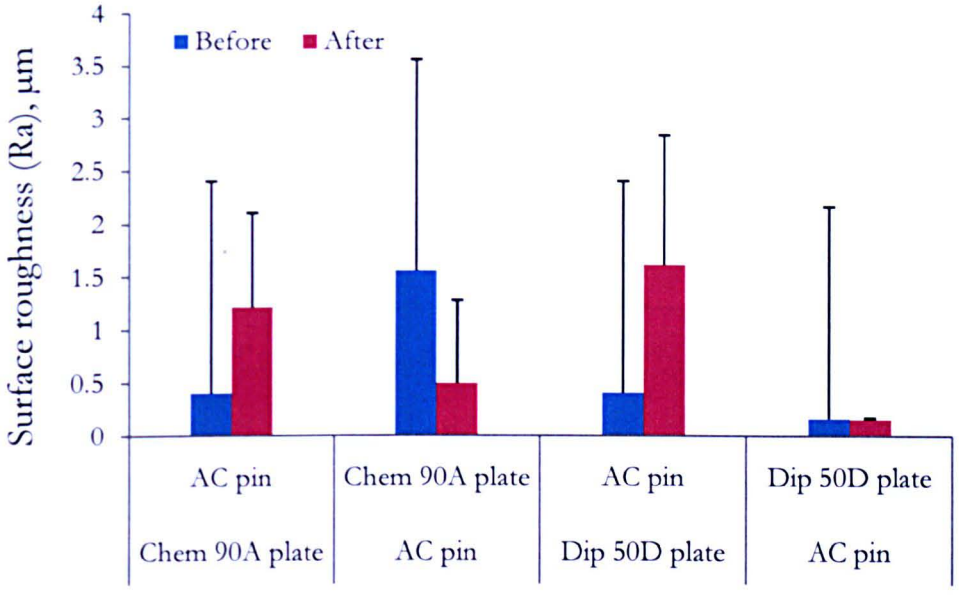

Figure 4.24 Surface roughness of AC pins and corresponding thermoset polyurethane plates before and after reciprocation in PBS. AC, articular cartilage (n=10 before, n=3 after); Chem 90A, Chemtura 90A (n=3); Dip 50D, Diprane 50D (n=3). ANOVA ($p > 0.05$; error bars 95% confidence limits) revealed no differences.

AC pins were reciprocated against thermoplastic polyurethane plates and Figure 4.25 shows the Ra of both the AC pins and polyurethane plates before and after testing. No differences were seen in Ra any of the materials.

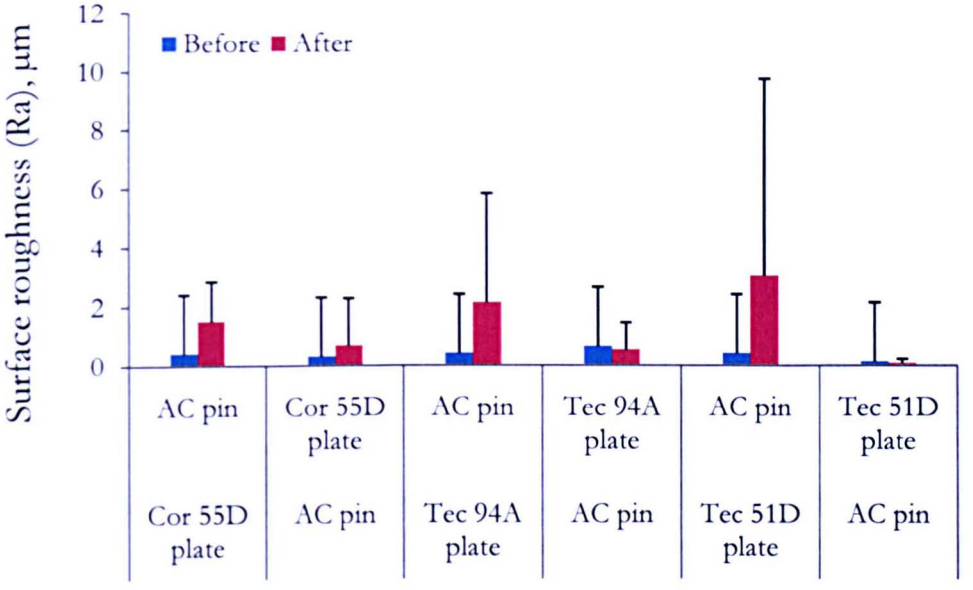

Figure 4.25 Surface roughness of AC pins and corresponding TPU plates before and after reciprocation in PBS. AC, articular cartilage (n=10 before, n=3 after); Chem 90A, Chemtura 90A (n=3); Dip 50D, Diprane 50D (n=3). ANOVA ($p > 0.05$; error bars 95% confidence limits) revealed no differences.

The Ra of pins and plates for Chemtura 90A and Diprane 50D were measured before and after friction tests where they were reciprocated against themselves (Figure 4.26). No significant differences were found before and after testing within each group.

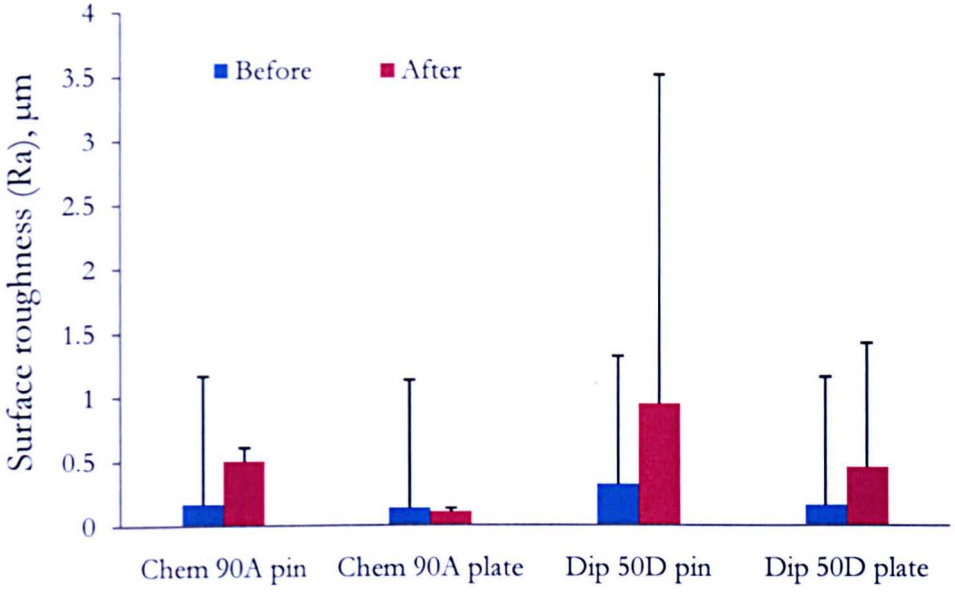

Figure 4.26 Surface roughness of thermoset pins and corresponding thermoset polyurethane plates before and after reciprocation in PBS + 25%FBS. Chem 90A, Chemtura 90A (n=3); Dip 50D, Diprane 50D (n=3). ANOVA ($p > 0.05$; error bars 95% confidence limits) revealed no differences.

4.4.5 *Contact angles*

4.4.5.1 *Static contact angles*

The contact angles of all polyurethane plates were measured six times for each group (Figure 4.27). The Corethane 55D plate had a significantly lower contact angle (70°) than the other polyurethane plates, suggesting Corethane 55D was more hydrophilic. There were no significant differences between any of the other groups. All other groups had a static contact angle > 90°, suggesting they were more hydrophobic than Corethane 55D.

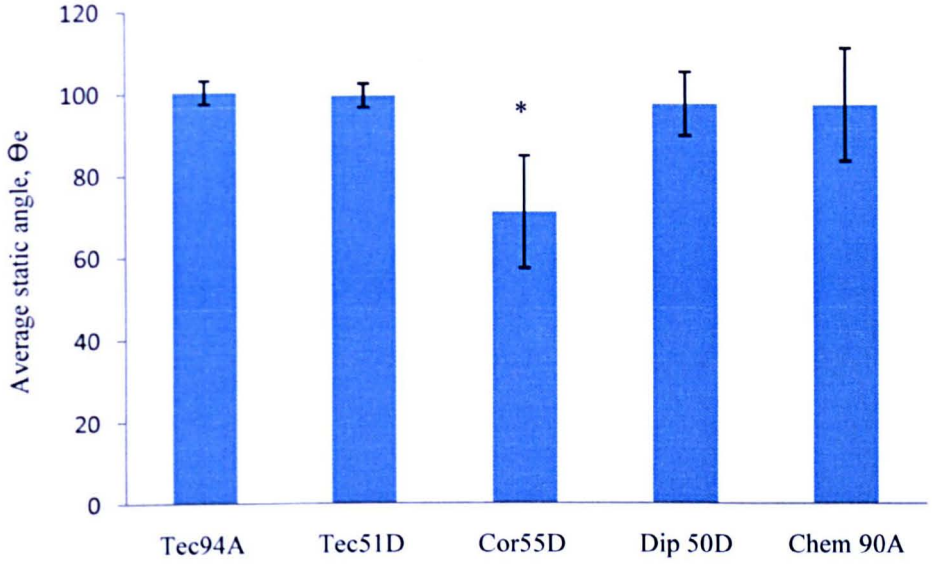

Figure 4.27 Average static contact angles for thermoset PUs and TPUs. Dip 50D, Diprane 50D; Chem 90A, Chemtura 90A; AC, articular cartilage; Cor 55D, Corethane 55D; Tec 94A, Tecoflex 94A; Tec 51D, Tecoflex 51D. ANOVA, $p < 0.05$; error bars: 95% confidence limits; n=6, * $p < 0.05$ statistically lower than all other polyurethane plates

4.4.5.2 *Dynamic contact angles*

4.4.5.2.1 *Receding angles*

Both Corethane 55D and Chemtura 90A plates had a significantly lower receding angle than the other polyurethane plates, however, Chemtura 90A was significant higher than Corethane 55D (Figure 4.28). There were no significant differences between the other groups. The receding angle of Corethane 55D was 39°, again suggesting the material was hydrophilic. While, the other polyurethanes had a receding angle greater than 50°, also suggesting they were hydrophilic.

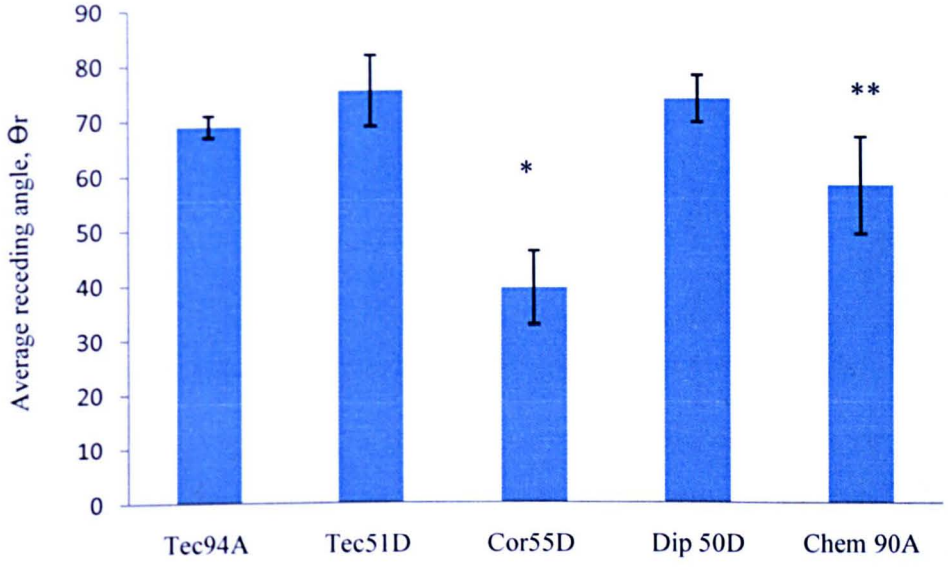

Figure 4.28 Average receding contact angles for thermoset PUs and TPUs. Dip 50D, Diprane 50D; Chem 90A, Chemtura 90A; Cor 55D, Corethane 55D; Tec 94A, Tecoflex 94A; Tec 51D, Tecoflex 51D. ANOVA, $p < 0.05$; error bars: 95% confidence limits; n=6, * $p < 0.05$ statistically lower than the other polyurethane plates and, ** $p < 0.05$ statistically lower the other polyurethane plates except Corethane 55D.

4.4.5.2.2 *Advancing angles*

Again, the Corethane 55D plate had a statistically lower advancing angle (84°) compared to the other polyurethanes, further suggesting that Corethane 55D was more hydrophilic than the other polyurethanes (Figure 4.29). The other polyurethanes had advancing angles greater than 100°.

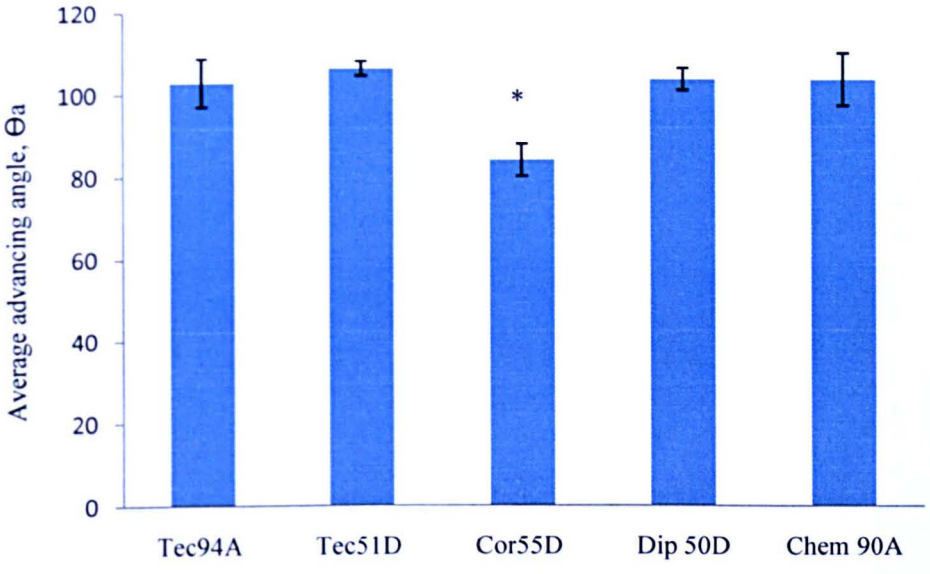

Figure 4.29 Average advancing contact angles for thermoset PUs and TPUs. Dip 50D, Diprane 50D; Chem 90A, Chemtura 90A; Cor 55D, Corethane 55D; Tec 94A, Tecoflex 94A; Tec 51D, Tecoflex 51D. ANOVA, $p < 0.05$; error bars: 95% confidence limits; n=6, * $p < 0.05$ statistically lower than the other polyurethane plates.

4.5 Discussion

4.5.1 Friction of articular cartilage

It has been reported that the friction coefficient of articular cartilage (AC) ranges between 0.002 - 0.3 μm (Forster and Fisher, 1996) and the present study demonstrated a low coefficient of friction for AC-AC (negative control) throughout the 1 h test period, within range of the previous studies. The load applied to AC was initially supported by the interstitial fluid, and as time increased the fluid pressurisation decreased (indicating a time-dependent response), to allow the solid phase to support the load (Armstrong *at al.*, 1984; Ateshian *et al.*, 1994; Kelkar *at al.*, 1999). The unloaded areas of the AC plates (negative control) during reciprocation were able to rehydrate, which also contributed to the low coefficient of friction seen with the negative control (AC-AC). This finding was concurrent with Northwood and Fisher (2007) who also reported a coefficient of friction of 0.05 (± 0.015), for AC-AC throughout a 1 h test period (0.5 MPa contact stress), which is comparable to the values in this present study (0.05 ± 0.03), even though the contact stress was 2.5 MPa. As load was applied to the AC, fluid migrated toward the unloaded areas and appeared to be time-dependent evident by the nonlinear response but steady-state was achieved in less than 1 h. However, the deformation and recovery tests indicated interstitial fluid flow back into the previously loaded areas was slower upon load removal, taking approximately 1 h to recover (not fully as some permanent deformation occurred). Baker and Seedhom (2001) proposed swelling pressure was much higher when AC was loaded compared to the pressure gradient after load removal. The swelling pressure and elastic modulus (stiffness) of AC has been reported to be related to proteoglycan concentration, therefore cartilage with a high elastic modulus would experience a high swelling pressure (Maroudas, 1973). This would suggest that stiff cartilage would recover faster than soft cartilage but this is not the case, in fact stiff cartilage has been reported to have a slower recovery rate due to the directly related lower permeability (Barker and Seedhom, 2001).

The positive (polyethylene, PE) control (PE-AC) exhibited a significantly higher coefficient of friction compared to the negative control (AC-AC). The average peak friction coefficient for the negative control (AC-AC) was 0.06 (± 0.03), and the positive control (PE-AC) was 0.17 (± 0.10). This suggested that the lubrication system operating in the negative control was possibly boundary/mixed lubrication and the positive control was boundary lubrication.

Boundary lubrication suggested that no lubricating fluid film existed between the opposing surfaces of the positive control and that the asperities had made contact resulting in protein rubbing, suggesting wear (adhesive) had occurred. This was evident by the visible damage on the cartilage plates (positive control) caused by the PE pin, which was confirmed by the increased surface roughness (Ra). The proteins on the cartilage surface may have been sheared causing high friction but also formed a protective layer on the PE pin surface, evident as a gel-like material covering the surface, which was difficult to remove. Protection by the proteins may explain the Ra of the PE pins after testing, as they were not significantly different to the Ra before the test, even though there was damage to the AC plate. The Ra of the AC pins and AC plates (negative control) had not changed after testing, nor was there any visible sign of tissue damage, further suggesting mixed lubrication was in operation. Mixed lubrication exists in the presence of a fluid film (same thickness as the Ra of the opposing surfaces) with fewer contacting asperities resulting in low or no wear. Since the average peak friction value was 0.06 for the negative control (AC-AC), this indicated a mixed lubrication.

It is important to note a gel-like material had collected around the perimeter of the 10 mm length wear scar on the cartilage plates, which was viscous but did not detach from the surface when pulled, possibly due to the collagen fibers present in the superficial layer (Wilson *et al.*, 2005; Aigner *et al.*, 2006). Graindorge *et al.* (2006) reported that the surface amorphous layer (SAL) is a discontinuous layer extending from the superficial zone of AC, which is thought to prevent fibrillation (Forster and Fisher, 1999), however, it is possible that the gel-like material seen in the present study was a mixture of the SAL and superficial layer tissue (although, the gel-like material was not identified in the present study).

AC pins against stainless steel (SS) plates exhibited a significantly higher coefficient of friction than PE-SS for the latter half of the test period, but this did not significantly affect the surface topography of the AC pins, nor was there a significant change in Ra of the PE pins. The average peak friction of the negative (AC-SS) control was 0.30 ($\pm$ 0.06), which was significantly higher than the positive (PE-SS) control (0.12, $\pm$ 0.03). The lubrication system operating in the AC-SS and PE-SS tests appeared to be boundary lubrication.

The cartilage surface proteins and proteins in the bovine serum (lubricant used in PE-SS tests) appeared to have played a protective role (possibly through surface adsorption) towards the AC and PE pin surfaces, although the high peak friction values (undesirable for AC-SS) suggested protein-protein rubbing (Scholes and Unsworth, 2006). Against polyurethane (PU) plates, the friction coefficient of articular cartilage continued to increase throughout the test, providing further supporting evidence that the fluid phase supported the load and suggesting biphasic behaviour. The biphasic behaviour was confirmed in the long term tests as the friction characteristics of articular cartilage showed a time- and load-dependent response owing to the biphasic nature of the tissue because the interstitial fluid pressure subsided (at approximately 150 minutes) to allow the solid phase to support the load (Armstrong *at al.*, 1984; Ateshian *et al.*, 1994; Kelkar *at al.*, 1999); an observation reported by others (Forster and Fisher, 1996; Northwood and Fisher, 2007).

The friction coefficients of AC pins against thermoplastic polyurethane (TPU) plates and AC-Diprane 50D were significantly higher than AC-Chemtura 90A. The average peak friction values of AC-Corethane, AC-Tecoflex 51A and, AC-Tecoflex 94A were 0.25 ± 0.03, 0.23 ± 0.08 and, 0.26 ± 0.06, respectively. This indicated a boundary lubrication system for the TPUs. The average peak friction values of AC-Chemtura 90A was 0.24 (± 0.11), while AC-Diprane 50D had an average peak friction of 0.28 (± 0.03). Again, boundary lubrication was in operation with shearing of adsorbed proteins, resulting in an undesirable high friction coefficient for the thermoset PUs.

Incidentally, the interstitial fluid may have been almost nonexistent at the surface of the AC pin because suction was produced at the AC-PU surface. This has also been observed at the interface of cartilage pins against glass (Ateshian, 2009). The surface topography of AC pins and opposing PU plates did not significantly change during the test period. However, after the test it was noticed that the TPUs had deformed under load, but the thermoset PU plates had not. This suggested that the TPUs were more compliant than the thermoset PU plates, but the indentation, deformation and recovery tests did not confirm this, as there were no significant differences between the two types of PUs. Articular cartilage deformed to a greater extent than the PUs, suggesting AC was more compliant. However, AC exhibited significantly higher permanent deformation and normalised permanent deformation.

4.5.2 *Friction of polyvinyl alcohol (PVA)/polyvinyl pyrrolidone (PVP) hydrogels*

The coefficient of friction for each PVA/PVP hydrogel against AC plates showed no significant differences when compared to the positive (PE) and negative controls (AC) against AC plates and stainless steel plates. However, this did not correlate with the Ra of the PVA/PVP hydrogel pins before and after testing. The AC and stainless steel plates significantly increased the surface roughness (Ra) of the H2A and H1B pins. In contrast, both plate types appeared to have a polishing effect on the H2B hydrogel pins, as the Ra significantly decreased after the test. Boundary layer proteins have been found to be advantageous or detrimental to bearing surfaces, in that they provide protection or undergo severe rubbing (Katta *et al.*, 2006; Nakashima *et al.*, 2007). It was apparent that the PVA/PVP hydrogels had laterally deformed after each test and the contacting face of each PVA/PVP hydrogel pin was measured after each test. The average diameter of the pins was 9.5 mm, as opposed to the original 9 mm diameter (altering the contact stress of the surface contacting area from 1.26 MPa to 1.13 MPa). The deformation (indentation) curves of the PVA/PVP hydrogels followed the same trend as the AC and, there were no significant differences seen between the PVA/PVP hydrogels and AC pins, supporting evidence of their biphasic (Covert *et al.*, 2003; Bodugoz-Senturk *et al.*, 2009) and viscoelastic (Covert *et* al., 2003; Katta *et* al., 2006; Pan *et* al., 2006; Wu *et al.*, 2007) properties. However, the percentage permanent deformation (and normalised permanent deformation) of H2B and H2A hydrogels were significantly lower than AC. The water content of articular cartilage has been reported to be between 60-80% (Buckwalter *et al.*, 1997), and plays an important role in the biphasic nature of cartilage. The water content of the PVA/PVP hydrogels used in the present study range between 65-72% (Hickey and Peppas, 1995) and the incorporation of PVP increased the mechanical properties; the comparable deformation further indicated that the PVA/PVP hydrogels also possess biphasic properties.

The peak friction coefficients of H1B-AC, H2B-AC and H2A-AC were 0.17 ± 0.17, 0.15 ± 0.17 and, 0.15 ± 0.06, indicating boundary lubrication was operating. This may explain the significant differences seen in the Ra of the PVA/PVP hydrogels after the test period, however, there were no significant topographical changes to the opposing AC plates. The friction values of the PVA/PVP hydrogels against AC plates were not significantly different to the positive and negative controls, possibly due to the wear of the PVA/PVP hydrogel pins.

It has already been mentioned that the articular cartilage plates were able to rehydrate when reciprocated against an articular cartilage pin, which in turn maintained a low coefficient of friction (Northwood and Fisher, 2007). It is possible that the AC plates were able to rehydrate when reciprocated against the PVA/PVP hydrogel pins, and this may explain why there were no significant differences in the coefficient of friction between the groups. This may be feasible as the PVA/PVP hydrogels contained 65-72% water and the contact stress was low (but still physiologically relevant). Water may have squeezed out of loaded PVA/PVP hydrogels over time contributing to the lubrication between surfaces (Ma *et al.*, 2009). Ma *et al.* (2009) proposed that polymer chains in PVA/PVP hydrogels change their orientation and relative positions when loaded thus, squeezing out interstitial fluid. This was in line with the findings in the present study, as all PVA/PVP hydogels experienced mixed lubrication against stainless steel counterfaces in contrast to the boundary lubrication seen when the PVA/PVP hydrogels were reciprocated against AC plates. The mixed lubrication seen with the PVA/PVP hydrogels against stainless steel plates in bovine serum in the present study was also reported by Ma *et al.* (2009) who used PVA/PVP hydrogels. The boundary lubrication experienced by the PVA/PVP hydrogels and AC plates suggested proteins sheared at the surface (Katta *et al.*, 2009). The PVA/PVP hydrogels expanded laterally, as seen by Katta *et al.* (2009).

The peak friction values of H1B, H2B and H2A were 0.04 ± 0.08, 0.22 ± 0.06 and, 0.19 ± 0.03, respectively against stainless steel plates. As the PVA/PVP hydrogels, this indicated that a mixed lubrication system was in operation, however, the advantageous and detrimental actions of proteins (from the bovine serum in the lubricant) and asperities on the stainless steel plate significantly changed the surface topography of the PVA/PVP hydrogels.

4.5.3 Friction of thermoset polyurethanes

The thermoset polyurethanes (PUs), Diprane 50D-AC and Chemtura 90A-AC had significantly higher friction coefficients than the negative control (AC-AC), but were not statistically different to the positive control (PE-AC). This correlated with the damage seen on the AC plates after the test period where a gel-like material was present on the surface, also seen with the positive control. Against stainless steel plates the thermoset PU pins exhibited significantly higher friction than the negative control (AC-SS) and the positive control (PE-SS). However, the surface roughness (Ra) of the pins after the test period

when reciprocated against AC and stainless steel plates showed no significant differences, indicating a protective boundary layer was present. Like the positive control, a gel-like material was seen on the surface of the thermoset pins when reciprocated against AC plates. The average peak friction coefficients of the thermoset PUs (no significant differences), which for Diprane 50D-AC was 0.15 (± 0.04) and Chemtura 90A-AC was 0.13 (± 0.03). This indicated boundary lubrication with possible protein shearing leading to high friction.

There were no significant differences between the average peak friction values for the thermoset PUs against stainless steel plates as Diprane 50D-SS was 0.41 (±0.13) and Chemtura 90A-SS was 0.39 (± 0.11). The average peak values indicated that boundary lubrication was the mode of operation.

4.5.4 Friction of thermoplastic polyurethanes

The thermoplastic polyurethanes (TPUs) did not damage the cartilage plates unlike the positive control (PE-AC) and thermoset pins. The friction coefficient of the TPUs against AC plates was not significantly different to the negative control (AC-AC); and they did not visibly damage the cartilage plates but, they did deform the plates under the loaded area. Interestingly, the Ra of the AC plates opposing Corethane 55D and Tecoflex 51D pins significantly increased after the test period (Figure 4.24). While, the Ra of AC plates opposing Tecoflex 94A pins did not change significantly, nor did the Ra of the TPU pins. These findings suggested that a protective boundary layer may have existed. The coefficient of friction for the TPUs against stainless steel plates were only significantly higher than the positive control (PE-SS) for the first few minutes of the test and the negative control (AC-SS) for the first 10 minutes of the test.

Corethane 55D-AC, Tecoflex 51D-AC and Tecoflex 94A-AC all had average peak friction coefficients of 0.08 ± 0.04, 0.09 ± 0.05 and, 0.04 ± 0.03, respectively. It appeared that Tecoflex 94A-AC experienced a mixed lubrication regime, however, Corethane 55D-SS and Tecoflex 51D-SS appeared to be bordering boundary lubrication as the friction values were close to 0.1. Nevertheless, there were no significant differences between the TPUs but the findings correlated with the unaffected surface topography of the AC plates that opposed the Tecoflex 94A pins. There were no significant changes to the surface topography of the TPU pins. The average peak friction values of Corethane 55D-SS,

Tecoflex 51D-SS and Tecoflex 94A-SS were 0.21 ± 0.05, 0.23 ± 0.08 and, 0.23 ± 0.08, respectively. These values indicated the TPUs experienced boundary lubrication.

Caravia *et al.* (1993) reported that microelastohydrodynamic lubrication created local pressure areas which deformed the surface of Tecoflex PUs and friction remained low because surface asperities on the soft materials were compressed. Caravia *et al.* (1993) compared the friction characteristics of two Tecoflex PUs (one with an elastic modulus of 8 MPa and one with an elastic modulus of 20 MPa) and found microelastohydrodynamic lubrication was more apparent with the softer PU (8 MPa). The elastic modulus of the TPUs used in the present study was close to the 8 MPa PU used in the study by Caravia *et al.* (2003). However, the elastic modulus of the thermoset PUs were much lower (Chapter 3) than the TPUs, yet the friction coefficient of both types of PUs used in the present study were not significantly different to each other, suggesting that elastic modulus of the PUs did not influence lubrication.

After statistically comparing the friction of the thermoset and TPU pins against AC plates, it was evident that that friction of both Diprane 50D-AC and Chemtura 90A-AC were significantly higher than Tecoflex 94A-AC throughout the test period. However, Chemtura 90A-AC was only significantly higher than Corethane 55D-AC and Tecoflex 51D for the first 10 minutes, while Diprane 50D-AC was significantly higher than both TPUs for the first 20 minutes of the test period. The Ra of PE, TPUs and thermoset PU pins did not significantly change after testing against AC plates. However, the AC plates which reciprocated against the thermoset PUs, Tecoflex 51D, Corethane 55D and PE pins had worn, evident by the increased Ra of the AC plates. This indicated that friction had no relationship to wear of AC plates because the thermoset PUs against AC plates and the positive control (PE-AC) exhibited a statistically higher coefficient of friction compared to Tecoflex 51D-AC, Corethane 55D-AC which were statistically similar to the negative control (AC-AC).

4.5.5 *Friction comparison for thermoset and thermoplastic polyurethanes*

It was initially thought that the frictional dissimilarity between the thermoset polyurethanes (PUs) and thermoplastic polyurethanes (TPUs) may have been affected by the wettability, material chemistry or geometry of the pins and that all these may have contributed to the increased friction and gel-like material seen on the articular cartilage plates. The PUs and polyethylene (PE) pins all had a truncated head and it was believed the truncated heads of the thermoset PUs and PE exhibited 'sharper' edges (which damaged the AC plates), compared to TPUs. Therefore, two types of stainless steel pins were manufactured (School of Mechanical Engineering, University of Leeds, UK).

The stainless steel pins were produced with both a radius head represented the surface of the articular cartilage pins and a truncated head to represent the 'sharp edges' (as stainless is not compliant) of the PU and PE pins. Surprisingly, the coefficient of friction of both the radius and truncated stainless steel pins against cartilage plates were not significantly different to the negative control [AC-AC] (Figure 4.30). The stainless steel pins did not cause any visible signs of damage to the AC plates but they had deformed the AC plates under load.

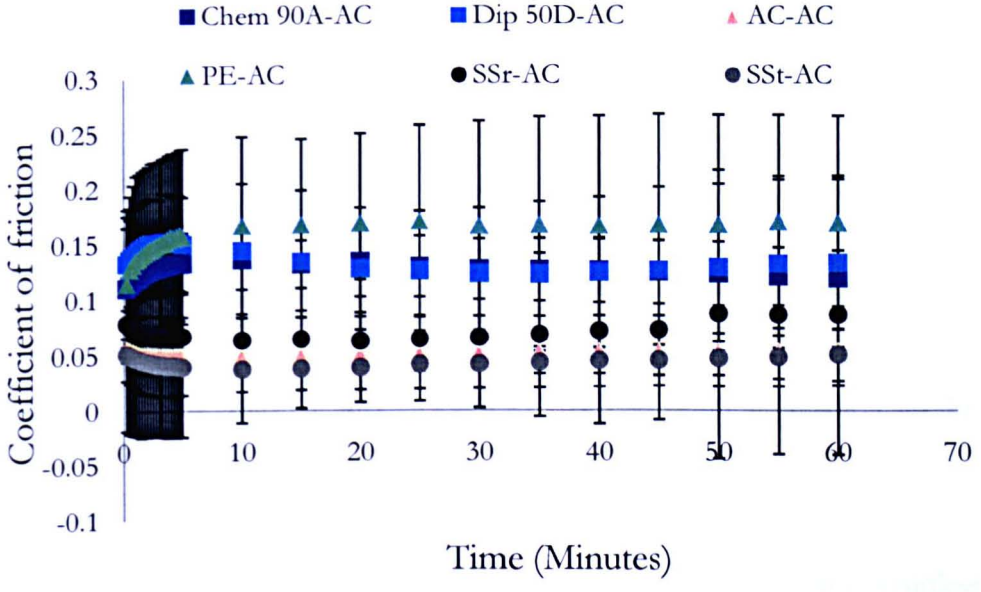

Figure 4.30 The stainless steel pins were reciprocated against articular cartilage plates in PBS under a 160 N load (contact stress 2.5 MPa) for 1 h. Friction characteristics of articular cartilage plates when reciprocated against articular cartilage (negative control), stainless steel (radius and truncated head), polyethylene (positive control) and, thermoset PU pins for 1 h. AC, articular cartilage; PE, polyethylene; SSr, stainless steel radius head;

SSt, stainless steel truncated head. ANOVA (error bars: 95% confidence limits; n=6 for AC, thermoset PUs and PE, n=3 for SSr and SSt) revealed no differences between AC-AC, SSt-AC and SSr-AC ($p > 0.05$).

In contrast, Diprane 50D-AC and the positive control (PE-AC) had a coefficient of friction significantly higher than the truncated stainless steel pins (SSt) throughout the test. Chemtura 90A-AC was higher than the SSt pins for the majority of the test (between 1 and 55 minutes). However, the coefficient of friction for the radius stainless steel (SSr) pins against AC, were statistically lower than Diprane 50D-AC (between 1.75 to 20 minutes), Chemtura 90A-AC (between 2.75 to 10 minutes) and positive control (between 1.75 to 60 minutes). The friction coefficient of the SSr and SSt pins against AC plates were also compared to the TPUs against AC plates, but no significant differences were evident, suggesting geometry was not the causative factor of dissimilar friction values between thermoset and TPUs (Figure 4.31).

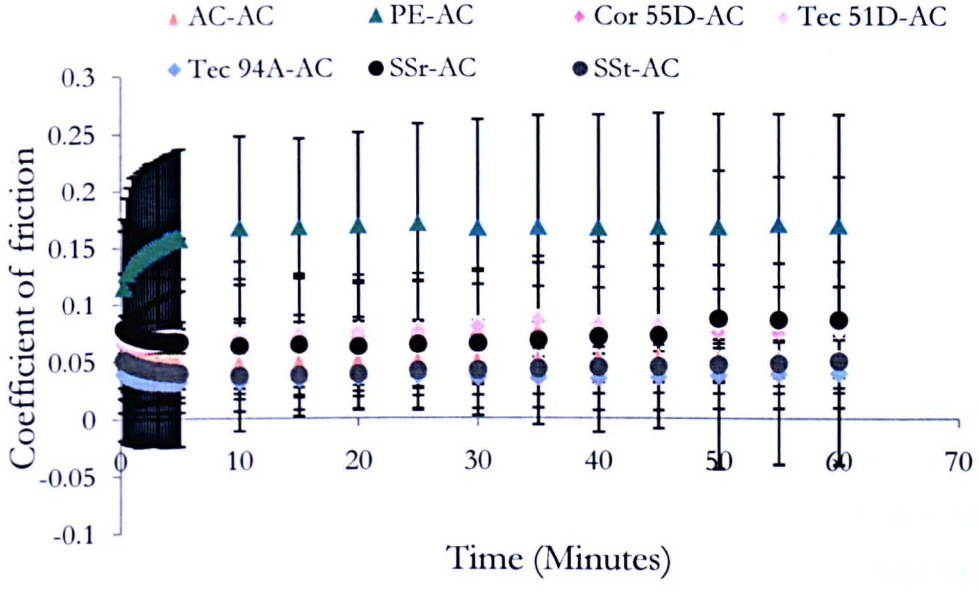

Figure 4.31 Friction characteristics of articular cartilage (negative control), stainless steel (radius and truncated head) polyethylene (positive control) and, TPU pins when reciprocated against articular cartilage plates for 1 h in PBS at a contact stress of 2.5 MPa. AC, articular cartilage; PE, polyethylene; SSr, stainless steel radius had; SSt, stainless steel truncated head. ANOVA (error bars: 95% confidence limits; n=6 for AC, thermoset PUs

and PE, n=3 for SSr and SSt) revealed no differences between SSt-AC, SSr-AC and the TPUs against articular cartilage plates ($p > 0.05$).

As the SSr-AC and SSt-AC showed no significant differences in friction when compared to each other, this further supported the case that geometry had no effect on friction or damage to the AC plates. Therefore, the higher friction coefficient of the thermoset PUs may have been due to the wettability or the surface chemistry of the materials. The wettability of the PUs was investigated by measuring the contact angles. Corethane 55D had significantly lower contact angles than the other PUs, suggesting this material was more hydrophilic (Figure 4.32).

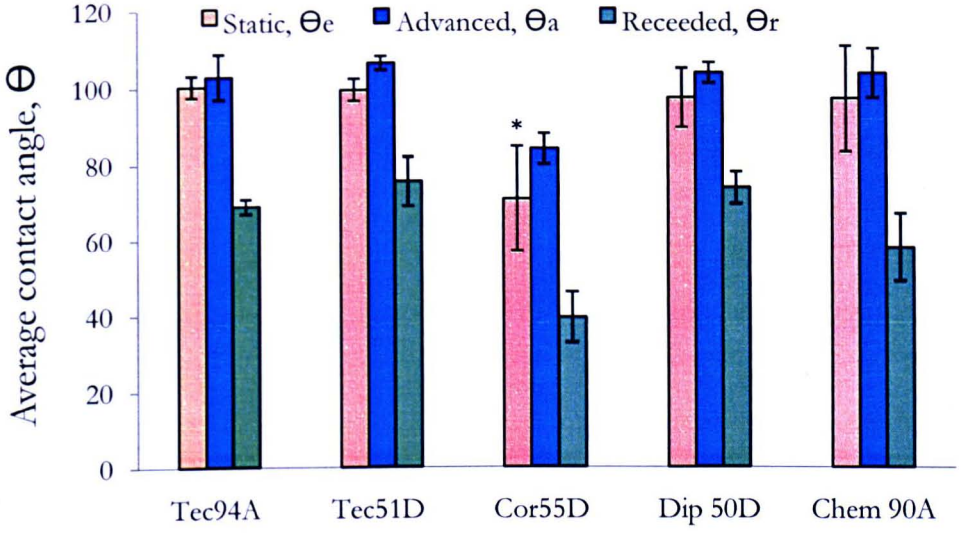

Figure 4.32 Static, advancing and receding contact angles (deionised water) of thermoset PUs and TPUs. Dip 50D, Diprane 50D; Chem 90A, Chemtura 90A; Cor 55D, Corethane 55D; Tec 94A, Tecoflex 94A; Tec 51D, Tecoflex 51D. ANOVA, $p < 0.05$; T-Method; Error bars: 95% confidence limits; n=6, * $p < 0.05$ statistically lower than the other materials.

The wettability and geometry results further suggested that the surface chemistry of the materials was the major factor for the differing friction values of the thermoset and TPUs.

Caravia *et al.* (1995) evaluated cyclic loading and continuous artificial joint motion for Tecoflex 93A against Tecoflex 93A, which initially gave high start up friction values before

decreasing to a steady state after continuous sliding. These authors observed a start up friction coefficient of nearly 4.0 and damage to both surfaces which was apparent in the present study, which attempted to reciprocate the TPUs pins against the corresponding PU plates, but the friction was so high that a 'stick slip' motion caused parts of the friction rig to become loose and these experiments were discontinued.

Diprane 50D pins against Diprane 50D plates exhibited a significantly higher friction coefficient compared to Chemtura 90A-Chemtura 90A plates. The high friction of the Diprane 50D-Diprane 50D did not have an adverse effect on the surface roughness, possibly due to the proteins present in the foetal bovine serum (used as lubricant). There were also no significant differences in surface roughness of the AC pins and thermoset PU plates after testing, possibly due to the presence of proteins on the cartilage surface. The average peak friction values of Chemtura 90A-Chemtura 90A and Diprane 50D-Diprane 50D were 0.27 ± 2.21 and 0.09 ± 0.90, respectively. Both tests were operating in boundary lubrication, though the friction of Chemtura 90A-Chemtura is undesirable. The thermoset PU against thermoset PU surfaces may have had a greater contact area due to the materials being compliant. The surface asperities may have been deformed thus increasing the adhesive forces, which lead to high friction values (Caravia *et al.*, 1993). It was possible water may have been squeezed out of the PU surfaces due to deformation of the asperities. Caravia *et al.* (1993) proposed the release of water from the PUs against PUs contributed to an increase in the surface contact area. This would also have accounted for the high friction values obtained in the study (Caravia *et al.*, 1993).

4.6 Conclusion

Only the hydrogels articulated in the favourable mixed lubrication regime and no signifcant differences in friction were evident compared to the positive and negative controls against articular cartilage (AC) and stainless steel plates. However, the hydrogels experienced significant changes to their surface topography. Diprane 50D and Chemtura 90A and polyethylene pins significantly damaged the AC plates and a gel-like viscous material collected around the perimeter of the wear scar, which had also attached to the surface of the pins

The different friction characteristics of polyethylene and thermoset polyurethanes compared to thermoplastic polyurethanes were possibly due to the surface chemistry of the

materials (and not the geometry or wettability), which was unrelated to the hydrophobic and hydrophilic properties of the materials. The thermoplastic polyurethanes have similar friction characteristics to the negative control (AC-AC), and exhibit lower friction coefficients compared to the thermoset polyurethanes when articulated against stainless steel plates. Tecoflex 94A had the most favourable friction characteristics against AC plates, indicating that Tecoflex 94A could be a potential cartilage substitution candidate not only because of the low friction coefficient but also due to the lack of damage caused to the AC plates.

Chapter Five

Wear and Wear Particle Analysis

5.1 Introduction

There are a number of surgical interventions and medical devices used for the replacement (in part or whole) of knee and hip joints. The development of degenerative diseases such as osteoarthritis makes it necessary to replace a natural joint. Initially, total joint (both knee and hip) replacements were conducted in patients over the age of 65, but more recently the age range has decreased dramatically to include those in the age group of 45-65 (Katz, 2006). The occurrence of inflammatory joint diseases (i.e. osteoarthritis and rheumatoid arthritis) has increased over the years, and in turn has increased the requirement for surgical intervention. This may be a result of patients not tolerating the pain, and hence seeking medical interventions earlier, rather than an increased number of people developing these diseases. Total joint replacements are invasive procedures and revision operations are on the increase. Prostheses may only last 10 to 15 years post-implantation as a result of adverse biological reactions from the individual, due to the generation of wear particles (from the prostheses) which leads to osteolysis and aseptic loosening.

The generation of wear particles is a major issue associated with all joint replacements (Matthews *et al.*, 2000). Wear particles promote the recruitment of various cell types, particularly macrophages, as these cells phagocytose the particles in order to try to digest them and eliminate them from the body. Macrophages release cytokines (such as interleukin-1 beta [IL-1β], interleukin-6 [IL-6], interleukin-8 [IL-8] and tumour necrosis factor-alpha [TNF-alpha]), which stimulate or inhibit the secretion of more cytokines (in an anabolic or catabolic manner) from other cell types and this action eventually leads to osteolysis. Pre-osteoclasts are one such cell type affected by the release of these cytokines, and it is these cells (when mature) that are responsible for the bone resorption at the prosthesis interface, which leads to implant loosening. The uptake of wear particles is highly dependent on their size (Wang *et al.*, 1997) and it has been reported that particles in the size range of 1.0-10μm elicit the biological response that leads to osteolysis and implant

loosening (Green *et al.*, 1998; Matthews *et al.*, 2000; Tipper *et al.*, 2006). Furthermore, the long term effects of these ingested particles are not fully understood.

In considering novel early intervention therapies which preserve healthy cartilage, wear particle generation from potential cartilage substitution biomaterials were investigated. It was important to determine whether or not these particles would potentially activate macrophages to release pro-inflammatory cytokines. The release of these cytokines could potentially result in further damage to the surrounding articular cartilage if the materials were to be implanted. TNF-alpha is known to inhibit collagen type II (Aigner *et al.*, 2003) as well as mediate the release of IL-1β, IL-6 and IL-8 (Choy *et al.*, 2001). IL-1β has been reported to inhibit the formation of type II collagen and proteoglycans but stimulate the release of destructive metalloproteinases leading the cartilage degradation (Van den Berg, 1999; Choy *et al.*, 2001; Aigner *et al.*, 2003). IL-6 is stimulated by IL-1β and IL-6 increases the secretion of the cartilage destructive, metalloproteinases (Van den Berg, 1999; Westacott, 1996). Inhibition of proteoglycan formation in cartilage is caused by IL-6 (Martel-Pelletier *et al.*, 1999), which also increases the release of IL-1β and TNF-alpha (Raman *et al.*, 2003). It has been reported that IL-8 induces neutrophils to secrete superoxides and proteases which leads to cartilage destruction (Raman *et al.*, 2003).

The aim of this chapter was to investigate the wear of thermoset (Diprane 50D and Chemtura 90A) and thermoplastic (Corethane 55D, Tecoflex 51D and Tecoflex 94A) polyurethanes and compare to ultra high molecular weight polyethylene (GUR1120). Particles were generated using multidirectional wear rigs to generate clinically relevant sized particles and the size and particle volume were determined. The particles generated from the polyvinyl alcohol/polyvinyl pyrrolidone (PVA/PVP) hydrogels were not sized because high levels of surface damage occurred making them unfavourable materials.

5.2 Materials and Methods

A single station multidirectional pin-on-plate wear rig (Section 2.4.5.2) was used to generate aseptic wear particles from ultra high molecular weight polyethylene (Section 2.3.6), thermoset (Section 2.3.4) and thermoplastic (Section 2.3.5) polyurethane. These materials were reciprocated against rough stainless steel plates (Ra = 0.07 – 0.08 μm) in Rosslyn Park Memorial Institute 1640 culture medium (RPMI) 1640 + 25% (v/v) foetal bovine serum (FBS) (refer to Sections 2.2.3 and 2.2.5). A known volume of the particles (for calculations

see Sections 2.4.7 and 2.4.8) were digested and isolated from the lubricants and filtered through a series of pre-weighed (known pore-sized) filters (Section 2.4.6), in order to compare particle sizes (Section 2.4.9.3) to polyethylene particles. A six station multidirectional pin-on-plate wear rig (Section 2.4.5.1) was utilised to generate wear particles from the thermoplastic polyurethanes when reciprocated against smooth (Ra = 0.01 - 0.03 μm) and rough (Ra = 0.07 – 0.09 μm) stainless steel plates (Section 2.3.9) in a phosphate buffered saline lubricant (Section 2.2.2). The particles generated against both surfaces were sized and compared. FBS (25% (v/v)) was added to the PBS lubricants which were digested and the particles isolated (through a series of known pore-sized filters). The particles generated in PBS were compared to those spiked with serum in terms of size and area in order to determine whether the digestion protocol had any adverse effects on the generated particles. All particles were visualised using a field emission gun environmental scanning electron microscope (Section 2.4.9.2) and sized using Image-Pro® Plus (Section 2.4.9.3).

5.3 Results

5.3.1 Wear factors

As previously mentioned the the polyvinyl alcohol/polyvinyl pyrrolidone (PVA/PVP) hydrogel wear tests to generate wear particles in PBS (using the six station pin-on-plate multidirectional wear rig) were stopped early because the pins had worn quickly (less than 20 hours). The wear factors of each PVA/PVP hydrogel are shown in Table 5.1. H1B had worn at a signifcantly higher ($p < 0.05$) rate than the H2B and H2A hydrogels. No signifcant differences were found with each material when articulated against smooth and rough stainless steel plates.

Table 5.1 Wear factors of PVA/PVP hydrogel pins

Materials	Stainless steel plate	Wear factor (mm^3/Nm)
H1B	Rough	1.06×10^{-5}
H1B	Smooth	1.05×10^{-5}
H2B	Rough	3.12×10^{-6}
H2B	Smooth	2.93×10^{-6}
H2A	Rough	2.92×10^{-6}
H2A	Smooth	3.11×10^{-6}

The wear factors of the thermoplastic polyurethanes are shown in Table 5.2 when reciprocated against smooth and rough stainless steel plates in PBS (using the 6-station pin-on-plate multidirectional wear rig). Tecoflex 94A had a signifcantly lower ($p < 0.05$) wear factor compared to the other materials when articulated against both surfaces. No significant differences were found with the material samples when articulated against smooth and rough stainless steel plates.

Table 5.2 Wear factors of thermoplastic polyurethane pins

Materials	Stainless steel plate	Wear factor (mm^3/Nm)
Tecoflex 51D	Rough	5.41×10^{-6}
Tecoflex 51D	Smooth	6.43×10^{-6}
Tecoflex 94A	Rough	2.13×10^{-5}
Tecoflex 94A	Smooth	2.20×10^{-5}
Corethane 55D	Rough	6.30×10^{-6}
Corethane 55D	Smooth	5.93×10^{-6}

The wear factors were calculated for polyethylene, thermoset and thermoplastic polyurethane pins which were articulated against rough stainless steel plates in the aseptic single station pin-on-plate multidirectional wear rig (Table 5.3). Tecoflex 51D and Corethane 55D had higher wear factors than the other all other materials (Table 5.3).

Table 5.3 Wear factors of various pins after generation of sterile wear particles

Materials	Wear factor (mm^3/Nm)
Chemtura 90A	3.99×10^{-5}
Diprane 50D	2.40×10^{-5}
Tecoflex 51D	1.05×10^{-4}
Corethane 55D	1.03×10^{-4}
Tecoflex 94A	9.76×10^{-5}
Polyethylene	6.35×10^{-5}

5.3.2 *Comparison between the LEO FEGSEM and Quanta™ FEGESEM*

The size distribution of Chemtura 90A wear particles was determined as described in Section 5.3.8. The particle size distributions of Chemtura 90A were comparable in the 0.1-1.0 μm and > 10 μm size range when imaged using both microscopes (Figures 5.1 A and B). Though, less particles were measured in the < 0.1 μm size range when the particles were imaged on the LEO FEGSEM, the size distributions were similar to those imaged on the Quanta™ FEGESEM.

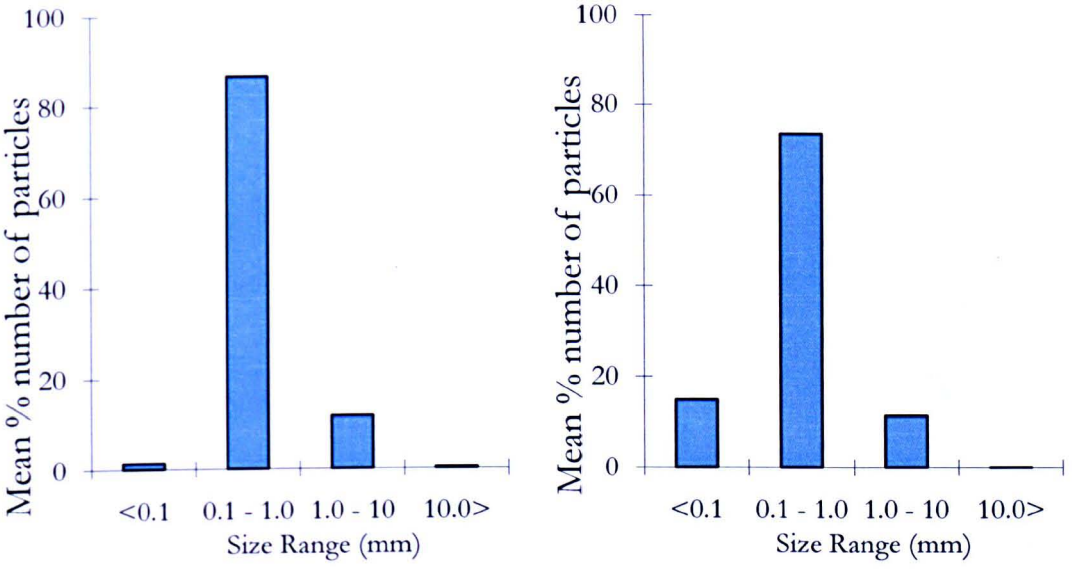

Figure 5.1 Size distribution of Chemtura 90A wear particles after imaging on the A) LEO FEGSEM and, B) Quanta™ FEGESEM

All images in Sections 5.3.3 to 5.3.7 were captured using the Quanta™ FEGESEM.

5.3.3 Particles generated on smooth stainless steel plates in phosphate buffered saline for validation of strong alkali digestion method

Tecoflex 94A, Tecoflex 51D and Corethane 55D (n=4) wear particles were generated on smooth stainless steel plates in phosphate buffered saline (PBS) using the six station multidirectional wear rig. A volume of 1 mm^3 of particles were isolated by filtering lubricants through a 10, 1 and, 0.015 μm pore-sized filters and images of the particles are shown in Figure 5.2 on 1 μm pore-sized filters.

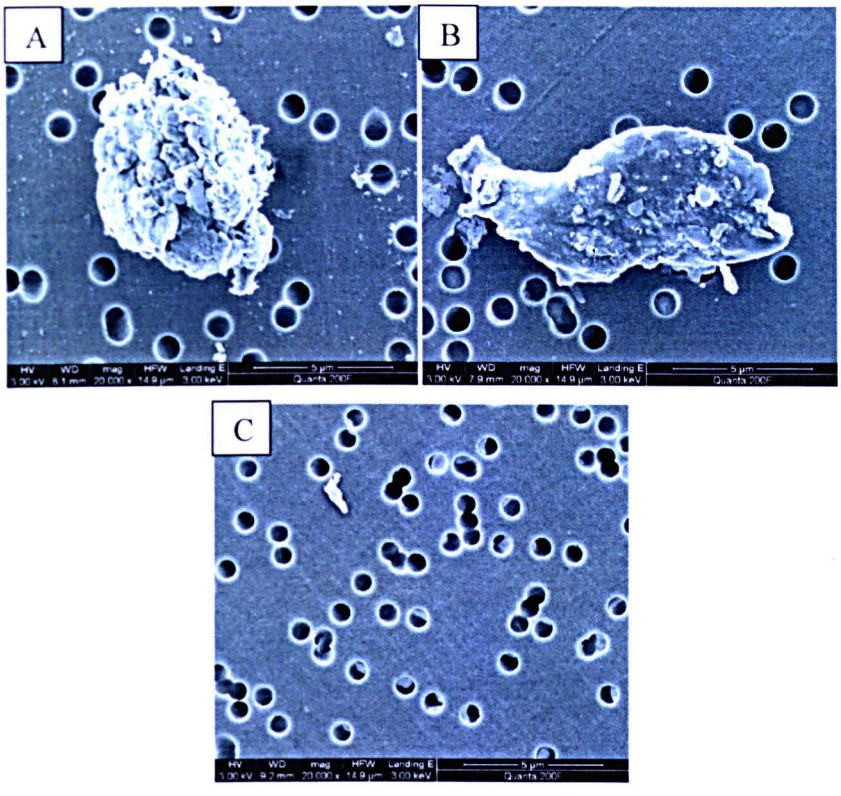

Figure 5.2 Wear particles generated on smooth stainless steel plates in PBS and filtered through a 1 μm pore-sized filter. A) Tecoflex 51D agglomerated flake-like particle (20K Mag), B) Tecoflex 94A flake-like particle (20K Mag) and, C) Corethane 55D fibril-like particle (20K Mag)

The particles were characterised in terms of shape and size using Image-Pro® Plus. Tecoflex 51D generated a higher percentage number of particles in the submicron size range (< 0.1 μm) closely followed by sizes in the range of 0.1 – 1.0 μm (Figure 5.3). The particles < 0.1 μm had a low percentage area while particles in the 0.1-1.0 μm size range had the largest percentage area compared to the other particle size ranges. The lowest percentage number of particles were in the 1.0-10 μm and > 10 μm size ranges, however, only the particles in the 0.1 – 1.0 μm size range occupied a larger percentage area compared to those > 10 μm in size.

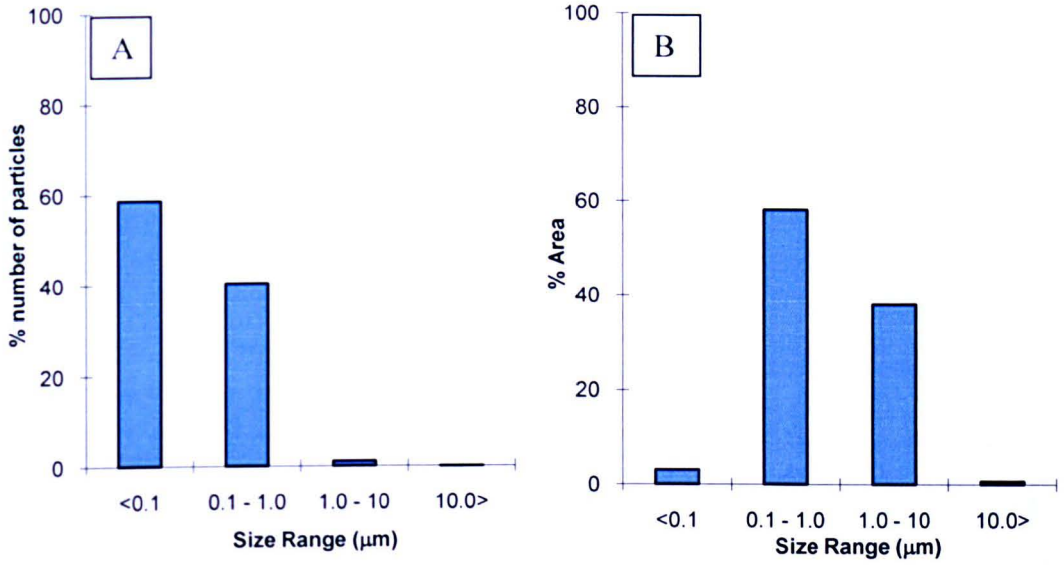

Figure 5.3 Tecoflex 51D generated wear particles on smooth stainless steel plates in PBS showing, A) percentage number of particles and, B) percentage area of wear particles as a function of particle size

Tecoflex 94A generated particles on smooth stainless steel plates in PBS of < 0.1 μm in size had the highest number of particles but the lowest percentage area (Figure 5.4). Particles in the size range of 0.1-1.0 μm were the second highest in percentgae number of particles but the highest percentage area. However, the second highest percentage area were those particles in the size range of 1.0-10 μm even though the percentage number of particles were the lowest. No particles were seen > 10 μm in size.

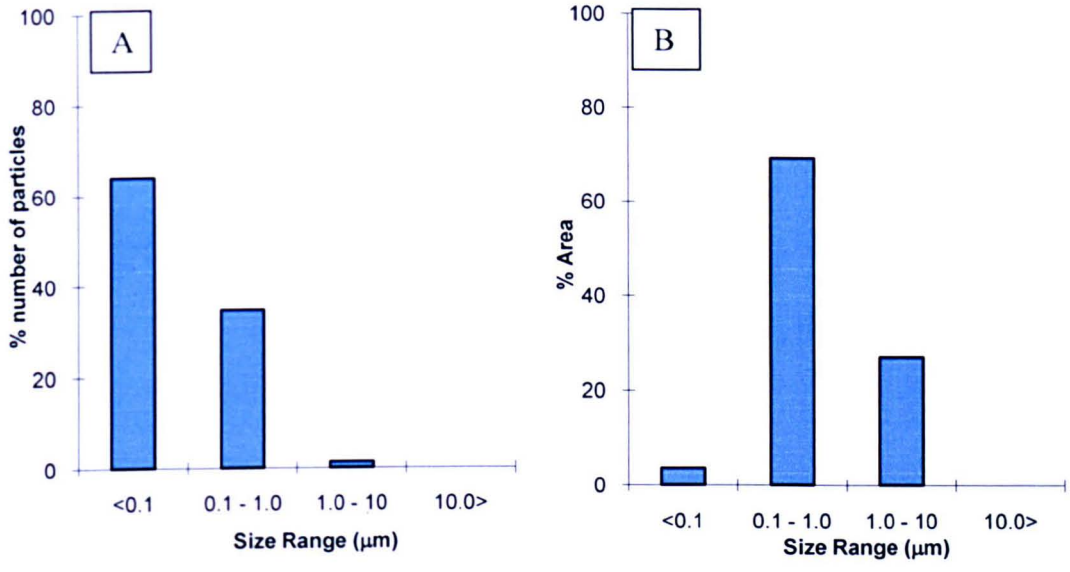

Figure 5.4 Tecoflex 94A generated wear particles on smooth stainless steel plates in PBS showing, A) Percentage number of particles and, B) percentage area of wear particles as a function of particle size

Corethane 55D particles generated on smooth stainless steel plates in PBS had the largest percentgae number of particles < 0.1 μm in size but had the lowest percentage area (Figure 5.5). Particles in the size range of 0.1-1.0 μm had the second highest percentage number of particles which were relative to the percentage area of the particles. The lowest percentage number of particles in the size range of 1.0-10 μm occupied the highest percentage area. No particles were seen > 10 μm in size.

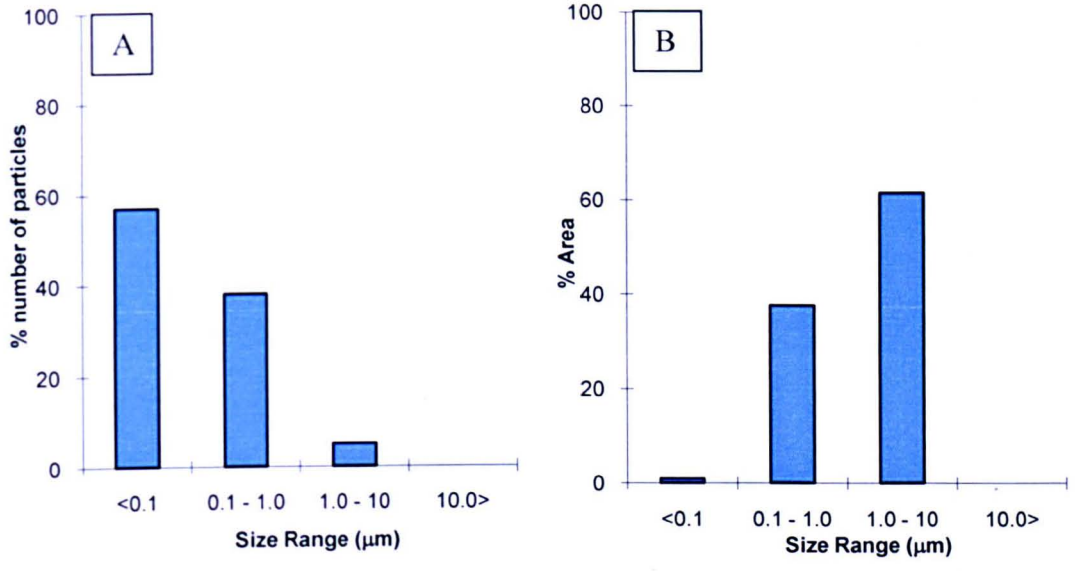

Figure 5.5 Corethane 55D generated wear particles on smooth stainless steel plates in PBS showing, A) Percentage number of particles and, B) percentage area of wear particles as a function of particle size

5.3.4 Particles generated on rough stainless steel plates in phosphate buffered saline for validation of strong alkali digestion method

Tecoflex 94A, Tecoflex 51D and Corethane 55D wear particles were generated on rough stainless steel plates in phosphate buffered saline (PBS) using the 6-station multidirectional wear rig. A volume of 1 mm^3 of particles were isolated by filtering lubricants through a 10, 1 and, 0.015 μm pore-sized filters and images of particles are shown in Figure 5.6 on 0.015 μm pore-sized filters.

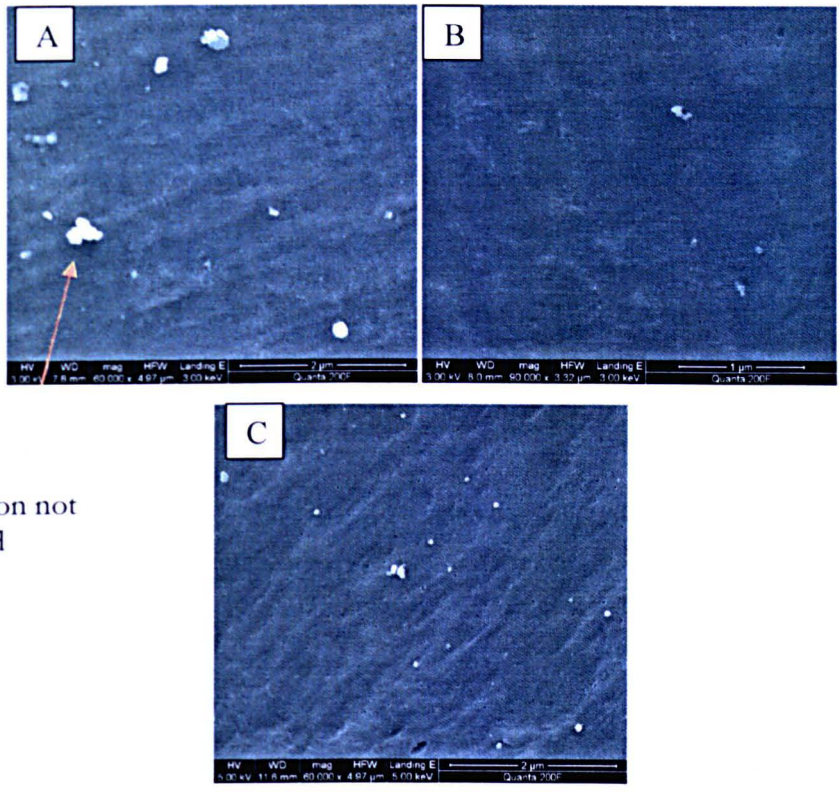

Figure 5.6 Wear particles generated on rough stainless steel plates in PBS and filtered through a 0.015 μm pore-sized filter. A) Flake-like Tecoflex 51D (60K Mag), B) flake Tecoflex 94A particles (90K Mag) and, C) Corethane 55D granules (60K Mag)

Tecoflex 51D particles were generated on rough stainless steel plates in PBS and the largest percentage number of particles were in the size ranges of < 0.1 μm and 0.1-1.0 μm (Figure 5.7). The lowest number of particles were in the 1.0-10 μm and >10 μm size ranges. However, the particles in the range of 0.1-1.0 μm and 1.0-10 μm had the highest percentgae area but the other two size ranges had the lowest percentage area.

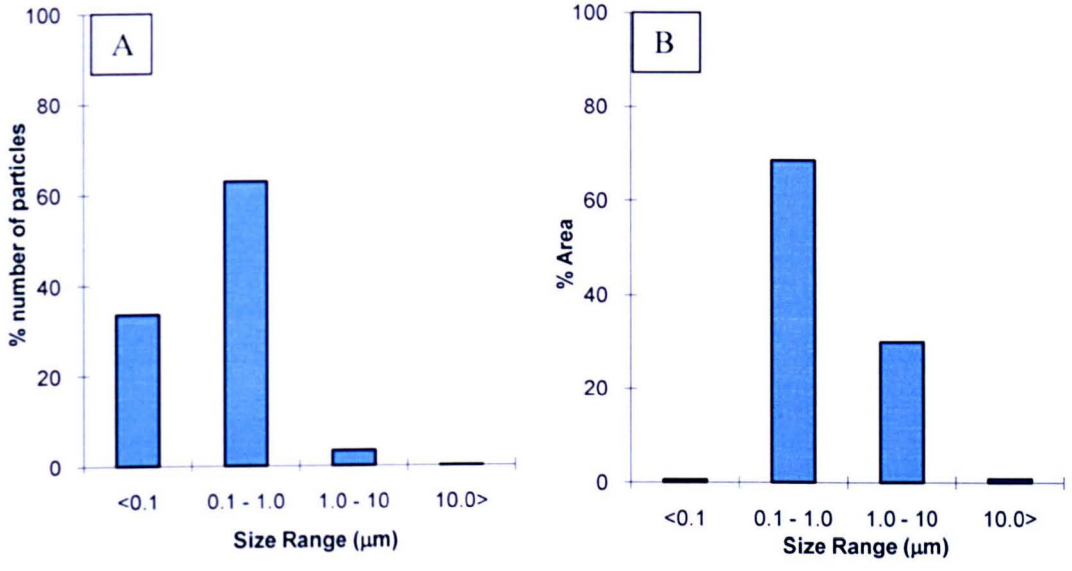

Figure 5.7 Tecoflex 51D generated wear particles on rough stainless steel plates in PBS showing, A) Percentage number of particles and, B) percentage area of wear particles as a function of particle size

Tecoflex 94A particles were generated on rough stainless steel plates in PBS exhibited high percentage number of particles in the size ranges of < 0.1 μm and 0.1-1.0 μm, but only the particles in the 1.0-10 μm size range had the largest percentage area of the two size ranges (Figure 5.8). Particles between 1.0-10 μm in size had the largest percentage area with a low percentage number of particles. The lowest percentage number of particles with the lowest percentage area were those particles > 10 μm in size.

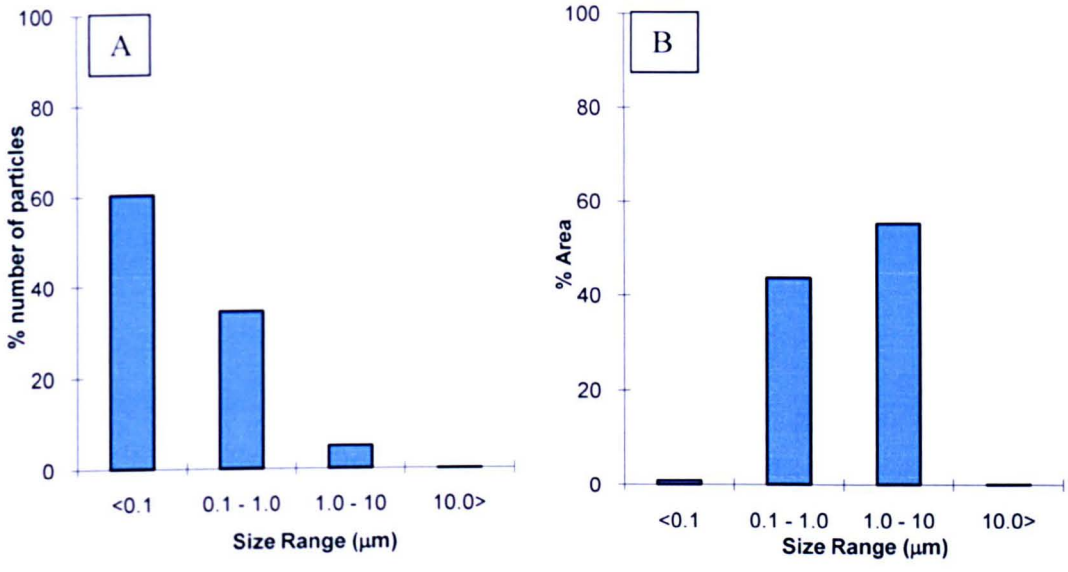

Figure 5.8 Tecoflex 94A generated wear particles on rough stainless steel plates in PBS showing, A) Percentage number of particles and, B) percentage area of wear particles as a function of particle size

Particles were generated on rough stainless steel plates (in PBS) with Corethane 55D and the largest percentage number of particles were less than 0.1 μm in size but had the lowest percentage area (Figure 5.9). A low percentage number of particles in the 0.1-1.0 μm size range was apparent with the largest percentage area. No particles were seen above 10 μm in size.

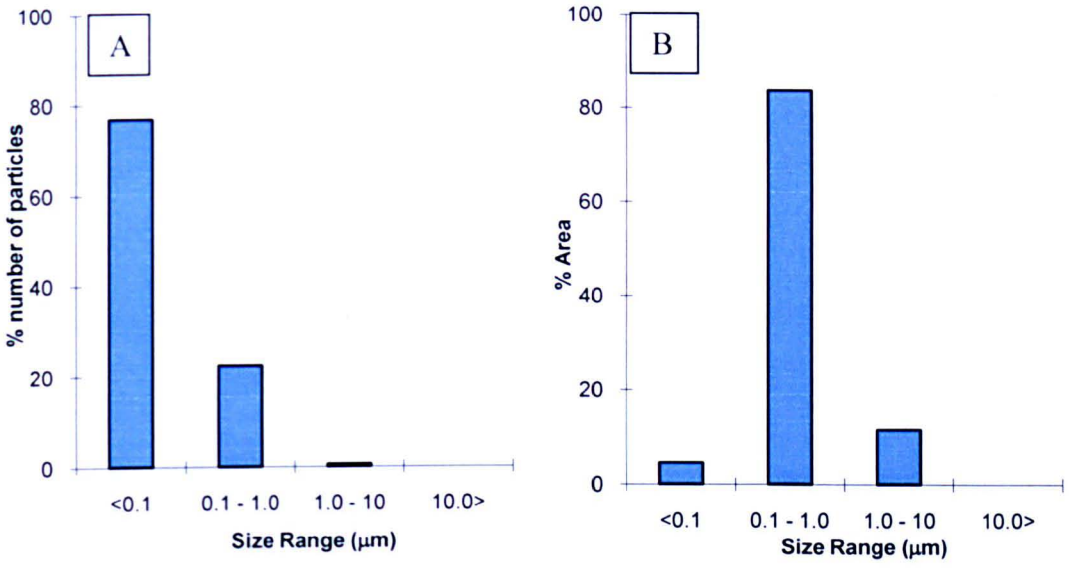

Figure 5.9 Corethane 55D generated wear particles on rough stainless steel plates in PBS showing, A) Percentage number of particles and, B) percentage area of wear particles as a function of particle size

5.3.5 Characterisation of thermoplastic polyurethane particles after digestion with strong alkali - comparison with particles generated in phosphate buffered saline and recovered without alkali digestion

Tecoflex 94A, Tecoflex 51D and Corethane 55D wear particles were generated on smooth stainless steel plates in phosphate buffered saline (PBS) using the six station multidirectional wear rig. The lubricants (1 mm^3 volume) were spiked with 25% (v/v) FBS in order to determine whether the alkali digestion method had an adverse effect on the particle size. Particles were isolated and the lubricants filtered through a 10, 1 and, 0.015 μm pore-sized filters and images of the particles are shown in Figure 5.10 on 10 μm pore-sized filters.

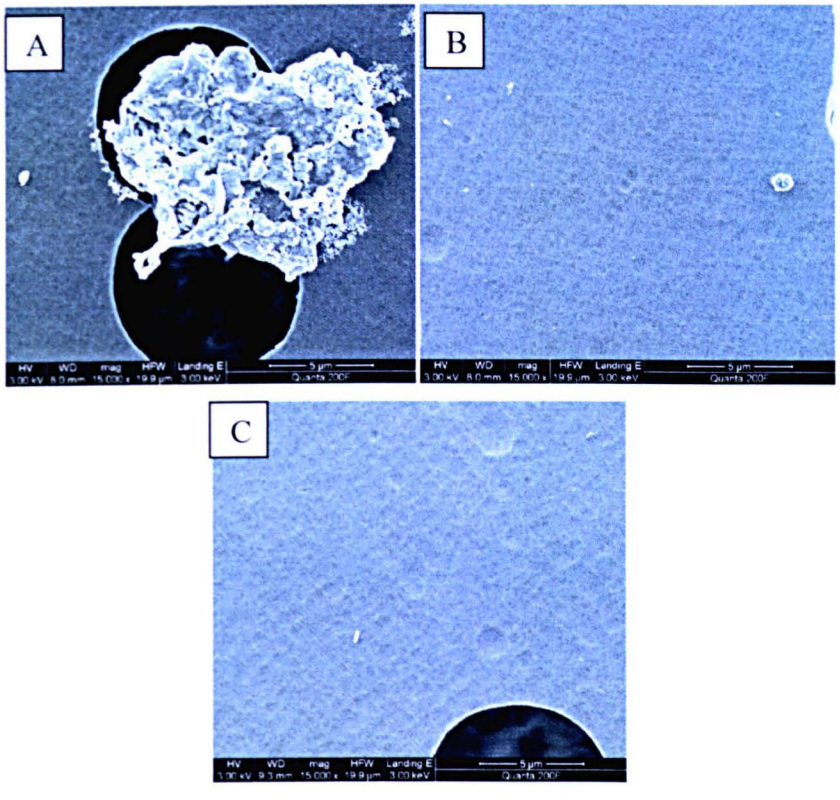

Figure 5.10 Particles generated on smooth stainless steel plates, isolated from PBS + 25% (v/v) FBS and filtered through a 10 μm pore-sized filter. A) a agglomerated flake-like Tecoflex 51D particle (15k Mag), B) a flake-like Tecoflex 94A particle (15k Mag) and, C) a fibril-like Corethane 55D wear particle (15k Mag)

Tecoflex 51D particles were highest in percentage number less than 0.1 μm and between 0.1-1.0 μm, however, these particles had low percentage areas (Figure 5.11). The lowest percentage number of particles were those in the size ranges of 1.0-10 μm and > 10 μm, but particles in the 1.0-10 μm had the highest percentage area.

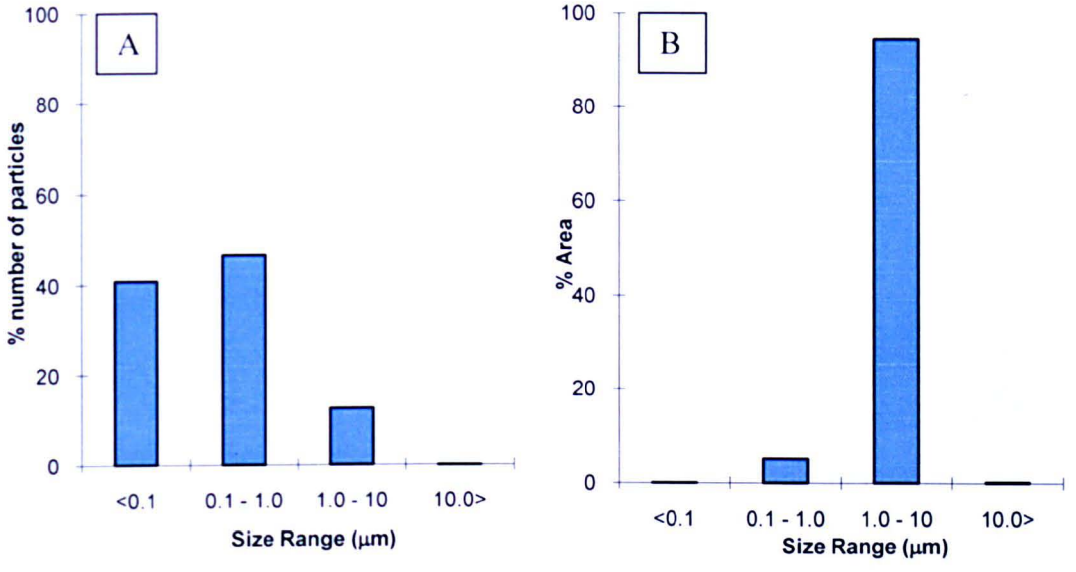

Figure 5.11 Tecoflex 51D generated wear particles on smooth stainless steel plates in PBS + 25% (v/v) FBS showing, A) Percentage number of particles and, B) percentage area of wear particles as a function of particle size

The lowest size range of Tecoflex 94A particles had the largest percentage number of particles (Figure 5.12). The percentage number of particles decreased with increasing particle size, however, percentage area increased with size range.

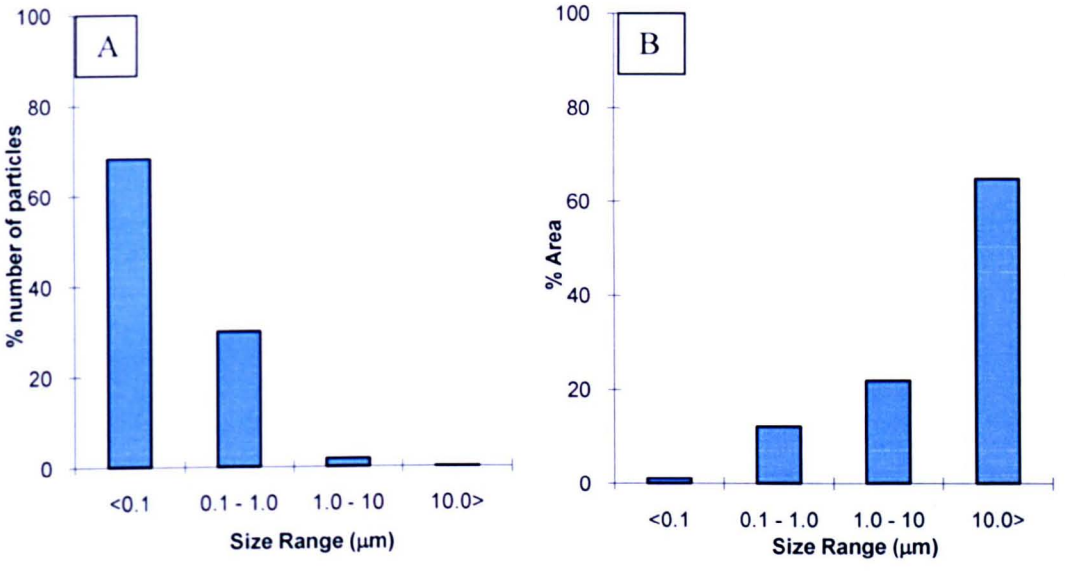

Figure 5.12 Tecoflex 94A generated wear particles on smooth stainless steel plates in PBS + 25% (v/v) FBS showing, A) Percentage number of particles and, B) percentage area of wear particles as a function of particle size

The two lowest size ranges of Corethane 55D particles had the highest percentage number of particles (Figure 5.13). Particle sizes in the 0.1-1.0 μm and 1.0-10 μm ranges had the largest percentage area but the lowest and highest size ranges had the lowest percentgae areas.

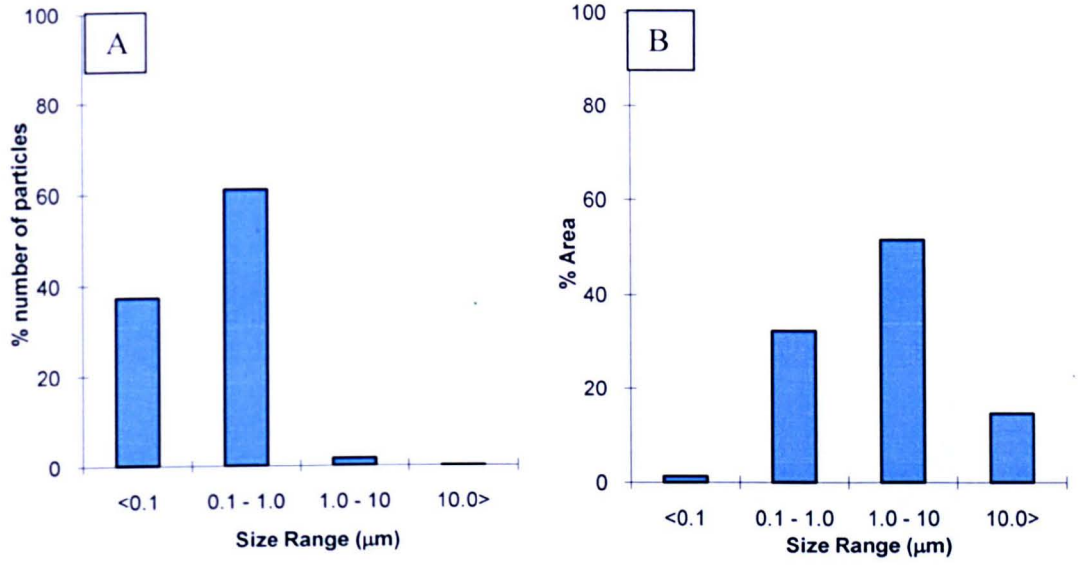

Figure 5.13 Corethane 55D generated wear particles on smooth stainless steel plates in PBS + 25% (v/v) FBS showing, A) Percentage number of particles and, B) percentage area of wear particles as a function of particle size

5.3.6 Characterisation of thermoplastic polyurethane particles after digestion with strong alkali - comparison with particles generated in phosphate buffered saline and recovered without alkali digestion

Tecoflex 94A, Tecoflex 51D and Corethane 55D wear particles were generated on rough stainless steel plates in phosphate buffered saline (PBS) using a six station multidirectional wear rig. The PBS lubricants (1 mm^3 volume) were spiked with 25% (v/v) FBS in order to determine whether the alkali digestion method had an adverse effect on the particle size. Particles were isolated and the lubricants filtered through a 10, 1 and, 0.015 μm pore-sized filters and images of the particles are shown in Figure 5.14 on 1 μm pore-sized filters.

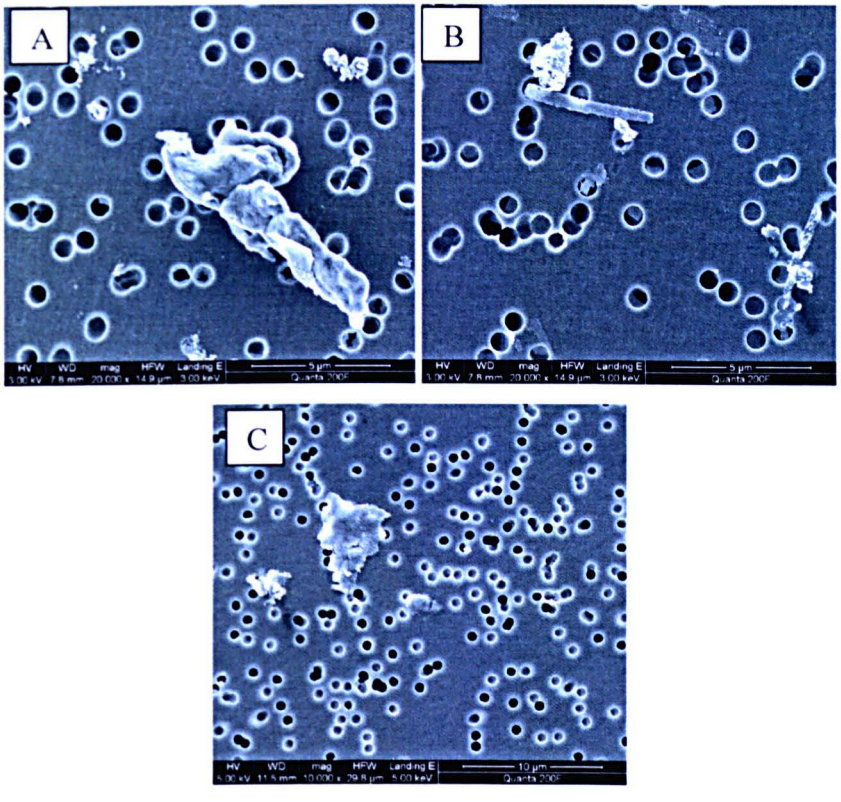

Figure 5.14 Particles generated on rough stainless steel plates, isolated from PBS + 25% (v/v) FBS and filtered through a 1 μm pore-sized filter. A) Tecoflex 51D flake-like particle (20k Mag), B) Tecoflex 94A flake-like particle (60k Mag) and, C) Corethane 55D flake-like particle on (10k Mag)

The highest percentage number of Tecoflex 51D particles were in the 0.1-1.0 μm and the other size ranges had low percentgae number of particles (Figure 5.15). Particles in the size range of < 0.1 μm had the lowest percentgae area, while particles in the other size ranges were higher.

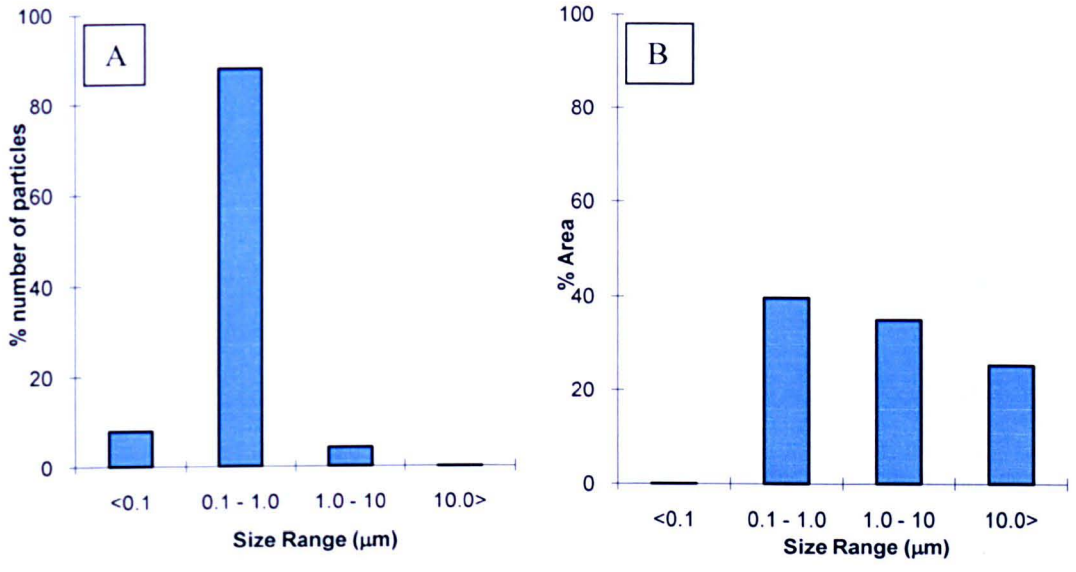

Figure 5.15 Tecoflex 51D generated wear particles on rough stainless steel plates in PBS + 25% (v/v) FBS showing, A) Percentage number of particles and, B) percentage area of wear particles as a function of particle size

Tecoflex 94A particles in the size ranges of < 0.1 μm and 0.1-1.0 μm had the highest percentage number of particles with the lowest percentgae area (Figure 5.16). In contrast the highest percentage area of particles in the 1.0-10 μm and > 10 μm size ranges had the lowest percentgae number of particles.

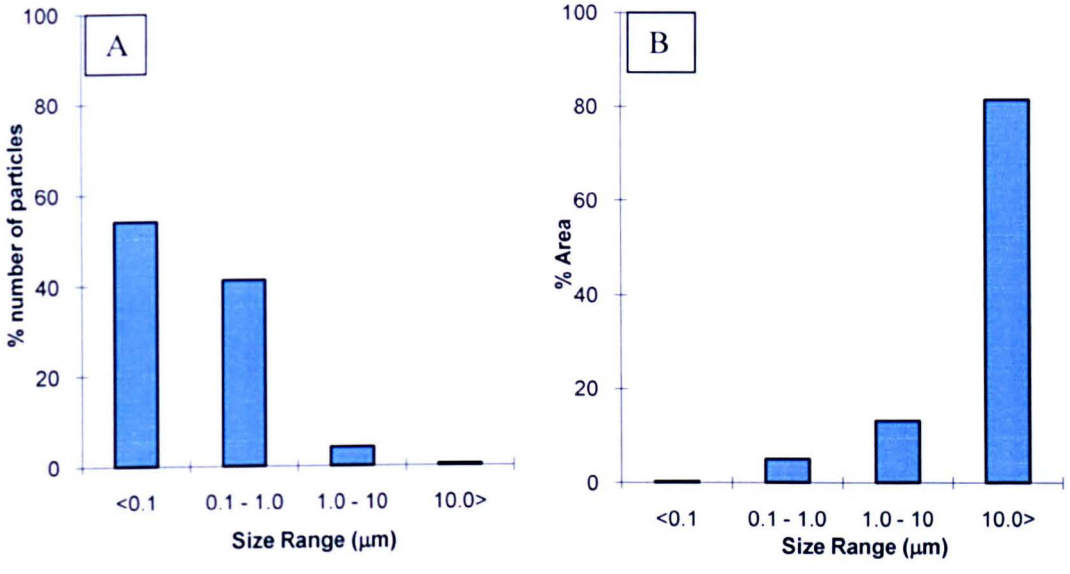

Figure 5.16 Tecoflex 94A generated wear particles on rough stainless steel plates in PBS + 25% (v/v) FBS showing, A) Percentage number of particles and, B) percentage area of wear particles as a function of particle size

The Corethanee 55D particles in size ranges of < 0.1 μm and 1.0-10 μm had similar percentage number of particles, but percentage area was higher in particles of the 1.0-10 μm size range (Figure 5.17). Particle sizes between 0.1-1.0 μm had the largest percentage number but percentage area was lower than 1.0-10 μm and > 10 μm particle sizes. Particles larger than 10 μm in size had the lowest percentgae number of particles.

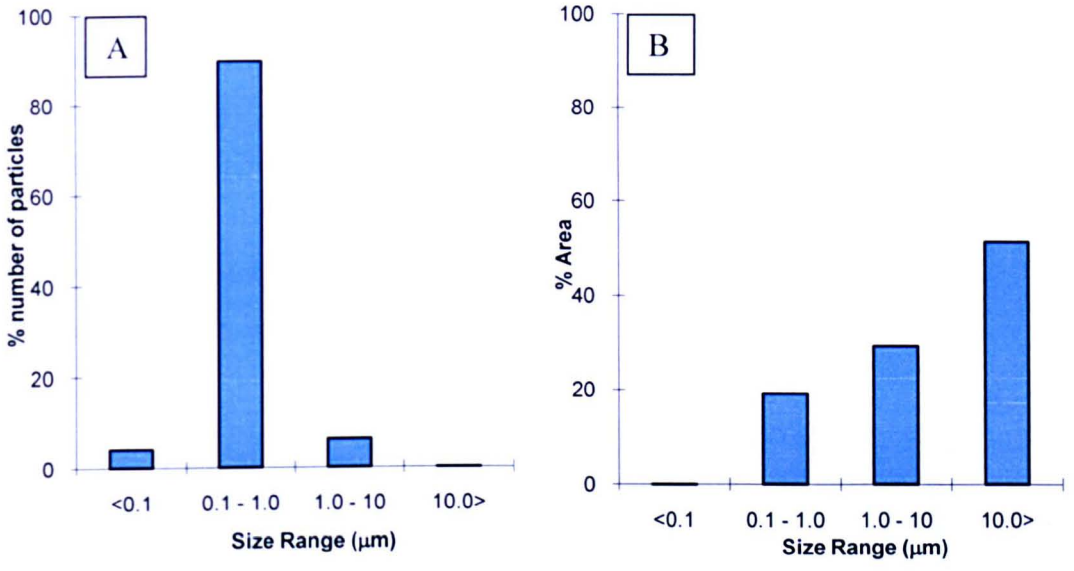

Figure 5.17 Corethane 55D generated wear particles on rough stainless steel plates in PBS + 25% (v/v) FBS showing, A) Percentage number of particles and, B) percentage area of wear particles as a function of particle size

5.3.7 *Particles generated on rough stainless steel plates and isolated from Rosslyn Park Memorial Institute 1640 medium + 25% (v/v) foetal bovine serum*

Chemtura 90A (n=4), Diprane 50D (n=4), polyethylene (n=1), Tecoflex 94A (n=1), Tecoflex 51D (n=1) and Corethane 55D (n=1) wear particles were generated on rough stainless steel plates in Rosslyn Park Memorial Institute 1640 medium (RPMI) + 25% (v/v) foetal bovine serum (FBS) using a single station multidirectional aspetic wear rig to be used in cell culture studies (Chapter 6), and to compare particle sizes to polyethylene particles. A volume of 1 mm^3 of wear particles were isolated and the lubricants and filtered through a 10, 1 and, 0.015 μm pore-sized filters and images of the particles are shown in Figure 5.18. A control sample of RPMI + 25% (v/v) FBS lubricant was digested and which was filtered through the above mentioned pore-sized filters. Particles seen in the controls were subtracted from the material samples during analysis.

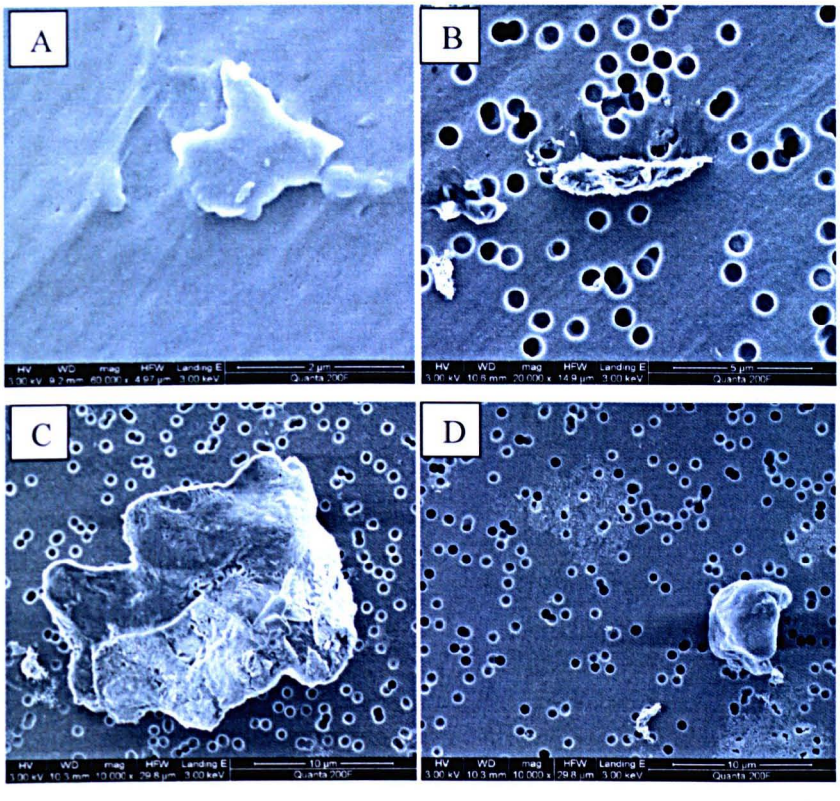

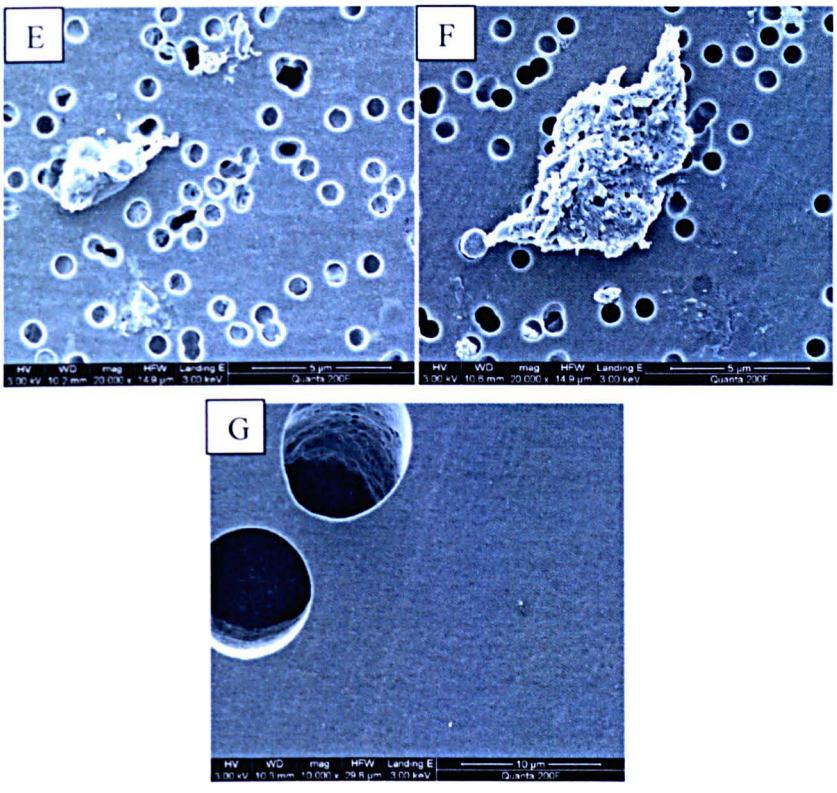

Figure 5.18 Particles generated on rough stainless steel plates, isolated from RPMI + 25% (v/v) FBS and filtered through various pore-sized filters. A) Chemtura 90A flake-like wear particle on 0.015 μm filter paper, 60k Mag, B) Diprane 50D fibril-like particle on 1 μm filter paper, 20k Mag, C) Tecoflex 51D flake-like wear particle on 1 μm, 10k Mag, D) Corethane 55D flake- and fibril-like wear particles on a 10 μm filter, 20K Mag, E) polyethylene wear particle on a 1 μm filter, 20K Mag, F) Tecoflex 94A flake-like wear particle on a 1 μm filter, 20K Mag and, G) Control 25% (v/v) FBS lubricant with granule-like wear particles on a 10 μm filter, 10K Mag

Chemtura 90A particles had the highest percentage number of particles in the 0.1-1.0 μm size range followed by particles less than 0.1 μm and 1.0-10 μm in size (Figure 5.19). The lowest percentage number of particles were those larger than 10 μm in size. Particles between 1.0-10 μm in size had the larger percentgae area followed by those particles larger than 10 μm in size. The lowest percentage area were particles less than 0.1 μm and between 0.1-1.0 μm.

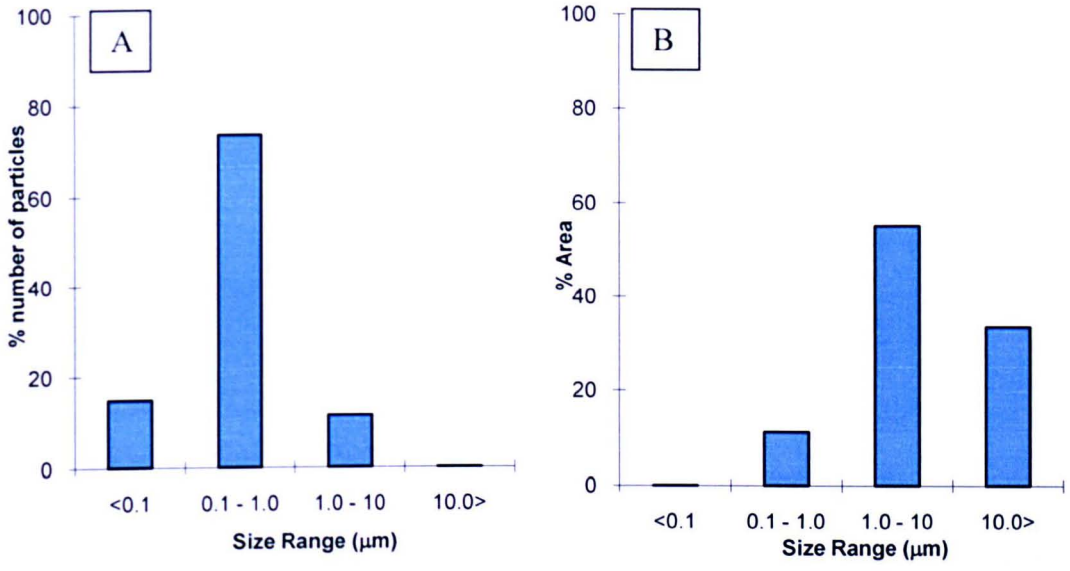

Figure 5.19 Chemtura 90A generated wear particles on rough stainless steel plates in RPMI + 25% (v/v) FBS showing, A) Percentage number of particles and, B) percentage area of wear particles as a function of particle size

The smallest particles size range of Diprane 50D had the largest percentage number of particles. The percentage number of particles decreased with increased particles size (Figure 5.20). The percentage area was highest in particle size ranges 1.0-10 μm followed by particles in the size ranges of 0.1-1.0 μm and > 10 μm, with the lowest percentgae area for those particles less than 0.1 μm in size.

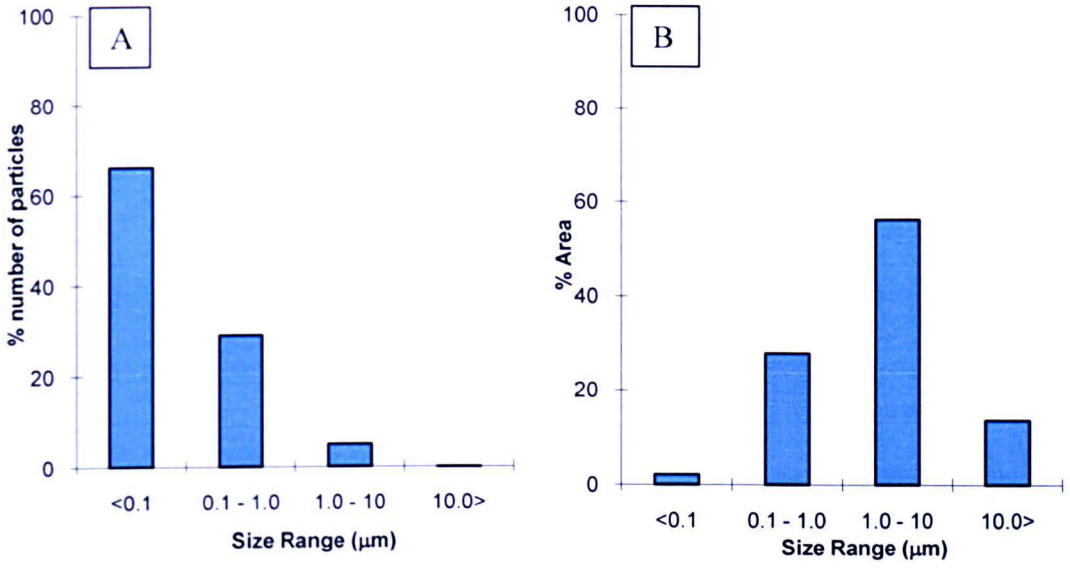

Figure 5.20 Diprane 50D generated wear particles on rough stainless steel plates in RPMI + 25% (v/v) FBS showing, A) Percentage number of particles and, B) percentage area of wear particles as a function of particle size

The largest percentage number of Tecoflex 51D particles were those partcles in the 0.1-1.0 μm size range and also had the highest percentage area, though the percentage areas were similar to those in the 1.0-10 μm and > 10 μm size ranges (Figure 5.21). Particles (< 0.1 μm) with the lowest percentage area had the second highest percentage number of particles.

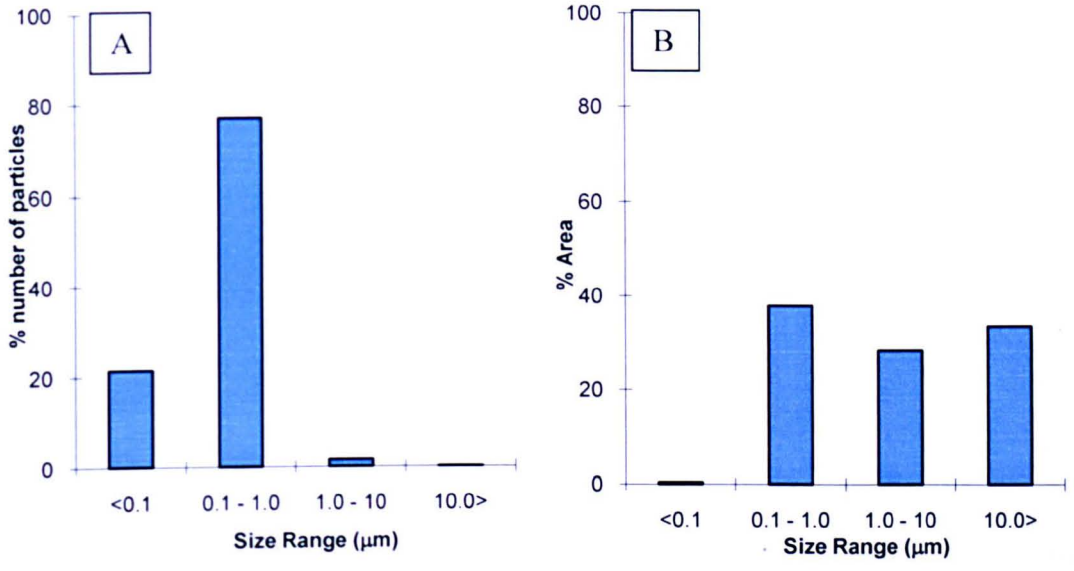

Figure 5.21 Tecoflex 51D generated wear particles on rough stainless steel plates in RPMI + 25% (v/v) FBS showing, A) Percentage number of particles and, B) percentage area of wear particles as a function of particle size

The largest percentage number of Corethane 55D particles were those partcles in the 0.1-1.0 μm size range followed by particles less than 0.1 μm and the two higher size ranges had the lowest percentage number of particles (Figure 5.22). Particles in the 1.0-10 μm had the largest percentage area followed by particles in the size ranges of 0.1-1.0 μm and > 10 μm. The lowest percentage area were from particles less than 0.1 μm in size.

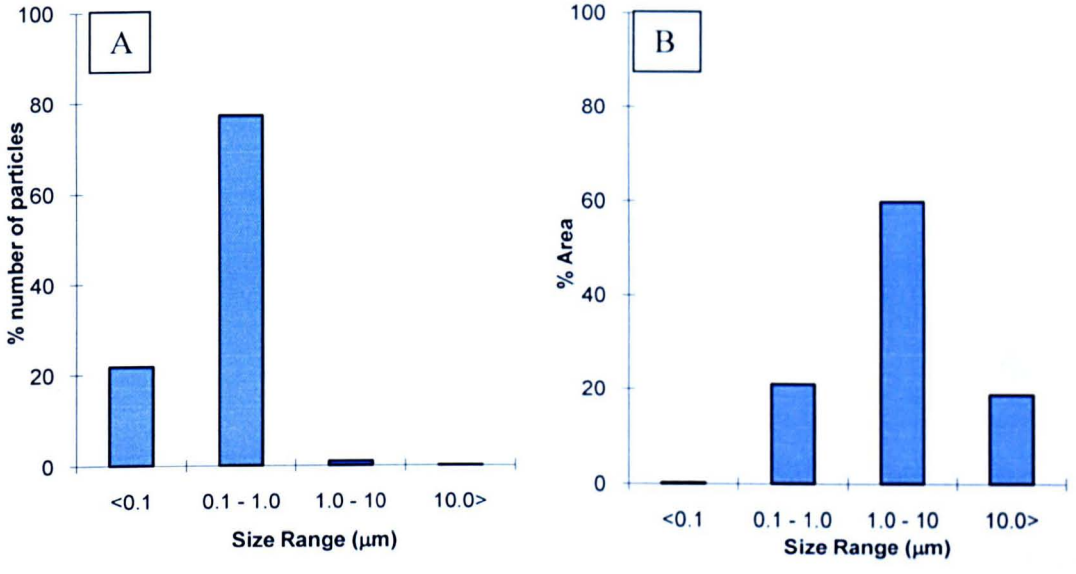

Figure 5.22 Corethane 55D generated wear particles on rough stainless steel plates in RPMI + 25% (v/v) FBS showing, A) Percentage number of particles and, B) percentage area of wear particles as a function of particle size

Polyethylene particles exhibted a similar size ditrubtion of the percentgae number of particles to both Tecoflex 51D and Corethane 55D with the largest number of particles in the 0.1-1.0 μm size range (Figure 5.23). The percentage areas of the particles increased as particle size increased.

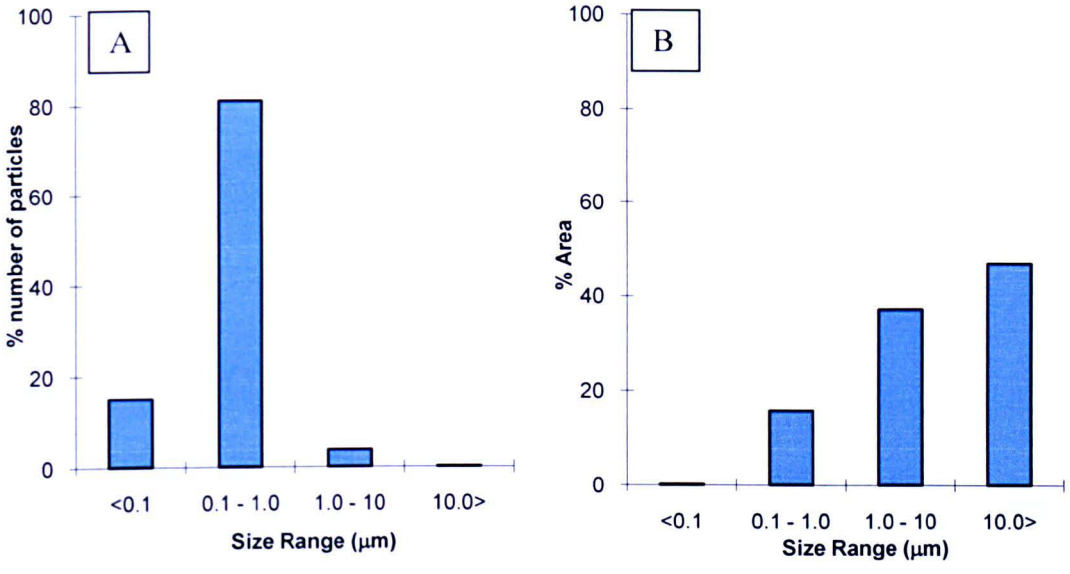

Figure 5.23 Polyethylene generated wear particles on rough stainless steel plates in RPMI + 25% (v/v) FBS showing, A) Percentage number of particles and, B) percentage area of wear particles as a function of particle size

Again, Tecoflex 94A particles showed a similar size distribution to Corethane 55D, polyethylene and Tecoflex 51D particles (Figure 5.24). However, the percentage area of the particles was highest for the 1.0-10 μm sized particles followed by those in the 0.1-1.0 μm size range and particles with the lowest percentage area were those less than 0.1 μm and greater than 10 μm in size.

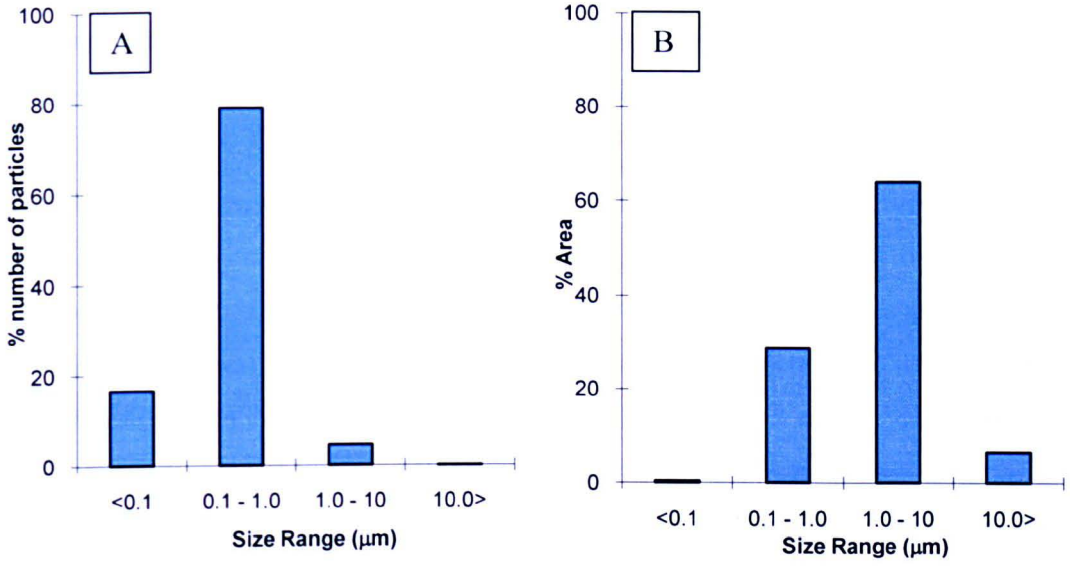

Figure 5.24 Tecoflex 94A generated wear particles on rough stainless steel plates in RPMI + 25% (v/v) FBS showing, A) Percentage number of particles and, B) percentage area of wear particles as a function of particle size

5.4 Discussion

It has been reported that polyethylene (PE) particles generated *in vivo* at the articulating surfaces of implants are generally less than 10 μm in size with few particles being several millimetres in size and particle sizes at the lower end are thought to be the most biologically active (Gelb *et al.*, 1994). However, PE particles in the submicrometer size range are commonly found in vivo (Matthews *et al.*, 2000). In the present study the majority of the particles generated were less than 10 μm in size. In this study wear particles were generated from thermoset (Diprane 50D and Chemtura 90A) and thermoplastic (Corethane 55D, Tecoflex 51D and 94A) polyurethanes (PUs) and compared to particles generated by PE.

Smooth and rough stainless steel plates were used to generate the thermoplastic polyurethane (TPU) particles using the six station pin-on-plate multidirectional wear rig which were compared to observe which bearing surface generated the most clinically

relevant sized particles. The particles were generated in phosphate buffered saline (PBS) and a volume of 1 mm^3 of particles was filtered before sizing. Addition of 25% (v/v) foetal bovine serum (FBS) was introduced to the same volume of particles which were then digested in a strong alkali to determine whether the digestion method had any adverse effects on the particles. The size and area distributions from each lubricant were then compared. PVA/PVP hydrogel wear particles were also generated in the six station pin-on-plate multidirectional wear rig, however, due to the deformation and high level of surface damage, the experiments were stopped early.

In preliminary tests, aseptic wear particles were generated from the thermoset PUs in a single station pin-on-plate multidirectional wear rig. However, due to time constraints wear particles were not generated from these materials using the six station pin-on-plate multidirectional wear rig. Therefore, it was not possible to determine whether the strong alkali digestion was detrimental to the particles. PE and TPU aseptic wear particles were also generated using the single station pin-on-plate multidirectional wear rig (in Rosslyn Park Memorial Institute 1640 medium (RPMI) + 25% (v/v) FBS), in order to perform cell culture studies (Chapter 6) and compare particle sizes to the PE particles. The size and area distributions of the thermoplastic wear particles were compared to those of the PE wear particles and to the TPU particles generated using the six station pin-on-plate multidirectional wear rig.

The wear factors indicated that Tecoflex 94A had a significantly lower level of wear compared to Tecoflex 51D and Corethane 55D when particles were generated in the six station pin-on-plate multidirectional wear rig. However, there were no significant differences in wear when bearing surfaces were compared. Tecoflex 51D and Corethane 55D had lower wear factors compared to the other materials when tested in the aseptic single station multidirectional pin-on-plate wear rig, this may indicate that the presence of serum had an effect on the wear.

Tecoflex 51D particles generated on smooth stainless steel plates (in PBS) exhibited similar particle size distributions to the same material particles generated on rough stainless steel plates. Comparing the particles generated on smooth plates for all three TPUs, particles less than 0.1 μm in size were the most frequently observed and particles in the 0.1-1.0 μm size range were the second most frequently observed. When thermoplastic PUs particles

were generated on rough stainless steel plates (in PBS) particles less than 1.0 μm in size were observed most frequently. Particles in size ranges 0.1-1.0 μm and 1.0-10 μm had the largest percentage area similar to particles generated on smooth stainless steel plates. Only Tecoflex 51D generated particles larger than 10 μm when articulated against smooth stainless steel plates, however, both Tecoflex 51D and Tecoflex 94A produced particles larger than 10 μm in size when articulated against rough stainless steel plates.

When lubricants were spiked into 25% (v/v) FBS and digested with strong alkali the size distributions of the TPU particles on smooth stainless steel plates were similar to those generated on rough stainless steel plates, except for the Corethane 55D particles. A volume of 1 mm^3 wear particles were retrieved from the lubricants spiked with 25% (v/v) FBS, indicating that the digestion method had not been detrimental to the thermoplastic wear particles. It was apparent that the samples contained particles larger than 10 μm in size when the particles had been subjected to alkali digestion compared to the particles isolated from PBS alone. Particles generated on smooth stainless steel plates a larger percentage number of particles contained less than 0.1 μm and between 0.1-1.0 μm in size (the submicron sized range particles), however, the percentage area distributions were more variable. Tecoflex 51D had a higher percentage number of particles in the 0.1-1.0 μm size range and the percentage areas were similar with particles in the 0.1-1.0 μm, 1.0-10 μm and > 10 μm ranges. This finding was similar to Corethane 55D, except particles larger than 10 μm in size accounted for the largest percentage area. Tecoflex 94A had the largest number of particles in the submicron size range, with particles larger than 10 μm exhibiting the largest percentage area.

All the PU materials articulated on rough stainless steel plates in RPMI + 25% (v/v) FBS exhibited a mode of percentage number of particles in either the 0.1-1.0 μm size range or the < 0.1 μm size range. Chemtura 90A, Diprane 50D, Corethane 55D and Tecoflex 94A exhibited a mode of area distrubtion in the 1.0-10 μm size range. Tecoflex 51D particles had similar percentage areas in the three size ranges above 0.1 μm. The percentage area increased when particle size increased for the PE particles.

Comparing the modes frequency for size and area of the particles generated against smooth plates in PBS, it was found that all three TPUs had a mode of frequency distribution of particles < 0.1 μm in size. However, the mode of area distribution for Tecoflex 51D and

94A was 0.1-1.0 μm, but 1-10 μm for Corethane 55D particles. When serum was added to the lubricants the mode of frequency distributions changed slightly. Tecoflex 51D and Corethane 55D had a frequency distribution in the 0.1-1.0 μm size range, while Tecoflex 94A remained the same at < 0.1 μm. The mode of area distribution remained the same for Corethane 55D (1-10 μm), however, Tecoflex 51D and Tecoflex 94A moved up a size range (1.0-10 μm and > 10 μm, respectively). This suggested that addition of serum may have caused the particles to aggregate. When the thermoplastic wear particles were generated on rough stainless steel plates in PBS the mode of frequency distribution of Tecoflex 51D was in the 0.1-1.0 μm size range (a size range higher compared to the particles generated on the smooth stainless steel plates), while the frequency distrubtion for Tecoflex 94A and Corethane 55D was < 0.1 μm (comparable to the particles generated on the smooth stainless steel plates). The mode of area distribution for Tecoflex 51D was in the size range of 0.1-1.0 μm (same as those particles generated on smooth stainless steel plates), however, the mode of area distribution for Tecoflex 94A and Corethane 55D were 1-10 μm and 0.1-1.0 μm (respectively), and had both moved up to the next size range compared to the particles generated against smooth stainless steel plates. When serum was added to the lubricants the mode of frequency distribution remained the same for Texoflex 94A and Tecoflex 51D, but moved up to the next size range for Corethane 55D to 0.1-1.0 μm compared to particles isolated from PBS. This suggested that the serum may have aggregated the particles. The mode of area distribution stayed the same for the Tecoflex 51D particles, however, the area distributions moved up to thenext size range for both Tecoflex 94A (> 10 μm) and Corethane 55D (> 10 μm), possibly caused the serum aggregating of particles.

When aseptic particles were generated in the single station wear in RPMI + 25% (v/v) FBS, the mode of frequency distribution for Diprane 50D and all the TPUs were in the size range of 0.1-1.0 μm, comparable to PE. However, the mode of frequency distribution for Diprane 50D was in the < 0.1 μm size range. The mode of area distribution for the thermoset PUs, Corethane 55D and Tecoflex 94A were in the 1.0-10 μm size range, but Tecoflex 51D had a mode of area distribution in the 0.1-1 μm size range. The mode of area distributions for all material samples were not comparable to PE which was in the > 10 μm size range.

The particle shapes (flake, granule, fibril) observed in this present study have been seen in other studies (Savio *et* al., 1994; Richards, 2008). It has been reported that ultra high molecular weight PE submicron particles are granular or round and 1-5 μm in size, while fibres and flakes of this material are between 5-25 μm in size (Savio *et* al., 1994). However, the flake-like PE particles observed in this study were less than 5 μm. It is known that different materials generate different size and shape particles, and this is possibly due to the composition of the materials. As already mentioned in the introduction of this chapter it was important to determine whether the size of particles generated in this study were clinically relevant. PE particles in the submicrometer size range are commonly found in vivo (Matthews *et al.*, 2000) and the mode of frequency for the particles generated in this study were in the submicron range and therefore comparable. However could potentially activate macrophages to release pro-inflammatory cytokines. It has been reported that PE particles less than 10 μm in size are thought to be the most biologically active (Gelb *et al.*, 1994). Therefore, it was necessary to perform cell culture studies using the generated aseptic wear particles to determine their biological activity. This is further discussed in Chapter 6.

5.5 Conclusion

Tecoflex 94A exhibited less wear compared to Corethane 55D and Tecoflex 51D in the absence of serum, however, serum may have affected the wear of Corethane 55D and Tecoflex 51D. The mode of frequency and frequency of area distributions remained the same for all materials tested suggesting the alkali digestion did not have any adverse affects on particle size. The mode of frequency for aseptic particles generated from Chemtura 90A and all the thermoplastic polyurethanes were the same as the polyethylene frequency (0.1-1.0 μm), suggesting the particles were clinically relevant in size

Chapter Six

Biological response to polyurethane and polyethylene wear particles

6.1 Introduction

This chapter focuses on cytokine (tumour necrosis factor-alpha [TNF-alpha], interleukin-1 beta [IL-1β], interleukin-6 [IL-6] and interleukin-8 [IL-8]) stimulated release when peripheral blood mononuclear cells (PBMNCs) were cultured with wear particles generated from thermoset polyurethanes (Chemtura 90A and Diprane 50D), thermoplastic polyurethanes (Tecoflex 94A and 51D and, Corethane 55D) and, ultra high molecular weight polyethylene (for further details see Chapter 5). The PVA/PVP hydrogels were not used as the surface damage occurred making them unfavourable (described in Chapter 5). The aim of this chapter was to determine the biological response of the ultra high molecular weight polyethylene, thermoset and thermoplastic polyurethanes.

6.2 Materials and Methods

Aseptic wear particles were generated (see Chapter 5) from ultra high molecular weight polyethylene (Section 2.3.6), thermoset (Section 2.3.4) and thermoplastic (Section 2.3.5) polyurethane in a single station multidirectional pin-on-plate wear rig (Section 2.4.5.2). These materials were reciprocated against rough (Ra = 0.07 – 0.08 μm) stainless steel plates (Section 2.3.9) in Rosslyn Park Memorial Institute 1640 culture medium 1640 + 25% (v/v) foetal bovine serum (Sections 2.2.3 and 2.2.5). Agarose gels (Section 2.4.10.1.2) contained aseptic wear particles at a concentration of 10 μm^3 particles per cell and 100 μm^3 particles per cell (Sections 2.4.7 and 2.4.8). Primary human peripheral blood mononuclear cells (Sections 2.4.10.1 to 2.4.10.1.3) were cultured with the wear particles for 12 and 24 h time periods. An MTT [3-(4,5-dimethylthiazol-2-yl)-2,5-diphenyltetrazolium bromide] assay

was performed to determine cell viability and cytokine release was assessed by enzyme-linked immunosorbent assay (Sections 2.4.10.3 to 2.4.10.3.4)

6.3 Results

6.3.1 Cell viability and cytokine release from cells from Donor 1

The addition of wear particles did not affect the cell viability of Donor 1 cells at 12 and 24 h, as no significant differences (ANOVA, $p < 0.05$) were evident between any of the groups compared to the negative control [cells only] (Figure 6.21).

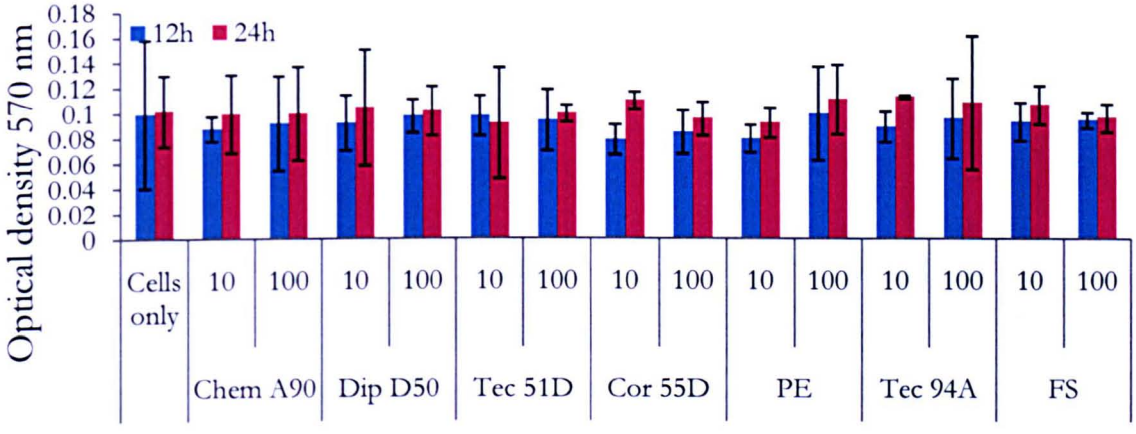

Figure 6.1 MTT assay showing PBMNC cell viability (Donor 1) at 12 and 24 hours at 10 μm^3 and 100 μm^3 particles per cell. Chem 90A - Chemtura 90A; Dip 50D – Diprane 50D, Tec 51D – Tecoflex 51D, Cor 55D – Corethane 55D, PE – polyethylene, Tec 94A – Tecoflex 94A, FS – 0.2 μm FluoShperes™. Mean ± 95% confidence intervals. Optical density (OD), 570 nm.

The positive control (FluoSpheres) stimulated the release of significantly higher tumour necrosis factor alpha (TNF-alpha) compared to the cells only negative control. Tecoflex 94A particles stimulated a significant release of TNF-alpha at 10 μm^3 per cell from cells from Donor 1, which was significantly higher than the cell only negative control at 12 h (hours). In addition, Tecoflex 94A particles also stimulated a significantly higher release of TNF-alpha at 100 μm^3 per cell compared to the negative control at 24h (Figure 6.2). There were no significant differences ($p > 0.05$) with any other particles compared to the negative control.

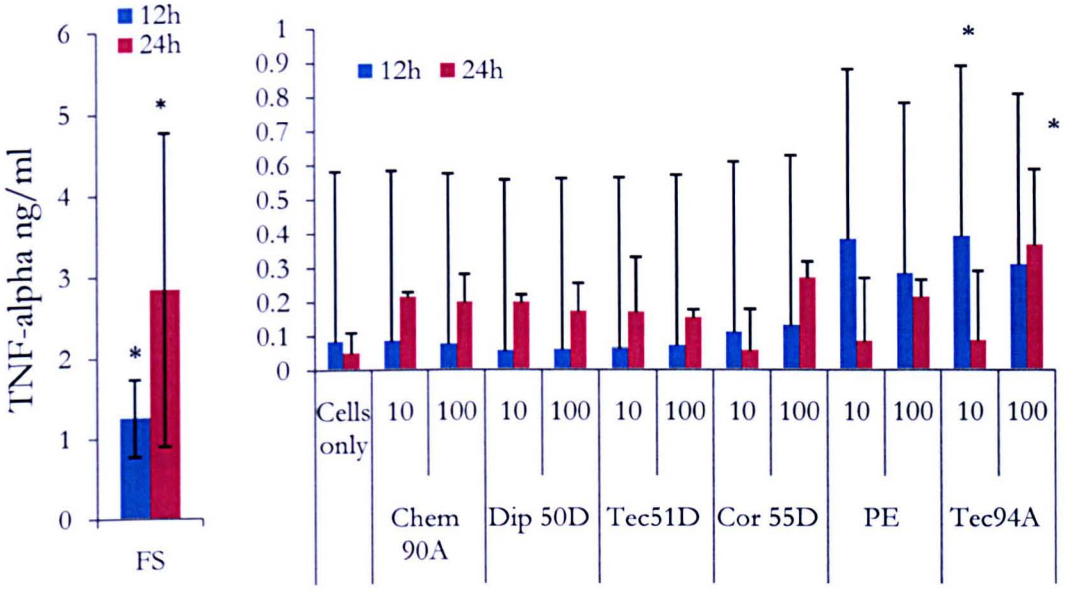

Figure 6.2 Mean (± 95% confidence interval) TNF-alpha release from PBMNC's from Donor 1 stimulated with Chemtura 90A (Chem 90A), Diprane 50D (Dip 50D), Tecoflex 94A (Tec 94A), Tecoflex 51D (Tec 51D), Corethane 55D (Cor 55), polyethylene (PE), and FluoSpheres™ (0.2 μm) at 10 μm^3 and 100 μm^3 particles per cell for 12 and 24 hours. Cell only (n = 3) were the negative control and FluoSpheres™ (FS) were the positive control Statistically higher TNF-alpha release compared to cells only at the same time point indicated by * ($p < 0.05$; ANOVA).

The positive control (FluoSpheres) stimulated the release of significantly higher interleukin-1 beta (IL-1β) compared to the cells only negative control. Chemtura 90A particles at 10 μm^3 and 100 μm^3 particles per cell concentrations stimulated significantly higher release of IL-1β compared to the cells only negative control at the 12 h time point (Figure 6.3). There were no statistical differences seen between particles from all other materials compared to the negative control and IL-1β secretion remained low. There were no significant differences ($p > 0.05$) with any other particles compared to the negative control.

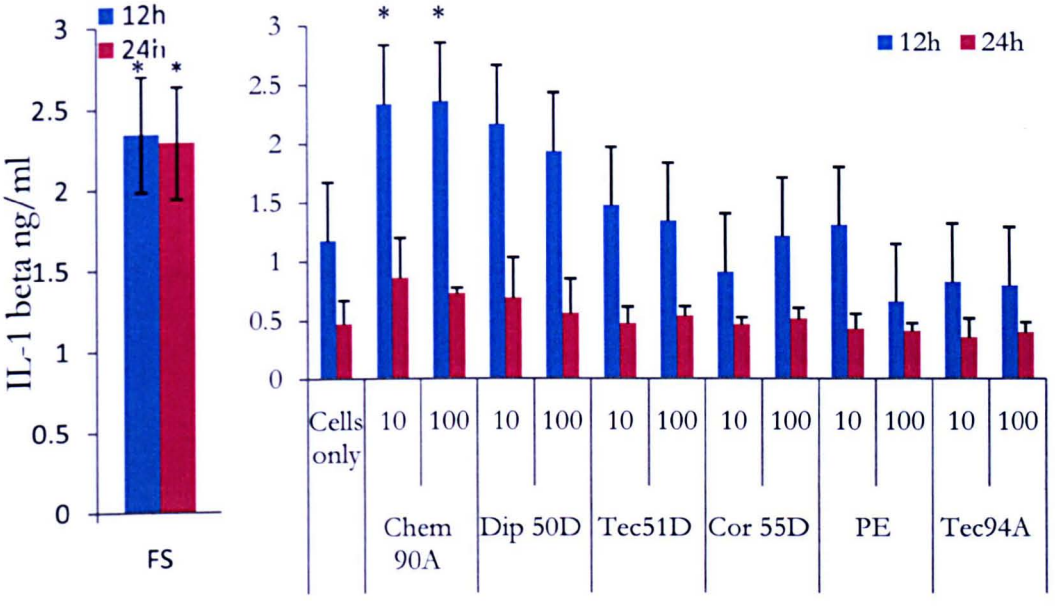

Figure 6.3 Mean (± 95% confidence interval) IL-1β release from PBMNC's from Donor 1 stimulated with Chemtura 90A (Chem 90A), Diprane 50D (Dip 50D), Tecoflex 94A (Tec 94A), Tecoflex 51D (Tec 51D), Corethane 55D (Cor 55), polyethylene (PE) and, 0.2 μm FluoSpheres™ (FS) at 10 μm^3 and 100 μm^3 particles per cell for 12 and 24 hours. Cell only (n = 3) were the negative control and FluroSpheres™ (FS) were the positive control. Statistically higher IL-1β release indicated by * ($p < 0.05$; ANOVA).

The positive control (FluoSpheres) stimulated the release of significantly higher interleukin-6 (IL-6) compared to the cells only negative control. At a ratio of 100 μm^3 particles per cell, Tecoflex 51D, PE (polyethylene) and, Tecoflex 94A stimulated significantly higher levels of secretion of IL-6 compared to the cells only negative control at 24 h. However, only Tecoflex 94A at 100 μm^3 particles per cell induced significantly higher cytokine release than the negative control at 12 h (Figure 6.4). There were no significant differences ($p > 0.05$) with any other particles compared to the negative control.

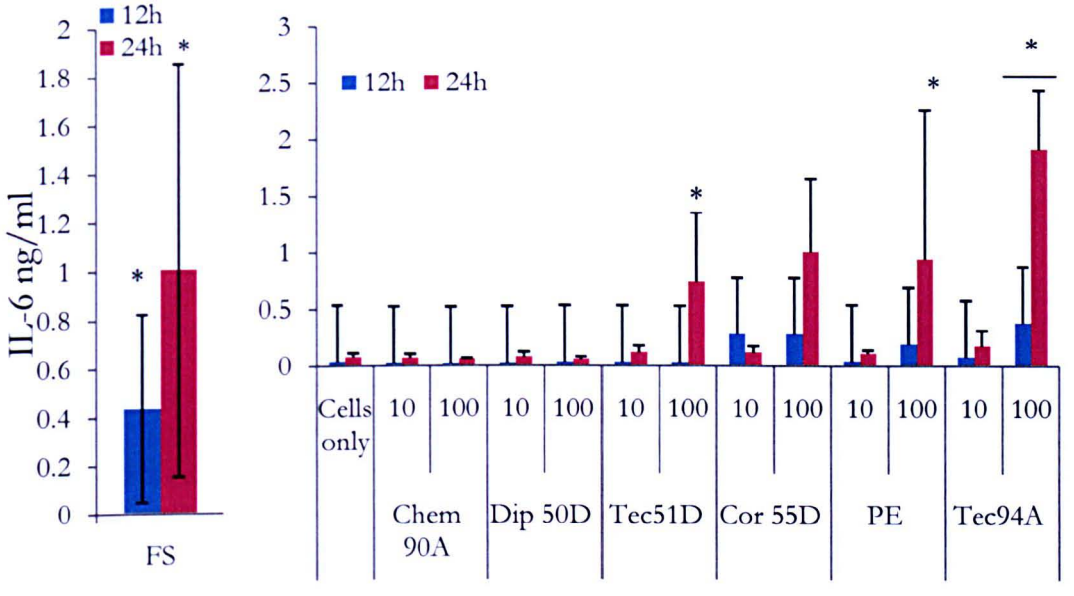

Figure 6.4 Mean (± 95% confidence interval) IL-6 release from PBMNC's from Donor 1 stimulated with Chemtura 90A (Chem 90A), Diprane 50D (Dip 50D), Tecoflex 94A (Tec 94A), Tecoflex 51D (Tec 51D), Corethane 55D (Cor 55) and, polyethylene (PE) at 10 μm^3 and 100 μm^3 particles per cell for 12 and 24 hours. Cell only (n = 3) were the negative control and 0.2 μm FluroSpheres™ (FS) were the positive control. Statistically higher IL-6 release indicated by *, — includes adjacent time point ($p < 0.05$; ANOVA).

The positive control (FluoSpheres) stimulated the release of significantly higher interleukin-8 (IL-8) compared to the cells only negative control. Cells were stimulated by Tecoflex 51D, Corethane 55D, polyethylene (PE) and, Tecoflex 94A at a concentration of 100 μm^3 particles per cell to secrete a significantly higher level of IL-8 at 24 h (Figure 6.5). The 10 μm^3 particles per cell concentration of Tecoflex 94A also stimulated a significant increase in IL-8 compared to the negative control (cells only) at 24 h. There were no significant differences ($p > 0.05$) with any other particles compared to the negative control.

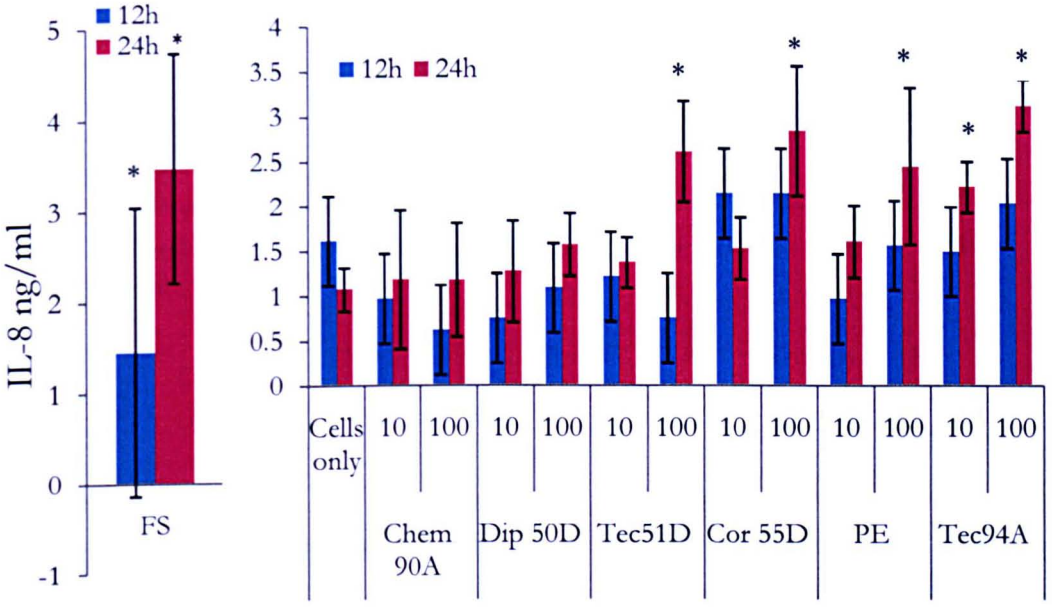

Figure 6.5 Mean (± 95% confidence interval) IL-8 release from PBMNC's from Donor 1 stimulated with Chemtura 90A (Chem 90A), Diprane 50D (Dip 50D), Tecoflex 94A (Tec 94A), Tecoflex 51D (Tec 51D), Corethane 55D (Cor 55) and, polyethylene (PE) at 10 μm^3 and 100 μm^3 particles per cell for 12 and 24 hours. Cell only (n = 3) were the negative control and 0.2 μm FluroSpheres™ (FS) were the positive control. Statistically higher IL-8 release indicated by * ($p < 0.05$; ANOVA).

6.3.2 *Cell viability and cytokine release from cells from Donor 2*

The addition of wear particles did not affect the cell viability of Donor 2 from cells at 12 and 24 h. No significant differences were apparent between any of the groups compared to the negative control [cells only] (Figure 6.6).

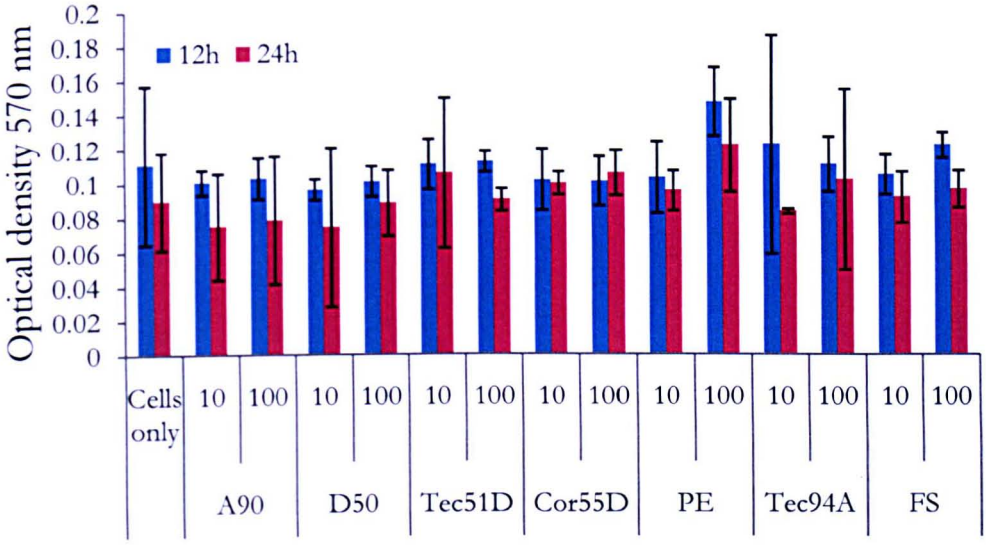

Figure 6.6 MTT assay showing PBMNC cell viability of Donor 2 at 12 and 24 hours at 10 μm^3 and 100 μm^3 particles per cell. Chem 90A - Chemtura 90A; Dip 50D – Diprane 50D, Tec 51D – Tecoflex 51D, Cor 55D – Corethane 55D, PE – polyethylene, Tec 94A – Tecoflex 94A, FS – 0.2 μm FluoShperes™. Mean ± 95% confidence intervals. Optical density (OD), 570 nm.

The positive control (FluoSpheres) stimulated the release of significantly higher tumour necrosis factor alpha (TNF-alpha) compared to the cells only negative control. At 12 h a significant increase in the release of TNF-alpha was observed when cells were exposed to Chemtura 90A (10 μm^3 particles per cell) and Tecoflex 94A (100 μm^3 particles per cell), compared to the cells only negative control (Figure 6.7). There were no significant differences in the release of TNF-alpha with all other materials compared to the negative control at 12 and 24 h. There were no significant differences ($p > 0.05$) with any other particles compared to the negative control.

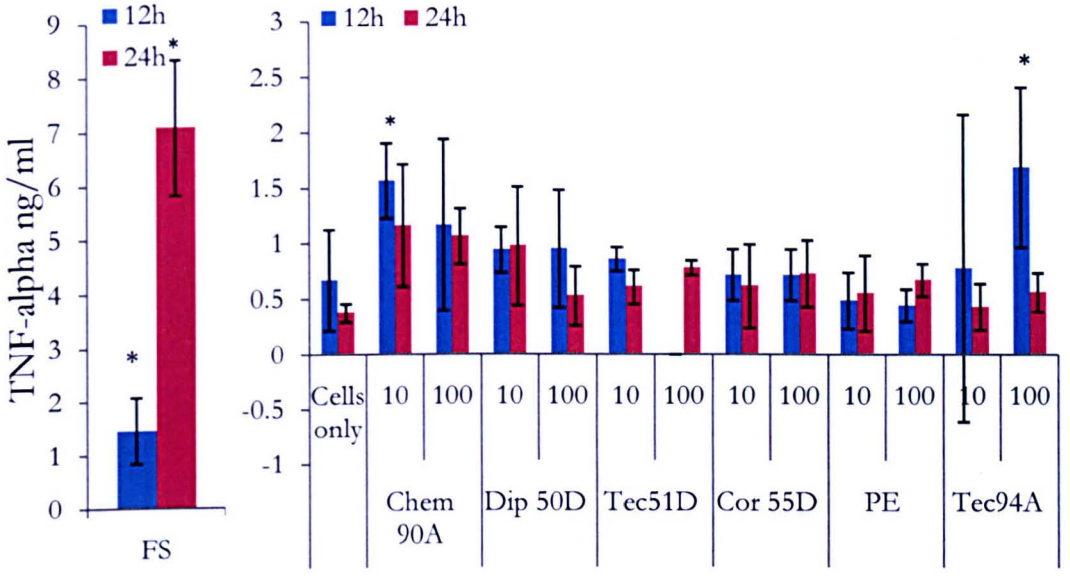

Figure 6.7 Mean (± 95% confidence interval) TNF-alpha release from PBMNC's from Donor 2 stimulated with Chemtura 90A (Chem 90A), Diprane 50D (Dip 50D), Tecoflex 94A (Tec 94A), Tecoflex 51D (Tec 51D), Corethane 55D (Cor 55) and, polyethylene (PE) at 10 μm^3 and 100 μm^3 particles per cell for 12 and 24 hours. Cell only (n = 3) were the negative control and 0.2 μm FluroSpheres™ (FS) were the positive control. Statistically higher TNF-alpha release indicated by * ($p < 0.05$; ANOVA).

The positive control (FluoSpheres) stimulated the release of significantly higher interleukin-1 beta (IL-1β) compared to the cells only negative control. Chemtura 90A particles (10 and 100 μm^3 particles per cell) stimulated a significant increase in the release of IL-1β at both 12 and 24 h compared to the cells only negative control. Diprane 50D particles (10 μm^3 particles per cell) had a significant effect on IL-1β secretion at both time points, however, at a concentration of 100 μm^3 particles per cell IL-1β was only significantly increased at 12

h (Figure 6.8). Tecoflex 51D particles (10 μm^3 particles per cell) stimulated a significant increase in IL-1β secretion and 12 and 24 h, but when stimulated with the 100 μm^3 particles per cell concentration, IL-1β was only significantly elevated at 24 h compared to the negative control. Corethane 55D had a significant enhancing effect on IL-1β secretion at 24 h at both concentrations. At 12 h both PE (10 and 100 μm^3 particles per cell) and Tecoflex 94A (100 μm^3 particles per cell) significantly increased IL-1β release, however, at 24 h PE (100 μm^3 particles per cell) and Tecoflex 94A (10 and 100 μm^3 particles per cell) caused significantly higher levels of IL-1β secretion compared to the negative control (cells only). There were no significant differences ($p > 0.05$) with any other particles compared to the negative control.

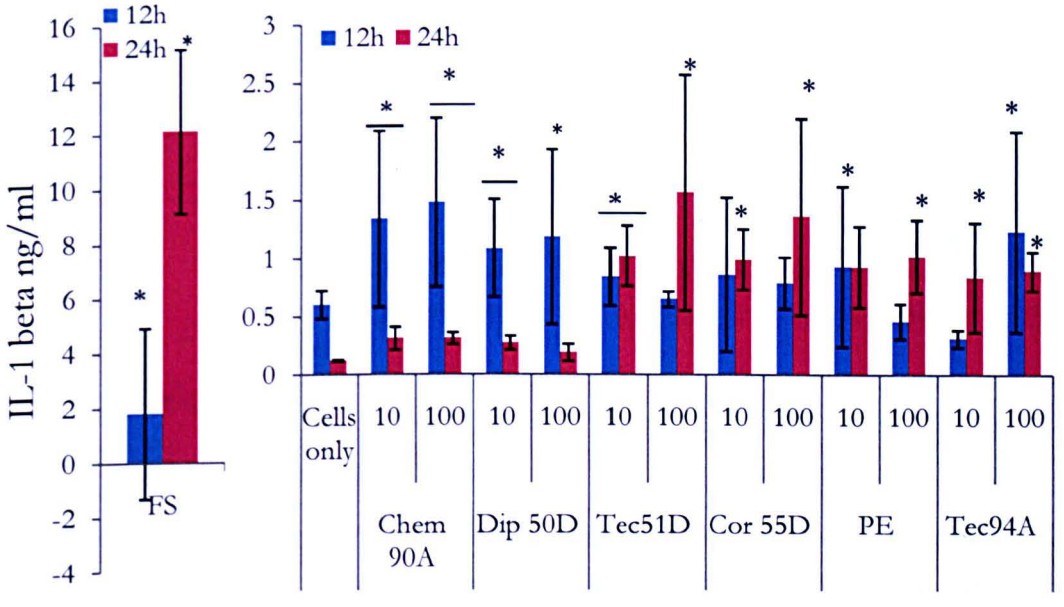

Figure 6.8 Mean (± 95% confidence interval) IL-8 release from PBMNC's from Donor 2 stimulated with Chemtura 90A (Chem 90A), Diprane 50D (Dip 50D), Tecoflex 94A (Tec 94A), Tecoflex 51D (Tec 51D), Corethane 55D (Cor 55) and, polyethylene (PE) at 10 μm^3 and 100 μm^3 particles per cell for 12 and 24 hours. Cell only (n = 3) were the negative control and 0.2 μm FluroSpheres™ (FS) were the positive control. Statistically higher IL-8 release indicated by *, —includes adjacent timepoint ($p < 0.05$; ANOVA).

The positive control (FluoSpheres) stimulated the release of significantly higher interleukin-6 (IL-6) compared to the cells only negative control. An elevated concentration of IL-6 was released at 24 h when cells were stimulated with particles of Diprane 50D at the 100 μm^3 particles per cell (Figure 6.9). However, at 12 h a significant increase in the release of IL-6 was observed when cells were stimulated by polyethylene (10 μm^3 particles per cell), Tecoflex 94A (10 and 100 μm^3 particles per cell) compared to the negative control. There were no significant differences ($p > 0.05$) with any other particles compared to the negative control.

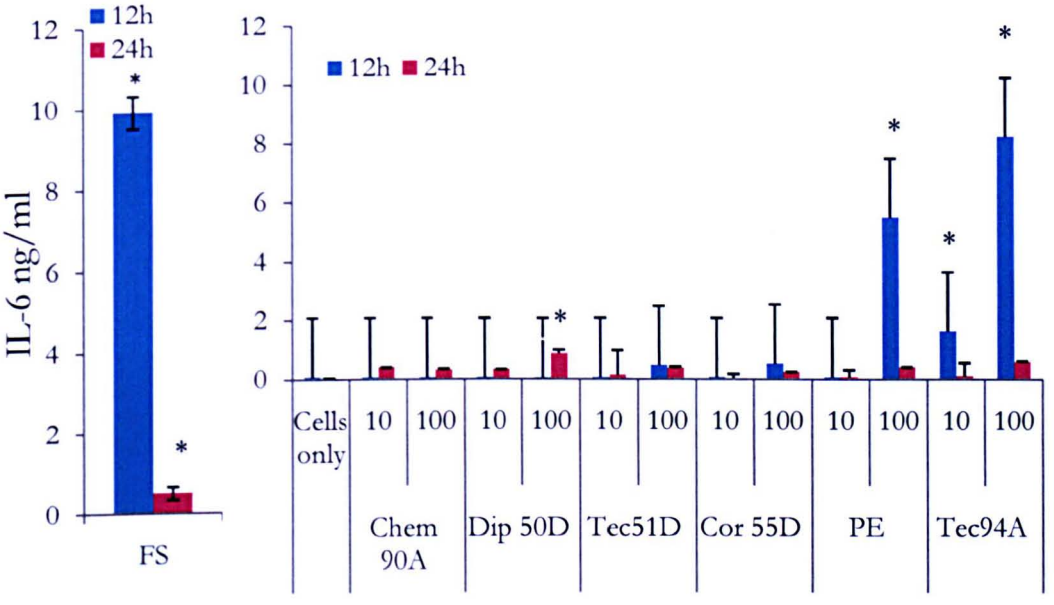

Figure 6.9 Mean (± 95% confidence interval) IL-1β release from PBMNC's from Donor 2 stimulated with Chemtura 90A (Chem 90A), Diprane 50D (Dip 50D), Tecoflex 94A (Tec 94A), Tecoflex 51D (Tec 51D), Corethane 55D (Cor 55) and, polyethylene (PE) at 10 μm^3 and 100 μm^3 particles per cell for 12 and 24 hours. Cell only (n = 3) were the negative control and 0.2 μm FluroSpheres™ (FS) were the positive control. Statistically higher IL-1β release indicated by * ($p < 0.05$; ANOVA).

The positive control (FluoSpheres) stimulated the release of significantly higher interleukin-8 (IL-8) compared to the cells only negative control. At 12 h, particles of Chemtura 90A, Tecoflex 51D and, Corethane 55D at the 100 μm^3 particles per cell concentration, significantly increased the secretion of IL-8 (Figure 6.10). However, only particles of Tecoflex 94A and Tecoflex 51D (100 μm^3 particles per cell) stimulated significantly higher levels of IL-8 secretion at 24 h. Chemtura 90A particles at the 100 μm^3 particles per cell concentration was the only material to provoke a significant increase in the release of IL-8 at 12 h. There were no significant differences ($p > 0.05$) with any other particles compared to the negative control.

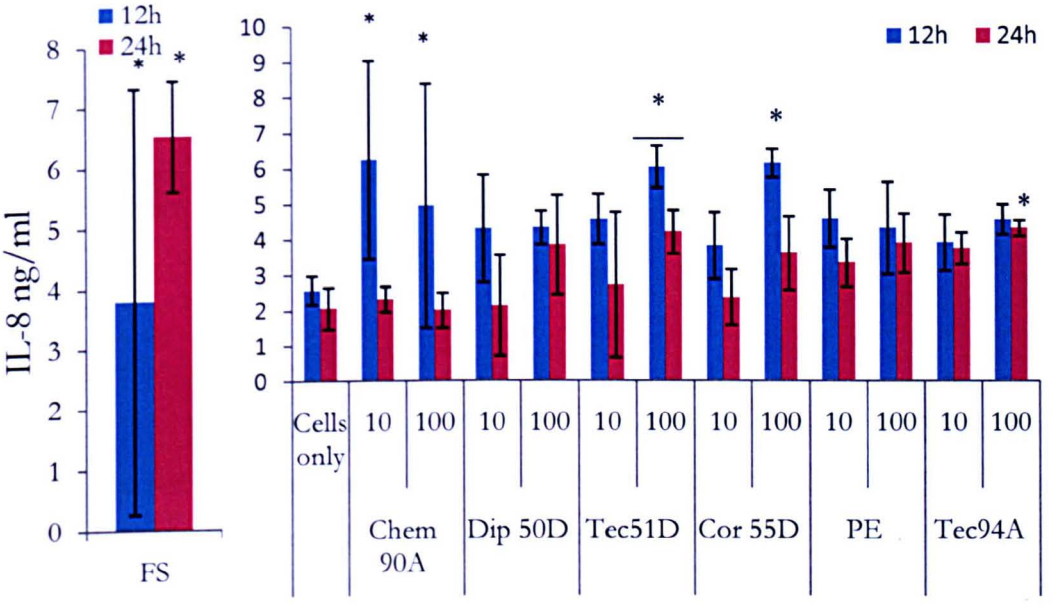

Figure 6.10 Mean (± 95% confidence interval) IL-6 release from PBMNC's from Donor 2 stimulated with Chemtura 90A (Chem 90A), Diprane 50D (Dip 50D), Tecoflex 94A (Tec 94A), Tecoflex 51D (Tec 51D), Corethane 55D (Cor 55) and, polyethylene (PE) at 10 μm^3 and 100 μm^3 particles per cell for 12 and 24 hours. Cell only (n = 3) were the negative control and 0.2 μm FluoSpheres™ (FS) were the positive control. Statistically higher IL-6 release indicated by *, — includes adjacent time point ($p < 0.05$; ANOVA).

6.3.3 *Cell viability and cytokine release from cells from Donor 3*

The addition of wear particles to the culture system did not affect the cell viability of cells from Donor 3 at 12 and 24 h, as no significant differences were evident between any of the groups compared to the cells only negative control (Figure 6.11).

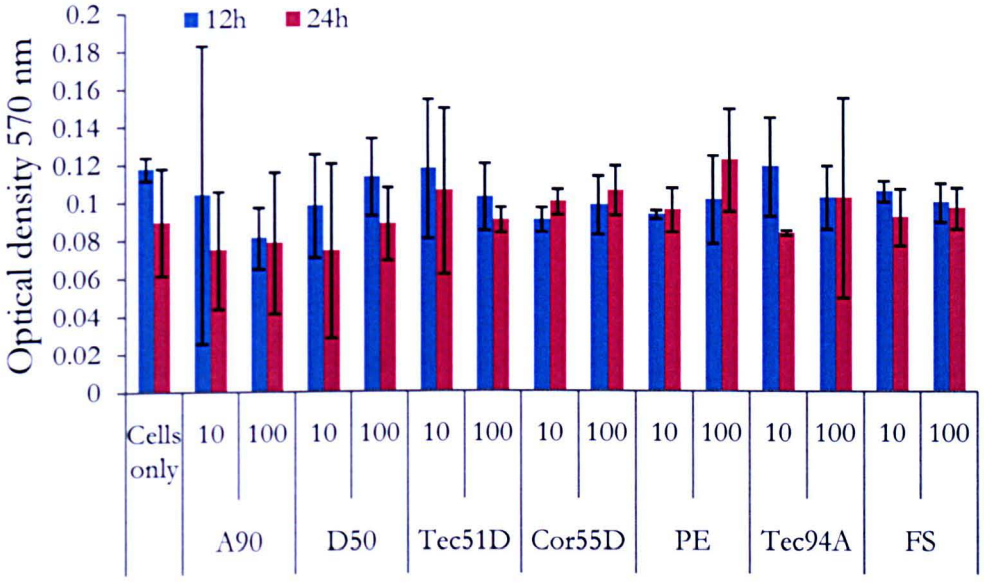

Figure 6.11 MTT assay showing PBMNC cell viability of Donor 3 at 12 and 24 hours at 10 μm^3 and 100 μm^3 particles per cell. Chem 90A - Chemtura 90A; Dip 50D – Diprane 50D, Tec 51D – Tecoflex 51D, Cor 55D – Corethane 55D, PE – polyethylene, Tec 94A – Tecoflex 94A, FS – 0.2 μm FluoSpheres™. Mean ± 95% confidence intervals. Optical density (OD), 570 nm.

The positive control (FluoSpheres) stimulated the release of significantly higher tumour necrosis factor alpha (TNF-alpha) compared to the cells only negative control. At 12 h, TNF-alpha was secreted at significantly higher levels (compared to the negative control) when cells were stimulated with Chemtura 90A particles (10 μm^3 particles per cell), Diprane 50D (100 μm^3 particles per cell), PE (100 μm^3 particles per cell) and, Tecoflex 94A (10 and 100 μm^3 particles per cell). While Tecoflex 51D and Corethane 55D (10 and 100 μm^3 particles per cell) and PE (10 μm^3 particles per cell) significantly elevated the release of TNF-alpha at 24 h compared to the cells only negative control (Figure 6.12). There were no significant differences ($p > 0.05$) with any other particles compared to the negative control.

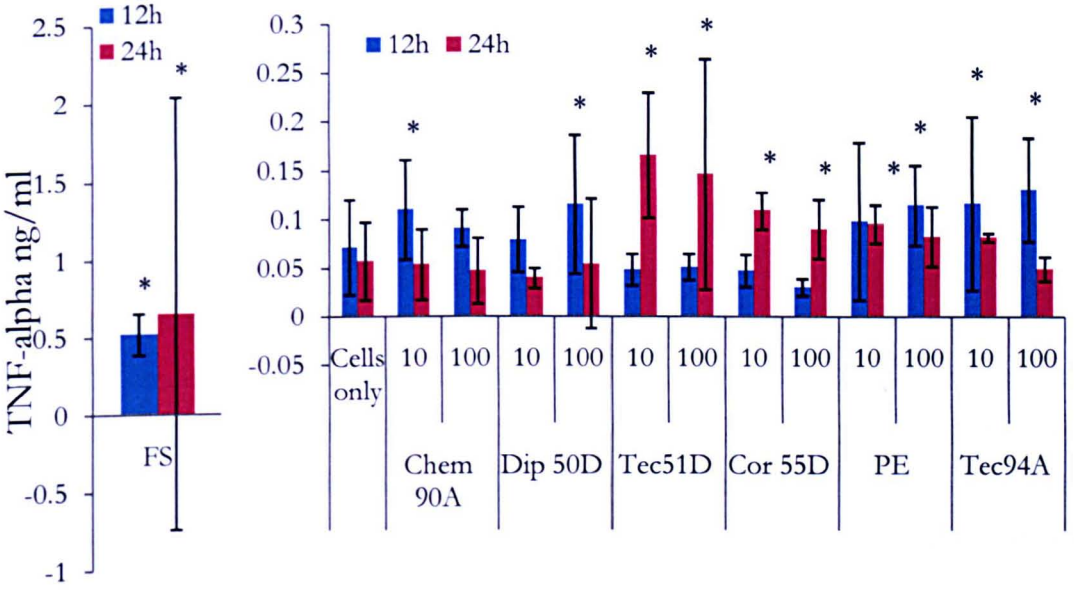

Figure 6.12 Mean (± 95% confidence interval) TNF-alpha release from PBMNC's from Donor 3 stimulated with Chemtura 90A (Chem 90A), Diprane 50D (Dip 50D), Tecoflex 94A (Tec 94A), Tecoflex 51D (Tec 51D), Corethane 55D (Cor 55) and, polyethylene (PE) at 10 μm^3 and 100 μm^3 particles per cell for 12 and 24 hours. Cell only (n = 3) were the negative control and 0.2 μm FluoSpheres™ (FS) were the positive control. Statistically higher TNF-alpha release indicated by * ($p < 0.05$; ANOVA).

The positive control (FluoSpheres) stimulated the release of significantly higher interleukin-1 beta (IL-1β) compared to the cells only negative control. Only Chemtura 90A particles (10 μm^3 particles per cell) caused significant increase in the secretion of IL-1β at 12 h compared to the negative control (Figure 6.13).

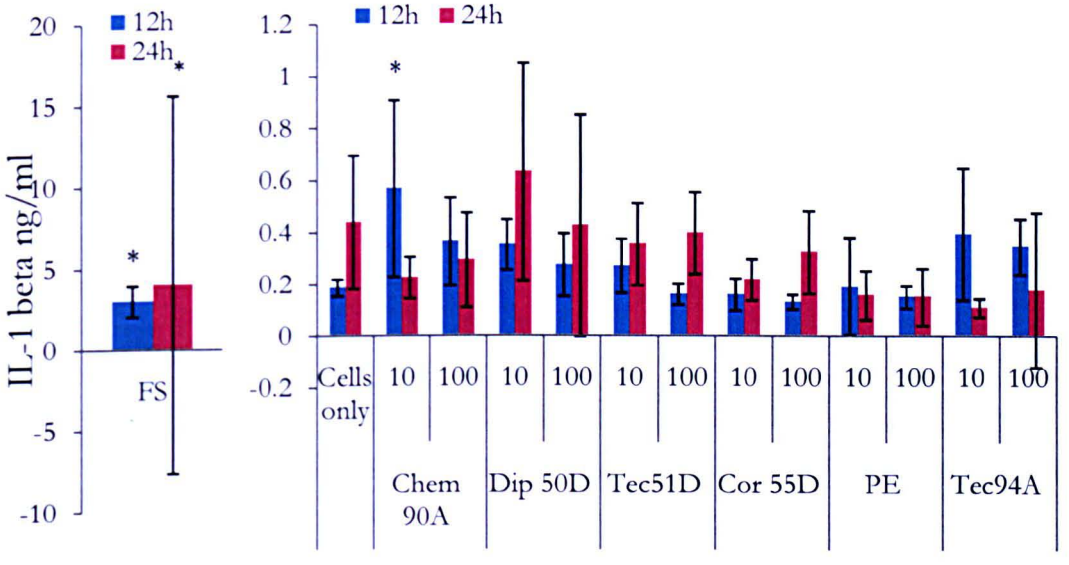

Figure 6.13 Mean (± 95% confidence interval) IL-1β release from PBMNC's from Donor 3 stimulated with Chemtura 90A (Chem 90A), Diprane 50D (Dip 50D), Tecoflex 94A (Tec 94A), Tecoflex 51D (Tec 51D), Corethane 55D (Cor 55) and, polyethylene (PE) at 10 μm^3 and 100 μm^3 particles per cell for 12 and 24 hours. Cell only (n = 3) were the negative control and 0.2 μm FluoSpheres™ (FS) were the positive control. Statistically higher IL-1β release indicated by * ($p < 0.05$; ANOVA).

The positive control (FluoSpheres) stimulated the release of significantly higher interleukin-6 (IL-6) compared to the cells only negative control. At 12 h a significant increase of IL-6 was released when cells were stimulated with polyethylene wear particles at a concentration of 100 μm^3 particles per cell compared to the negative control (Figure 6.14). There were no significant differences ($p > 0.05$) with any other particles compared to the negative control.

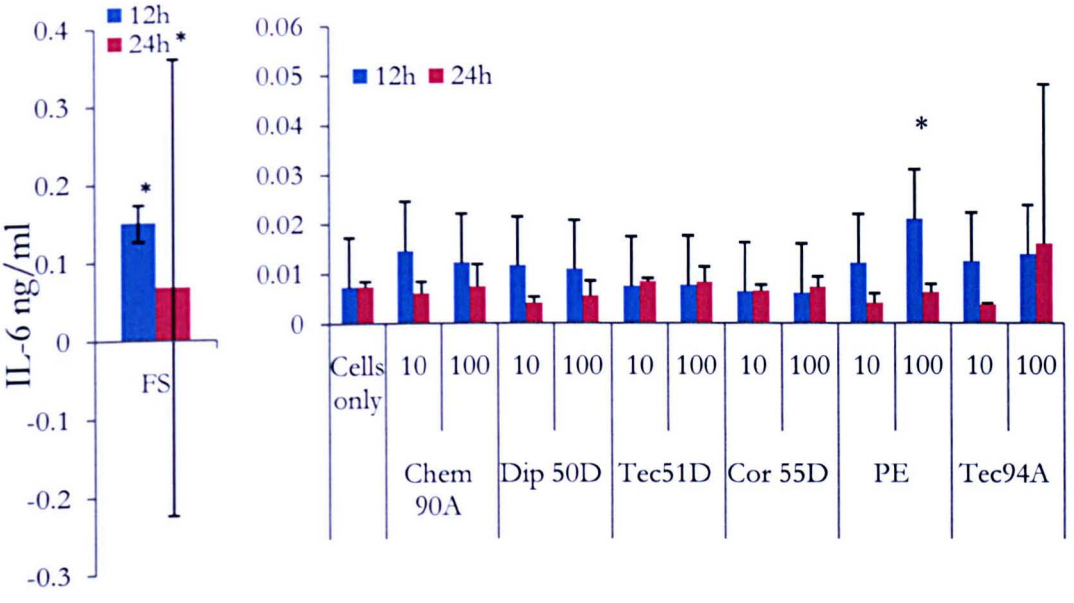

Figure 6.14 Mean (± 95% confidence interval) IL-6 release from PBMNC's from Donor 3 stimulated with Chemtura 90A (Chem 90A), Diprane 50D (Dip 50D), Tecoflex 94A (Tec 94A), Tecoflex 51D (Tec 51D), Corethane 55D (Cor 55) and, polyethylene (PE) at 10 μm^3 and 100 μm^3 particles per cell for 12 and 24 hours. Cell only (n = 3) were the negative control and 0.2 μm FluoSpheres™ (FS) were the positive control. Statistically higher IL-6 release indicated by * ($p < 0.05$; ANOVA).

The positive control (FluoSpheres) stimulated the release of significantly higher interleukin-8 (IL-8) compared to the cells only negative control. IL-8 release was not significantly higher than the negative control when cells were cultured with particles any of the material at 12 and 24 h (Figure 6.15).

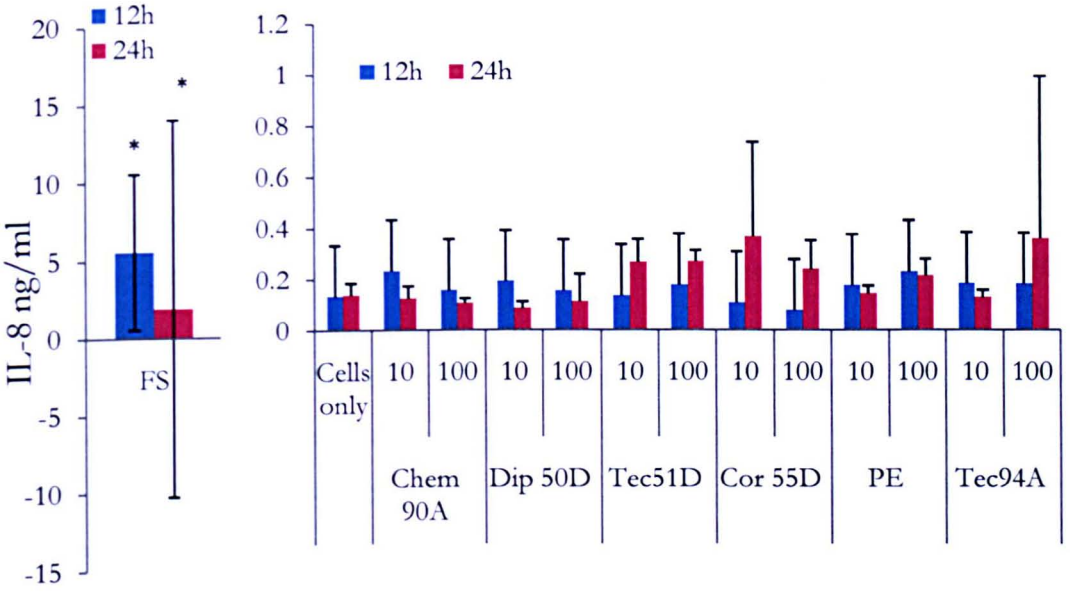

Figure 6.15 Mean (± 95% confidence interval) IL-8 release from PBMNC's from Donor 3 stimulated with Chemtura 90A (Chem 90A), Diprane 50D (Dip 50D), Tecoflex 94A (Tec 94A), Tecoflex 51D (Tec 51D), Corethane 55D (Cor 55) and, polyethylene (PE) at 10 μm^3 and 100 μm^3 particles per cell for 12 and 24 hours. Cell only (n = 3) were the negative control and 0.2 μm FluoSpheres™ (FS) were the positive control. Statistically higher IL-8 release indicated by * ($p < 0.05$; ANOVA).

6.4 Discussion

Polyurethanes as bulk materials are noted for their favourable biocompatible properties and have been used in the clinical setting for a number of years (Lambda *et al.*, 1998; Possard *et al.*, 2004). Clinical applications include catheters, tubing, and vascular grafts (Lambda *et al.*, 1998; Possard *et al.*, 2004). However, their biocompatibility has generally been tested in bulk form, as opposed to wear particles. A biological response is more likely if the material is small in size, as this will allow phagocytes to ingest the material (Gelb *et al.*, 1994). However, not all wear particles elicit a biological response and it has been documented that the induction of pro-inflammatory cytokines is dependent on material chemistry, volume,

shape (Wang *et* al., 2004; Purdue *et al.*, 2006), exposure time (Wang *et* al., 2004) and size (Green *et al.*, 1998). It is known that certain particle size ranges are highly biologically active in terms of inflammatory cytokine release from macrophages, for instance, polyethylene wear particles have been reported to elicit a biological response at < 10 μm in size and particularly the submicron size range (Campbell *et al.*, 1995; Tipper *et al.*, 2000). This coincides with a study that reported polyethylene particles were phagocytosed by macrophages in the size range of 0.2-10 μm (Green *et al.*, 1998).

Matthews *et al.* (2000) cultured primary human peripheral blood mononuclear cells with polyethylene (GUR1120) particles to elicit a biological response from three donors. As with the present study, Matthews *et al.* (2000) found that each donor responded differently in terms of the elevated concentration of cytokines released and demonstrated that particle size and volume played critical roles in macrophage stimulation. Varying individual responses to wear particles were also observed by Richards (2008), who also demonstrated that peak cytokine release generally occurred at 24h of exposure to wear particles. Exposure time played an important part in this finding, however, the size, shape and material chemistry may also have played a role. Particle size and shape of the materials used in this study are discussed in Chapter 5.

Polyethylene, thermoset and thermoplastic wear particles at two concentrations were cultured with cells from three donors. The elevated release of cytokines (TNF-alpha, IL-1β, IL-6 and IL-8) from the cells from each donor was determined by ELISA and are shown in Table 6.1.

Table 6.1 Polyethylene, thermoset and thermoplastic polyurethanes wear particles stimulated cells from donors to release significantly elevated levels of cytokines.

Material	Donor 1	Donor 2	Donor 3
Chemtura 90A	1	T, 1, 8	T, 1, 6
Diprane 50D	-	1, 6	T
Corethane 55D	8	1, 8	T
Tecoflex 51D	6, 8	1, 6, 8	T
Polyethylene	T, 1, 6, 8	T, 1, 6, 8	T
Tecoflex 94A	T, 6, 8	1, 6	T, 6

T = tumour necrosis factor-alpha, 1 = interleukin 1β, 6 = interleukin-6, 8 = interleukin-8

Results in Table 6.2 show that Diprane 50D was the least biologically active material, as cells from only two donors were stimulated to release elevated levels of cytokines. However, all other material samples had stimulated cells from all three donors to release elevated levels of cytokines. Diprane 50D and Corethane 55D were the only materials to stimulate cells from donors to significantly release three cytokines. This indicated that these two materials were the least biologically active because the other material samples stimulated the cells from each donor to release elevated levels of all four cytokines.

6.5 Conclusion

Chemtura 90A, Tecoflex 51D, polyethylene and Tecoflex 94A materials were the most biologically active while Diprane 50D and Corethane 55D were the least biologically active materials. However, Diprane 50D is not a medical grade material and thus would not be used as a biomaterial. The results in this study indicate that the biological activity of particles from various materials is donor specific. This suggests that pre-clinical testing of material particles with the patients' own cells could be beneficial when considering a device choice for individual patients.

Chapter Seven

Discussion

There are over 100 types of arthritis that affect bones, joints and muscles and the most common one being osteoarthritis (www.nhs.uk). It is estimated that 8.5 million individuals suffer from osteoarthritis (OA) in the UK and it is more prevalent in women than men over the age of 50. Historically, this debilitating disease was thought to be part of the ageing process, even though it can affect the young and old. OA involves the destruction of articular cartilage (AC), bone and the surrounding tissues of the joints (Aigner *et al.*, 2006). OA is prevalent in the knee and hip but, can also appear in the hands, lower spine, shoulders, elbows, wrists and feet. As the cartilage wears, the underlying subchondral bone becomes exposed and comes in contact with the opposing side of the joint. This eventually leads to joint stiffening and eventually a loss of joint movement, however, not all individuals suffer from pain.

Approximately, 20% of people in the age range of 45-64 years suffer from pain due to osteoarthritis in the knee and around 25% of people > 50 years old are disabled from severe knee pain and approximately 12% of adults > 65 years experience pain due to hip OA (www.nhs.uk). OA cannot be cured but there are many options available to manage this disease such as, exercise, diet, medications and surgical interventions (Polster *et al.*, 2005; Pylawka *et al.*, 2005; Ge *et al.*, 2006; Malviya *et al.*, 2006). For individuals suffering from severe OA in which all other options are not effective, total joint replacements (TJRs) are the last resort. Initially, TJRs (both knee and hip) were conducted in patients over the age of 65, however, more recently the age range has decreased dramatically to include those in the age group of 45-65 (Katz, 2006). OA morbidity in younger individuals has lead to a direct economic burden as the disease affects individuals of 'working' age and imposes an indirect burden which impacts on the health care system. The National Joint Registry reported that approximately 160,000 TJRs (hip and knee) are performed every year in England and Wales, and around the same number of revision operations (knee and hip) are

completed every year (www.njrcentre.org.uk). In the private health sector hip replacements cost between £7,000 and £9,000 and knee replacements cost between £8,000 and £10,000, albeit part of the costs account for post-operative care (Private Health Care UK, www.privatehealth.co.uk).

Although TJRs restore joint function and dramatically improve the individual's quality of life, the prosthesis may only last 10 to 15 years post-implantation as a result of adverse biological reactions, which eventually leads to osteolysis and aseptic loosening and inevitably leading to a revision operation (Ingham and Fisher, 2005). TJRs are extremely invasive procedures and early interventions are aimed to be less destructive to the joint. Therefore, early interventions (such as cartilage substitution therapies) are imperative to manage joint degenerative diseases and preserve the natural joint as much as possible. Such novel therapies have the potential to delay the time when a total joint replacement will be required. This thesis aimed to determine and further understand the friction and wear characteristics of potential novel cartilage substitution biomaterials and native articular cartilage and to establish the biocompatibility of generated wear particles.

Thermoset (Chemtura 90A and Diprane 50D) and thermoplastic polyurethanes (Tecoflex 94A, Tecoflex 51D and, Corethane 55D) as well as polyvinyl alcohol/polyvinyl pyrrolidone (PVA/PVP) hydrogels (H1B, H2B and H2A) were investigated. The mechanical properties of the polyurethanes (PU) showed that the thermoplastic polyurethanes (TPUs) were not as stiff or as ductile compared to the manufacturer's datasheets. The TPUs were also less ductile but much stiffer than the thermoset PUs. It was also evident that the shore hardness A PUs were more ductile than the shore hardness D PUs, which was to be excepted since shore A PUs are 'softer' than shore D PUs. The chemistry of each PU used in this thesis differed slightly and may have had an effect on the mechanical properties (Chapter 3).

The friction characteristics of native AC against itself were low and comparable to the literature (Forster and Fisher, 1996; Northwood *et al.*, 2007). This thesis demonstrated that articular cartilage is biphasic in nature (Armstrong *at al.*, 1984; Ateshian *et al.*, 1994; Kelkar *at al.*, 1999) which is very much dependent on time and load (Forster and Fisher, 1996; Northwood and Fisher, 2007). AC is a viscoelastic tissue and this behaviour was demonstrated in the indentation tests which were in line with previous studies. Friction,

indentation and recovery tests showed that AC was more compliant compared to the PUs and hydrogels. Hydrogels have been reported to possess biphasic properties (Covert *et al.*, 2003; Bodugoz-Senturk *et al.*, 2009), however, this was not clear with the results in this thesis as they did not exhibit the characteristic 'biphasic' curve during friction testing that is so typical of articular cartilage. However, the indentation tests did indicate that the hydrogels and thermoset PUs exhibit similar viscoelastic properties to AC. The TPUs, however, had statistically lower viscoelasticity than AC.

The friction characteristics of the TPUs and hydrogels against AC plates were favourable (not significantly different to the negative control AC against AC) compared to the thermoset PUs whose friction coefficients were significantly higher than the TPUs and hydrogels, and were also statistically higher AC against AC. The material with the most desirable coefficient of friction was Tecoflex 94A, although there were no significant differences between the TPUs (against AC plates) and the negative control (AC against AC). However, after 20 minutes (to the end of the test) of friction testing the friction coefficients of Tecoflex 51D and Corethane 55D were not statistically different to the thermoset PUs against AC plates. The thermoset PUs visibly damaged the AC plates possibly caused by adhesive wear. There was also evidence of a gel-like tissue on the surface of the pins and it was possible that surface proteins (although this material was not biochemically or histologically tested) may have acted as a protective layer as no significant changes were found on the surface topography of the thermoset PU pins after the test.

It appeared that the PUs operated in boundary lubrication while, the hydrogels operated in a mixed lubrication regime, which was more favourable as less wear would occur between opposing surfaces. However, significant changes to the surface topography of the hydrogels suggested that the PVA/PVP hydrogels would not be suitable cartilage substitution biomaterials. The results suggested that an increase in porosity (hydrogels containing gluconic acid) with an increase in PVA content may have had an effect on the wear of the materials. The AC plates appeared to have a 'polishing' effect on the surface of the H2B hydrogels, while the surface roughness of the H1B and H2A hydrogels significantly increased after testing. Multidirectional wear tests had an adverse effect on the surface topography of the PVA/PVP hydrogels and tests were stopped early because of this, further supporting that these materials would not be suitable cartilage substitution biomaterials.

The differences in the coefficient of friction between the thermoset PUs and TPUs could possibly be due to the surface chemistry of the materials as the wettability and geometry of the PUs pins did not account for the significantly higher coefficient of friction of the thermoset PUs (against AC). Tecoflex 94A seemed to be the most ideal cartilage substitution candidate because it did not damage the surface of the articular cartilage plate exhibited a statistically similar friction coefficient to AC (and was significantly lower than the thermoset PUs throughout the friction tests). It is important to note that the orientation of these materials was vital to the frictional characteristics when AC pins articulated against the PU plates, the friction properties of the PUs were completely different (compared to PU pins against AC plates) because friction continued to increase, however, this was an attribute of the biphasic nature of the cartilage tissue and the compliance of the PU plates.

Wear particles were generated using the thermoset PUs and TPUs and it was evident that these materials produced the largest number of particles in two size ranges (< 0.1 μm and 0.1-1.0 μm) irrespective of the wearing surface (smooth or rough stainless steel plates). However, particles in the size range of 0.1-1.0 μm generally occupied the largest percentage area, but were closely followed by particles in the 1.0-10 μm size range. Articular cartilage pins were also articulated against smooth stainless steel plates, rough stainless steel plates and TPU plates using the six station wer rig, however, the wear particles were not observed using the FEGESEM due to time contraints.

When aseptic PU (thermoset and thermoplastic) and polyethylene (control) wear particles were cultured with peripheral blood mononuclear cells it was evident that Chemtura 90A, Tecoflex 51D, Tecoflex 94A and polyethylene were biologically active as they stimulated all three donors to release significant elevated levels of cytokines. Although Tecoflex 94A was the ideal material to be used as a cartilage substitute because of the low friction coefficient and low wear (in the absence of serum), it was one of the least biocompatible materials. The least active materials in terms of the number of cytokines (three out of four) released by the cells from the donors were Diprane 50D and Corethane 55D. The results indicated that the biological activity of particles from various materials is donor specific, suggesting that pre-clinical testing of material particles with the patients' own cells could be beneficial when considering a device choice for individual patients. Due to time constraints cells from only three donors were used in the biocompatibility experiments, however, it would

have been preferred if blood from at least five donors were used. Time constriants also permitted the invesigation of the biological activity of articular cartilage wear particles with macrophages (an original objective of this thesis).

This thesis showed that the wear properties of Diprane 50D were undesirable and thus would unlikely be used as a potential cartilage substitution biomaterial, in conjunction with this Diprane 50D is not a medical grade material. The friction characteristics of Diprane 50D (against AC) were also unfavourable, however, the coefficient of friction for Corethane 55D (against AC) was statistically similar to AC against AC, even though after 20 minutes of testing the friction was statistically similar to Diprane 50D. The wear properties of Corethane 55D were more desirable compared to Diprane 50D and although the friction of Corethane 55D were similar to Diprane 50D during part of the tests, the properties of this material may be improved.

7.1 Overall Conclusion

The results in this thesis show that Tecoflex 94A exhibited a similar coefficient of friction to native articular cartilage and generally had a lower coefficient of friction compared to the other materials. However, the PVA/PVP hydrogels were the only materials to operated in a favourable mixed lubrication regime. Tecoflex 94A also had a low wear factor compared to the other thermoplastic materials (Corethane 55D and Tecoflex 51D), however, the particles were generated in the absence of serum. In contrast, the presence of serum resulted in low wear factors for both Corethane 55D and Tecoflex 51D (compared to Tecoflex94A), suggesting serum had affected the wear of the materials. TPUs possessed better mechanical properties to the thermoset PUs (Diprane 50D and Chemtura 90A). The biological activity of Tecoflex 94A was undesirable, however, Corethane 55D and Diprane 50D were the least biologically active materials.

7.2 Future Work

Information about how these materials would operate *in vivo* could be determined by natural joint simulators, in which the materials would be implanted (as osteochondral plugs) into natural whole joints. These experiments would show the effect of the materials on the opposing side of the joint as well as the effect on the surrounding tissues. Generating wear particles from articular cartilage and determining the size and volume of the particles would increase our understanding of cartilage wear. It would also be of interest to establish

whether these particles were biologically active when cultured with macrophages. It has been reported that chondrocytes change phenotype under pathological conditions and release cytokines (i.e. TNF-alpha, IL-1β) they would not normally secrete (Sandell *et al.*, 2001), thus leading to further destruction of surrounding cartilage. Culturing cartilage wear particles with chondrocytes may provide more information about the pathological conditions and thus, increase our knowledge of the mechanisms involved in degenerative diseases such as osteoarthritis. Polyurethanes and hydrogels are some of the few materials that can be manipulated to improve material properties, for instance, changing the chain extender in a polyurethane material can alter the softness of the material (Lambda *et al.*, 1998), or chemical addition (i.e. gluconic acid) can increase the internal porosity of a hydrogel (Fray *et al.*, 2007). Since many polyurethane materials have been developed with many different components, there is much room for improvement of these materials. By altering the components within these materials it may be possible to develop potential cartilage substitution biomaterials that not only possess similar mechanical (like the PVA/PVP hydrogels) and frictional characteristics (like Tecoflex 94A) compared to native articular cartilage but also generate limited particles that do not have a significant effect on cytokine release (like Diprane 50D and Corethane 55D).

8.0 References

Aigner, T., Sachse, A., Gebhard, P., and Roach, H. I. (2006) Osteoarthritis: Pathobiology-targets and ways for therapeutic intervention, *Advanced Drug Delivery Reviews* **58**(2): 128-149.

Aigner, T. and Stove, J. (2003) Collagens-major component of the physiological cartilage matrix, major target of cartilage degeneration, major tool in cartilage repair, *Advanced Drug Delivery Reviews* **55**(12): 1569-1593.

Anderson, J. M. (2001) Biological Responses to Materials, *Annu. Rev. Mater. Res* **31**: 81-110.

Armstrong, C. G., Mow, V. C. (1984) An analysis of the unconfined compression of articular cartilage *J Biomech Eng* **106**:165-73

Arner, E. C. (2002) Aggrecanase-mediated cartilage degradation, *Current Opinion in Pharmacology* **2**:322-329.

Aspden, R. M. (1994) Fibre reinforcing by collagen in cartilage and soft connective tissues, *Proc. R. Soc. Lond* **258**(1352): 195-200.

Ateshian, G. A. (2009) The role of interstitial fluid pressurization in articular cartilage lubrication *Journal Biomechanics* **42**(9):1163-1176

Atesian, G.A., Lai, W. M., Zhu W. B., Mow, V. C. (1994) An asymptotic solution for the contact of two biphasic cartilage layers *J Biomechanics* **27**(11):1347-1360

Ballantine, G. C. and Stachowiak, G. W. (2002) The effect of lipid depletion on osteoarthritic wear, *Wear* **253**: 383-393.

Barbaro, V., Bosi, C., Caiazza, S., Cgristolini, P., Ialonga, D., and Rosa, P. (1985) Implant effects on polyurethane and silicone cardiac pacing leads in humans: Insulation measurements and SEM observations, *Biomaterials* **6**: 28-32.

Barker M. K, Seedhom, B. B. (2001) The relationship of the compressive modulus of articular cartilage with its deformation response to cyclic loading: does cartilage optimize its modulus so as to minimise the strains arising in it due to the prevalent laoding regime? *Rheumatology* **40**:274-284

Bellemans, J., Vandenneucker, H., and Vanlauwe, J. (2005) Total knee replacement, *Current Orthopaedics* **19**: 446-452.

Bellucci. G., Seedhom. B. B. (2001) Mechanical behavior of articular cartilage under tensile cyclic load *Rheumatology* **40**:1337-1345

Bessis, N. and Boissier, M. C. (2001) Novel proinflammatory interleukins: potential therapeutic targets in rheumatoid arthritis, *Joint Bone Spine* **68**(6):477-481.

Bhosale, A. M., Richardson, J. B. (2008) Articular cartilage:structure, injuries and review of management *British Medical Bulletin* **87**:77-95

Bhushan, B. (2002) *Introduction to Tribology*, New York: John Wiley & Sons. ISBN 0 471 15893 3

Bodugoz-Senturk. H., Macias. C. E., Kung. J. H., Muratoglu. O. K. (2009) Poly(vinyl alcohol)-acrylamide hydrogels as load-bearing cartilage substitute *Biomaterials* **30**: 589-596

Brook, I. M., Hatton, P. V. (1998) Glass-ionomers: bioactive implant materials *Biomaterials* **19**(6):565-571

Buckwalter, J. A. and Makin, H. J. (1997) Instructional course lectures, The American academy of orthopaedic surgeons – Articular cartilage. Part I: Tissue design and chondrocyte – Matrix interactions, *J. Bone Joint Surg Am* **79**: 600-611.

Caravia, L., Dowson, D., and Fisher, J. (1993) Start up and steady state friction of thin polyurethane layers, *Wear* **160**:191-197.

Caravia, L., Dowson, D., Fisher, J., Corkhill, P. H., and Tighe, B. J. (1995) Friction of hydrogel and polyurethane elastic layers when sliding against each other under a mixed lubrication regime, *Wear* **181-183**: 236-240.

Carl, A., Ledet, E., Yuan, H., and Sharan, A. (2004) New developments in nucleus pulposus replacement technology, *The Spine Journal* **4**: 325S-329S.

Carlsson, L. V., Albrektsson, B. E. J., and Regner, L. R. (2006) Minimally invasive surgery vs conventional exposure using the Miller-Galante unicompartmental knee arthroplasty: A randomised radiostereometric study, *The Journal of Arthroplasty* **21**(2):151-156.

Caterson, B., Flannery, C. R., Hughes, C. E., and Little, C. B. (2000) Mechanisms involved in cartilage proteoglycan catabolism, *Matrix Biology* **19**: 333-344.

Cheung, H. Y., Lau, K. T., Lu, T. P., and Hui, D. (2007) A critical review on polymer-based bio-engineered materials for scaffold development, *Composition Part B: Engineering* **38**(3): 291-300.

Choy, E. H. S., and Panayi, G. S. (2001) Cytokine pathways and joint inflammation in rheumatoid arthritis, *N Engl J Med* **344**(12): 907-916.

Covert, R. J., Ott, R. D., and Ku, D. N. (2003) Friction characteristics of a potential articular cartilage biomaterial, *Wear* **255**: 1064-1068.

Daughaday, W. H., Rotwein, P. (1989) Insuling-like growth factors I and II. Peptide, messenger ribonucleic acid and gene structures, serum, and tissue concentrations. *Endocr Rev* **10**(1):68-91.

Darwis, D., Stasica, P., Razzak, M. T., and Rosiak, J. M. (2002) Characterisation of poly(vinyl alcohol) hydrogel for prosthetic intervertebral disc nucleus, *Radiation Physics and Chemistry* **63**: 539-542.

Dowson, D., Jin, Z. M. (1992) Microelastohydrodynamic lubrication of low-elastic-modulus solids on rigid substrates *J Phys D: Appl Phys* **25**A116-A123

Dudler, J., Renggli-Zulliger, N., Busso, N., Lotz, M., and So. A. (2000) Effect of interleukin 17 on proteoglycan degradation in murine knee joints, *Ann Rheum Dis* **59**(7): 529-532.

Durwood, B.R, Baer, G. D., Rowe, P. J. (1999) Functional human movement: measurement and analysis. Butterworth-Heinemann. ISBN 0-7506-26070.

Eisenberg, S. P., Evans, R. J., Arend, W. P., Verderber, E., Brewwe, M. T., Hannum, C. H., and Thompson, R. C. (1990) Primary structure and functional expression from complementary DNA of a human interleukin-1 receptor antagonist, *Nature* **343**(6256):341-346.

Etter, H., Althaus, R., Eugster, H. P., Santamaria-Babi L. F., Wber, L., and Moser, R. (1998) IL-4 and IL-13 downregulate rolling adhesion of leukocytes to IL-1 or TNF-alpha-activated endothelial cells by limiting the interval of E-selectin expression *Cytokine* **10**:395-403

Eyre, D. (2002) Collagen of articular cartilage, *Arthritis Res* **4**: 30-35.

Fan, Z., Bau, B., Yang, H., and Aigner, T. (2004) IL-1[beta] induction of IL-6 and ILF in normal articular human chondrocytes involves the ERK, p38 and NF[kappa]B signalling pathways, *Cytokine* **28**(1): 17-24.

Fray, M. E. L., Pilaszkiewicz, A., Sweiszkowski, W., Kurzydlowski, K. J. (2007) Morphology assessment of chemically modified and cryostructured poly(vinyl alcohol) hydrogel *European Polymer Journal* **43**:2035-2040

Freeman, M. A. R. (1979) Adult articular cartilage 2nd Ed. Pitman Medical Publishing ISBN 0-272-79430-9.

Forsey, R. (2004) Development of cartilage damage models for a tribological investigation of therapeutic lubricants in osteoarthritis, *PhD Thesis*, University of Leeds.

Forster, H., and Fisher, J. (1996) The influence of loading time and lubricant on the friction of articular cartilage, *Proc Instn Mech Eng Part H* **210**(2): 109-119.

Forster, H., and Fisher, J. (1999) The influence of continuous sliding and subsequent surface on the friction of articular cartilage, *Proc Instn Mech Engrs Part H* **213**: 329-345.

Galvin, A. L., Tipper, J. L., Ingham, E., Fisher, J. (2005) Nanometer size wear debris generated from crosslinked and non-crosslinked ultra high molecular weight polyethylene in artificial joints *Wear* **259**(7-12):977-983

Ge, Z., Hu, Y., Heng, B. C., Yang, Z., Ouyang, H., Lee, E. H., and Cao, C. (2006) Osteoarthritis and therapy, *Arthritis & Rheumatism* **55**(3): 493-500.

Gelb, H., Schumacher, H. R., Cuckler, J., Baker D.G. (1994) *In vivo inflammatory response to polymethylmethacrylate particulate debris. Effect of size, morphology and surface area. Journal of Orthopedic Research* **12**:83-92

Gelse, K., Poschl, E., and Aigner, T. (2003) Collagens – structure, function, and biosynthesis, *Advanced Drug Delivery Reviews* **55**(12):1531-1546.

Gerwin, N., Hops, L., and Lucke, A. (2006) Intraarticular drug delivery in osteoarthritis, *Advanced Drug Delivery Reviews* **58**:226-242.

Gleghorn, J. P., Bonassar, L. J. (2008) Lubrication mode analysis of articular cartilage using Stribeck surfaces *Journal of Biomechanics* **41**:1910-1918

Gibson, A. J., McDonnell, S. M., Price, A. J. (2006) Matrix_induced Autologous Chondrocyte Implantation *Operative Techniques in Orthopaedics* **16**:262-265

Goins, M. L., Wimberley, D. W., Yuan, P. S., Fitzhenry, L. N., and Vaccaro, A. R. (2005) Nucleus pulposus replacement: an emerging technology, *The Spine Journal* **5**: 317S-324S.

Graindorge, S. L., Ferrandez, W., Ingham, E., Jin, Z., Twigg, P., and Fisher, J. (2006) The role of the surface amorphous layer of articular cartilage in joint lubrication, *J. Engineering in medicine* **220 Part H**: 597-607.

Graindorge, S., Ferrandez, W., Jin, Z., Ingham, E., Grant, C., Twigg, P., and Fisher, J. (2005) Biphasic surface amorphous layer lubrication of articular cartilage, *Medical Engineering & Physics* **27**(10): 836-844.

Green, T. R., Fisher, J., Stone, M., Wroblewski, B. M., and Ingham, I. (1998) Polyethylene particles of a 'critical size' are necessary for the induction of cytokines by macrophages *in vitro*, *Biomaterials* **19**: 2297-2302.

Grimaud, E., Blanchard, F., Charrier, C., Gouin, F., Redini, F., and Heymann, D., (2002) Leukaemia inhibitory factor (LIF) is expressed in hypertrophic chondrocytes and vascular sprouts during osteogenesis, *Cytokine* **20**(5):224-230.

Hansen, U., Seidler, D. G., and Bruckner, P. (2006) Supramolecular organisation of heterotypic fibrils by decorin, *Matrix Biology* **25**(Supplement1) S73:178.

Hayes, W. C., Bodine A. J. (1972) Flow-independent viscoelastic properties of articular cartilage matrix, *Journal of Biomechancis* **11**:407-419

Hickey. A. S., Peppas. N. A. (1995) Mesh size and diffusive characteristics of semicrystalline poly(vinyl alcohol) membranes prepared by freezing/thawing techniques *Journal of Membrane Science* **107**:229-237

Hoffman, A. S. (2002) Hydrogels for biomedical applications, *Advanced Drug Delivery Reviews* **43**:3-12.

Hui, W., Bell, M. C., Carroll, G. J., and Layton, M. J. (1998). Modulation of cartilage proteoglycan metabolism LIF binding protein, *Cytokine* **10**(3): 220-226.

Hutchings, I. M. (1992) Tribology: Friction and wear of engineering materials. Edward Arnold, London.

Ingham, E., Fisher, J. (2005) The role of macrophages in osteolysis of total joint replacement *Biomaterials* **26**(11): 1271-1286

Jin, Z. M., Dowson, D., and Fisher, J. (1993) Wear and friction of medical grade polyurethane sliding on smooth metal counterfaces, *Wear* **162-164**: 627-630.

Jin, Z., Williams, S., Tipper. J., Ingham, I., and Fisher, J. (2006) Tribology of hip joints from natural hip joints, cartilage substitution, artificial replacements to cartilage tissue engineering, *Journal of Biomechanical Science and Engineering* **1**(1): 69-81.

Joosten, L. A. B., Helsen, M. M. A., Van de Loo, F. A. J., and Van den Berg, W. B. (1996) Anticytokine treatment of established type II collagen-induced arthritis in DBA/1 mice, *Arthritis & Rheumatism* **39**(5): 797-809.

Jovanovic, D. V., Di Battista, J. A., Martel-Pelletier, J., Jolicoeur, F. C., He, Y., Zhang, M., Mineau, F., and Pelletier, J. P. (1998) IL-17 stimulates the production and expression of proinflammatory cytokines, IL-β and TNF-α, by human macrophages, *J Immunol* **160**(7): 3513-3521.

Katta, J., Marcolongo, M., Lowman, A., Mansmann, K. A. (2006) Friction and wear behaviour of poly(vinyl alcohol)/poly(vinyl pyrrolidone) hydrogels for articular cartilage replacement *Journal of Bomedical Materials Research Part A* 471-479

Katta, J., Jin. Z., Ingham, E., Fisher, J. (2009) Effect of nominal stress on the long term friction, deformation and wear of native and glycosaminoglycan deficient articlar cartilage *Osteoarthritis and Cartilage* **17**:662-668

Katz, J. N. (2006) Total joint replacement in osteoarthritis, *Best Practice & Research Clinical Rheumatology* **20**(1): 145

Kelkar, R., Ateshian, G.A (1999) Contact creep of biphasic cartilage layers *J Appl Mech Trans ASME* **66**(1):137-145

Knudson, C. B., and Knudson, W. (2001) Cartilage proteoglycans, *Cell & Developmental Biology* **12**: 69-78.

Kuettner, K. E. (1992) Biochemistry of articular cartilage in health and disease, *Clinical Biochemistry* **25**(3): 155-163.

Lambda, N. M. K., Woodhouse, K. A., Cooper, S. L. (1998) Polyurethanes in biomedical applications. ISBN 08 493 451 70

Lotz, M. H. S., and Kuhn, K. (1999) Mechanisms of chondrocyte apoptosis, *Osteoarthritis and Cartilage* **7**: 389-391.

Ma, R., Xiong, D., Miao, F., Zhang, J., Peng, Y. (2009) Friction properties of novel PVA/PVP hydrogels as artificial cartilage *Journal of Biomedical Materials Research Part A* **93A**(3):1016-1019

Malviya, A., and McCaskie, A. (2006) Surgery for osteoarthritis, *Medicine* **34**(9): 369-372.

Marcelino, J., and McDevitt, C. A. (1995) Attachment of articular cartilage chondrocytes to the tissue form of type VI collagen, *Biochimica et Biophysica Acta (BBA) – Protein Structure and Molecular Enzymology* **1249**(2): 180-188.

Marieb, E. (2004) Human anatomy and physiology 6th Ed. ISBN 0-321-20413-1.

Martel-Pelletier, J., Alaaeddine, N., and Pelletier, J. P. (1999) Cytokines and their role in the pathophysiology of osteoarthritis, *Frontiers in Bioscience* **4**: 694-703.

Martini, F. H., and Bartholomew, E. F. (2007) Essentials of anatomy & physiology, *Benjamin Cummings* ISBN 978-0321567024

Maroudas, A. A. (1976) A balance between swelling pressure and collagen tension in normal and degenerate cartilage *Nature* **260**:808-809

Matthews, J. B., Besong, A. A., Green, T. R., Stone, M. H. Wroblewski, B. M., Fisher, J., and Ingham, E. (2000) Evaluation of the response of primary human peripheral blood mononuclear phagocytes to challenge with in vitro generated clinically relevant UHMWPE particles of known size and dose, *J Biomed Mater Sci* **52**: 296-307.

McCredie, A. J., Stride, E., Saffari, N. (2009) Quasi-static elastography comparsion of hyaline cartilage structures, *Journal of Physics: Conference Series* **195** 012004. DOI: 10.1088/1742-6596/195/1/012004.

M^{c}Cutchen, C. W. (1962) The frictional properties of animal joints, *Wear* **5**: 1-17.

M^{c}Cutchen, C. W., and Lewis, P. R. (1959) Experimental evidence for weeping lubrication in mammalian joints, *Nature* **4695**: 1285.

Mente, P. L., and Lewis, J. L. (1994) Elastic modulus of calcified cartilage is an order of magnitude less than that of subchondral bone, *J Orthop Res* **12**: 637-647.

Miller, M. J. S., Ahmed, S., Bobrowski, P., and Haqqi, T. M. (2004) Suppreeion of human cartilage degradation and chondrocyte activation by a unique mineral supplement (SierraSil) and a cat's claw extract, Vincaria, *The Journal of American Nutraceutical Association* **7**(2) 32-39.

Monfort, J., Tardif, G., Reboul, P., Mineau, F., Roughly, P., Pelletier, J. P., and Martel-Pelletier, J. (2006) Degradation of small leucine-rich repeat proteoglycans by matrix metalloprotease-13: identification of a new biglycan cleavage site, *Arthritis Research & Therapy* **8**(1): R26.

Mortellaro, C. M. (2003) Pathophysiology of osteoarthritis, *Veterinary Research Communications* **27**(1): 75-78.

Mow, V. C., Hayes, W. C. (1997) Basic Orthopaedic Biomechanics 2nd Ed. *Lippincott-Raven* ISBN 978-0397516841

Mow, V. C., Lai, W. M., Eisenfeld, J., and Redler, I. (1974) Some surface characteristics of articular cartilage – II. On the stability of articular surface and a possible biomechanical factor in etiology of chondrodegeration and structures, *Journal of Biomechanics* **7**(5): 457-468.

Mow. V. C., Mak. A. F., Lai. W. M. (1984) Viscoelastic properties of proteoglycan subunits and aggregates in varying solution concentrations *Journal of Biomechanics* **17**(5):325-338

Mow, V. C., Ratcliffe, A., and Poole, A. R. (1992) Cartilage and diarthrodial joints as paradigms for hierarchical materials and structures, *Biomaterials* **13**(2): 67-97.

Muir, H. (1981) Proteoglycans – State of the art, *Seminars in Arthritis and Rheumatism* **11**(1): 7-10.

Muir, H. (1995) The chondrocyte, architect of cartilage – Biomechanics, structure, function and molecular biology of cartilage matrix macromolecules, *Bioassays* **17**(12): 1039-1048.

Nakase, T., Miyaji, T., Tomita, T., Kaneko, M., Kuriyama, K., Myoui, A., Sugamoto, K., Ochi, T., and Yoshikawa, H. (2003) Localisation of bone morphogenetic protein-2 in human osteoarthritic cartilage and osteophyte, *Osteoarthritis and Cartilage* **11**(4): 278-284.

Nakashima, K., Sawae, Y., Murakami, T. (2007) Effect of conformational changes and differences of proteins on frictional properties of poly(vinyl alcohol) hydrogel *Tribology International* **40** 1423-1427

Neame, P. J., Tapp, H., and Azizan, A. (1999) Noncollagenous, nonproteoglycan macromolecules of cartilage, *Cellular and molecular Life Sciences* **55**(10): 1327-1340.

Northwood, E., and Fisher, J. (2007) Investigation of the friction and surface degradation of innovative chondroplasty materials against articular cartilage, *Proc Inst Mech Eng [H]* **221**(3): 263-279.

Ozbilgin, M. K., Inan, S. (2003) The roles of transforming growth factor type β3 (TGF-β3) and mast cells in the pathogenesis of scleroderma *Clin Rheumatol* **22**:189-95.

Palastanga, N., Soames, R., Field, D. (2006) Anatomy and human movement: Structure and function *Butterworth Heinemann* ISBN 978-0-7506-8814-7

Pan, Y., Xiong, D., and Ma, R. (2006) A study on the friction properties of poly (vinyl alcohol) hydrogel as articular cartilage against titanium alloy, *Wear* ***In press***

Pascual, E., and Jovani, V. (2005) Synovial fluid analysis, *Best Practice & Research Clinical Rheumatology* **19**(3): 371-386.

Park, C. C., Morel, J. C. M., Amin, M. A., Connors, M. A., Harlow, L. A., and Koch, A. E. (2001) Evidence of IL-18 as a novel angiogenic mediator, *J Immunol* **167**(3): 1644-1653.

Pilaszkiewicz, A., Fray, M. E. L., Sweiszkowski, W, Kurzydlowski, K. J. (2005) Chemically and physically crosslinked poly(vinyl alcohol) hydrogels for cartilage repair *e-Polymers* **P-013**:1-6

Podsiadlo, P., Kuster, M. S., and Stachowiack, G. W. (1997) Numerical analysis of wear particles from non-arthritic and osteoarthritic human knee joints, *Wear* **210**: 318-325.

Polster, J., and Recht, M. (2005) Postoperative MR evaluation of chondral repair in the knee, *European Journal of Radiology* **54**(2):206-213.

Poole, A. R. (2003) What type of cartilage repair are we attempting to attain? *J. Bone Joint Surg Am* **85**: 40-44.

Poole, A. R., Flint, H. M., Beaumont, W. B., (1987) Morphologival and functional interrelationships of articular cartilage matrices *J Anat* **138**: 113-138.

Poole, A. R., Kojima, T., Yasuda, T., Mwale, F., Kobayashi, M., and Laverty, S. (2001) Composition and structure of articular cartilage: A template for tissue repair, *clinical Orthopaedics and Related Research* **391**: S26-S33.

Porth, C. M., Kunert, M. P. Pathophysiology: concepts of altered health states, 6th Ed. (2002) Lippincott Williams & Wilkins. ISBN 0-7817-28819

Purdue, P. E., Koulouvaris, P., Nestor, B. J., Sculo, T. P (2006) The central role of wear debris in periprosthetic osteolysis *HSSJ* **2**:102-113

Pylawka, T., Kank, R.W., Cole, B.J: Articular Cartilage Injuries. In Schepsis AA and Busconi B (eds). Sports Medicine, Orthopaedic Surgery Essentials, pp 418-429, Lippincott & Williams, Philadelphia, Pensylvania, 2006

Quigley, F.P., Buggy, M., Birkinshaw, C. (2002) Selection of elastomeric materials for compliant –layered total hip arthroscopy *Proc Instn Mech Engrs Part H: Journal Engineering in Medicine* **216**:77-83

Raman, R., Pape, H. C., and Giannoudis, P.V. (2003) Cytokines in orthopaedic practice: a review, *Current Orthopaedics* **17:** 378-385.

Richards, L. (2008) Biological activity of nanometer sized polymer particles *PhD* University of Leeds

Rosiak, J. M., and Yoshii, M. (1999) Hydrogels and their medical applications, *Nuclear Instruments and Methods in Physics Research B* **151**: 56-64.

Sandell, L. J., and Aiger, T. (2001) Articular cartilage and changes in arthritis an introduction: Cell biology of osteoarthritis, *Arthritis Res* **3**:107-113.

Santerre, J. P., Woodhouse, K., Laroche, G., and Labow, R. S. (2005) Understanding the biodegradation of polyurethanes: From classical implants to tissue engineering materials, *Biomaterials* **26**: 7457-7470.

Savio, J. A., Overcamp, L. M., Black, J. (1994) Size and shape of biomaterial wear debris *Clinical Materials* **15**: 101-147

Scholes. S. C., Unsworth. A. (2006) The effect of proteins on the friction and lubrication of artificial joints *Proc IMechE Part H: J Engineering in Medicine* **220**:687-693

Soder, S., Hambach, L., Lissner, R., Kirchner, T., and Aigner, T. (2002) Ultrastructural localisation of type VI collagen in normal adult and osteoarthritic human articular cartilage, *Osteoarthritis and Cartilage* **10**(6): 464-470.

Springer, B. D., Scott, R. D., Sah, A. P., and Carrington, R. (2006) McKeever hemiarthroplasty of the knee in patients less than sixty years old, *J. Bone Joint Surg Am*, **88**:366-371.

Stewart. T. D., Hall. R.M (2006) Basic biomechanics of human joints: Hips, knees and the spine *Current Orthopaedics* **20**: 23-31

Stoltz, J. F. (2004) *Mechanobiology: Cartilage and Chondrocyte*, Amsterdam: IOS Press. ISBN 1 58603 436 7

Stone, K. R., Walenbach, A. W., Freyer, A., Turek. T. J., and Speeder, D. P. (2006) Articular cartilage grafting to full-thickness articular cartilage knee joint lesions:A 2- to 12- year follow-up, *Arthroscopy: The Journal of Arthroscopic and Related Surgery* **22**(3):291-299.

Stove, J., Schneider-Wald, B., Scharf, H. P., and Schwarz, M. L. (2006) bone morphogenetic protein 7 (bmp-7) stimulates proteoglycan synthesis in human osteoarthritic chondrocytes in vitro, *Biomedicine & Pharmacotherapy* **60**(10): 639-643.

Tipper, J. L., Galvin, A. L., Williams, S., McEwen, H. M. J., Stone, M. H., Ingham, E., and Fisher, J. (2006) Isolation and characterization of UHMWPE wear particles down to ten nanometers in size from *in vitro* hip and knee joint simulators, *J Biomed Mater Res* **78A**: 473-480.

Tipper, J. L., Ingham, E., Hailey, J., Besong, A. A., Wroblewski, B. M., Stome, M. H., and Fisher, J. (2000) Quantitative comparison of polyethylene wear debris, waer rate and head damage in retrieved Charnley hip prostheses, *Biomed Mater Engng* **12**:189-201.

Tu, C. F., Fort, T (2004) A study of fiber-Capstan friction. Stribeck curves *Tribology International* **37** 701

Van den Berg, W. (1999) The role of cytokines and growth factors in cartilage destruction in osteoarthritis and rheumatoid arthritis, *Z Rheumatol* **58**: 136-141.

Van de Loo, F. A. J., Joosten, L. A. B., Van Lent, P. L. M., Arntz, O. J., and Van den berg, W. B. (1995) Role of interleukin-1, tumour necrosis factor alpha, and interleukin-6 in cartilage proteoglycan metabolism and destruction, *Arthritis & Rheumatism* **38**(2): 164-172.

Van Roon, J. A., Van Roy, J. L., Duits, A., Lafeber, F. P., and Bijlsma, J. W. (1995) Proinflammatory cytokine production and cartilage damage due to rheumatoid synovial T helper-1 activation is inhibited by interleukin-4, *Ann Rheum Dis* **54**(10): 836-840.

Van Roon, J. A., Van Roy, J. L., Gmelig-Mehling, F., Lafeber, F. P., and Bijlsma, J. W. (1996) Prevention and reversal of cartilage degradation in rheumatoid arthritis by interleukin-10 and interleukin-4, *Arthritis & Rheumatism* **39**(5): 829-835.

Van Snick, J. (1990) Interleukin-6: An overiew, *Annu Rev Immunol* **8**: 253-278.

Walker, P. S., Dowson, D., Longfield, M. D., and Wright, V. (1968) "Boosted lubrication" in synovial joints by fluid entrapment and enrichment, *Ann Rheum Dis* **27**: 512-520.

Walker, P. S., Unsworth, A., Dowson, D., Sikorski, J., and Wright, V. (1970) Mode of aggregation of hyaluronic acid protein complex on the surface of articular cartilage, *Ann Rheum Dis* **29**: 591-602.

Wang, W., Ferguson, D. J. P., Quinn, J. M. W., Hamish, A., Simpson, R. W., and Athanasou, N. A. (1997) Biomaterial particle phagocytosis by bone-resorbing osteoclasts, *J Bone Joint Surg (Br)* **79-B**: 849-856.

Ward, W. K., Slobodzian, E. P., Tiekotter, K. L., and Wood, M. D. (2002) The effect of microgeometry, implant thickness and polyurethane chemistry on the foreign body response to subcutaneous implants, *Biomaterials* **23**: 4185-4192.

Westacott, C. I., and Sharif, M. (1996) Cytokines in osteoarthritis: Mediators or markers of joint destruction? *Seminars in Arthritis and Rheumatism* **25**(4): 254-272.

Wilson, W., Van Donkelaar, C. C., Van Rietbergen, R., and Huiskes, R. (2005) The role of computational models in the search for the mechanical behaviours and damage mechanisms of articular cartilage, *Medical Engineering & Physics* **27**: 810-826.

Whittle, M. W. (1996) Gait Analysis: an introduction. Butterworth-Heinemann. ISBN 0-7506-22229.

Wu. G., Wang. C., Zhang. W. (2007) The factors of speeds and loads on the tribological properties of PVA-H/HA composites *Journal of Applied Polymer Science* **106**:3908-3914

Yagi, R., McBurney, D., Laverty, D., Weiner, S., and Horton, W. E. (2005) Intrajoint comparison of gene expression patterns in human osteoarthritis suggest a change in chondrocyte phenotype, *Journal of Orthopaedic Research* **23**: 1128-1138.

Zheng, M. H., King, E., Kirilak, Y *et al* (2004) Molecular characterisation of chondrocytes in autologous chondrocyte implantation *Int J Mol Med* **13**:623-628

Zoltnik, A., Moore, K. W. (1991) Interleukin 10 *Cytokine* **3**:366-371

Appendix I

General chemicals used throughout this thesis are shown in Table I-i.

Table I-i General chemicals used in this study indicating suppliers and storage requirements

Reagent	Supplier	Storage
Agarose	Helena Biosciences Europe, Gateshead, UK	Room temperature
Bovine serum albumin (BSA)	Sigma-Aldrich Ltd., Dorset, UK	Stored at 4°C
Carbon paste	Agar scientific, Stanstead, Essex, UK	Room temperature
Chloroform	VWR International, Poole, UK	Room temperature. Solvents cupboard.
ELISA kits (TNFα, IL-1β, IL-6, IL-8)	IDS, Michigan, USA	Stored at 4°C
Ethanol	VWR International, Poole, UK	Flammables cupboard, room temperature
Household detergent	Procter & Gamble, Surrey, UK	Room temperature
Foetal bovine serum (FBS)	Lonza, Basel, Switzerland	Mycoplasma and virus screened. FBS was heat inactivated for 1 hour at 56°C then aliquoted. Stored at -20°C.
HEPES N-(2-hydroxyethyl) piperazine-N'-(2-ethanesulfonic acid)	Sigma-Aldrich Ltd., Dorset, UK	1M solution stored at room temperature
Isopropanol	VWR International, Poole, UK	Flammables cupboard, room temperature
L-Glutamine	Invitrogen Life Technologies Ltd., Paisley, UK	Aliquoted 200mM mL^{-1} solution and stored at -20°C

Latex beads (1.1 μm diameter)	Invitrogen Life Technologies Ltd., Paisley, UK	1% w/v in tissue culture medium. Stored at -20°C
Lymphoprep®	Nycomed UK Ltd., Birmingham, UK	Stored at 4°C
Methanol	VWR International, Poole, UK	Flammables cupboard, room temperature
Microbiological culture plates: Heated blood agar (HBA) Nutrient agar (NA) Saboraud dextrose agar (SAB)	Media Laboratory, Institute of Molecular and Cell Biology, University of Leeds, UK	Stored at 4°C. Before use, plates were dried for 20-30 minutes at 36°C.
PBS tablets	Oxoid Ltd, Hampshire, U.K	One PBS tablet dissolved in 100 mL ultrapure sterile water as stated by the manufacturer and stored at room temperature
Penicillin/Streptomycin	Invitrogen Life Technologies Ltd., Paisley, UK	Aliquoted and stored at -20°C. 5000 U mL^{-1} penicillin and 5000 U mL^{-1} streptomycin
Potassium hydroxide (KOH)	Fisher Scientific, Loughborough, Leicestershire, UK	To 10 ml of lubricant 6.25 g of KOH was added. Stored at room temperature
Pyrogen-free ultra pure water	Fresenius Kabi Warrington, USA	Room temperature
Rosslyn Park Memorial Institute (RPMI) 1640 culture medium (R0883)	Sigma-Aldrich Company Ltd., Poole, Dorset, UK	Stored at 4°C
Silica gel (0.7% w/v)	Merck, Darmstadt, Germany	Incubated at 160°C for 1 h until a colour change was achieved from blue (hydrated) to brown (dehydrated). Stored at room temperature

Trigene	Scientific Laboratory Systems	Room temperature. Diluted in water to 1:100 before use.
Trypan blue	Sigma-Aldrich Company Ltd., Poole, Dorset, UK	Room temperature. Made up in 10ml PBS at pH 7.4
Tween 20	Sigma-Aldrich Company Ltd., Poole, Dorset, UK	Room temperature
Virkon	Sigma-Aldrich Company Ltd., Poole, Dorset, UK	Room temperature

General equipment and materials used throughout this thesis are shown in Table I-ii.

Table I-ii General equipment and consumables in this study indicating suppliers

Equipment/Material	Supplier
Aluminium stub holder	Agar Scientific Ltd, Stanstead, Essex, UK
Automatic pipette boy (Pipetboy®)	Scientific Laboratory Supplies (SLS) Ltd., Nottingham, UK
Balance GX-2000 EC, accuracy 0.01g	A&D Instruments Ltd, Abington, Oxford, UK
Bovine femurs	John Penny & Company, Rawden, Leeds, UK
Centaur 2 plate spinner	MSE Scientific Instruments, West Sussex, UK
Chemtura LF blend 90A polyurethane	PPL Polyurethane Products Ltd., Retford, UK
Class I laminar flow hood	Bassaire, Southampton, UK
Class II laminar flow hood (Hera safe)	Heraeus, Germany
CO_2 gas cylinder	British Oxygen Company Ltd (BOC), Manchester, UK
CO_2 Incubator (MCO-20 AIC)	Sanyo Biomedical Europe BV
Contacting form talysurf profilometer 120L and associated pieces; ball calibrator, Ra Standard and Taylor-Hobson Ultra software	Taylor Hobson Ltd, Leicester, UK

Corethane 55D polyurethane (rebranded Bionate® by Polymer Technology Group [PTG], USA)	Corvita Corporation, USA; which was acquired by PTG. PTG has since been acquired by Royal DSM N.V., and are now known as DSM PTG (Berkeley, USA).
Dissection kit including metal plates, 9 mm diameter drill corer, 9 mm diameter drill bit, 9 mm diameter serrated corer, holding bath, clamps, jig, concave plates and plunger	School of Mechanical Engineering, University of Leeds, UK
Diprane 50D polyurethane	PPL Polyurethane Products Ltd., Retford, UK
Double sided carbon pads	Agar scientific, Stanstead, Essex, UK
Dry heat oven	Sanyo Biomedical Europe BV
Durometer D700 and digital reader	Zwick, Ulm, Germany
Electric drill (Skil 14.4 V)	SilverLine, Somerset, UK
ELISA Maxisorp® plates	Manufactured by Nunc AS, Roskilde, Denmark, supplied by Fisher Scientific, UK
ELISA MutilSkan Spectrum	Thermo Labsystems, MA, USA
Eppendorf pipettes	Sarstedt Aktlengesellschaft & Co., Nümbrecht, Germany
Freezer (Electrolux) -20°C	Jencons PLC, East Grinstead, UK
Fridge	Jencons PLC, East Grinstead, UK
Fume hood	Whiteley Fume Extraction Solutions Ltd., Bradford, UK
Gilson pipettes (P20, P200 & P1000)	Fisher Scientific, Loughborough, Leicestershire, UK
Glass universals	Institute of Molecular and Cell Biology, University of Leeds, UK
Glassware for filtering	Sartorius, Goettingen, Germany
Heavy duty hacksaw 300 mm	SilverLine, Somerset, UK

Haemocytometer	Marienfeld, Germany
High speed centrifuge rotors	Kendro Laboratory Products Ltd., Hertfordshire, UK
High speed Sorvall Evolution RC Centrifuge	Kendro Laboratory Products Ltd., Hertfordshire, UK
Hydrogels (H1B, H2B and H2A)	Provided by Dr. Wojciech Swieszkowski from Warsaw University, Poland
Indentation rig and all related pieces (custom-made)	School of Mechanical Engineering, University of Leeds, UK
Instron Tensile Tester 3365 and Bluehill software	Instron Service UK, High Wycombe, UK
Image Pro Plus (6.1) software	Media Cybernetics, Maryland, USA
Ion generator	Stat Attack P0294, Amersham, Buckinghamshire , UK
Labview 9 software	National Instruments Ltd., Berkshire, UK
LEO 1530 field emission gun scanning electron microscope	LEO Electron Microscopy Limited, Cambridge, UK
Magnetic stirrer	Scientific Laboratory Systems
Medical grade stainless steel (316)	Clarke Kilroy Metal Supplies, Leeds, UK
Mettler Toledo Analytical balance, accuracy 10μg	AT21 comparator, European Instruments, Oxford, UK
Microdrop Analyser and Build 306 software	First Ten Angstroms, Portsmouth, VA, USA
MSE Microcentaur	MSE Scientific Instruments, West Sussex, UK
MSE MISTRAL 3000i (bench centrifuge)	MSE Scientific Instruments, West Sussex, UK
Nikon profile projector (model V -16D)	Nippon Kogaku K. K., Tokyo, Japan
Non-contacting white light interferometer (WLI) NT 33005, and Vision 32 software	Veeco, MA, USA
Nunc 96-well plates (MTT assay)	Manufactured by Nunc AS, Roskilde, Denmark, supplied by Fisher Scientific, UK
Olympus Light Microscope	Mazurek, Warwickshire, UK

(VK40)	
Orbital shaker	Dynatech Ltd., West Sussex, UK
Petri dishes	Bibby Sterilin, Staffordshire, UK
Pipette tips (1-20 μL, 1-200μL & 101-1000 μL	Starlab, Ahrensburg, Germany
Plastic pipettes (1 mL, 10 mL, 25 mL)	Bibby Sterilin, Staffordshire, UK
Platinum (for coating stubs)	Cressington Scientific Instruments Ltd., Watford, UK
Polycarbonate filter membranes (10, 1.0 and 0.015 μm)	Whatman, Maidstone, Kent, UK
Pump, model FB70157 (50 Hz)	Fisher Scientific, Loughborough, Leicestershire, UK
Quanta™ Field Emission Gun Environmental Electron Microscope (FEGESEM)	FEI, Hanover, Germany
Single station multidirectional pin-on-plate aseptic wear rig and related pieces; bath , pin holder, spacer, collet and weights	School of Mechanical Engineering, University of Leeds, UK
Single station multidirectional pin-on-plate friction rig and related pieces; bath , pin holder, spacer, collet and lead weights	School of Mechanical Engineering, University of Leeds, UK
Six-station multidirectional wear pin-on-plate rig and all related pieces; bath inserts, polymer baffles, stainless steel toothed racks, stainless steel plates, spacer, collets, polymer gear wheels , bridges, connecting rods, load arms, long handled allen key, pin holder, load arms, bath well, lead weights	School of Mechanical Engineering, University of Leeds, UK
Stainless steel medical grade 316L pins and plates	School of Mechanical Engineering, University of Leeds, UK
Sorvall® polypropylene oak ridge bottles, 250 mL	DuPont Ltd., Stevenage, Herts., UK
Sputter coater and film thickness	Cressington Scientific Instruments Ltd., Watford, UK

monitor (208 HR)	
Sterile & non-sterile dispenser tips	BDH-Merck, VWR International, Poole, UK
Sterile hypodermic needles, 21 G X 1½ "	Terumo Europe, Belgium
Syringes (1, 10 and 20 mL)	Plastipak®, NHS supplies, UK
Talymap Gold software	Taylor Hobson Ltd, Leicester, UK
Tecoflex 51D/94A polyurethane	Thermedics™ (now known as The Lubrizol Corporation, USA)
Ultra high molecular weight polyethylene	Hoechst (now known as Ticona), Germany
Ultra sonication bath	Grant Instruments (Cambridge) Ltd., Herts., UK
Vacuette with sodium heparin	Greiner Bio-one GmbH (455051), Austria
TRIMOS vernier scale	Draper Expert, Middlesex, UK
Vortex mixer (TopMix FB15024)	Fisher Scientific, Loughborough, Leicestershire, UK
Water bath	Fisher Scientific, Loughborough, Leicestershire, UK
XT microscope server FEGESEM software (version 3.2.5)	FEI, Hanover, Germany

Appendix II

The injection moulding temperatures recommended by the manufacturer for Tecoflex 51D and 94A are shown in Table II-i.

Table II-i Guideline temperatures for Tecoflex 51D and 94A

Material	Rear	Front	Nozzle	Melt	Mould
Tecoflex 94A	325	350	360	< 410	50-110
Tecoflex 51D	360	375	380	< 410	50-120

Temperatures are in degrees Fahrenheit (tolerance ± 25)

The recommended optimum temperatures for Corethane 55D were 370 – 428°F. Temperatures used were the same as Tecoflex 51D.

Appendix III

FluoSpheres (FS) calculations (Richards, 2008):

Number of microspheres = $\frac{6C \times 10^{12}}{\rho \times \pi \times \varphi^3}$

Where, ρ = density (1.05), φ = diameter (μm), C = concentration (g/ml)

FluoSpheres 0.2 μm in size contained 2 % solids

Number of microspheres = $(6 \times 0.02) \times 10^{12} / (1.05 \times \pi \times (0.02)^3)$

$= 4.547 \times 10^{15}$ particles. ml^{-1}

Volume of each microsphere = $4/3\ \pi\ r^3$

Therefore, the volume of 1 FluoSphere was equal to 4.189×10^{-6} μm^3

In 1 ml there were 4.547×10^{15} FluoSphere particles. μl^{-1}

Total volume of FluoSphere particles was $4.547 \times 10^{15} \times 4.189 \times 10^{-6}$ μm^3

$= 1.905 \times 10^7$ μm^3. ml^{-1}

For example, 1: 10 μm^3 cell: particle volume ratio of 0.2 μm sized FS

FluoSpheres (10 μl) were added to 990 μl transport medium (RTM), giving a 1: 100 particle stock.

Therefore, there were 4.547×10^{15} particles. μl^{-1} in 1ml thus, 4.547×10^{13} particles. μl^{-1} in 1ml of the 1: 100 stock particle solution.

A volume of 1 FluoSphere = 4.189×10^{6} μm^3

Therefore, the volume of particles in stock solution = 4.189×10^{-6} μm^3 x 4.547×10^{13}

$= 1.91 \times 10^8 \mu m^3$

Require 3×10^5 cells per well therefore, 3×10^6 particles per well for 1: 10 μm^3 cell: particle volume ratio were required

$$\frac{1.91 \times 10^8 \mu m^3}{3 \times 10^6 \text{ particles/ well}} = 63.5 \text{ dilution factor}$$

So, in 1000 µl,
1000/63.5 = 15.7 per well

A total volume of 3 ml was made up in the agarose gels (2 % v/v agarose) and of this 200 µl was added to each well

Therefore, $\frac{3000}{200} = 15$ wells possible

So, 15.7 x 15 = 236 µl from stock was added

1 ml agarose + 1764 µl RTM + 236 µl 0.2 µm 1: 100 FS stock

1: 100 μm^3 cell: particle volume ratio of 0.2 µm sized FS

Total volume of particles in stock $= 4.189 \times 10^{-6} \mu m^3 \times 4.547 \times 10^{15}$

$= 1.91 \times 10^{10}$ particles/µl

Require 3×10^5 cells per well therefore, 3×10^7 particles per well for 1: 100 μm^3 cell: particle volume ratio.

$$\frac{1.91 \times 10^{10}}{3 \times 10^7 \text{ particles/ well}} = 636.7$$

Therefore, 1000/636.7 = 1.57 dilution factor per well

For a total of 15 wells

15 x 1.57 = 23.6 µl required from 0.2 µm FS as purchased.

1 ml agarose + 1976.4 µl RTM + 23.6 µl 0.2 µm FS stock

Appendix IV

Conference Oral Presentations

Engineering Postgraduate Symposium (2008), Leeds, UK – 1st prize

European Society of Biomechanics, ESB (2008), Lucerne, Switzerland

Biomaterials and Tissue Engineering Group (BiTEG) conference (2010), York, UK

Leeds Annual Conference, (2010), Leeds, UK

Conference poster presentations

Faculty of Engineering Symposium (2007), Leeds, UK

DePuy International Symposium (2007), Leeds, UK

Faculty of Engineering Symposium (2008), Leeds, UK – 3rd prize

Engineering Postgraduate Symposium (2008), Leeds, UK